Nuclear Science
NEA/NSC/DOC(2003)21

ISBN 92-64-02152-3

NEA NUCLEAR SCIENCE COMMITTEE
NEA COMMITTEE ON SAFETY OF NUCLEAR INSTALLATIONS

PRESSURISED WATER REACTOR MAIN STEAM LINE BREAK (MSLB) BENCHMARK

Volume IV: Results of Phase III on Coupled Core-plant Transient Modelling

by

N. Todorova, K. Ivanov and B. Taylor
Nuclear Engineering Program
Pennsylvania State University
University Park, PA 16802, USA

NEA3129

US NUCLEAR REGULATORY COMMISSION
NUCLEAR ENERGY AGENCY
ORGANISATION FOR ECONOMIC CO-OPERATION AND DEVELOPMENT

ORGANISATION FOR ECONOMIC CO-OPERATION AND DEVELOPMENT

Pursuant to Article 1 of the Convention signed in Paris on 14th December 1960, and which came into force on 30th September 1961, the Organisation for Economic Co-operation and Development (OECD) shall promote policies designed:

- to achieve the highest sustainable economic growth and employment and a rising standard of living in Member countries, while maintaining financial stability, and thus to contribute to the development of the world economy;
- to contribute to sound economic expansion in Member as well as non-member countries in the process of economic development; and
- to contribute to the expansion of world trade on a multilateral, non-discriminatory basis in accordance with international obligations.

The original Member countries of the OECD are Austria, Belgium, Canada, Denmark, France, Germany, Greece, Iceland, Ireland, Italy, Luxembourg, the Netherlands, Norway, Portugal, Spain, Sweden, Switzerland, Turkey, the United Kingdom and the United States. The following countries became Members subsequently through accession at the dates indicated hereafter: Japan (28th April 1964), Finland (28th January 1969), Australia (7th June 1971), New Zealand (29th May 1973), Mexico (18th May 1994), the Czech Republic (21st December 1995), Hungary (7th May 1996), Poland (22nd November 1996), Korea (12th December 1996) and the Slovak Republic (14 December 2000). The Commission of the European Communities takes part in the work of the OECD (Article 13 of the OECD Convention).

NUCLEAR ENERGY AGENCY

The OECD Nuclear Energy Agency (NEA) was established on 1st February 1958 under the name of the OEEC European Nuclear Energy Agency. It received its present designation on 20th April 1972, when Japan became its first non-European full Member. NEA membership today consists of 28 OECD Member countries: Australia, Austria, Belgium, Canada, Czech Republic, Denmark, Finland, France, Germany, Greece, Hungary, Iceland, Ireland, Italy, Japan, Luxembourg, Mexico, the Netherlands, Norway, Portugal, Republic of Korea, Slovak Republic, Spain, Sweden, Switzerland, Turkey, the United Kingdom and the United States. The Commission of the European Communities also takes part in the work of the Agency.

The mission of the NEA is:

- to assist its Member countries in maintaining and further developing, through international co-operation, the scientific, technological and legal bases required for a safe, environmentally friendly and economical use of nuclear energy for peaceful purposes, as well as
- to provide authoritative assessments and to forge common understandings on key issues, as input to government decisions on nuclear energy policy and to broader OECD policy analyses in areas such as energy and sustainable development.

Specific areas of competence of the NEA include safety and regulation of nuclear activities, radioactive waste management, radiological protection, nuclear science, economic and technical analyses of the nuclear fuel cycle, nuclear law and liability, and public information. The NEA Data Bank provides nuclear data and computer program services for participating countries.

In these and related tasks, the NEA works in close collaboration with the International Atomic Energy Agency in Vienna, with which it has a Co-operation Agreement, as well as with other international organisations in the nuclear field.

FOREWORD

The PWR MSLB Benchmark began in 1999. Four workshops have taken place since then. The first workshop was held in Washington DC, USA (April 1997), the second in Madrid, Spain (June 1998), the third in Garching near Munich, Germany (March 1999) and the fourth in Paris, France (January 2000). The participants in these workshops recognised that in performing these series of exercises they would be working at the edge of current developments in neutronics and thermal-hydraulics coupling. The benchmark also provided a common background understanding of key issues. At the outset, participants agreed that the PWR MSLB Benchmark would be published in four volumes.

Volume 1 of the *PWR MSLB Benchmark: Final Specifications* was issued by the OECD/NEA in April 1999 [NEA/NSC/DOC(99)8]. A small team at Pennsylvania State University (PSU) was responsible for authoring the final specification, co-ordinating the benchmark activities and answering any questions. The team also analysed the solutions submitted by benchmark participants and provided reports summarising the results for each phase. In performing these tasks, the PSU team collaborated with Adi Irani and Nick Trikouros of GPU Nuclear Inc.

Volume 2 of the *PWR MSLB Benchmark: Results of Phase I on Point Kinetics* was issued by the OECD/NEA in December 2000 [NEA/NSC/DOC(2000)21]. The second report of the series summarised the results of Phase I of the benchmark (point kinetics). The report identified the key parameters and important issues of thermal-hydraulic system modelling of the MSLB transient with specified point kinetics parameters. Phase I helped the participants to initialise and test their system code models for further use in Phase III, which addressed coupled three-dimensional (3-D) kinetics/system thermal-hydraulics simulations.

Volume 3 of the *PWR MSLB Benchmark: Results of Phase II on Coupled 3-D Kinetics Core Thermal-hydraulics Boundary Conditions Model* was issued by the OECD/NEA in June 2002 [NEA/NSC/DOC(2000)21]. The third volume summarised the results for Phase II of the benchmark (coupled-core boundary conditions model) and identified the key parameters and important issues of coupled-core modelling of the MSLB transient with specified core inlet and outlet thermal-hydraulic boundary conditions. As was the case with Phase I, Phase II helped the participants to initialise and test their coupled 3-D kinetics/ core thermal-hydraulics code models for further use in Phase III.

Volume 4 of the *PWR MSLB Benchmark* summarises the results of Phase III concerning best-estimate coupled core-plant system transient modelling. The report contains brief descriptions of the coupled codes used (for modelling 3-D core/plant system) as provided by the participants (Appendix A). In addition, the report gives detailed descriptions (including graphs where useful) of the models used (Appendix B). These model descriptions are presented as answers to the questionnaire for Phase III so that compliance with the specifications can be verified. The list of deviations from the specifications, if any, is provided and any specific assumptions are stated. Based on the information supplied, the benchmark co-ordinators and the report reviewers decided whether the solution provided models with sufficient precision. Solutions that deviated from the modelling in ways not compatible with the specifications were not included in the statistical evaluation procedure.

Appendices A and B are included in both the hard copy of the report as published by the OECD/NEA and the electronic copy as distributed on CD-ROM. Due to the large amount of data contained in Appendices C and D (approximately 600 pages), they are only provided on CD-ROM. Appendix C contains the mean solutions for each data type and parameters generated using the statistical methodology developed by PSU. These solutions are used as reference results for code-to-code comparisons with the participants' results. The participants' deviations and figures of merit for each parameter are presented in Appendix D.

Acknowledgements

This report is dedicated to the students of Penn State University, the next generation of nuclear engineers, who are the reason why we are here.

The authors would like to thank Dr. H. Finnemann from Siemens – former member of the NEA/NSC, Dr. S. Langenbuch from the *Gessellschaft für Reaktorsicherheit* (GRS), Professor J. Aragones from *Universidad Politecnica Madrid* (UPM) – current member of the NEA/NSC, and Professor F. D'Auria of University of Pisa (UP) – member of the NEA/CSNI, whose support and encouragement in establishing and carrying out this benchmark were invaluable.

This report is the sum of many efforts, the participants, the funding agencies and their staff (the US Nuclear Regulatory Commission and the Organisation of Economic Co-operation and Development). Special appreciation goes to the report reviewers: Professor J. Aragones from UPM, Dr. S. Langenbuch from GRS and R. Boeer from FRAMATOME ANP GmbH. Their comments and suggestions were very valuable and significantly improved the quality of this report. We would like to thank them for the effort and time involved.

Particularly noteworthy were the efforts of Farouk Eltawila assisted by David Ebert, both of the US Nuclear Regulatory Commission. With their help, funding was secured, enabling this project to proceed. We also thank them for their excellent technical advice and assistance.

The authors wish to express their sincere appreciation for the outstanding support offered by Dr. Enrico Sartori, who not only provided efficient administration, organisation and valuable technical recommendations, but most importantly provided friendly counsel and advice.

Finally, we are grateful to Amanda Costa for having devoted her competence and skills to the preparation of this report for publication.

TABLE OF CONTENTS

List of figures

List of tables

LIST OF ABBREVIATIONS

1-D	One-dimensional
2-D	Two-dimensional
3-D	Three-dimensional
ANL	Argonne National Laboratory
APSR	Axial power shape rods
ARI	All rods in
ARO	All rods out
BC	Boundary conditions
BE	British Energy
BOC	Beginning of cycle
BP	Burnable poison
CA	Control assembly
CEA	Commissariat á l'énergie atomique
CSA	Computer system analysis
EDF	Electricité de France
EFPD	Effective full power days
EOC	End of cycle
EOT	End of transient
EPRI	Electric Power Research Institute
FA	Fuel assembly
FZK	Forschungszentrum Karlsruhe
FZR	Forschungszentrum Rossendorf
GPU	General Power Utility
GRS	Gesellschaft für Anlagen- und Reaktorsicherheit mbH
HFP	Hot full power
HZP	Hot zero power
KAERI	Korean Atomic Energy Research Institute
LWR	Light water reactor
MSLB	Main steam line break
NEA	Nuclear Energy Agency
NEM	Nodal expansion method
NP	Normalised power
NPP	Nuclear power plant
NRC	Nuclear Regulatory Commission
OECD	Organisation for Economic Co-operation and Development
PSU	Pennsylvania State University
PWR	Pressurised water reactor
SRW	Stuck rod worth
T-H	Thermal-hydraulic
TMI-1	Three Mile Island – Unit 1
TR	Tripped rod
TRW	Tripped rod worth
UP/UZ	University of Piza/ University of Zagreb
UPM	Universidad Politecnica de Madrid
UPV	Universidad Politecnica de Valencia
VTT	Technical Research Centre of Finland

Chapter 1

INTRODUCTION

Incorporation of full three-dimensional (3-D) models of the reactor core into system-transient codes allows for a "best-estimate" calculation of interactions between the core behaviour and plant dynamics. Recent progress in computer technology has made feasible the development of coupled system thermal-hydraulic (T-H) and neutron-kinetics code systems. Considerable efforts have been made in various countries and organisations in this direction. To verify the capability of the coupled codes to analyse complex transients with coupled core-plant interactions and to fully test thermal-hydraulic coupling, appropriate light water reactor (LWR) transient benchmarks need to be developed on a higher "best-estimate" level. The previous sets of transient benchmark problems addressed separately system transients (designed mainly for T-H system codes with point kinetics models) and core transients (designed for T-H core boundary conditions models coupled with a three-dimensional neutron kinetics model). The Nuclear Energy Agency (NEA) of the Organisation for Economic Co-operation and Development (OECD), under the sponsorship of the US Nuclear Regulatory Commission (NRC), has recently completed a PWR Main Steam Line Break (MSLB) Benchmark against coupled T-H and neutron kinetics codes. A small benchmark team from the Pennsylvania State University (PSU) has been responsible for developing the benchmark specification, assisting the participants and co-ordinating the benchmark activities.

The PWR MSLB Benchmark problem uses a three-dimensional neutronics core model to verify the capability of coupled codes to analyse complex transients with coupled core-plant interactions and to fully test the thermal-hydraulic coupling. The benchmark problem is based on real plant design and operational data for Three Mile Island – Unit 1 Nuclear Power Plant (TMI-1 NPP). The purpose for this benchmark is three-fold:

- To verify the capability of system codes to analyse complex transients with coupled core-plant interactions.
- To fully test the 3-D neutronics/thermal-hydraulic coupling.
- To evaluate discrepancies between the predictions of coupled codes in best-estimate transient simulations.

The purposes of this benchmark are met through the application of three exercises (phases), which are described in Volume 1 of the *PWR MSLB Benchmark: Final Specifications* [1]. Volume 2 summarised the results of Phase 1 of point kinetics [2]. The purpose of the first exercise was to test the thermal-hydraulic system response, based on the point-kinetics plant simulations, which modelled the entire primary system. The participants were provided with compatible point-kinetics model inputs that preserve axial and radial power distribution, and scram reactivity obtained using a 3-D core neutronics model and a complete system description. Volume 3 summarised the results of Phase II. The purpose of this phase is to test the neutronics response to imposed thermal-hydraulic boundary conditions. The participants were provided with transient boundary conditions (radial distribution of mass flow rates at the core inlet, and core average pressure versus time at both the core inlet and

outlet); and a complete core description. This report (Volume 4) summarises the results for Phase III. This exercise combines elements of the first two exercises in the benchmark and is an analysis of the transient in its entirety.

As mentioned above, this report presents the final results for the third exercise of the PWR MSLB Benchmark problem, the best-estimate coupled core-plant transient modelling. This report contains twenty-two results received from sixteen participants representing twenty-five organisations from ten countries. Table 1.1 provides a list of participants who have submitted information to the PSU benchmark team for the third exercise, along with the codes used to perform the analysis. A more detailed description of each code is presented in Appendix A, and the modelling assumptions made by each participant are given in Appendix B. Some participants have submitted results from different versions of the same code and/or using different models, or couplings of different codes. Chapter 2 contains a description of the third benchmark exercise including core and neutronics data, a definition of the core T-H boundary conditions model, details about neutronic/thermal-hydraulic coupling, and a summary of the states and transient scenarios, calculated in this exercise. Chapter 3 discusses the statistical methodology employed in the benchmark to generate mean solutions. These mean solutions are presented in Appendix C and are used as reference solutions. Chapter 4 provides comparative analysis of the final results for the third exercise. The comparisons of results for each participant are provided in Appendix D. Chapter 5 provides a brief summary of the conclusions drawn from this exercise.

Table 1.1. List of participants in Phase III of the PWR MSLB Benchmark

Participant number	Company name	Country	Code
1	BE/Tractebel (1)	UK/Belgium	RELAP5/PANTHER
2	CEA (1)	France	CATHARE/FLICA4/CRONOS2
3	CEA (2)	France	CATHARE/FLICA4/CRONOS2
4	CSA/GPUN	USA	RETRAN-3-D
5	FRAMATOME ANP/FZK	Germany	RELAP5/PANBOX
6	FZR	Germany	DYN3-D/R-AHTLET
7	GRS	Germany	Q-C/ATHLET
8	JAERI	Japan	THYDE-NEU
9	KAERI	Korea	MARS/MASTER
10	PSU	USA	TRAC-PF1/NEM
11	Purdue/NRC	USA	RELAP5/PARCS
12	UP/UZ	Italy/Croatia	RELAP5/PARCS
13	UP/UZ	Italy/Croatia	RELAP5/QUABOX
14	UPC	Spain	RELAP5/PARCS
15	UPM	Spain	SIMTRAN/RELAP5
16	UPV	Spain	TRAC-PF1/NEM
17	VTT	Finland	TRAB-3-D/SMABRE

Chapter 2

DESCRIPTION OF THIRD BENCHMARK EXERCISE

Phase III of the OECD/NRC PWR MSLB Benchmark combines elements of the first two exercises and is an analysis of the transient in its entirety. While the purpose of the first exercise was to test the system response using specified point kinetics parameters and that of the second exercise was to test the core neutronics response to imposed thermal-hydraulic conditions, the third exercise seeks to test the coupled core/plant system transient modelling using the models developed in the first and second exercises.

The reference design for the PWR is derived from the reactor geometry and operational data of the TMI-1 NPP (see Figure 2.1). The full thermal-hydraulics (T-H) system model is coupled with the 3-D core model. The set of data given in the *Final Specifications* [1] in the pertinent tables and figures completely defines the third PWR MSLB benchmark exercise.

2.1 Description of MSLB scenario

The analysed transient is a MSLB in a PWR that may occur as a consequence of the rupture of one steam line upstream of the cross-connect. The event is characterised by significant space-time effects in the core caused by asymmetric cooling and an assumed stuck-out control rod after the reactor trip. Major concerns for the MSLB accident include the return-to-power and criticality. Because of this, the MSLB scenario was based on assumptions that conservatively maximise the consequences for a return-to-power. Two versions of this scenario were specified. The first version is the original scenario that is employed in the current licensing practice. For this scenario, point-kinetics models usually predict return-to-power, while despite the conservative assumptions the 3-D models do not. Participants requested the second scenario to better test the predictions of coupled 3-D kinetics/ thermal-hydraulic codes. In this scenario, the 3-D models are also expected to predict return-to-power. Both versions have the same initial steady-state conditions and follow the same sequence of events. The difference is in the value of the tripped rod worth. In the 3-D kinetics simulations, the point-kinetics tripped-rod worth values are matched by two different rodded cross-section libraries to be used in each scenario version – **nemtabr.norp** and **nemtabr.rp**. The third exercise uses a modified linear interpolation routine (which allows extrapolation) – **lint4d.3rdExercise**.

The limiting MSLB for TMI-1 (a B&W-designed PWR) is at hot full power (HFP) because the steam generator (SG) liquid inventory increases with the power level. The worst case overcooling occurs at the maximum power level, which corresponds to the maximum liquid inventory in the SG.

The double-ended rupture of one steam line is assumed to occur upstream of the cross-connect (see Figures 2.2 and 2.3). Figure 2.2 shows the detailed RETRAN steam line nodalisation, while Figure 2.3 shows a simplified steam line modelling used for this MSLB simulation. The 24-inch (60.96 cm) main steam line and 8-inch (20.32 cm) cross-connect rupture results in the highest break flow assumption and maximises the RCS cool-down. The worst single failure is the failure in the open position of the feedwater-regulating valve to the broken SG. This failure in the open position causes

feedwater flow from the intact SG to cross over to the broken SG across the common header and maximises the feedwater flow to the broken SG. The feedwater flow is eventually terminated by closure of the feedwater block valve, which is conservatively assumed to close 30 seconds after the break occurs.

Subsequent to break initiation, and following reactor scram, the steam line turbine stop valves are assumed to slam shut, isolating the intact SG. The 8-inch (20.32 cm) cross-connect between the two steam lines of the broken SG remains open.

All four RCS pumps are assumed to operate during the event since maximising the primary to secondary heat transfer will cause maximum RCS cool-down. No credit is taken for pressuriser heater operation. This conservative assumption enhances the RCS depressurisation.

The reactor trip occurs when the neutron power reaches 114% of 2 772 MWt or when the primary system pressure reaches 1 945 psia (13.41 MPa) – 1 900 psia + 30 psia error + 15 psia absolute – at the hot leg pressure tap. The high neutron flux trip has a delay of 0.4 seconds; the low RCS pressure delay is 0.5 seconds. These values represent the delay from the time the trip condition is reached to the time the control rods are free to fall and bound the actual delays for TMI-1.

High-pressure injection (HPI) starts when the primary system pressure drops to 1 645 psia (11.34 MPa) with a 25-second delay. HPI is expected to activate because of the large overcooling that occurs during this transient. No credit is taken for negative reactivity insertion from boron addition. No other emergency core coolant system (ECCS) action is expected.

Since the primary-to-secondary heat transfer is the driving force behind the RCS cool-down and the depressurisation, the steam generator inventory is maximised to provide the largest cool-down capacity. An initial steam inventory of 57 320 lbm (26 000 kg) was assumed. One can obtain the desired mass by either decreasing the aspirator flow until the downcomer quality is just saturated, or adjusting the initial void fraction in the bundle region of the SG. In addition to the initial inventory, the mass of the feedwater between the feedwater isolation valve and the downcomer of the broken steam generator, which was calculated to be 35 500 lbm (16 103 kg), is modelled and contributes to the overcooling and depressurisation of the RCS. For the purposes of this benchmark the additional feedwater is modelled as an extended boundary condition of feedwater rate.

Vessel mixing is based on test data from Duke Power Company's Oconee Plant, also designed by B&W. These tests define the amount of mixing that occurs within the vessel as a ratio of the difference in hot leg temperatures to the difference in cold leg temperatures:

$$\text{Ratio} = [T_{hot}(\text{intact}) - T_{hot}(\text{broken})][T_{cold}(\text{intact}) - T_{cold}(\text{broken})]^{-1}$$

There is 20% mixing in the lower plenum and 80% mixing in the upper plenum, and the ratio (dT_{hot}/dT_{cold}) was conservatively chosen to be equal to 0.5. In order to be able to simulate this mixing, the reactor vessel in the RETRAN model was modified to include two equal parallel flow paths by splitting the downcomer, the lower plenum, the core and the upper plenum as shown in Figure 2.4. For the most part, these parallel flow paths behave independently, with the exception of common connections with the bypass and upper head volumes. These common flow paths keep the loop pressures in balance but contribute little to mixing of loop flows. The desired amount of loop flow mixing is obtained by exchanging energy between the two lower plenum volumes and the two upper plenum volumes with non-conducting heat exchangers. A proportional-integral control system is used to compute the ratio each time step from the hot and cold leg temperatures, compare the instantaneous

value of the ratio to the target value and adjust the energy exchange between the plenum volumes to match the target ratio of 0.5. Consistent with the experimental results, 20% of the energy was exchanged between lower plenum volumes and 80% between upper plenum volumes.

Different code predictions are compared and evaluated in regard to:

- Time and value of the power peak before reactor trip.
- Time and value of a power peak after reactor trip.
- Whether the system remains critical after the momentary return to power (if it occurs) for the transient duration.

2.2 Core neutronics model and cross-section library

The radial geometry of the reactor core is shown in Figure 2.5. Radially, the core is divided into cells 21.811 cm (0.7156 ft) wide, each corresponding to one fuel assembly (FA), plus a radial reflector (shaded area) of the same width. There are a total of 241 assemblies, 177 FA and 64 reflector assemblies. The reactor core is divided into 24 axial layers with a height (starting from the bottom) of: 14.88 cm (0.4882 ft); 4.71 cm (0.1545 ft); 10.17 cm (0.3514 ft); 8 × 14.88 cm; 2 × 29.76 cm (0.9764 ft); 8 × 14.88 cm; 12.266 cm (0.4024 ft); 2.614 cm (0.0858 ft); 14.88 cm, adding up to a total active core height of 357.12 cm (11.717 ft). Both the upper and lower axial reflector have a thickness of 21.811 cm (0.7156 ft). The axial nodalisation scheme accounts for material changes in the fuel design and for the exposure and moderator temperature (spectral history) variations.

The participants are free to choose the mesh for their calculation according to the numerical capabilities of the code. However, the output should give volume-averaged results on the specified mesh in the format described in Chapter 6 of the *Final Specifications*.

The PWR core contains fuel assemblies with different ^{235}U enrichments and different numbers of burnable absorber rods. The axial and radial distributions of the enrichment and absorbers can be found in Tables 2.9 and 2.10; the geometric data for the FA is given in Table 2.6. The available gap width is 0.00955 cm. For the neutronics problem, each of the FAs is considered to be homogeneous.

The radial arrangement of the control assemblies (CA) is shown in Figure 2.6. Sixty-one (61) of these CAs, grouped into seven groups, consist of full-length control rods. The rods contain a strong neutron absorber over a length that spans most of the active core region. In addition, the position of a control rod insertion in cm is given from the bottom of lower reflector. The total CA length, which coincides with the absorber length, is 342.7055 cm (11.244 ft). No tip of control rods is defined. The position of the lower CA absorber edge from the bottom of the lower reflector is 36.2255 cm (1.189 ft) for a completely inserted CA, and 378.931 cm (12.4323 ft) for a completely withdrawn CA. Measured in units of steps, complete insertion and withdrawal of a CA correspond to 0 and 971 steps, respectively. Each step is 0.3531 cm (0.139 in). If one multiplies 971 × 0.3531 and summates with 36.2255, the result is 379.0856 cm. The top edge of the core region is 378.931 cm, i.e. there is a difference of 0.1546 cm, which is not modelled in this benchmark. Here, the definition “completely withdrawn” means withdrawn from the active core, i.e. out of the core. The real completely withdrawn position in terms of steps is 1 000 steps, i.e. at 36.2255 + 353.1 = 389.3255 cm from the bottom of lower reflector, which is in the region of upper reflector and is not modelled in this benchmark. In addition, eight of the CAs (Group 8) consist of part-length control rods (axial power-shaping rods or APSR) whose presence is already accounted for in the cross-section tables.

Two neutron energy and six delayed neutron groups are modelled. The energy release per fission for the two prompt neutron groups is 0.3213×10^{-10} and 0.3206×10^{-10} W-s/fission and is considered to be independent of time and space. Table 2.7 shows the decay constants and fractions of delayed neutrons. No delayed energy release is considered.

The ANS-79 decay heat standard is the recommended decay heat standard model. In total, 71 decay-heat groups are used: 69 groups are used for the three isotopes ^{235}U, ^{239}Pu and ^{238}U with the decay-heat constants defined in the 1979 ANS standard plus the heavy-element decay heat groups for ^{239}U and ^{239}Np with constants given in Table 2.8. The participants should use the assumption of an infinite operation at power 2 772 MWt. For participants who are not capable of using the ANS-79 decay heat standard, a file of the decay heat evolution throughout the transient for both scenario versions has been provided. These predictions are obtained using the PSU coupled code TRAC-PF1/NEM [3] in order to avoid the uncertainties coming from using different decay-heat models. The effective decay-heat energy fraction of the total thermal power (the relative contribution in the steady state) is equal to 0.07143.

Thirty assembly types define the core geometry by 438 un-rodded and 195 rodded compositions. The corresponding sets of cross-sections are provided. Each composition is defined by material properties (due to changes in the fuel design) and burn-up. Burn-up dependence is a three-component vector of variables: exposure (GWd/t), spectral history (T_{mod}) and burnable poison (BP) history. Table 2.9 shows the definition of assembly types and Figure 2.7 presents the radial distribution of these assembly types within the reactor geometry. The 2-D assembly type map is shown in one-eighth core symmetry sector together with the assembly exposure values at the end of cycle (EOC). The axial locations of compositions for each assembly are shown in Table 2.10.

For each composition, the benchmark defines a complete set of diffusion coefficients and macroscopic cross-sections for scattering, absorption and fission as a function of the moderator density and fuel temperature. The cross-sections implicitly take into consideration the assembly discontinuity factors (ADFs) in order to minimise the size of the cross-section tables. The group inverse neutron velocities are also provided for each composition. Dependence of the cross-sections on the above variables is specified through a two-dimensional table look-up. Each composition is assigned to a cross-section set containing separate tables for the diffusion coefficients and cross-sections, with each point in the table representing a possible core state. The expected range of the transient is covered by the selection of an adequate range for the independent variables shown in Table 2.11. A linear interpolation scheme is used to obtain the appropriate total cross-sections from the tabulated ones based on the reactor conditions being modelled. The original interpolation procedure provided by PSU does not perform a linear extrapolation outside of the density boundaries, which can lead to an underestimation of the moderator density feedback. Subsequently the original interpolation procedure was modified to perform linear extrapolation of out-of-bounds values. At the fourth benchmark workshop the participants decided to use the modified interpolation procedure for Phase III [4]. Table 2.12 shows the definition of a cross-section table associated with thermal-hydraulic conditions. Table 2.13 shows the macroscopic cross-section table structure for one cross-section set. All cross-section sets are assembled into a cross-section library. Separate libraries provide cross-sections for rodded **(nemtabr)** (numerical nodes with a CA) and un-rodded compositions **(nemtab)**. Here we list some of the features of each library:

- The first line of data shows the number of data points used for the independent thermal-hydraulic parameters, i.e. fuel temperature, moderator density, boron concentration and moderator temperature.

- Each cross-section set is in the order shown in Table 2.13. Each table is in the format described in Table 2.12. More information on the format is presented in Appendix B of the *Final Specifications* [1]. First, the values of the independent thermal-hydraulic parameters (fuel temperature and moderator density) that are used to specify that particular set of cross-sections will be listed, followed by the values of the cross-sections.* Finally, the group inverse neutron velocities complete the data for a given cross-section set.

- The dependence on fuel temperature in the reflector cross-section tables is also modelled. This is because the reflector cross-sections are generated by performing 1-D transport calculations, including the next fuel region. In order to simplify the reflector feedback modelling the following assumptions are made for this benchmark: an average fuel temperature value equal to 600 K is used for the radial reflector cross-section modelling in both the initial steady-state and transient simulations, and an average coolant density for radial reflector equal to the inlet coolant density. For the axial reflector regions the following assumptions are made: for the bottom – the fuel temperature is equal to the inlet coolant temperature (per T-H channel or cell) and the coolant density is equal to the inlet coolant density (again per channel); for the top – the fuel temperature is equal to the outlet coolant temperature (per channel) and the coolant density is equal to the outlet coolant density (per channel).

- There is a second rodded library, generated for a hypothetical return-to-power scenario with 3-D kinetic models. It is named **nemtabr.rp**. The magnitude of the return to power is small; however, this is the maximum one can obtain by modifying the rodded thermal absorption cross-section for control rod Groups 1 to 6. This additional non-realistic scenario (even accounting for all the conservative assumptions used in the licensing practice) is defined upon the request of participants for more comprehensive testing of coupled 3-D kinetics/ thermal-hydraulics models.

2.3 Neutronic/thermal-hydraulic coupling

The feedback or coupling between neutronics and thermal-hydraulics can be defined by choosing user-supplied mapping schemes (spatial mesh overlays) in the radial and axial core planes.

Some of the inlet perturbations (inlet disturbances of both temperature and flow rate) are specified as a function of the position across the core inlet. This requires either 3-D modelling of the vessel or some type of a multi-channel model.

For the purposes of this benchmark (Phase III), it is recommended that an assembly flow area of 40.061 in^2 (0.0262 m^2) be used in the core T-H multi-channel models.

2.4 Initial steady-state conditions

The reactor is assumed to be at the end of cycle (EOC), 650 EFPD (24.58 GWd/MT average core exposure), with a boron concentration of 5 ppm, and equilibrium Xe and Sm concentration. Control rod groups from 1 to 6 are completely withdrawn (wd) – see Table 2.15. Group 7 is 90% wd, or 900 steps (354.0155 cm) from the bottom of lower reflector except the rod at position N12, which is

* Please note that the provided absorption cross-sections already take the xenon thermal cross-sections into account; however, at the participants' request, the xenon cross-sections are listed in the cross-section sets.

stuck throughout the transient and is out of the core. The position of Group 7 in terms of insertion from the top of core region is 26.9155 cm. The position of Group 8 is modelled implicitly through the cross-sections and the participants do not have to account for it in their control rod models.

The initial RCS pressure is at the nominal operating value of 2 170 psia (14.96 MPa). The initial pressuriser liquid level is set to the typical HFP pressuriser level of 220 temperature-compensated inches (558.8 cm). The initial cold leg temperature is 555°F (564°K). The initial HFP steady-state parameters are summarised in Table 2.14.

The initial steady state for the MSLB simulation, as described above, is to be calculated at EOC HFP conditions (used as initial steady state for the transient simulation). In order to obtain a critical initial steady state for the transient calculations the number of neutrons produced per fission is divided by the effective multiplication factor, k_{eff}, for the initial steady state. This adjustment procedure should be applied to the provided cross-section tables.

2.5 Transient calculations

Table 2.1 summarises the key assumptions for performing the coupled 3-D kinetics/system thermal-hydraulics MSLB analysis. Below we describe the assumptions that require additional explanation.

- *Steam flow and break modelling*. The rupture of the steam line occurs upstream of the cross-connect. This leads to the highest break flow assumption and maximises the reactor coolant system (RCS) cool-down. The main steam line piping length of about 146.98 ft (44.8 m) is included in the model (see Figure 2.2).

- *Main steam flow to turbine*. As shown in Figure 2.2 each SG has two steam lines to the turbine. For the intact SG, the steam lines are combined for modelling purposes, while for the broken SG, they are modelled separately. The initial steam flow from the intact SG to the turbine is 1 679 lbs/sec (761.59 kg/sec) and from each of the steam lines on the broken SG the flow is half of this value, i.e. 839.5 lbs/sec (380 795 kg/sec). At the time of the break, the steam from the broken steam lines will go directly to the break. The steam flow from the intact SG will continue to the turbine until the turbine stop valves close. The steam flow from the intact SG will not go to the break, because the steam lines are equipped with check valves to prevent reverse flow.

- *Break size*. The main steam line is specified as a 24-inch (60.96 cm) pipe. This value corresponds to the outside diameter of the pipe. The break area should be based on the pipe inside diameter, which is 22.06 in (56.03 cm). The 8-inch (20.32 cm) cross-connect corresponds to the inside pipe diameter.

- *Break location*. The steam line nodalisation and break location can be identified in Figure 2.2. The steam line break is the double-ended rupture of one 24-inch steam line, and is represented by junctions 178 and 179 below. The 8-inch cross-connect is represented by junction 360. The simplified main steam line model, shown in Figure 2.3, is developed for the purposes of this benchmark.

- *Main steam safety valves*. The MSSVs are modelled for the intact SG only, and the small safety plus three (271-273) safety valve banks are modelled (compare Figures 2.2 and 2.3). The flow

increases from zero to rated flow between the open set point and 3% above the open set point. The flow area for the small safety valve is approximately 0.0276 ft^2 (2.567×10^{-3} m^2) and 0.111 ft^2 (1.03×10^{-2} m^2) for the other valves. A description of the MSSVs is given in Table 2.2.

- *Main feedwater and emergency feedwater flows.* The mechanical failure of the feedwater regulating valve in the broken SG in the open position is assumed. The feedwater flow (FW) is eventually terminated by closure of the feedwater block valve, with the conservative assumption of a delay of 30 seconds after the break occurs. The FW in the broken SG is assumed to be ramped to the new value over the time indicated (see Table 2.3). After 30 seconds an extended boundary condition models the additional feedwater between the feedwater isolation valve and the downcomer of the broken SG. The mass of feedwater between the isolation valve and the broken steam generator nozzle, which is specified as 35 500 lbm (16 103 kg) is approximated as a constant flow of 3 000 lbm/sec (1 362 kg/sec) over 12 seconds (see Table 2.3). The main FW to the intact SG should be kept constant until reactor trip and then ramped to zero in 10 seconds (see Table 2.4). It is anticipated that for the purposes of this benchmark, 100 seconds of transient time will be sufficient for a return to power to be seen if it occurs. Consequently, emergency feedwater flow (EFW) need not be modelled as liquid levels in the broken SG will only reach the 10-inch (25.4 cm) actuation set point just prior to 100 seconds.

- *Reactor trip*. For the first and third exercises, the reactor scram occurs at a high neutron flux of 114% of 2 772 MWt (with a 0.4 second delay) or at a low RCS pressure of 1 945 psia (13.41 MPa) with a 0.5 second delay. For the second exercise, reactor scram is modelled to occur at 6.65 seconds into the transient. The high neutron flux set point is reached at 6.61 seconds and the insertion of control rod groups begin after the specified 0.4-second delay. Subsequent to the reactor trip signal, the most reactive control rod (the position of the rod is N12) is assumed stuck in its fully withdrawn position. The control rod movement during the scram in the second and third exercises is modelled with a speed of 155.773 cm/sec.

- *High-pressure injection*. The high-pressure injection (HPI) system triggers when primary system pressure drops to 1 645 psia (11.34 MPa) with a 25-second delay. The HPI is modelled taking credit for two pumps; the total flow versus pressure is shown in Table 2.5. No credit is taken for the negative reactivity insertion from boron addition.

- *SG conductors*. The secondary side heat conductors on the SG, downcomers and steam annulus should be given zero thickness and zero heat transfer coefficient. This will increase the cool-down for this event.

- *Containment modelling*. The containment response is not modelled and is assumed to remain at atmospheric pressure during the transient.

Table 2.1. MSLB analysis assumptions

Parameter	Value
Vessel mixing	$dT_{hot}/dT_{cold} = 0.5$
Boron injection	No credit taken for boron injection
Steam line break	24-inch rupture (60.96 cm)
Critical flow model	Moody, cont. coeff. = 1.0
High flux trip set point	114%
High flux trip delay time	0.4 sec
Decay heat multiplier	1.0
Turbine stop valve closure time	0.5 sec
MFW flow	Flow vs. time
EFW flow	No credit
HPI flow	Flow vs. pressure
High pressure trip set point	2 370 psia/16.34 MPa
High pressure trip delay	0.6 sec
Low pressure trip	1 945 psia/13.41 MPa
Low pressure trip delay	0.5 sec

Table 2.2. Description of MSSVs per OTSG

Description of safety valves	Open setpoint		Close setpoint		Rated flow per valve at 3% accumulation	
	psia	Bar	psia	Bar	lbm/hr	kg/hr
Small safety (1 valve)	1 055.0	72.73	1 012.5	69.8	194 900	88 407
Safety bank 1 (1 valve)	1 065.0	73.42	1 022.0	70.46	824 265	373 887
Safety bank 2 (2 valves)	1 065.0	73.42	1 022.0	70.46	792 610	359 528
Safety bank 3 (2 valves)	1 075.0	74.11	1 031.5	71.12	799 990	362 875

Table 2.3. Main feedwater flow boundary conditions to broken SG

Time (sec)	Flow (lb/sec / kg/sec)
0	1 679.0/761.59
10	4 000.0/1 814.4
30	3 000.0/1 360.8
42	3 000.0/1 360.8
45	0.0/0.0

Table 2.4. Main feedwater flow boundary conditions to intact SG

Time (sec)	Flow (lb/sec / kg/sec)
0	1 679.0/761.59
Reactor trip	1 679.0/761.59
10 seconds after reactor trip	0.0/0.0
35	0.0/0.0

Table 2.5. HPI flow versus pressure

Flow (gpm / kg/sec)	Pressure (psia/MPa)
470.0/28.43	15/0.103
455.2/27.53	615/4.24
390.0/23.59	1 215/8.38
360.0/21.77	1 515/10.45
345.0/20.87	1 615/11.14
315.0/19.05	1 815/12.51
190.0/11.49	2 415/16.65

Table 2.6. FA geometry data

Parameter	Value
Pellet diameter	9.391 mm/0.3697 in
Clad diameter (outside)	10.928 mm/0.43 in
Clad wall thickness	0.673 mm/0.0265 in
Fuel rod pitch	14.427 mm/0.568 in
Guide tube diameter (outside)	13.462 mm/0.53 in
Guide tube diameter (inside)	12.650 mm/0.498 in
Geometry	15×15
Number of fuel pins	208
Number of guide tubes	16
Number of in-core instrument positions per fit	1

Table 2.7. Decay constants and fractions of delayed neutrons

Group	Decay constant (s^{-1})	Relative fraction of delayed neutrons in %
1	0.012818	0.0153
2	0.031430	0.1086
3	0.125062	0.0965
4	0.329776	0.2019
5	1.414748	0.0791
6	3.822362	0.0197

Total fraction of delayed neutrons: 0.5211%.

Table 2.8. Heavy-element decay heat constants

Group no. (isotope)	Decay constant (s^{-1})	Available energy from a single atom (MeV)
70 (^{239}U)	4.91×10^{-4}	0.474
71 (^{239}Np)	3.41×10^{-6}	0.419

Table 2.9. Definition of assembly types

Assembly	Characteristics		
1	4.00 w/o	No BP	No Gd pins
2	4.95 w/o	3.5% BP	4 Gd pins
3	5.00 w/o	3.5% BP pulled	4 Gd pins
4	4.95 w/o	3.5% BP	4 Gd pins
5	4.40 w/o	No BP	No Gd pins
6	5.00 w/o	3.5% BP	4 Gd pins
7	4.85 w/o	No BP	4 Gd pins
8	4.85 w/o	No BP	4 Gd pins
9	4.95 w/o	3.5% BP pulled	4 Gd pins
10	4.95 w/o	3.5% BP	4 Gd pins
11	4.85 w/o	3.5% BP pulled	4 Gd pins
12	4.95 w/o	3.5% BP	4 Gd pins
13	5.00 w/o	3.5% BP pulled	4 Gd pins
14	5.00 w/o	No BP	8 Gd pins
15	4.95 w/o	No BP	8 Gd pins
16	4.95 w/o	3.5% BP pulled	4 Gd pins
17	4.95 w/o	3.5% BP	4 Gd pins
18	4.95 w/o	3.5% BP pulled	4 Gd pins
19	5.00 w/o	3.5% BP	4 Gd pins
20	4.40 w/o	No BP	No Gd pins
21	4.85 w/o	3.5% BP pulled	4 Gd pins
22	4.40 w/o	No BP	No Gd pins
23	4.95 w/o	3.5% BP	No Gd pins
24	4.95 w/o	3.5% BP pulled	4 Gd pins
25	5.00 w/o	No BP	8 Gd pins
26	5.00 w/o	No BP	4 Gd pins
27	5.00 w/o	No BP	No Gd pins
28	4.95 w/o	3.5% pulled	4 Gd pins
29	5.00 w/o	No BP	4 Gd pins
30		Radial reflector	

Table 2.10. Composition numbers in axial layers for each assembly type

Bottom

	1	2	3	4	5	6	7	8	9	10	11	12	13	14	15	16	17	18	19	20	21	22	23	24	25	26	27	28	29	30
1	24	24	24	24	24	24	24	24	24	24	24	24	24	24	24	24	24	24	24	24	24	24	24	24	24	24	24	24	24	24
2	1	16	34	49	64	79	94	109	124	139	154	169	184	199	214	229	244	259	274	289	304	319	334	349	364	379	394	409	424	25
3	2	17	35	50	65	80	95	110	125	140	155	170	185	200	215	230	245	260	275	290	305	320	335	350	365	380	395	410	425	25
4	3	18	36	51	66	81	96	111	126	141	156	171	186	201	216	231	246	261	276	291	306	321	336	351	366	381	396	411	426	25
5	4	19	37	52	67	82	97	112	127	142	157	172	187	202	217	232	247	262	277	292	307	322	337	352	367	382	397	412	427	25
6	5	20	38	53	68	83	98	113	128	143	158	173	188	203	218	233	248	263	278	293	308	323	338	353	368	383	398	413	428	25
7	6	21	39	54	69	84	99	114	129	144	159	174	189	204	219	234	249	264	279	294	309	324	339	354	369	384	399	414	429	25
8	7	22	40	55	70	85	100	115	130	145	160	175	190	205	220	235	250	265	280	295	310	325	340	355	370	385	400	415	430	25
9	7	22	40	55	70	85	100	115	130	145	160	175	190	205	220	235	250	265	280	295	310	325	340	355	370	385	400	415	430	25
10	7	22	40	55	70	85	100	115	130	145	160	175	190	205	220	235	250	265	280	295	310	325	340	355	370	385	400	415	430	25
11	7	22	40	55	70	85	100	115	130	145	160	175	190	205	220	235	250	265	280	295	310	325	340	355	370	385	400	415	430	25
12	8	23	41	56	71	86	101	116	131	146	161	176	191	206	221	236	251	266	281	296	311	326	341	356	371	386	401	416	431	25
13	8	23	41	56	71	86	101	116	131	146	161	176	191	206	221	236	251	266	281	296	311	326	341	356	371	386	401	416	431	25
14	8	23	41	56	71	86	101	116	131	146	161	176	191	206	221	236	251	266	281	296	311	326	341	356	371	386	401	416	431	25
15	8	23	41	56	71	86	101	116	131	146	161	176	191	206	221	236	251	266	281	296	311	326	341	356	371	386	401	416	431	25
16	9	27	42	57	72	87	102	117	132	147	162	177	192	207	222	237	252	267	282	297	312	327	342	357	372	387	402	417	432	25
17	9	27	42	57	72	87	102	117	132	147	162	177	192	207	222	237	252	267	282	297	312	327	342	357	372	387	402	417	432	25
18	9	27	42	57	72	87	102	117	132	147	162	177	192	207	222	237	252	267	282	297	312	327	342	357	372	387	402	417	432	25
19	9	27	42	57	72	87	102	117	132	147	162	177	192	207	222	237	252	267	282	297	312	327	342	357	372	387	402	417	432	25
20	10	28	43	58	73	88	103	118	133	148	163	178	193	208	223	238	253	268	283	298	313	328	343	358	373	388	403	418	433	25
21	11	29	44	59	74	89	104	119	134	149	164	179	194	209	224	239	254	269	284	299	314	329	344	359	374	389	404	419	434	25
22	12	30	45	60	75	90	105	120	135	150	165	180	195	210	225	240	255	270	285	300	315	330	345	360	375	390	405	420	435	25
23	13	31	46	61	76	91	106	121	136	151	166	181	196	211	226	241	256	271	286	301	316	331	346	361	376	391	406	421	436	25
24	14	32	47	62	77	92	107	122	137	152	167	182	197	212	227	242	257	272	287	302	317	332	347	362	377	392	407	422	437	25
25	15	33	48	63	78	93	108	123	138	153	168	183	198	213	228	243	258	273	288	303	318	333	348	363	378	393	408	423	438	25
26	26	26	26	26	26	26	26	26	26	26	26	26	26	26	26	26	26	26	26	26	26	26	26	26	26	26	26	26	26	26

Top

Table 2.11. Range of variables

T fuel (°K)	Void	T mod (°K)	Pressure (psia/MPa)	Rho M. (kg/m^3 / lb/ft^3)	Boron (ppm)
500.00	0.00	605.22	2200.0/15.17	641.40/8.2385	5.00
760.22	0.00	605.22	2200.0/15.17	641.40/8.2385	5.00
867.27	0.00	605.22	2200.0/15.17	641.40/8.2385	5.00
921.88	0.00	605.22	2200.0/15.17	641.40/8.2385	5.00
1500.00	0.00	605.22	2200.0/15.17	641.40/8.2385	5.00
500.00	0.00	579.35	2200.0/15.17	711.43/9.1379	5.00
760.22	0.00	579.35	2200.0/15.17	711.43/9.1379	5.00
867.27	0.00	579.35	2200.0/15.17	711.43/9.1379	5.00
921.88	0.00	579.35	2200.0/15.17	711.43/9.1379	5.00
1500.00	0.00	579.35	2200.0/15.17	711.43/9.1379	5.00
500.00	0.00	551.00	2200.0/15.17	769.47/9.8834	5.00
760.22	0.00	551.00	2200.0/15.17	769.47/9.8834	5.00
867.27	0.00	551.00	2200.0/15.17	769.47/9.8834	5.00
921.88	0.00	551.00	2200.0/15.17	769.47/9.8834	5.00
1500.00	0.00	551.00	2200.0/15.17	769.47/9.8834	5.00
500.00	0.00	545.00	1300.00/8.963	772.44/9.9216	5.00
760.22	0.00	545.00	1300.00/8.963	772.44/9.9216	5.00
867.27	0.00	545.00	1300.00/8.963	772.44/9.9216	5.00
921.88	0.00	545.00	1300.00/8.963	772.44/9.9216	5.00
1500.00	0.00	545.00	1300.00/8.963	772.44/9.9216	5.00
500.00	0.00	538.71	1000.00/6.895	781.31/10.035	5.00
760.22	0.00	538.71	1000.00/6.895	781.31/10.035	5.00
867.27	0.00	538.71	1000.00/6.895	781.31/10.035	5.00
921.88	0.00	538.71	1000.00/6.895	781.31/10.035	5.00
1500.00	0.00	538.71	1000.00/6.895	781.31/10.035	5.00
500.00	0.00	520.00	800.00/5.516	810.10/10.405	5.00
760.22	0.00	520.00	800.00/5.516	810.10/10.405	5.00
867.27	0.00	520.00	800.00/5.516	810.10/10.405	5.00
921.88	0.00	520.00	800.00/5.516	810.10/10.405	5.00
1500.00	0.00	520.00	800.00/5.516	810.10/10.405	5.00

Table 2.12. Key to macroscopic cross-section tables

T_{f1}	T_{f2}	T_{f3}	T_{f4}	T_{f5}
ρ_{m1}	ρ_{m2}	ρ_{m3}	ρ_{m4}	ρ_{m5}
ρ_{m6}	Σ_1	Σ_2	...	
		...	Σ_{29}	Σ_{30}

Where:

– T_f is the Doppler (fuel) temperature (°K)

– ρ_m is the moderator density (kg/m^3)

Macroscopic cross-sections are in units of cm^{-1}

Table 2.13. Macroscopic cross-section tables structure

```
**************************************************************************
        NEM – Cross-Section Table Input
*
*       T Fuel  Rho Mod.        Boron ppm.      T Mod.
        5       6       0       0
*
***********  X-Section Set #
 #
**************************************************************************
        Group No. 1
*
**************      Diffusion Coefficient Table
*
**************      Absorption X-Section Table
*
**************      Fission X-Section Table
*
**************      Nu-Fission X-Section Table
*
**************      Scattering From Group 1 to 2 X-Section Table
*
**************************************************************************
        Group No. 2
*
**************      Diffusion Coefficient Table
*
**************      Absorption X-Section Table
*
**************      Fission X-Section Table
*
**************      Nu-Fission X-Section Table
*
**************      Xenon Absorption Cross-Section Table
*
**************************************************************************
**************      Inv. Neutron Velocities
*
```

Table 2.14. Initial conditions for TMI-1 at 2 772 MWt

Parameter	Value
Core power	2 772.00 MWt
RCS cold leg temperature	555°F/563.76°K
RCS hot leg temperature	605°F/591.43°K
Lower plenum pressure	2 228.5 psia/15.36 MPa
Outlet plenum pressure	2 199.7 psia/15.17 MPa
RCS pressure	2 170.00 psia/14.96 MPa
Total RCS flow rate	38 806.2 lb/sec / 17 602.2 kg/sec
Core flow rate	35 389.5 lb/sec / 16 052.4 kg/sec
Bypass flow rate	3 416.7 lb/sec / 1 549.8 kg/sec
Pressuriser level	220 in/558.8 cm
Feedwater/steam flow per OTSG	1 679 lb/sec / 761.59 kg/sec
OTSG outlet pressure	930.00 psia/6.41 MPa
OTSG outlet temperature	571°F/572.63°K
OTSG superheat	35°F/19.67°K
Initial SG inventory	57 320 lbm/26 000 kg
Feedwater temperature	460°F/510.93°K

Table 2.15. Definition of steady state

T-H conditions	Control rod positions	Scenario version
HFP	Groups 1-6 ARO Group 7 is 90% wd N12 is 100% wd	1 and 2

ARO – all rods out; ARI – all rods inserted.

Figure 2.1. Original RETRAN nodalisation diagram

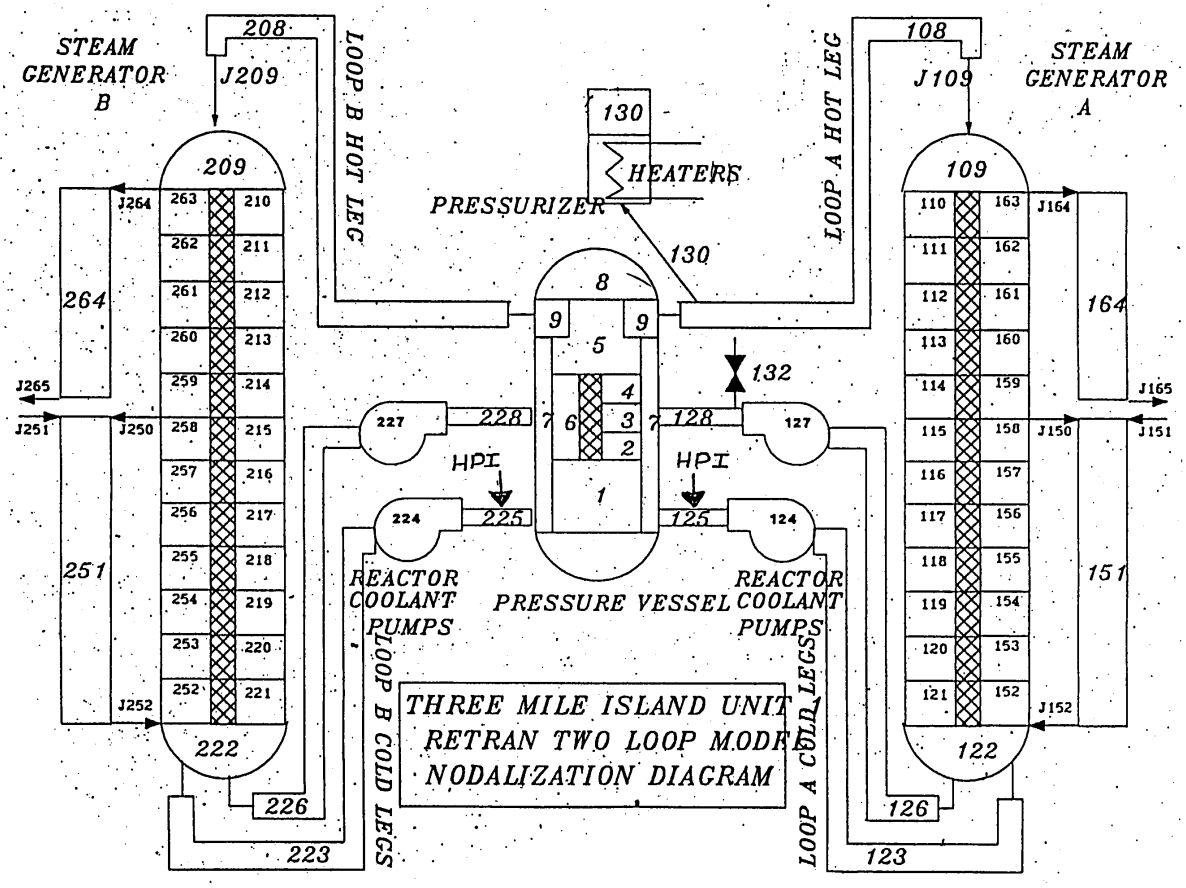

Figure 2.2. Original RETRAN steam line nodalisation

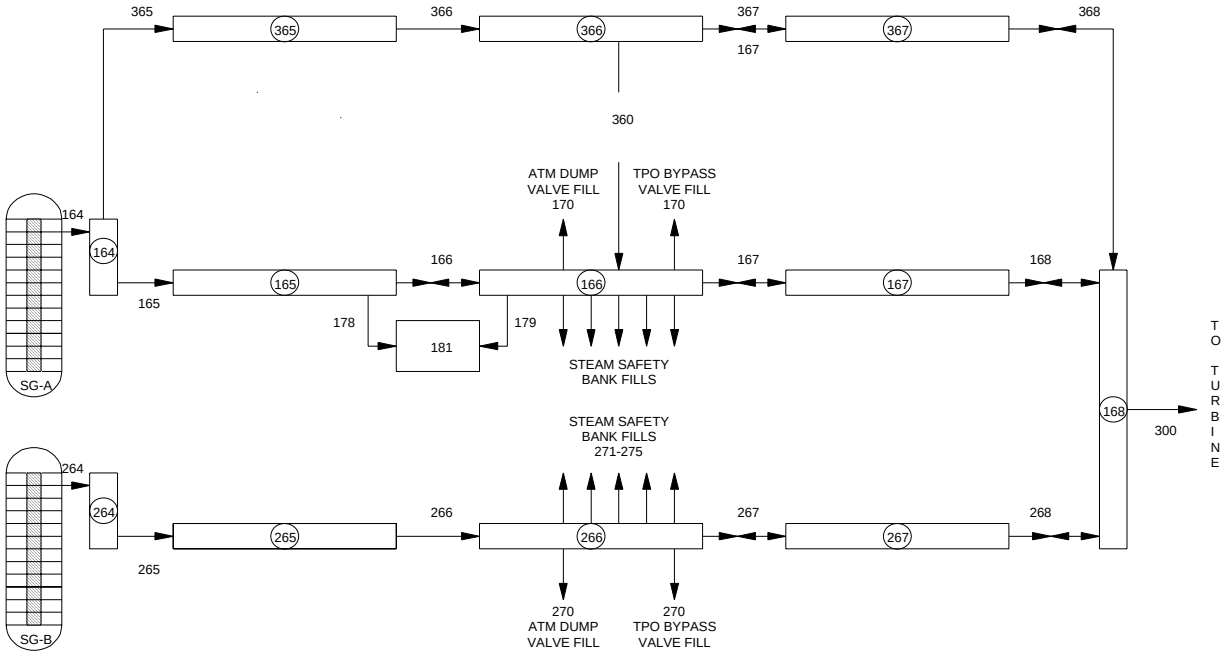

Figure 2.3. Simplified steam line modelling for MSLB

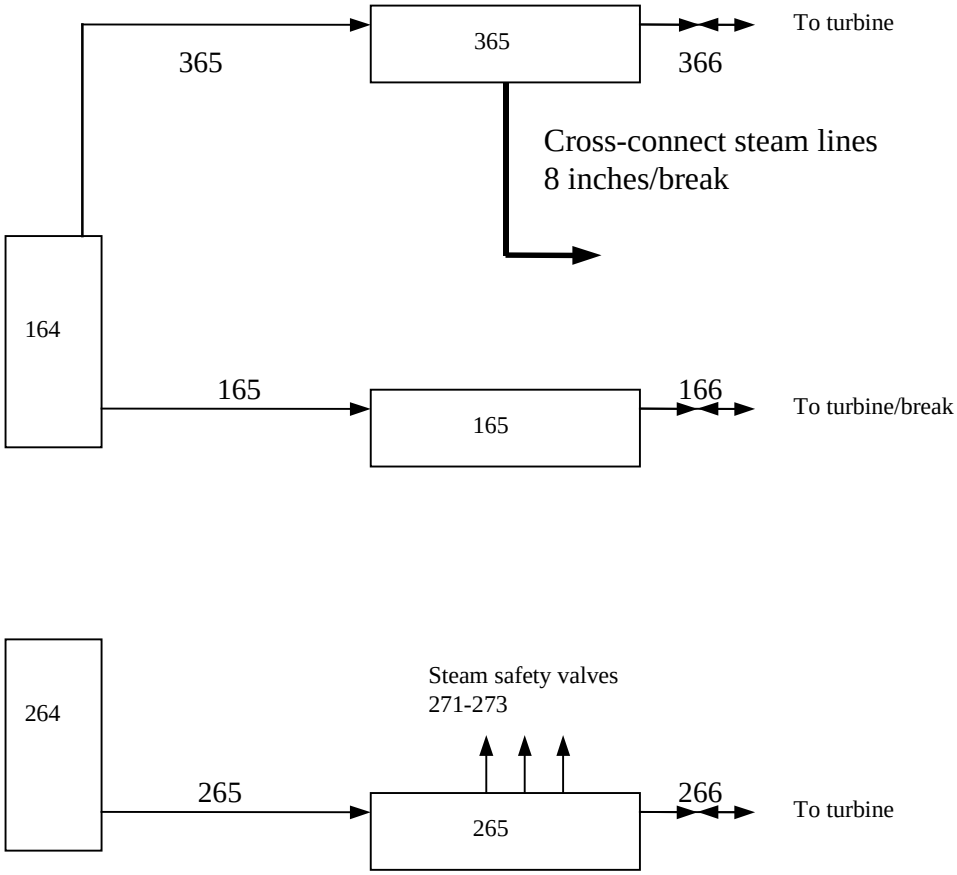

Figure 2.4. RETRAN two-channel model

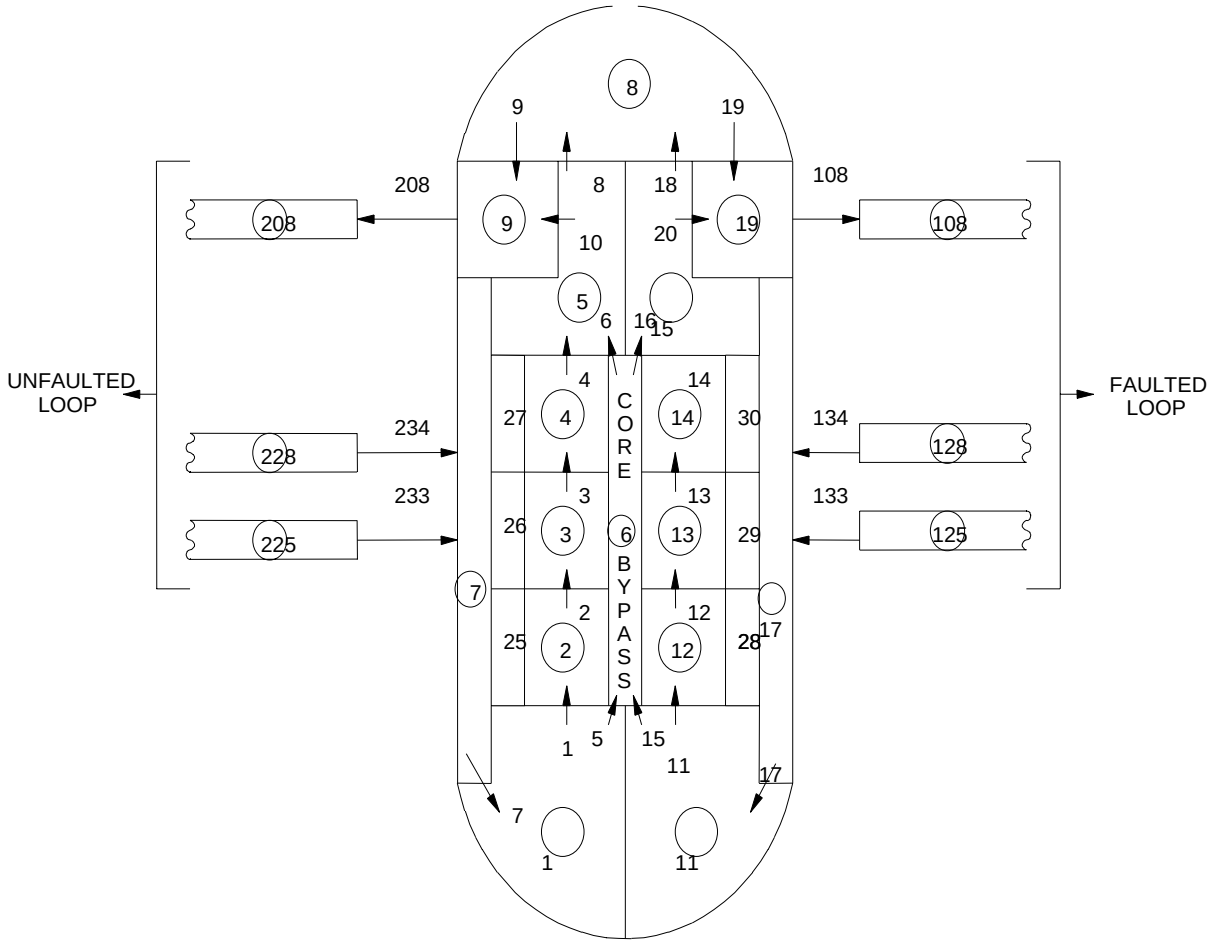

Figure 2.5. Cross-section of the reactor core

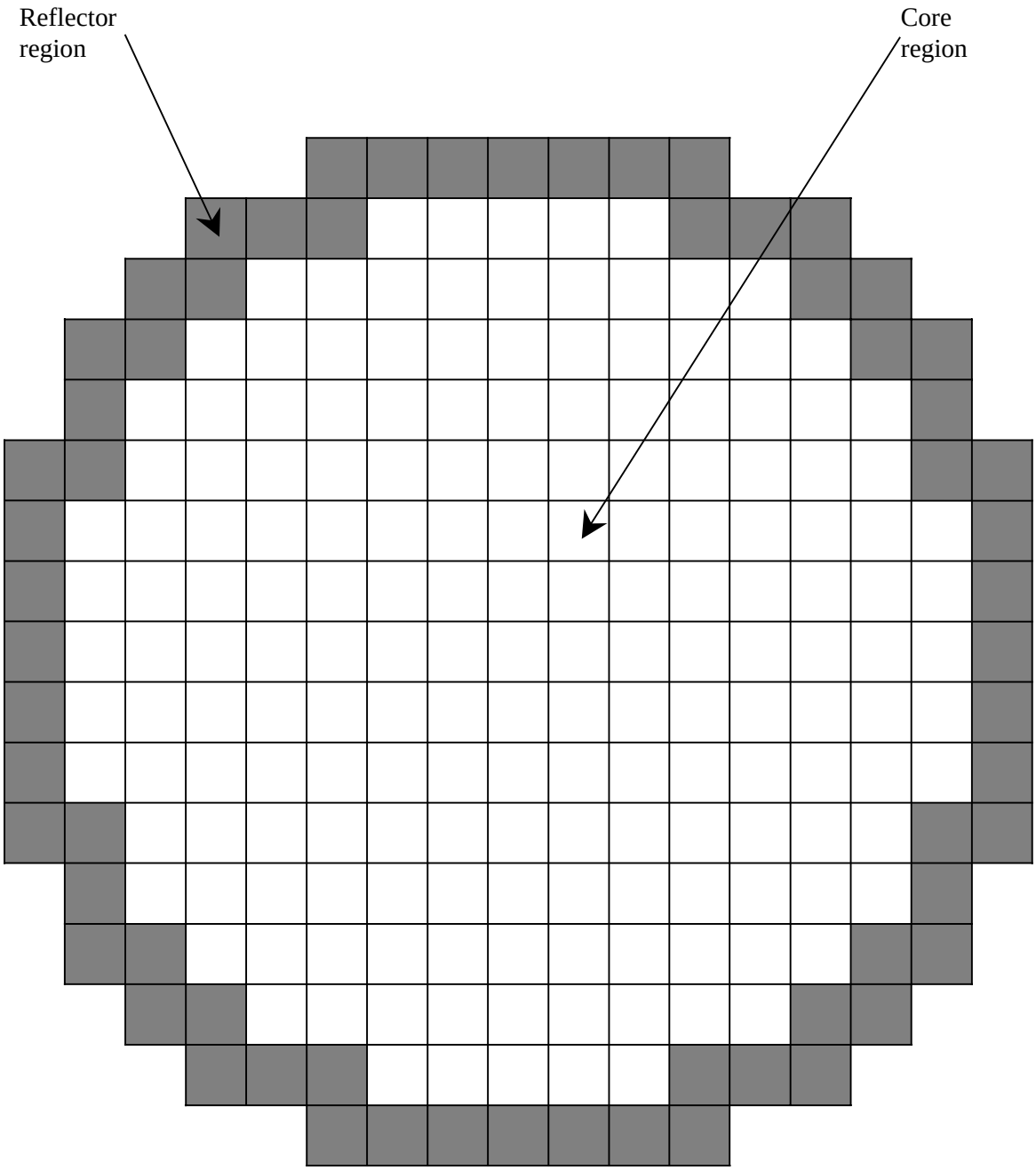

Figure 2.6. Arrangement of control rods

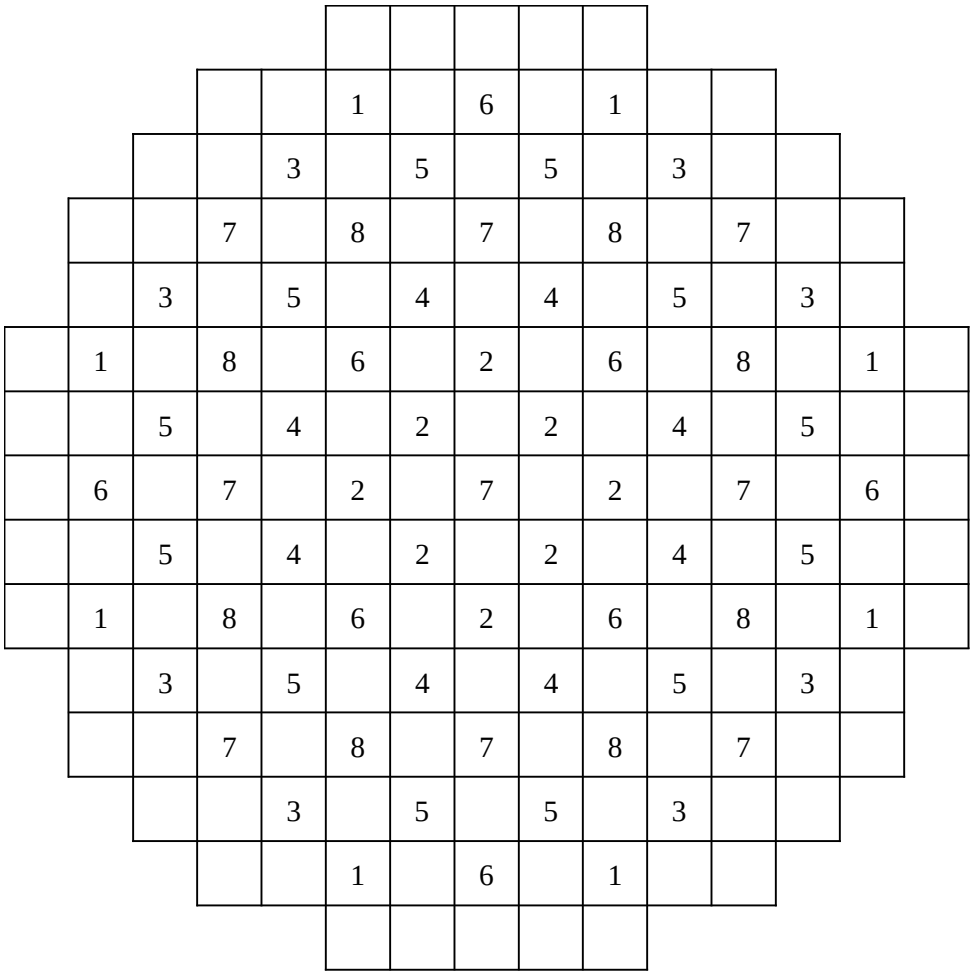

Bank	No. rods	Purpose
1	8	Safety
2	8	Safety
3	8	Safety
4	8	Safety
5	12	Regulating
6	8	Regulating
7	9	Regulating
8	8	APSR

Figure 2.7. Two-dimensional assembly-type map

	8	9	10	11	12	13	14	15
H	1 52.863	2 30.192	3 56.246	4 30.852	5 49.532	6 28.115	7 53.861	8 55.787
K		9 57.945	10 30.798	11 55.427	12 29.834	13 53.954	14 25.555	15 49.166
L			16 57.569	17 30.218	18 54.398	19 27.862	20 23.297	21 47.300
M				22 49.712	23 28.848	24 52.846	25 40.937	
N					26 48.746	27 23.857	28 41.453	
O						29 37.343	A B	
P								
R								

A – Type of fuel assembly

B – Assembly average burn-up in GWd/T

Chapter 3

STATISTICAL METHODOLOGY

Due to the lack of experimental data for the current phase of the benchmark problem, the reference solution for each requested parameter is based upon the statistical mean value of all submitted results. The comparisons to follow in this and later chapters are thus properly called code-to-code comparisons, rather than code-to-data comparisons. While perhaps not ideal, this method provides the strongest basis from which to complete a statistical analysis and comparison of the results for this exercise. In Section 3.1, the standard methods used to generate the reference solution will be presented. Special methods used for the analysis of normalised parameters are presented in Section 3.2, and some remaining issues are discussed in Section 3.3. Finally, in Section 3.4, a list of the parameters for which reference values have been calculated is provided.

3.1 Standard techniques for comparison of results

In Phase III of this benchmark problem, several types of data must be analysed and the results of all participants compared. These data types are:

1) Time history data.

2) Two-dimensional (2-D) radial distributions.

3) One-dimensional (1-D) axial distributions.

4) Integral parameter values.

It is necessary to develop a suite of statistical methods for each of these data types, to be applied whenever a comparison is desired. What follows is a description of each of these methods.

3.1.1 Time history data

In this exercise, various parameters such as power, temperature and coolant density are plotted as a function of time. Points of interest are isolated and submitted to a basic statistical analysis as described below.

- *Step 1: Isolate points of interest.* Such points include the highest return to power, the time of highest power before and after trip and values at the end of transient for all parameters. These points are identified for all time history sets, and the values of all participants are collected. For Phase III, these points are listed in Table 3.1.

Table 3.1. Points of interest for Phase III time histories

Time history	Point of interest	Scenario
Total power	Highest power before trip	2
Total power	Highest power after trip	2
Total power	Power at EOT	1, 2
Total power	Time of highest return to power	2
Fission power	Highest power before trip	2
Fission power	Highest power after trip	2
Fission power	Power at EOT	1, 2
Coolant density	Density at EOT	1, 2
Doppler temperature	Temperature at EOT	1, 2
Maximum nodal Doppler temperature	Temperature at EOT	1, 2

- *Step 2: Calculate mean value and standard deviation.* These two standard statistical values are calculated according to the formulae:

$$\bar{x} = \frac{\sum_{i}^{N} x_i}{N} \tag{3.1}$$

$$\sigma = \pm\sqrt{\frac{\sum_{i}^{N} (x_i - \bar{x})^2}{N-1}} \tag{3.2}$$

  Mean values and standard deviations are calculated at each of the points defined in Step 1, to be used in the remaining steps.

- *Step 3: Determine and report the deviation and figure of merit for each participant's value.* The deviation, *e*, which is merely the difference between the participant's value and the mean as determined in Step 2, is calculated according to:

$$e_i = (x_i - \bar{x}) \tag{3.3}$$

After calculating the deviation, the figure of merit, Φ, can be determined according to the formula:

$$\Phi_i = \frac{e_i}{\sigma} \tag{3.4}$$

This figure of merit provides a means for comparison that is perhaps easier to interpret than the raw deviations, relating the participant's deviation to the overall standard deviation. After calculating the deviations and figures of merit, comparison values are tabulated.

3.1.2 Two-dimensional (2-D) radial distributions

Phase III contains many steady state and transient snapshots of the radial distribution through the core for certain parameters. Due to the two-dimensional nature of such data, it is difficult to plot the results as with time history data and 1-D distributions. However, the same statistical methods can be used to generate mean values, standard deviations and participant deviations, and figures of merit.

- *Step 1: Calculate mean and standard deviation for each 2-D cell.* These reference values are calculated according to Eqs. (3.1) and (3.2). Such an analysis results in a 2-D map for both mean values and standard deviations, rather than a single value for each parameter. Comparisons can thus be made for each cell, rather than only specific cells of interest.

- *Step 2: Tabulate deviations and figures of merit.* For each participant, a map will be generated that shows deviations from the mean at each radial position. A second map will report the figures of merit.

3.1.3 One-dimensional (1-D) axial distributions

Phase III also contains many steady-state and transient snapshots of the axial distribution of certain parameters through the core. These parameters will usually be a function of height, and can thus be displayed as an x-y plot. Similar methods of statistical analysis will be applied as with the previous two data types.

- *Step 1: Calculate mean and standard deviation for each 1-D cell.* This analysis is similar to that for the 2-D distributions, and 1-D maps will be generated for the mean values and standard deviations in each axial layer.

- *Step 2: Determine deviations and figures of merit.* For each participant, a single table will be prepared that shows deviations from the mean and figures of merit at each axial position.

3.1.4 Integral parameters

These parameters include such values as multiplication factor, power peaking factors and axial offset. In this case, there is no need to condition the data by isolating points of interest. Likewise, there are no curves to analyse. Thus, the mean value and standard deviation should be sufficient to facilitate a comparison of the results.

- *Step 1: Calculate mean and standard deviation.* Reference values are calculated according to Eqs. (3.1) and (3.2).

- *Step 2: Determine deviations and figures of merit.* These values are calculated according Eqs. (3.3) and (3.4).

3.2 Statistical analysis of normalised parameters

In Phase III, three parameters are provided as normalised relative distributions: 2-D core-averaged radial power, 1-D core-averaged axial power and 1-D axial power at the position of the stuck rod. These parameters must be given special attention during the statistical analysis because under certain circumstances the normalisation will become skewed. Treating each of these parameters separately, the procedure for generating a comprehensive analysis that preserves the normalisation will be discussed.

3.2.1 Two-dimensional (2-D) core-averaged radial power distribution

This parameter is collected for the steady-state case and transient snapshots. The goal of the statistical analysis is to derive an average normalised power for each assembly:

$$\overline{NP_i} = \frac{\overline{p_i}}{\overline{p_{FA}}} \tag{3.5}$$

where, for N participants, $\overline{p_i}$, the average power density in radial assembly location i, is:

$$\overline{p_i} = \frac{1}{N}\sum_{j=1}^{N} p_{ij} \tag{3.6}$$

and $\overline{p_{FA}}$, the averaged assembly power density, is:

$$\overline{p_{FA}} = \frac{1}{N}\sum_{j=1}^{N} p_{FA,j} \tag{3.7}$$

Thus,

$$\overline{NP_i} = \frac{\sum_{j=1}^{N} p_{ij}}{\sum_{j=1}^{N} p_{FA,j}} \tag{3.8}$$

In the initial steady-state case the total core power is specified as Q = 2 772 MW for the hot-full-power (HFP) conditions, so that the average power per fuel assembly is the same for all participants and:

$$\overline{NP_i} = \frac{1}{N}\frac{\sum_{j=1}^{N} p_{ij}}{p_{FA,c}} = \frac{1}{N}\sum_{j=1}^{N}\frac{p_{ij}}{p_{FA,c}} = \frac{1}{N}\sum_{j=1}^{N} NP_{ij} \tag{3.9}$$

where, given the total number of fuel assemblies, M, is 177:

$$p_{FA,c} = \frac{Q}{M} \tag{3.10}$$

Thus, for the steady-state cases the standard techniques described above can be applied directly to the normalised values provided by each participant. For the transient snapshots, however, where total power level and power per assembly vary among the participants, the following corrected procedure must be applied.

- *Step 1: Convert normalised values into absolute values.* Absolute values are achieved by multiplying the normalised value in each 2-D cell for each participant by the average power per assembly for the same participant, where the latter value is the total core power for that participant divided by 177 fuel assemblies.

- *Step 2: Calculate participant-averaged average power per assembly*. All participant values for total core power are averaged by the standard averaging technique to get the average core power. This value is divided by the number of fuel assemblies, 177, to get the average power per assembly, averaged over all participants. The same result can be obtained by averaging directly, with Eq. (3.1), all participants' values for average power per assembly.

- *Step 3: Generate mean solution using absolute values.* The map of absolute mean values is generated by the standard averaging procedure.

- *Step 4: Re-normalise mean solution.* Normalisation is attained by dividing each cell of the absolute map by the average power per assembly calculated in Step 2.

Unfortunately, the standard deviation and figure of merit can not be included in a normalised form, since the meaning of these statistical functions would be lost. Therefore, three maps must be provided instead of the usual two. Mean values and standard deviations are provided using absolute powers, and are accompanied by maps of the normalised mean values. Participant deviations and figures of merit are calculated relative to the absolute mean solution.

3.2.2 One-dimensional (1-D) core-averaged axial power distribution

This parameter is also collected for every steady-state case and transient snapshot, and the final specifications require that all participants divide the core into 24 equal axial nodes. Where this is the case, the statistical analysis will be similar to that for the radial power distribution. The normalised mean axial power for a given axial node is given by:

$$\overline{NP_{z,i}} = \frac{\overline{p_{z,i}}}{\overline{\overline{p_z}}} \tag{3.11}$$

where $\overline{p_{z,i}}$, the average power density axial layer *i*, is given by:

$$\overline{p_{z,i}} = \frac{1}{N}\sum_{j=1}^{N} p_{z,ij} \tag{3.12}$$

and $\overline{\overline{p_z}}$, the core-averaged axial power density, is:

$$\overline{\overline{p_z}} = \frac{1}{N}\sum_{j=1}^{N} p_{z,j} = \frac{1}{N}\sum_{j=1}^{N} \frac{p_{FA,j}}{24} \tag{3.13}$$

Thus,

$$\overline{NP_{z,i}} = \frac{\sum_{j=1}^{N} p_{z,ij}}{\sum_{j=1}^{N} \frac{p_{FA,j}}{24}} \tag{3.14}$$

For the steady-state cases, where the total power level, *Q*, and the average power per assembly are constant for all participants:

$$\overline{NP_{z,i}} = \frac{1}{N}\frac{1}{24}\sum_{j=1}^{N}\frac{p_{z,ij}}{p_{FA,j}} = \frac{1}{N}\sum_{j=1}^{N} NP_{z,ij} \tag{3.15}$$

As a result, the standard techniques for 1-D distribution can be applied for the steady-state cases; however, for the transient snapshots, where the average power per assembly will vary among the participants, the following procedure must be utilised.

- *Step 1: Convert normalised values into absolute values.* Absolute values are achieved by multiplying the normalised value in each axial node for each participant by the average power per node in the average assembly for the same participant, where the latter value is the total core power for that participant divided by 177 fuel assemblies and 24 axial nodes.

- *Step 2: Calculate participant-averaged average power per axial node.* All participant values for total core power are averaged by the standard averaging technique to get the average core power. This value is divided by the number of fuel assemblies, 177, to get the average power per assembly, which is finally divided by 24 to get the average power per axial node, averaged over all participants. The same result can be obtained by averaging directly all participants' values for average power per axial node, using Eq. (3.1).

- *Step 3: Generate mean solution using absolute values.* The table of absolute mean values is generated by the standard averaging procedure.

- *Step 4: Re-normalise mean solution.* Normalisation is attained by dividing each cell of the absolute map by the average power per node calculated in Step 2.

Once again, the standard deviation and figure of merit can not be included in a normalised form and two axial tables will be provided. Absolute mean values and standard deviations are provided along with re-normalised mean values in one table. Participant deviations and figures of merit, calculated relative to the absolute values, are presented in a second table. It should be noted that this procedure could be applied only where the participants have used 24 equal axial layers. Results from participants who do not adhere to this specification must first have their data converted to 24 equal nodes via a cell-volume weighting procedure.

3.2.3 One-dimensional (1-D) axial power distribution in the stuck rod

This parameter is collected for the HFP steady-state case and all transient snapshots, and is treated in a similar manner as for the core-averaged axial power. Again, the specifications request that the stuck rod assembly be divided into 24 equal nodes. In the case of the steady state at HFP, where the distributions are based on the known whole-core volume normalisation, the standard techniques can be applied. For the transient snapshots, the power in the stuck rod varies among the participants and the average normalised power per node is given by:

$$\overline{NP_{z,i}} = \frac{\sum_{j=1}^{N} p_{z,ij}}{\sum_{j=1}^{N}\frac{p_{N12,j}}{24}} \tag{3.16}$$

where the total power in the stuck rod assembly at position N12 can be extracted from each participant's 2-D core-averaged radial power distribution. The following method must be applied in every transient case:

- *Step 1: Convert normalised values into absolute values.* The absolute values are found by multiplying the normalised value in each axial node for each participant by the average power per 3-D node in the core for the same participant, where the latter value is the total core power divided by 177 assemblies and 24 axial nodes.

- *Step 2: Calculate participant-averaged average power per axial node.* All participant values for total core power are averaged by the standard averaging technique to get the average core power. This value is divided by the number of cells in the core – 177 assemblies times 24 axial layers – to get the average power per 3-D node, averaged over all participants.

- *Step 3: Generate mean solution using absolute values.* The map of absolute mean values is generated by the standard averaging procedure.

- *Step 4: Re-normalise mean solution.* Normalisation is attained by dividing each cell of the absolute map by the average power per node calculated in Step 2.

As with the previous two parameters, the results are reported in the form of mean values and standard deviations of the absolute values along with a re-normalised mean solution. Participant deviations and figures of merit are again calculated relative to the absolute mean solution

3.2.4 Multiple code dependencies

It has been noted that some of the sets of results that have been submitted for this exercise are not fully independent of each other. That is, certain participants have submitted multiple sets from codes that differ from each other to varying degrees. In some cases, the differences are significant, and involve quite different kinetics models. In other cases, the differences are subtler, involving different nodalisation schemes. In the case of codes with only subtle differences, it may not be appropriate to treat the results as fully separate, and therefore subject to independent treatment in the averaging techniques described above.

To account for this circumstance, a two-step averaging process has been developed whereby sets of results that are determined to be "dependent" on each other are first averaged together, and the subsequent mean participant values are then included in the final averaging process. However, after examining the descriptions of each code that has been used in developing the submitted results, it was determined that such a two-step averaging process is not necessary in the present case, and so has not been applied.

3.2.5 Reference results

Analysis is performed for one steady-state case, four transient snapshots and five time histories. The initial steady state (Case 2) is performed at HFP. Transient snapshots are taken at the highest power before scram (State 5), highest power after scram for Scenario 2 (State 6), EOT for Scenario 1 (State 7) and EOT for Scenario 2 (State 8).

The reference solutions for all parameters are provided in Appendix C, with the steady-state values presented first, followed by transient snapshot parameters, and ending with the time history solutions. The parameters that are analysed and which can be found in Appendix C are listed below:

- For the initial HFP steady state the following parameters are analysed: k_{eff}; 2-D normalised power (NP) distribution; core-averaged axial power distribution; the power-peaking factors F_{xy}, F_z , axial offset, 2-D maps for inlet coolant temperature, inlet flow rate and outlet coolant temperature; axial distributions for the stuck rod (position N12) – relative power (normalised to the core power level), coolant density, mass flow rate and Doppler temperature.

- Snapshots at time of maximum power before reactor trip, at time of maximum power after reactor trip, and at 100 seconds of the transient – the same data as for the HFP steady state except the total and fission power levels are analysed instead of $k_{eff.}$

- Time histories in two parts – system thermal-hydraulic parameters: loop steam line and RCS pressures, loop cold and hot leg temperatures, break flow rates, loop steam generator masses and exchange powers and total integrated steam and liquid break flows; and core parameters (volume averaged without the reflector region): total power, fission power, coolant density and Doppler temperature. In addition, the maximum nodal Doppler temperature vs. time is compared.

As can be seen above, the local parameter distributions are monitored at the position of the stuck rod. Since the local parameter predictions are sensitive to the spatial coupling schemes it was decided at the third benchmark workshop [5] that in the final report these results would be compared in two groups: one cluster for very detailed spatial mesh overlays (one neutronics node per thermal-hydraulic cell/channel) – this is called the 177 channel cluster – and one separate cluster for coarse mesh overlays –called the 18 channel cluster. Subsequently, separate mean solutions and standard deviations are produced for these two clusters.

The participant deviations and figures of merit are presented in Appendix D, and are listed in the same order as the reference solutions. In each case, where separate tables are necessary for each participant, these are listed in alphabetical order.

Chapter 4

RESULTS AND DISCUSSION

The tables and the figures in this chapter provide a comparison of the participants' results with the reference solution. The comparison is made for the parameters that have the greatest effect on the initial steady state and the two versions of the transient scenario. In each case, the tables show values of the standard deviation and the figure of merit (as defined in Chapter 3) for each participant's result for a given parameter. Selected figures included in this chapter show the scatter of data about the reference (mean) solution.

The analysis of results is grouped into three sections. Section 4.1 discusses the steady-state results at initial conditions. Section 4.2 presents the analysis of results for the transient snapshots. For these two groups of results the discussion is further subdivided into three subsections: singular (integral) parameter values, 1-D axial distributions and 2-D radial distributions. The transient time-history data is discussed in Section 4.3. The complete detailed comparison of the participants' results is provided in Appendix D (which is divided into four parts: D.1. Integral parameters, D.2. One-dimensional (1-D) axial distributions, D.3. Two-dimensional (2-D) radial distributions and D.4. System and core averaged time evolutions).

4.1 Steady-state results

4.1.1 Integral parameters

The initial steady state is at HFP conditions. Keeping in mind that that the participants are provided with the cross-section libraries and the linear interpolation routine, one can conclude that the discrepancies for this state result from:

- Different methods for solving the steady-state diffusion problem and different neutronics nodalisation schemes in radial plane (1 node per assembly – 1 npa – vs. 4 npa schemes and in the axial direction).

- Differences in core thermal-hydraulic models used by participants, such as 1-D parallel channels vs. 3-D models; coarse mesh (18 channels/cells in radial plane) vs. fine mesh (177 channels/cells); as well as heat-structure nodding and mapping schemes.

The following integral parameters were compared: multiplication factor (k_{eff}), radial and axial power peaking factors (Fxy and Fz), and axial offset (AO). Please note that all of these parameters are unitless. These comparisons are summarised in Tables 4.1-4.4. In each case the participants are in reasonable agreement. The JAERI results show the largest deviations for Fz and AO, though are in reasonable agreement for k_{eff} and in Fxy. One reason for the differences is that JAERI utilised a smaller number of axial layers (i.e. coarser axial nodalisation) for the core thermal-hydraulics model, which affects the accuracy of the results.

4.1.2 One-dimensional (1-D) axial distributions

4.1.2.1 One-dimensional (1-D) core-averaged axial power distributions

The results for 1-D core-averaged axial power distribution are compared and analysed for the above-described initial steady state, which is a HFP state. Figure 4.1 presents a comparison of participants' predictions and mean distribution in the form of graph. The participants are in good agreement and the results form a single cluster around the mean solution. The local deviations increase towards the bottom and the top of the core. Since the spatial distribution of the thermal-hydraulic feedback plays an important role, the observed deviations are probably due to the utilisation of different thermal-hydraulics models, nodding and mapping schemes. Another probable reason for the differences are the core inlet and outlet thermal-hydraulic conditions, which are determined by the system models and their interactions with core models. The participants utilise two different types of core thermal-hydraulics models with different degrees of detailed spatial nodalisation. The majority of submitted results are based on parallel-channel models (which is basically 1-D modelling) ranging between 18 and 177 channels (for example FZR and UPM) in the radial plane. Some of the participants used 3-D core thermal-hydraulics models also with different degrees of spatial detail in the radial plane – from 18 T-H cells (PSU and UPV) to 177 T-H cells (CEA/IPSN). NRC/Purdue used 18 core thermal-hydraulic channels and 177 heat structures, i.e. each neutronic assembly has separate a heat structure. The axial nodalisation used by the participants is also different, ranging from 7 to 28 axial T-H nodes. Interestingly, the different distributions have very similar shapes for the initial steady state for the transient. The trends intersect in the central part of the core and are slightly shifted at the core ends (see Figure 4.1). This indicates that the distribution of the mass flow is very important, coming from the lower plenum in the core.

4.1.2.2 One-dimensional (1-D) axial distributions in the stuck rod

The local parameter distributions are monitored at the position of the stuck rod for the initial steady state. These results are compared in two groups: one cluster for very-detailed spatial-mesh overlays – this is called the 177 channel cluster, and another cluster for coarse-mesh overlays – called the 18 channel cluster (see Figures 4.2 and 4.3). The figures illustrate the effect of the T-H model on the local power distributions, which is a result of the local distributions of the T-H feedback parameters – moderator (coolant density) and Doppler temperature (see Figures 4.4 and 4.5). The deviations in local coolant-density predictions at the core inlet are relatively small and are caused by the differences in the T-H system and vessel models of the participants. The deviations become more pronounced towards the core exit because of the differences (as for example parallel 1-D channel vs. complete 3-D core modelling) in the coupled-core models (although all of them are detailed 177 channel/ cell models). This fact certainly causes larger deviations in the relative power distributions. The axial distributions of the local Doppler temperature have similar shape and display small deviations. Only the UPM results at the core bottom and top regions show larger deviations that are the consequence of differences in the fuel rod/heat structure modelling.

4.1.3 Two-dimensional (2-D) radial distributions

4.1.3.1 Two-dimensional (2-D) core-averaged radial power distributions

For the initial HFP steady state (State 2) the following parameters are analysed: 2-D normalised power (NP) distribution, 2-D maps for inlet coolant temperature, inlet flow rate and outlet coolant temperature. The 2-D mean distributions are provided in Appendix C, while the participants'

deviations are calculated for each radial node and provided in the form of 2-D maps in Appendix D. The discrepancies among participants' results are due to the differences in neutronics models, thermal-hydraulics models and utilised spatial-mesh overlays (coupling schemes). The differences in neutronics models are mostly due to the radial nodalisation scheme (one node per assembly – 1 npa vs. 4 npa schemes) and the spatial discretisation method used. The participants' methods and models are described in Appendices A and B.

For the HFP case (State 2) the thermal-hydraulic feedback is modelled and impacts the 2-D power distributions. The effect is stronger as compared to the results of Phase II [3]. In Phase III every participant predicts the core inlet flow rate and coolant temperature distributions based on its own system, vessel and mixing models and, as a result, the deviations in the 2-D radial power distributions are greater. The majority of the participants utilised parallel 1-D fluid volumes for the vessel T-H modelling and the specified mixing ratio was obtained by implementing junctions with appropriate flow areas in the lower and upper plenums. PSU, KAERI and UPV used 3-D vessel fluid-dynamics capabilities, which explicitly model the radial cross-flow between the thermal-hydraulic cells of the vessel plenums, thus accounting for thermal loop mixing in a best-estimate manner.

4.2 Transient snapshots

Transient snapshots are taken at the highest power before scram (State 5), highest power after scram for Scenario 2 (State 6), EOT for Scenario 1 (State 7), and EOT for Scenario 2 (State 8). As in the case of the steady-state results, the comparison and the analysis also include three types of data: integral parameters, 1-D axial distributions and 2-D radial distributions.

4.2.1 Integral parameters

The following integral parameters are compared and analysed for the transient snapshots: the total and fission power levels (in MW), the time of maximum power before the scram and maximum return to power after scram for the second transient scenario (in seconds), radial and axial power peaking factors (Fxy and Fz), and axial offset (unitless). The mean solutions are provided in Appendix C. The participants' deviations are given in Appendix D and are summarised in Tables 4.5 through 4.16.

For each case the participants are in reasonable agreement. The most interesting snapshot is 6 (return to power for the second transient scenario). BE/Tractebel, JAERI and UP/UZ 1 predict the highest power peaks after the scram, while the GRS result shows the highest power level at the end of the transient for the second scenario. This power over-prediction during the transient can be attributed to several facts – the thermal-hydraulics system modelling during the transient, approximations introduced in the core neutronics model (explained above), the correlations for fuel properties vs. temperature used being different than specified, and different relations for Doppler temperature. There is a good agreement between different codes' predictions of the timing of the return to power, except FZR (predicts later peak) and UP (predict earlier peak) The results of FZR and UP bound the other participants' results. Comparing the two sets of results of CEA/IPSN gives the opportunity to observe and quantify how the modelling of the core/plant interactions influences the transient predictions. In both cases the same system and coupled-core models are used. The difference is in the coupling between the core and system models, as explained above.

4.2.2 One-dimensional (1-D) axial distributions

4.2.2.1 One-dimensional (1-D) core-averaged axial power distribution

During the comparison of the participants' results, more pronounced deviations in the relative core-averaged axial shapes were observed for the transient snapshots after reactor scram where the decay-heat component of total power becomes dominant. While the participants' results for the snapshots at maximum power before scram (State 5 – see Figure 4.6) and after scram (State 6 – see Figure 4.7) form clusters similar to the initial steady-state comparison their results for the EOT snapshots for both transient scenarios (see Figures 4.8 and 4.9) show much larger deviations. Based on the results of a sensitivity study performed by PSU, it was suggested that this anomaly is connected to spatial decay-heat modelling. The time evolution of the core-averaged decay-heat power is provided to the participants for both scenarios (no return to power and return to power). This average value at each time step should be re-distributed spatially according to the fission-power spatial distribution, and the spatial-decay distribution should follow the fission-power distribution at the initial HFP nominal steady-state conditions. Some participants instead distributed the decay heat by following the fission-power distribution at each time step, which introduced the deviations. This can be seen especially for the EOT snapshots – States 7 and 8 (see Figures 4.8 and 4.9). For example, the JAERI results are obtained by redistributing the decay heat following the fission-power distribution at each time step, and these results fall in the cluster, which has higher normalised power at the core bottom and lower normalised power at the core top. On the other hand, the CEA/IPSN results are obtained by distributing the decay heat following the initial steady-state fission-power distribution, and subsequently fall in the other cluster. In addition, some participants like KAERI and FZR used independent decay-heat data and models.

4.2.2.2 One-dimensional (1-D) axial distributions in the stuck rod position

The local parameter distributions are monitored at the position of the stuck rod, and are sensitive to the spatial coupling schemes. It was thus decided at the third benchmark workshop [6] that in the final report these results should be compared in two groups: one cluster for the very-detailed spatial mesh overlays (one neutronics node per thermal-hydraulic cell/channel), designated the 177-channel cluster, and another cluster for the coarse mesh overlays, designated the 18-channel cluster. Subsequently, separate mean solutions and standard deviations are produced for these two clusters.

During Phase II [3] it was noted that the core thermal-hydraulic models used by the participants could be an important source of deviations for local parameters, especially for the relative power at the position of the stuck rod. One node per assembly in radial plane is the standard neutronics model utilised by the participants; however, some core thermal-hydraulics models differ in the degree of spatial detail. Some participants applied the 18-channel/cell models, while others used a more refined model with one channel/cell per fuel assembly, or 177 thermal-hydraulic channels/cells. Accordingly, for the comparisons, the results for all local parameters have been divided into two clusters, one for those codes using 18 channels and the other for those with the more refined model (177 channels).

During the course of the MSLB transient, a power spike is seen at the position of the stuck rod. However, in the 18-channel model this assembly is averaged with several of the surrounding assemblies while mapping the neutronics model to the thermal-hydraulics model. This has a significant effect on underestimating the feedback in this part of the core. Conversely, the 177-channel model is expected to more accurately predict the feedback (as a result of a better spatial feedback resolution), and therefore the relative power shape near the stuck rod. Figures 4.10 through 4.13 and 4.18 through 4.21 show the axial normalised-power shapes averaged over all participants in each of the two clusters and

confirm this expectation. The mean curves in these figures show that the averaged 18-channel results differ in the upper half of the core at the position of the stuck rod when compared to similar results from a 177-channel model. The standard deviations for the 18-channel model are also much larger as compared to those of the 177-channel model. For the representative of the snapshot of highest power after scram for the second transient scenario [RP (State 6)] the axial distributions of the feedback parameters in the stuck rod position are also shown for both clusters to illustrate the effect of the spatial feedback distributions (see Figures 4.14 through 4.17). Some of these results (for example PSU) have a stepwise shape because a coarse mesh (six axial nodes) was used in the thermal-hydraulic core nodalisation, i.e. the values of the feedback parameters are the same for several neutronics nodes mapped to one thermal-hydraulics node in axial direction.

4.2.3 Two-dimensional (2-D) radial distributions

4.2.3.1 Two-dimensional (2-D) core-averaged radial power distributions

For the transient snapshots (States 5, 6, 7 and 8), the following 2-D nodal radial distributions are compared: normalised power (NP), inlet coolant temperature, inlet flow rate and outlet coolant temperature. The mean distributions are provided in Appendix C, while the participants' deviations are calculated for each radial node and provided in a form of 2-D maps in Appendix D.

The discrepancies observed in the core-averaged radial distributions (especially for the return-to-power scenario) are mostly due to the spatial coupling schemes: from very detailed spatial mesh overlays (one neutronics node per thermal-hydraulic cell/channel) to coarser mesh overlays. During the course of the MSLB transient, a power spike is seen at the position of the stuck rod. However, in the 18-channel model this assembly is averaged with several of the surrounding assemblies when mapping the neutronics model to the thermal-hydraulics model. This mapping leads to underestimating the feedback in this part of the core. On the other hand, the 177-channel model is expected to more accurately predict the feedback (as a result of a better spatial feedback resolution), and therefore the relative power shape near the stuck rod. This can be seen very clearly from the comparisons of participants' results for the snapshot (State 6) taken at the time of highest return to power for Transient Scenario 2. In summary, the maximum observed deviations in radial power distributions between the coarse-mesh 18-channel models and the fine-mesh 177-channel models are about 15% (for Snapshot 6), where up to 5% are due to the different thermal-hydraulic nodalisation and mapping schemes and up to 10% are due to different heat structure nodalisation and mapping schemes. The coupled-core model of NRC/Purdue, which uses 18 thermal-hydraulic channels and 177 heat structures, is an example of a successful compromise in terms of computational efficiency and accuracy.

4.3 Time histories

The plots in this section provide a comparison of the participants' results for the parameters that have the greatest effect on the MSLB transient for each transient scenario. These parameters include system parameters such as temperatures, pressures, break flow rates and steam generator masses. In addition, core time histories (core volume averaged without the reflector region) are analysed and compared in the following order: total power, fission power, coolant density and Doppler temperature. Total reactivity and the maximum nodal Doppler temperature vs. time are also compared.

The mean curves for the time histories are provided in Appendix C (supplied on the CD-ROM). The standard deviations are represented as error bars at each time step. The participant deviations and

figures of merit are presented in Appendix D (also supplied on the CD-ROM), and are listed in the same order as the reference solutions. In this section, selected comparisons of the time histories for each of the two transient scenarios are presented and analysed.

In each case, the figures (Figures 4.22 through 4.71) graphically illustrate the agreement or disagreement of participants' predictions. Statistical evaluation is employed to generate a mean solution, which is also shown in the plots. The table of sequence of events and figures for each parameter are discussed in more detail below. Note that the two sets of CEA/IPSN results are produced with CATHARE/CRONOS2/FLICA-4 using different coupling schemes between core and plant system models. The two sets of UP/UZ results are produced with two coupled code systems – RELAP5/PARCS and RELAP5/QUBBOX, which utilise two different core neutronics solvers. CEA/IPSN 1 results are calculated with CATHARE using a 1-D system and core models and the 3-D FLICA-4 model is used only to provide feedback to CRONOS2. CEA/IPSN 2 results are calculated with the 3-D CRONOS2/ FLICA-4 model with 177 T-H cells coupled with the CATHARE system model via exchange of boundary conditions.

Sequence of events

Table 4.17 summarises the timing of events during the transient for each participant. The modelling sequence of events for the MSLB transient is outlined in the *Final Specifications* [1]and has been discussed at the benchmark workshops and meetings. The two analysed transient scenarios (Scenario 1: NoRP and Scenario 2: RP) differ only in the worth of negative tripped rod reactivity inserted during the scram. The double-ended break occurs at 0.001 seconds. The break is followed by an immediate closure of the turbine isolation valve of the broken SG and all flow from the broken SG goes out to break. The reactor trip is modelled to occur at the high neutron flux trip set point (with a delay of 0.4 seconds) or at the low RCS pressure set point (with a delay of 0.5 seconds). The turbine trip begins at the reactor trip. At the turbine trip, the turbine isolation valve for the intact SG closes with a closure time of 0.5 seconds. As pressure increases in the intact steam line some of the safety relief valves (MSSVs) will open and subsequently close at the set points, defined in the final specification. High-pressure injection (HPI) occurs when the primary-system pressure drops to the defined set point with a 25-second delay.

Table 4.17 shows the variations among the participants in interpreting and modelling the sequence of events. Some participants initiate the break at 0.01 seconds. Further, there are different interpretations of the time of the turbine trip and the closure of the turbine isolation valve for the intact SG. Some participants interpret the time of reactor trip as the time when the trip condition is reached, while others consider the time when the reactor scram begins, i.e. taking into account the delay. While these differing interpretations may not be significant, they contribute to the differences in the participants' predictions at the beginning of the transient. Later into the transient all the participants do not see return to criticality, which is a different result than that obtained during Phase I using point kinetics models [2]. Depending on the scenario, the number of participants seeing return to power varies. BE/Tractebel, FRAMATOME ANP, JAERI and Purdue/NRC see return to power in both scenarios. Their results demonstrate that the return to power in the first scenario is smaller in magnitude and later in time as compared to the second scenario. CEA/IPSN, CSA/GPUN and FZK do not predict return to power for both scenarios. Finally, some participants (KAERI, PSU) do not see return to power in the first scenario and do see a return to power in the second scenario.

Break flow rate

Figures 4.22 through 4.24 (for the first scenario) and Figures 4.47 through 4.49 (for the second scenario) provide a comparison for the behaviour of the total, 24-inch and 8-inch break flow rates, respectively. The MSLB transient is initiated at 0.001 seconds by a double-ended break of the Loop A steam line upstream of the MSIVs. As expected, there is an initial peak in the flow out of the breaks when the transient is initiated. The second peak occurs after 30 seconds into the transients and coincides with the feedwater in the broken SG being ramped to zero. After this second peak, the flow rate of the breaks does go to zero as the SG blows dry. In each case, the participants' results are in reasonable agreement about the behaviour of this parameter, but there are a number of local deviations throughout the transient. These local deviations are caused by modelling differences in the steam line, the break, the break flow rate and the various other modelling assumptions and code correlations. For example, the differences in the steam-liquid interface friction in the SG influence the liquid entrainment into the steam line and into the break during the blow-down.

Pressures

Figures 4.25 through 4.29 (for the first scenario) and Figures 4.50 through 4.54 (for the second scenario) show comparisons for the pressures (core-average, broken and intact loop, broken and intact steam line, and pressuriser) throughout the transient. In each case, the participants are in reasonable agreement about the behaviour of the parameter and the results form a single cluster. Any local deviations in the pressure behaviour throughout the transient are caused by modelling differences in the reactor coolant system and stream lines, the modelling assumptions and the code correlations.

The depressurisation of the broken SG results in overcooling of the reactor coolant fluid (RCF), which results in a lower average temperature in the core region. As the RCS fluid cools down, it contracts, which results in a rapid decrease in the RCS pressure. The HPI low-pressure signal is received and HPI is activated with a 25-second delay. As a result of injecting cold water into the core region, the power begins to increase and the RCS pressure begins to even out. Comparing the mean solutions for the core-average and the broken and intact loop pressures during the transient for both scenarios, one can observe that they follow the same tendencies. However, the primary pressure decreases more during the first scenario and subsequently the values of the pressure at the end of transient are lower compared to those of the second scenario.

As expected, the broken steam line pressure decreases rapidly following the break as a result of the depressurisation in the broken SG. This large drop in steam-line pressure is followed by a slow depressurisation throughout the remainder of the transient, as the broken SG blows dry. The intact steam line sees a constant pressure until the turbine stop valve to the intact SG is closed, following the reactor trip signal, thus effectively isolating the intact SG. The pressure in the intact steam line increases slightly after the turbine stop valve closes because the reactor is trying to make up for the loss in the broken loop. As a result of this increase, the safety relief valves on the intact steam line start opening. Later into the transient, these valves are closing. Following the closure of the safety relief valves, the intact steam line sees a slight depressurisation throughout the remainder of the transient. The observed deviations in the participants' results are a consequence of modelling assumptions applied by the code user. For example, if a participant uses full mixing in the reactor pressure vessel, this would result in a higher energy transfer from the intact half to the broken half. While some local deviations exist, overall, these parameters show good agreement with the reference data.

Temperatures

Comparisons of the coolant core averaged, hot leg (broken and intact loop), cold leg (broken and intact loop), fuel (Doppler) temperature (core volume averaged without the reflector region) and maximum nodal Doppler temperature calculated by each code throughout the transient for both scenarios are shown in Figures 4.30 through 4.36 (first scenario) and in Figures 4.55 through 4.61 (second scenario). In each case, the behaviour of the parameter during the transient forms a single cluster. Any local deviations in the temperature behaviour throughout the transient are caused by modelling differences in the reactor coolant system, the modelling assumptions and the code correlations.

When the steam line break occurs, the pressure in the broken SG decreases rapidly and causes an increase of the flow rate within the SG. The increased flow rate results in an increase in the heat transfer and overcooling of the RCS fluid. The cold leg temperature plots show an immediate temperature decrease as a result of the broken SG depressurisation; however, the hot leg temperature plots show a more gradual decline. The reason is that the decreasing RCS temperature results in an increase in the core power, which initially offsets the broken SG's cooling effect. Following the initial decrease, the intact cold leg temperatures see a slight increase in temperature as a result of the closure of the turbine stop valve that isolates the intact SG. In the second half of the transient, there is an increase in the core power, and the overcooling effect from the broken SG becomes secondary. In addition to the increase in power, the broken SG loses its cooling capacity throughout the transient as it blows dry. The broken loop sees an increase in RCS temperature as a result of this power increase, while the intact loop see the temperature approaching a constant value in the later half of the transient. The deviations for the broken loop are fairly low for both the hot and cold legs.

This difference is caused by under-cooling in the broken SG and may be the result of different code correlations. As with the broken-loop temperatures, there are small deviations in the intact hot- and cold leg temperatures. This difference is explained by over-cooling of the intact cold leg, which is a result of mixing assumptions.

Overall, the deviations for the average moderator are relatively small. As expected, the fuel temperature time evolution follows the behaviour of the power plot throughout the transient. In summary, the fuel temperature deviations reflect the power deviations. Those reflect more or less the deviations in the break flow rates and inserted dynamic scram reactivity. In addition, the differences in fuel temperature predictions at the same power predictions and same coolant temperature predictions can be attributed to the heat structure modelling assumptions as the number of radial zones for the fuel rod.

Steam generator mass

Figures 4.41 and 4.42 (Scenario 1) and Figures 4.66 and 4.67 (Scenario 2) provide a comparison for the behaviour of the intact and broken steam generator masses throughout the transient. As expected, the mass in the broken SG decreases throughout the transient until it eventually blows dry. The intact SG mass increases initially as a result of the closure of the turbine isolation valve for the intact SG at the turbine trip. This mass eventually decreases because of the MSIV's action and further events and remains constant until the end of the transient. While there is general agreement about the behaviour of the masses in each SG, the analysis shows a great deal of disagreement about the values of the masses throughout the transient. This parameter shows the largest deviation out of all those presented in this report; however, this is not surprising when one considers the complexity involved in modelling the OTSG. Originally, it was thought that the SG mass discrepancy was the result of the differences in modelling of both the SG and the steam line. Since that time, the break nodalisation has been made

uniform and the participants have been provided with a great deal of additional information about the OTSG, both on the way it works and on the geometry. The initial mass of the SG has been modified to remove the artificial increase of 3 000 kg that a number of the participants were having trouble reproducing. Putting the SG masses back to 26 000 kg has helped to make the results more uniform; however, discrepancies still exist [2].

Overall, the masses for both SGs are fairly consistent amongst all participants. All the participants were provided with the same base deck from which to take SG information, as well as the same subsequent information. As a result, any differences in the value or behaviour of this parameter throughout the transient can be attributed to three major factors:

- Differences in the code models, which significantly influence the transient behaviour, like models for break flow rate, and steam-liquid interface friction or liquid entrainment during blow-down.

- Differences in the heat transfer correlations used within each participant's code. This is especially true for the participants who use proprietary correlations that are specific to U-tube SGs in their codes, as a behaviour of an OTSG is much different than a U-tube SG, and also involves superheat, something U-tube SG users do not have to worry about modelling.

- Differences in the noding of the SG, which can produce significant differences in the SG behaviour.

Since a lot of time was spent making sure that the participants' models for the SG are the same, additional information for the transient SG behaviour was requested and compared in Figures 4.43 through 4.46 (Scenario 1) and in Figures 4.68 through 4.71 (Scenario 2). This approach certainly helped to explain the observed differences in the participants' predictions.

Reactor power

A comparison of the fission power and the total power calculated by each code throughout the transient is shown in Figures 4.37 and 4.38 (Scenario 1) and in Figures 4.62 and 4.63 (Scenario 2). The power response and the magnitude of the return to power during the transient as predicted by different codes are functions of the total reactivity time evolution. When the break is initiated, the core sees a gradual rise in power in response to the temperature changes within the core region. A rapid power rise occurs when the over-cooled liquid from the broken SG reaches the core. The power rise continues until the reactor trips. After the trip, a sharp decrease in power results from the negative reactivity inserted into the core when the reactor scrams. The broken SG continues to over-cool the RCS fluid together with the cold water injected from the HPI system, and the reactor sees an increase in power later into the transient. This rise in power quickly decreases because the broken SG loses its cooling capability as its mass and pressure go to zero. As was the case during Phase I, although there is a general agreement about the behaviour of the power throughout the transient, there is a great deal of disagreement about the magnitude (if any) of the return to power. This disagreement is explained below, while discussing the differences in the predictions of the total-reactivity time evolution.

Scenario 1 is the best estimate, in which no return to power and criticality should be observed with coupled 3-D core/plant models in the second half of the transient. For this scenario the participants are in a good agreement and form a single cluster. As Figures 4.37 and 4.38 show, some small deviations in total and fission power as function of time can be seen before the scram and some participants do predict a small return to power after the scram. Looking at the time histories of the core averaged

coolant density and Doppler temperature (which are the instantaneous feedback parameters for the benchmark calculations, see Figures 4.35 and 4.40) one can attribute the small deviations at the beginning of transient to some differences in the feedback parameters. These differences are more pronounced in the Doppler feedback temperature values, and they are a result of the fact that not all of the participants are using the defined relation [1] for the Doppler feedback temperature. In case of the maximum nodal Doppler temperature, this fact affects not only the values at the beginning of the transient but also during the transient. After the scram, one observes also deviations in the core averaged coolant density. Some participants (UP/UZ2, UPV, VTT and FZR) predict core averaged coolant density around or greater than 810.10 kg/m^3 – the highest density reference point in the cross-section tables. This means that for some nodes these participants do utilise the added extrapolation capability to the modified cross-section interpolation routine, provided by the benchmark team to the participants. The deviations in the coolant density predictions have an effect on the power histories that is enforced by the deviations in the inserted negative dynamic scram reactivity (see Figure 4.39).

Scenario 2 is of special interest because the return-to-power phenomenon is enforced by decreasing the amount of negative tripped rod reactivity during the scram, which represents a very good test case for coupled codes. The participants' results for the total and the fission power (see Figures 4.62 and 4.63) form a cluster with larger local deviations observed after the scram and especially at the time of return to power (second peak) into the transient. These deviations can be explained by the differences in the participants' predictions of the total reactivity time behaviour and the core averaged coolant density and Doppler temperature (see Figures 4.60, 4.64 and 4.65). The power response and the magnitude of the return to power during the transient as predicted by different codes are functions of the total reactivity time evolution, which is discussed below.

The deviations at the first power peak for both scenarios are relatively small. The reasons for these deviations are differences in the high-flux trip delay time and the fact that all participants start at approximately the same initial total power level, although the initial fission power level varies, depending on the decay-heat model. The effective decay-heat energy fraction of the total thermal power (the relative contribution in the steady state) is specified to be equal to 0.07143, which assumes approximately 2 574 MW as the initial fission power level. The deviations for the total and fission power at the second peak are quite large, especially for the second scenario, with UP/UZ1 (total power) and UPM (fission power) having the greatest value in this case.

Reactivity

Figures 4.39 and 4.64 show comparisons for the behaviour of the total reactivity throughout the transient for both scenarios. The total reactivity has three components – negative tripped rod reactivity, positive moderator (coolant) density reactivity and Doppler feedback reactivity. Unlike the point kinetics simulations [2], where the inserted negative tripped-rod reactivity is specified (i.e. it is the same for all the codes), in coupled calculations the actual inserted negative reactivity during the scram (with assumption for the maximum worth control rod stuck out) can be different. There are two reasons for this difference; first, there are differences in the calculated static tripped rod worth with different coupled codes [3]; second, in the coupled calculations there is a dynamic simulation of the scram, which accounts for real changes in the reactor core, connected with flux re-distribution and local feedback conditions change at each time step. As a result the actual value of inserted tripped-rod (TR) reactivity is larger than the statically evaluated TR, and this effect of the 3-D dynamic scram simulation is predicted differently by different coupled codes (as shown in Figures 4.39 and 4.64 at the time of scram).

The moderator (coolant) reactivity component follows the moderator (coolant) density (see Figures 4.40 and 4.65). As the third exercise is a coupled 3-D core/system calculation the discrepancies in coolant density predictions are mostly due to both:

- Different density correlations and standards for water/steam property tables, incorporated into the codes.

- Discrepancies in the cold leg temperature predictions that mostly are due to differences in modelling the secondary side. It was observed that the major factors affecting the dynamics of the transient are break flow modelling (critical flow model), liquid entrainment, modelling of the aspirator flow and nodalisation of the SG downcomer. In addition, the disagreement can be attributed to differences in the SG heat-transfer correlations used within each participant's code.

The Doppler reactivity component follows the Doppler fuel temperature. The discrepancies in the core averaged Doppler temperature time evolutions (see Figures 4.35 and 4.60) are due to the relation used for calculating the Doppler fuel temperature, and the correlations for fuel properties vs. temperature, as well as to the radial and axial nodalisation of the heat structure used (fuel rod). Some participants submitted core averaged fuel temperature (based on pellet average temperature) instead of the Doppler temperature, which is defined as the weighted relation of pellet surface and centreline temperatures. Pellet average temperature is higher than the Doppler temperature since in the defined relation for the Doppler temperature in the *Final Specifications* [1] the higher weight is given to the surface temperature. For the maximum nodal Doppler temperature time evolution comparisons the deviations become more pronounced. This is because, in addition to the above-described sources of discrepancies, the detail of thermal-hydraulic modelling (including the heat structure model) and coupling with the core neutronics model contributes to increasing the deviations among the participants' results around the time of return to power. The maximum values of about 1 130 K are predicted by UPM and BE/Tractebel for the second transient scenario.

Table 4.1. Participant deviations and figures of merit for steady-state k_{eff}

Participants	Deviation	FOM
Mean = 1.0039	**Standard deviation = 0.0019**	
BE/Tractebel	-0.0004	-0.1957
CEA/IPSN 1	-0.0002	-0.0819
CEA/IPSN 2	0.0014	0.7349
CSA/GPUN	0.0009	0.4811
FRAMATOME ANP/FZK	-0.0012	-0.6098
FZR	-0.0010	-0.5007
GRS	-0.0039	-2.0051
JAERI	0.0019	0.9954
KAERI	0.0030	1.5620
PSU	0.0014	0.7251
Purdue/NRC	0.0012	0.6232
UP/UZ 1	-0.0005	-0.2732
UP/UZ 2	–	–
UPC	0.0009	0.4712
UPM	-0.0038	-1.9740
UPV	0.0001	0.0473
VTT	-0.0004	-0.1957

Table 4.2. Participant deviations and figures of merit for steady-state Fxy

Participants	Deviation	FOM
Mean = 1.3338	**Standard deviation = 0.0504**	
BE/Tractebel	–	–
CEA/IPSN 1	-0.0108	-0.2143
CEA/IPSN 2	-0.0098	-0.1944
CSA/GPUN	0.0036	0.0714
FRAMATOME ANP/FZK	0.0047	0.0933
FZR	-0.0093	-0.1845
GRS	-0.0077	-0.1528
JAERI	0.0258	0.5119
KAERI	0.0063	0.1250
PSU	0.0817	1.6210
Purdue/NRC	-0.0020	-0.0397
UP/UZ 1	-0.1496	-2.9683
UP/UZ 2	-0.0097	-0.1925
UPC	–	–
UPM	-0.0078	-0.1548
UPV	0.0712	1.4127
VTT	0.0134	0.2659

Table 4.3. Participant deviations and figures of merit for steady-state Fz

Participants	Deviation	FOM
Mean = 1.0989	**Standard deviation = 0.0745**	
BE/Tractebel	–	–
CEA/IPSN 1	-0.0237	-0.3178
CEA/IPSN 2	-0.0270	-0.3623
CSA/GPUN	-0.0063	-0.0851
FRAMATOME ANP/FZK	-0.0370	-0.4973
FZR	0.0028	0.0370
GRS	-0.0351	-0.4717
JAERI	0.2621	3.5180
KAERI	-0.0174	-0.2341
PSU	0.0081	0.1082
Purdue/NRC	-0.0289	-0.3885
UP/UZ 1	-0.0384	-0.5161
UP/UZ 2	-0.0279	-0.3751
UPC	–	–
UPM	-0.0359	-0.4825
UPV	0.0146	0.1967
VTT	-0.0096	-0.1294

Table 4.4. Participant deviations and figures of merit for steady-state axial offset

Participants	Deviation	FOM
Mean = -0.0233	**Standard deviation = 0.0527**	
BE/Tractebel	–	–
CEA/IPSN 1	-0.0022	-0.0415
CEA/IPSN 2	0.0001	0.0010
CSA/GPUN	-0.0098	-0.1863
FRAMATOME ANP/FZK	0.0248	0.4705
FZR	-0.0180	-0.3413
GRS	0.0114	0.2155
JAERI	-0.1759	-3.3387
KAERI	0.0420	0.7962
PSU	0.0500	0.9494
Purdue/NRC	0.0279	0.5302
UP/UZ 1	0.0077	0.1465
UP/UZ 2	0.0347	0.6586
UPC	–	–
UPM	0.0194	0.3673
UPV	-0.0063	-0.1195
VTT	-0.0057	-0.1080

Table 4.5. Participant deviations for transient total core power

Participant	5	6	7	8
Mean	**3 273.37**	**961.81**	**130.71**	**322.35**
BE/Tractebel	-41.57	174.09	-2.23	-69.96
CEA/IPSN 1	34.70	-150.32	-2.72	173.37
CEA/IPSN 2	52.28	-114.64	–	165.15
CSA/GPUN	20.93	39.79	-22.46	-165.70
FRAMATOME ANP/FZK	-37.93	12.49	-8.59	-47.58
FZR	43.03	-61.81	8.25	-27.85
GRS	-91.37	-309.01	-24.41	330.45
JAERI	–	110.89	19.03	4.93
KAERI	-6.57	26.54	-5.67	-81.47
PSU	51.63	-58.61	-12.21	-25.85
Purdue/NRC	1.03	54.09	0.37	-82.79
UP/UZ 1	-17.87	251.71	67.42	-6.67
UP/UZ 2	-27.40	16.46	-7.74	-5.99
UPC	–	–	–	–
UPM	14.42	66.37	0.76	-74.14
UPV	–	–	–	–
VTT	4.63	-58.01	-9.81	-85.95

Table 4.6. Participant figures of merit for transient total core power

Participant	5	6	7	8
Standard deviation	**40.90**	**135.71**	**22.36**	**127.91**
BE/Tractebel	-1.02	1.28	-0.10	-0.55
CEA/IPSN 1	0.85	-1.11	-0.12	1.36
CEA/IPSN 2	1.28	-0.84	–	1.29
CSA/GPUN	0.51	0.29	-1.00	-1.30
FRAMATOME ANP/FZK	-0.93	0.09	-0.38	-0.37
FZR	1.05	-0.46	0.37	-0.22
GRS	-2.23	-2.28	-1.09	2.58
JAERI	–	0.82	0.85	0.04
KAERI	-0.16	0.20	-0.25	-0.64
PSU	1.26	-0.43	-0.55	-0.20
Purdue/NRC	0.03	0.40	0.02	-0.65
UP/UZ 1	-0.44	1.85	3.02	-0.05
UP/UZ 2	-0.67	0.12	-0.35	-0.05
UPC	–	–	–	–
UPM	0.35	0.49	0.03	-0.58
UPV	–	–	–	–
VTT	0.11	-0.43	-0.44	-0.67

Table 4.7. Participant deviations for transient total fission power

Participant	5	6	7	8
Mean	**3 080.59**	**806.54**	**25.94**	**214.21**
BE/Tractebel	-49.09	196.36	3.93	-70.82
CEA/IPSN 1	37.73	-126.57	2.90	168.01
CEA/IPSN 2	51.33	-90.46	–	159.79
CSA/GPUN	17.11	64.37	-11.03	-158.30
FRAMATOME ANP/FZK	-43.77	35.26	-3.04	-54.17
FZR	39.61	-33.89	12.12	-31.41
GRS	-72.59	-277.14	-11.24	315.19
JAERI	–	–	–	–
KAERI	-7.39	75.68	0.80	-71.62
PSU	46.41	-31.55	-5.80	-3.81
Purdue/NRC	-0.99	79.53	3.85	-84.59
UP/UZ 1	–	–	–	–
UP/UZ 2	-33.22	45.59	0.87	-6.63
UPC	–	–	–	–
UPM	8.50	89.14	6.28	-81.01
UPV	–	–	–	–
VTT	6.41	-26.34	0.37	-80.61

Table 4.8. Participant figures of merit for transient total fission power

Participant	5	6	7	8
Standard deviation	**39.73**	**118.98**	**6.86**	**133.07**
BE/Tractebel	-1.24	1.65	0.57	-0.53
CEA/IPSN 1	0.95	-1.06	0.42	1.26
CEA/IPSN 2	1.29	-0.76	–	1.20
CSA/GPUN	0.43	0.54	-1.61	-1.19
FRAMATOME ANP/FZK	-1.10	0.30	-0.44	-0.41
FZR	1.00	-0.28	1.77	-0.24
GRS	-1.83	-2.33	-1.64	2.37
JAERI	–	–	–	–
KAERI	-0.19	0.64	0.12	-0.54
PSU	1.17	-0.27	-0.85	-0.03
Purdue/NRC	-0.03	0.67	0.56	-0.64
UP/UZ 1	–	–	–	–
UP/UZ 2	-0.84	0.38	0.13	-0.05
UPC	–	–	–	–
UPM	0.21	0.75	0.92	-0.61
UPV	–	–	–	–
VTT	0.16	-0.22	0.05	-0.61

Table 4.9. Participant deviations for transient time sequence

Participant	5	6
Mean	**6.50**	**65.51**
BE/Tractebel	-0.60	-1.01
CEA/IPSN 1	0.90	4.49
CEA/IPSN 2	0.48	5.02
CSA/GPUN	-0.50	-3.51
FRAMATOME ANP/FZK	-0.40	0.49
FZR	-1.15	12.34
GRS	0.92	1.73
JAERI	–	-3.21
KAERI	-0.20	1.49
PSU	0.49	0.04
Purdue/NRC	-0.33	0.31
UP/UZ 1	–	-8.01
UP/UZ 2	1.10	-0.51
UPC	-1.04	-0.65
UPM	-0.31	0.32
UPV	0.51	-9.28
VTT	0.10	-0.01

Table 4.10. Participant figures of merit for transient time sequence

Participant	5	6
Standard deviation	**0.71**	**4.86**
BE/Tractebel	-0.84	-0.21
CEA/IPSN 1	1.27	0.92
CEA/IPSN 2	0.68	1.03
CSA/GPUN	-0.70	-0.72
FRAMATOME ANP/FZK	-0.56	0.10
FZR	-1.62	2.54
GRS	1.30	0.36
JAERI	–	-0.66
KAERI	-0.28	0.31
PSU	0.69	0.01
Purdue/NRC	-0.46	0.06
UP/UZ 1	–	-1.65
UP/UZ 2	1.56	-0.11
UPC	-1.46	-0.13
UPM	-0.44	0.07
UPV	0.72	-1.91
VTT	0.14	0.00

Table 4.11. Participant deviations for transient Fxy

Participant	5	6	7	8
Mean	**1.4623**	**3.3078**	**2.4879**	**2.7305**
BE/Tractebel	-0.01	0.00	-0.48	-0.15
CEA/IPSN 1	0.03	0.18	1.29	0.55
CEA/IPSN 2	0.04	0.22	–	0.57
CSA/GPUN	0.08	–	–	–
FRAMATOME ANP/FZK	-0.06	0.09	-0.76	-0.25
FZR	-0.02	-0.07	-0.32	0.00
GRS	-0.03	0.53	-0.86	-0.27
JAERI	–	–	–	–
KAERI	–	–	–	–
PSU	-0.01	-0.16	1.37	0.13
Purdue/NRC	–	–	–	–
UP/UZ 1	–	–	–	–
UP/UZ 2	0.07	0.19	0.07	0.31
UPC	–	–	–	–
UPM	0.00	0.39	-0.33	-0.08
UPV	-0.08	-1.21	0.63	-0.56
VTT	0.00	-0.14	-0.61	-0.26

Table 4.12. Participant figures of merit for transient Fxy

Participant	5	6	7	8
Standard deviation	**0.0478**	**0.4539**	**0.8223**	**0.3577**
BE/Tractebel	-0.26	0.00	-0.59	-0.42
CEA/IPSN 1	0.58	0.39	1.57	1.53
CEA/IPSN 2	0.77	0.47	–	1.60
CSA/GPUN	1.69	–	–	–
FRAMATOME ANP/FZK	-1.27	0.19	-0.93	-0.69
FZR	-0.39	-0.15	-0.39	-0.01
GRS	-0.67	1.16	-1.04	-0.76
JAERI	–	–	–	–
KAERI	–	–	–	–
PSU	-0.29	-0.36	1.67	0.37
Purdue/NRC	–	–	–	–
UP/UZ 1	–	–	–	–
UP/UZ 2	1.46	0.43	0.09	0.88
UPC	–	–	–	–
UPM	-0.05	0.85	-0.40	-0.22
UPV	-1.65	-2.66	0.77	-1.55
VTT	0.07	-0.30	-0.74	-0.72

Table 4.13. Participant deviations for transient Fz

Participant	5	6	7	8
Mean	**1.1232**	**1.8603**	**1.4675**	**1.8937**
BE/Tractebel	-0.02	-0.07	-0.20	-0.11
CEA/IPSN 1	0.37	1.62	2.31	1.38
CEA/IPSN 2	0.38	1.66	–	1.41
CSA/GPUN	0.42	–	–	–
FRAMATOME ANP/FZK	0.28	1.53	0.26	0.59
FZR	0.32	1.38	0.70	0.83
GRS	0.31	1.97	0.16	0.57
JAERI	–	–	–	–
KAERI	–	–	–	–
PSU	0.33	1.28	2.39	0.97
Purdue/NRC	–	–	–	–
UP/UZ 1	–	–	–	–
UP/UZ 2	0.41	1.64	1.09	1.15
UPC	–	–	–	–
UPM	0.34	1.83	0.69	0.76
UPV	0.26	0.24	1.66	0.28
VTT	0.34	1.31	0.41	0.58

Table 4.14. Participant figures of merit for transient Fz

Participant	5	6	7	8
Standard deviation	**0.0373**	**0.2530**	**0.3783**	**0.2300**
BE/Tractebel	-0.43	-0.29	-0.53	-0.48
CEA/IPSN 1	9.82	6.42	6.10	6.02
CEA/IPSN 2	10.06	6.57	–	6.12
CSA/GPUN	11.24	–	–	–
FRAMATOME ANP/FZK	7.46	6.06	0.68	2.56
FZR	8.58	5.45	1.84	3.62
GRS	8.23	7.81	0.43	2.46
JAERI	–	–	–	–
KAERI	–	–	–	–
PSU	8.72	5.07	6.32	4.21
Purdue/NRC	–	–	–	–
UP/UZ 1	–	–	–	–
UP/UZ 2	10.96	6.48	2.89	5.00
UPC	–	–	–	–
UPM	9.02	7.24	1.83	3.29
UPV	6.97	0.94	4.38	1.22
VTT	9.17	5.18	1.09	2.52

Table 4.15. Participant deviations for transient axial offset

Participant	5	6	7	8
Mean	**0.0234**	**0.4679**	**0.2501**	**0.4589**
BE/Tractebel	-0.07	-0.12	-0.16	-0.12
CEA/IPSN 1	-0.11	0.04	0.08	0.09
CEA/IPSN 2	-0.09	0.05	–	0.09
CSA/GPUN	-0.08	–	–	–
FRAMATOME ANP/FZK	-0.06	-0.05	-0.18	-0.10
FZR	-0.10	-0.10	-0.12	-0.08
GRS	0.02	0.08	-0.15	-0.04
JAERI	–	–	–	–
KAERI	–	–	–	–
PSU	-0.02	0.00	0.28	0.12
Purdue/NRC	–	–	–	–
UP/UZ 1	–	–	–	–
UP/UZ 2	-0.02	-0.01	-0.15	-0.04
UPC	–	–	–	–
UPM	-0.05	-0.10	-0.13	-0.14
UPV	0.67	0.34	0.72	0.37
VTT	-0.09	-0.12	-0.19	-0.14

Table 4.16. Participant figures of merit for transient axial offset

Participant	5	6	7	8
Standard deviation	**0.2132**	**0.1325**	**0.2932**	**0.1573**
BE/Tractebel	-0.31	-0.87	-0.53	-0.73
CEA/IPSN 1	-0.51	0.30	0.26	0.56
CEA/IPSN 2	-0.40	0.36	–	0.58
CSA/GPUN	-0.38	–	–	–
FRAMATOME ANP/FZK	-0.30	-0.38	-0.61	-0.65
FZR	-0.45	-0.76	-0.42	-0.54
GRS	0.10	0.60	-0.49	-0.28
JAERI	–	–	–	–
KAERI	–	–	–	–
PSU	-0.08	0.03	0.96	0.79
Purdue/NRC	–	–	–	–
UP/UZ 1	–	–	–	–
UP/UZ 2	-0.09	-0.09	-0.53	-0.28
UPC	–	–	–	–
UPM	-0.24	-0.79	-0.45	-0.91
UPV	3.12	2.54	2.46	2.38
VTT	-0.44	-0.94	-0.65	-0.92

Table 4.17. Sequence of events for Phase III of the PWR MSLB Benchmark problem

Event / Scenario	BE/Tractebel		CEA/IPSN 1		CEA/ IPSN 2	CSA/GPUN		FRAMATOME/ ANP	
	NoRP	RP	NoRP	RP		NoRP	RP	NoRP	RP
Break opens	0.001	0.001	0.001	0.001	0.001	0.001	0.001	0.001	0.001
Break is fully open	N/A	N/A	N/A	N/A	N/A	N/A	N/A	N/A	N/A
Turbine isolation valve closes – broken SG	N/A	N/A	N/A	N/A	N/A	N/A	N/A	N/A	N/A
High neutron flux signal	N/A	N/A	N/A	N/A	N/A	N/A	N/A	5.68	5.68
Low RCS pressure set point	N/A	N/A	N/A	N/A	N/A	N/A	N/A	N/A	N/A
Reactor trip	5.9	5.9	7	7	6.48	6.04	6.04	6.08	6.08
Turbine valve close	N/A	N/A	7.4	7.4	6.98	6.54	6.54	6.58	6.58
Steam line B small safety valve opens	N/A	N/A	N/A	N/A	N/A	N/A	N/A	N/A	N/A
Steam Line B safety valve Group 1 opens	N/A	N/A	N/A	N/A	N/A	N/A	N/A	N/A	N/A
Steam line B safety valve Group 2 opens	N/A	N/A	N/A	N/A	N/A	N/A	N/A	N/A	N/A
Steam Line B safety valve Group 3 opens	N/A	N/A	N/A	N/A	N/A	N/A	N/A	N/A	N/A
HPI activation signal	N/A	N/A	N/A	N/A	N/A	N/A	N/A	11.69	12.19
Steam line B safety valve Group 3 closed	N/A	N/A	N/A	N/A	N/A	N/A	N/A	N/A	N/A
Steam line B safety valve Group 2 closed	N/A	N/A	N/A	N/A	N/A	N/A	N/A	N/A	N/A
Steam line B safety valve Group 1 closed	N/A	N/A	N/A	N/A	N/A	N/A	N/A	N/A	N/A
Steam line B small safety valve closed	N/A	N/A	N/A	N/A	N/A	N/A	N/A	N/A	N/A
HPI starts	N/A	N/A	36.11	36.2	36.51	39.19	40.29	36.7	37.2
Return to criticality	N/A	N/A	N/A	N/A	N/A	N/A	N/A	N/A	N/A
Point of maximum power after trip	67.2	64.5	N/A	N/A	N/A	N/A	N/A	67.2	65.8
Transient ends	100	100	100	100	100	100	100	100	100

Table 4.17. Sequence of events for Phase III of the PWR MSLB Benchmark problem (*cont.*)

Event / Scenario	FZR		JAERI		KAERI		Purdue/NRC		UP/UZ 1	
	NoRP	RP	NoRP	RP	NoRP	RP	NoRP	RP	NoRP	RP
Break opens	0	0	0.03	0.03	0.012	0.012	0.01	0.01	0	0
Break is fully open	0.1	0.1	N/A	N/A	N/A	N/A	N/A	N/A	N/A	N/A
Turbine isolation valve closes – broken SG	0.5	0.5	2.255	2.255	N/A	N/A	N/A	N/A	N/A	N/A
High neutron flux signal	4.95	4.95	N/A	N/A	5.958	5.958	N/A	N/A	N/A	N/A
Low RCS pressure set point	N/A	N/A	2.245	2.245	N/A	N/A	N/A	N/A	N/A	N/A
Reactor trip	5.35	5.35	2.755	2.755	6.358	6.358	6.17	6.17	7.9	7.9
Turbine valve close	5.85	5.85	N/A	N/A	6.858	6.858	6.67	6.67	8.4-12.4	8.4-12.4
Steam line B small safety valve opens	N/A	N/A	N/A	N/A	N/A	N/A	N/A	N/A	N/A	N/A
Steam Line B safety valve Group 1 opens	N/A	N/A	N/A	N/A	N/A	N/A	N/A	N/A	N/A	N/A
Steam line B safety valve Group 2 opens	N/A	N/A	N/A	N/A	N/A	N/A	N/A	N/A	N/A	N/A
Steam Line B safety valve Group 3 opens	N/A	N/A	N/A	N/A	N/A	N/A	N/A	N/A	N/A	N/A
HPI activation signal	14.12	14.9	4.74	4.75	N/A	N/A	N/A	N/A	N/A	N/A
Steam line B safety valve Group 3 closed	N/A	N/A	N/A	N/A	N/A	N/A	N/A	N/A	N/A	N/A
Steam line B safety valve Group 2 closed	N/A	N/A	N/A	N/A	N/A	N/A	N/A	N/A	N/A	N/A
Steam line B safety valve Group 1 closed	N/A	N/A	N/A	N/A	N/A	N/A	N/A	N/A	N/A	N/A
Steam line B small safety valve closed	N/A	N/A	N/A	N/A	N/A	N/A	N/A	N/A	N/A	N/A
HPI starts	39.12	39.9	29.75	29.77	36.67	36.67	35.8	35.94	46.3	46.4
Return to criticality	N/A	N/A	N/A	N/A	N/A	N/A	N/A	N/A	N/A	N/A
Point of maximum power after trip	N/A	N/A	66.9	62.3	N/A	67.02	68.68	65.82	N/A	N/A
Transient ends	100	100	N/A	N/A	100	100	100	100	100	100

Table 4.17. Sequence of events for Phase III of the PWR MSLB Benchmark problem (*cont.*)

Event / Scenario	UP/UZ 2		UPC	UPM		VTT	
	NoRP	RP	RP	NoRP	RP	NoRP	RP
Break opens	0	0	0	0.01	0.01	0	0
Break is fully open	N/A	N/A	N/A	N/A	N/A	N/A	N/A
Turbine isolation valve closes – broken SG	N/A	N/A	N/A	N/A	N/A	0.5	0.5
High neutron flux signal	N/A	N/A	N/A	N/A	N/A	6.2	6.2
Low RCS pressure set point	N/A	N/A	N/A	N/A	N/A	N/A	N/A
Reactor trip	7.603 (7.203+0.4)	7.603 (7.203+0.4)	5.462	6.18	6.18	6.6	6.6
Turbine valve close	8.104 (7.603+0.5)	8.104 (7.603+0.5)	N/A	6.68	6.68	8.15	8.2
Steam line B small safety valve opens	N/A	N/A	N/A	N/A	N/A	8.60	8.65
Steam Line B safety valve Group 1 opens	N/A	N/A	8.046	N/A	N/A	8.80	8.80
Steam line B safety valve Group 2 opens	N/A	N/A	8.171	N/A	N/A	8.80	8.80
Steam Line B safety valve Group 3 opens	N/A	N/A	8.164	N/A	N/A	9.00	9.05
HPI activation signal	21.078	21.414	N/A	N/A	N/A	11.4	11.6
Steam line B safety valve Group 3 closed	N/A	N/A	32.627	N/A	N/A	27.8	29.0
Steam line B safety valve Group 2 closed	N/A	N/A	32.627	N/A	N/A	33.3	36.7
Steam line B safety valve Group 1 closed	N/A	N/A	39.665	N/A	N/A	33.3	36.7
Steam line B small safety valve closed	N/A	N/A	N/A	N/A	N/A	36.2	40.3
HPI starts	46.078	46.414	35.59	35.9	36.03	36.5	36.7
Return to criticality	N/A	N/A	N/A	N/A	N/A	N/A	N/A
Point of maximum power after trip	N/A	N/A	64.86	69.7	65.83	N/A	N/A
Transient ends	100	100	100	100	100	100	100

Figure 4.1. Core-averaged axial power distribution, State 2

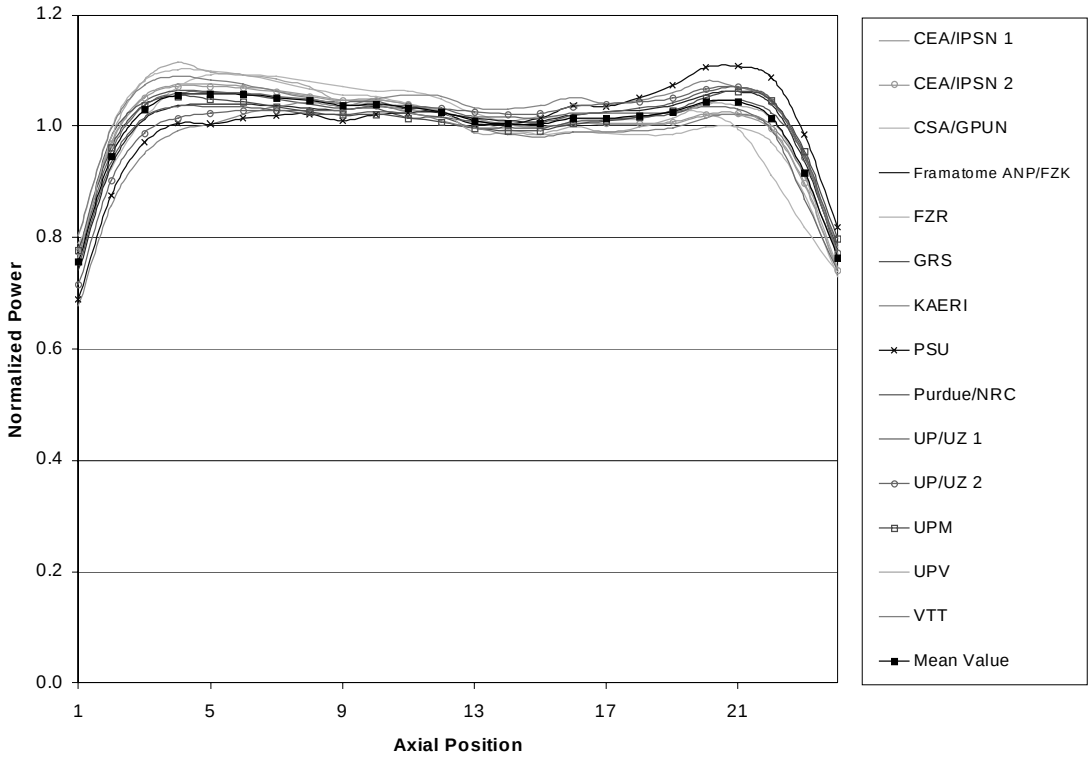

Figure 4.2. Normalised power distribution at the stuck rod (N12) – 18 channels, State 2

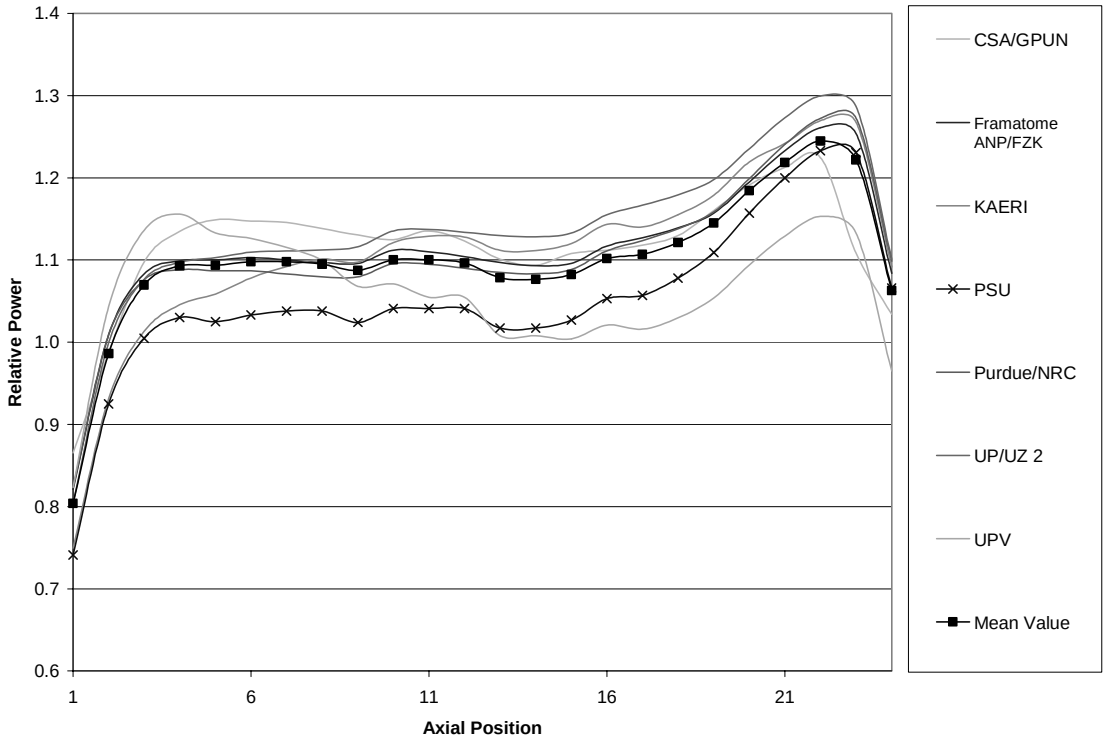

Figure 4.3. Normalised power distribution at the stuck rod (N12) – 177 channels, State 2

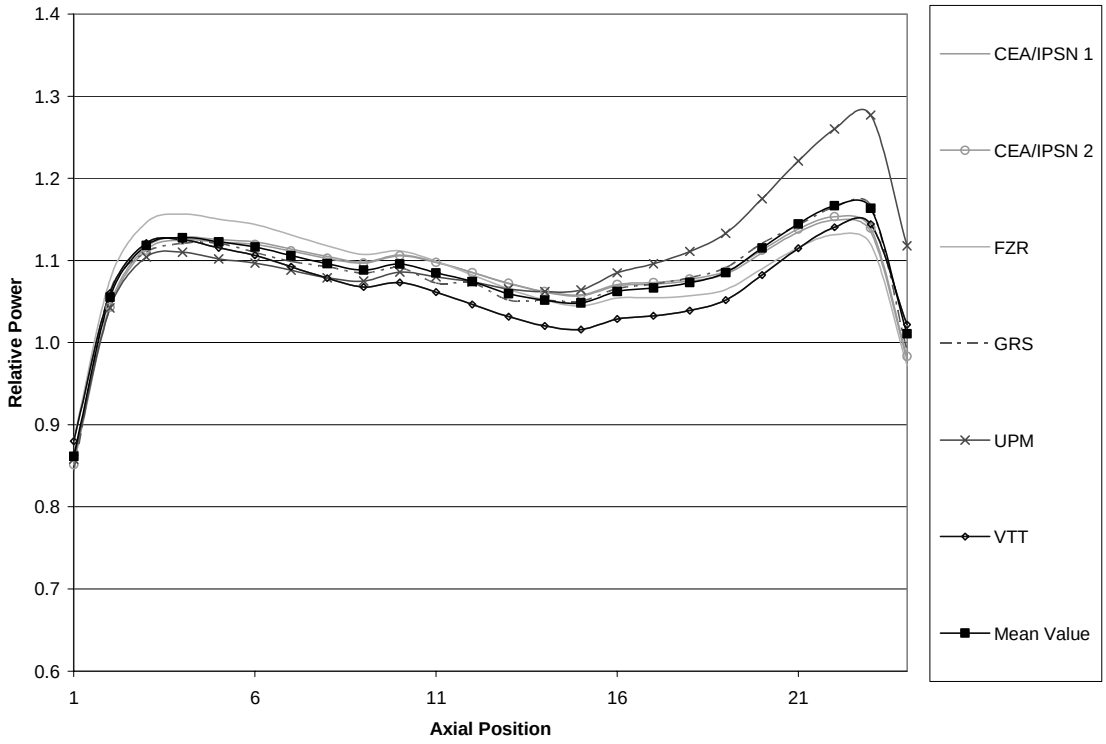

Figure 4.4. Coolant density at stuck rod (N12) – 177 channels, State 2

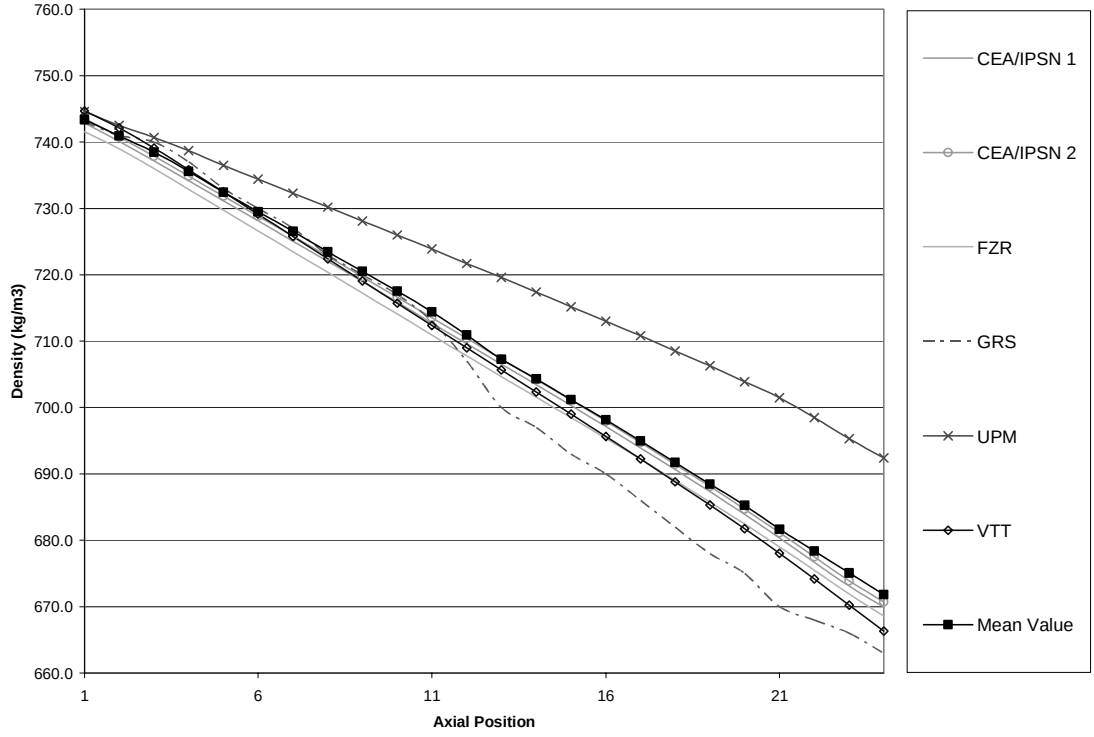

Figure 4.5. Doppler temperature at stuck rod (N12) – 177 channels, State 2

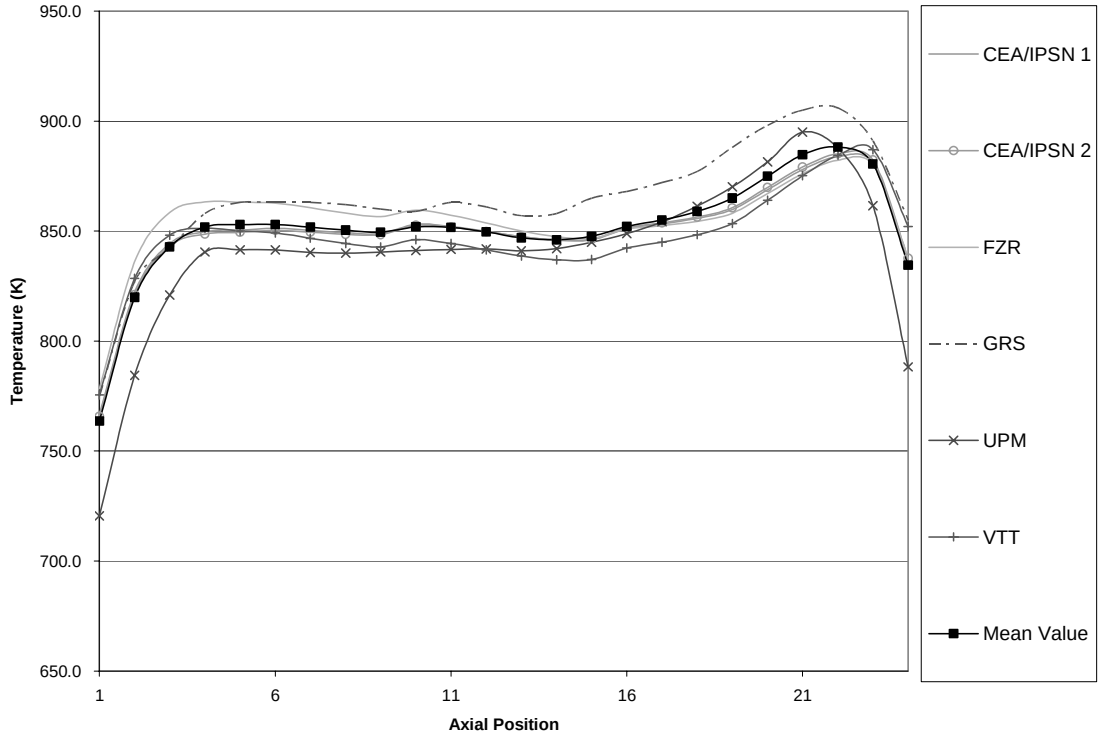

Figure 4.6. Core-averaged axial power, State 5

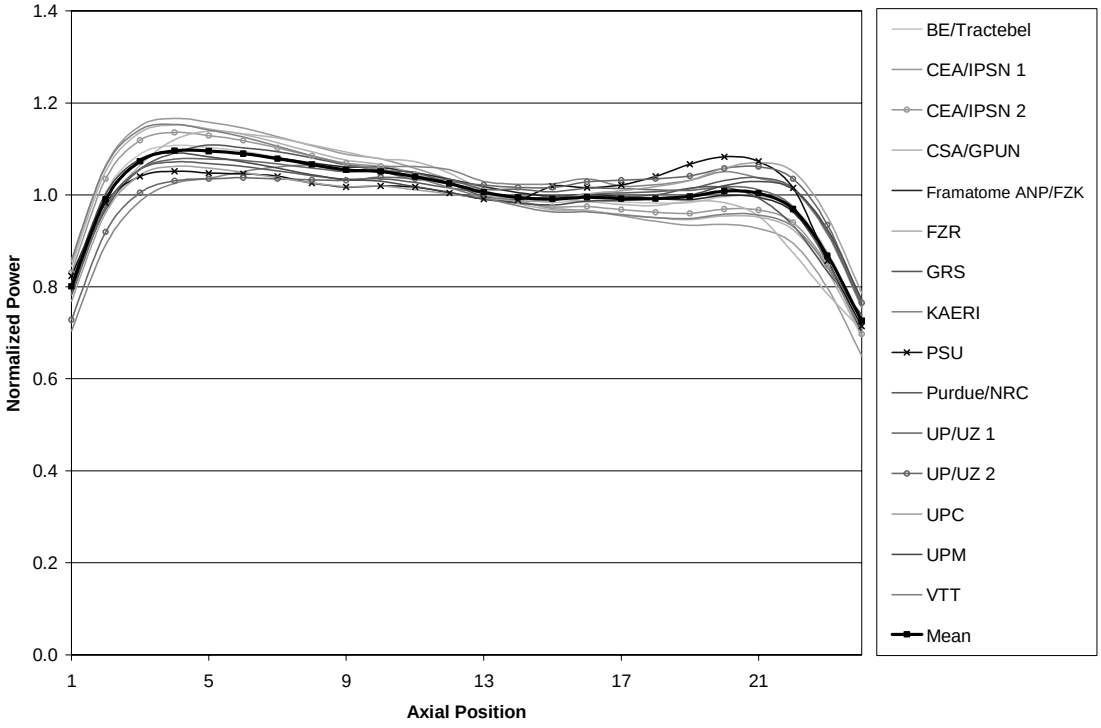

Figure 4.7. Core-averaged axial power, State 6

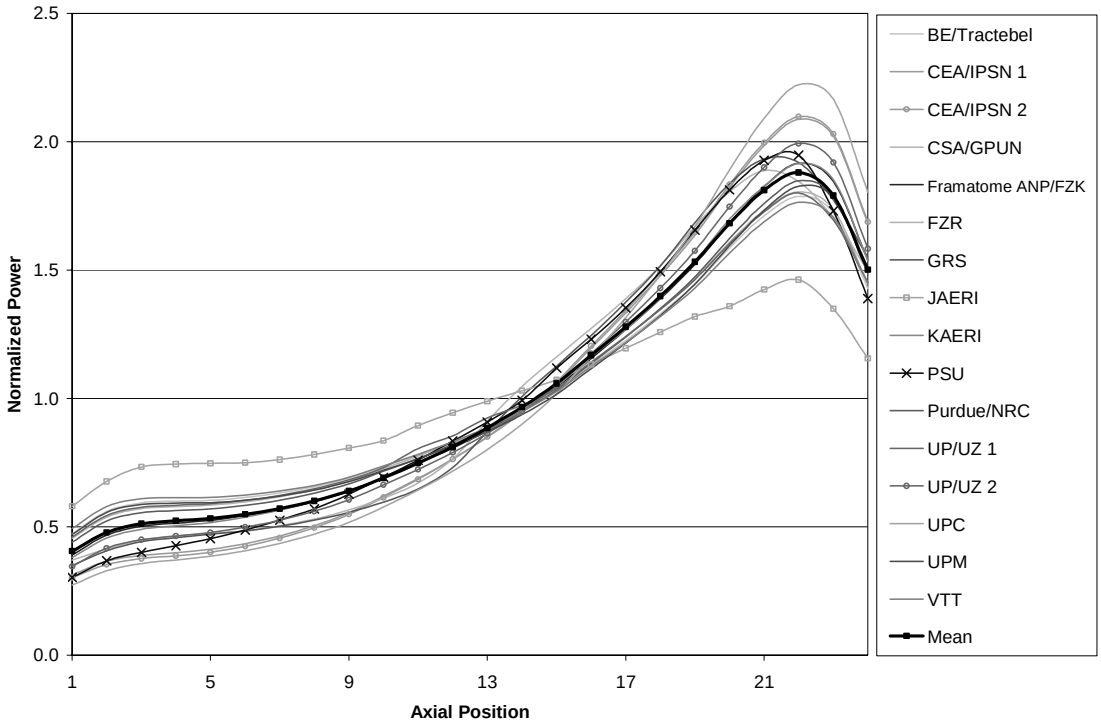

Figure 4.8. Core-averaged axial power, State 7

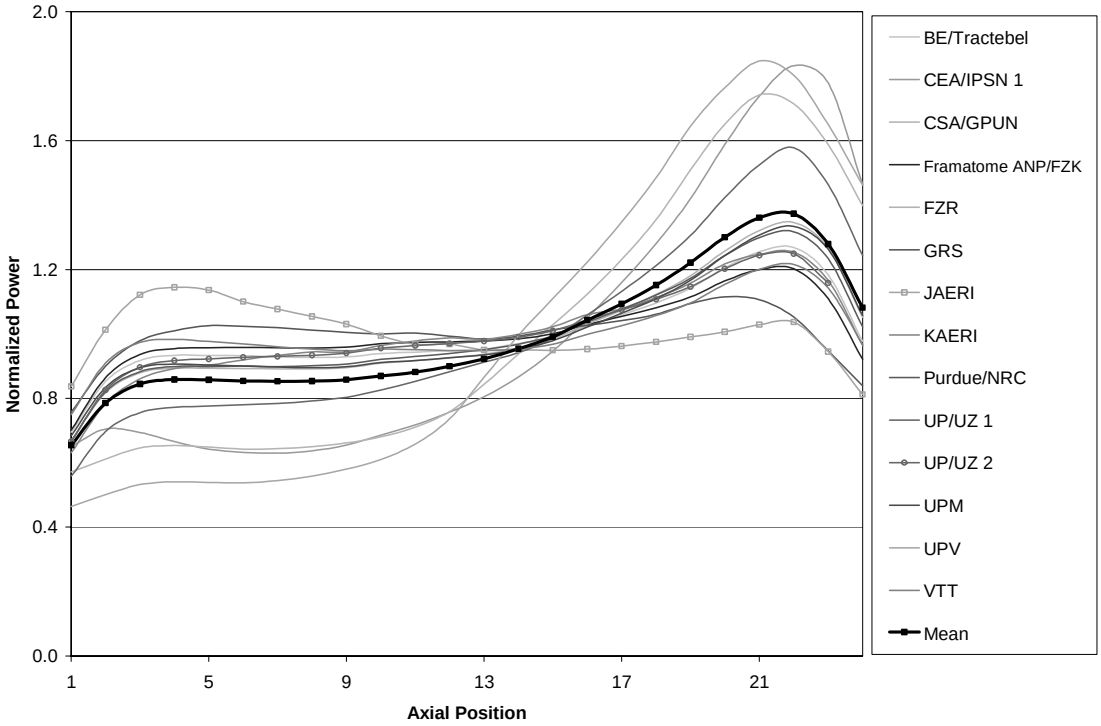

Figure 4.9. Core-averaged axial power, State 8

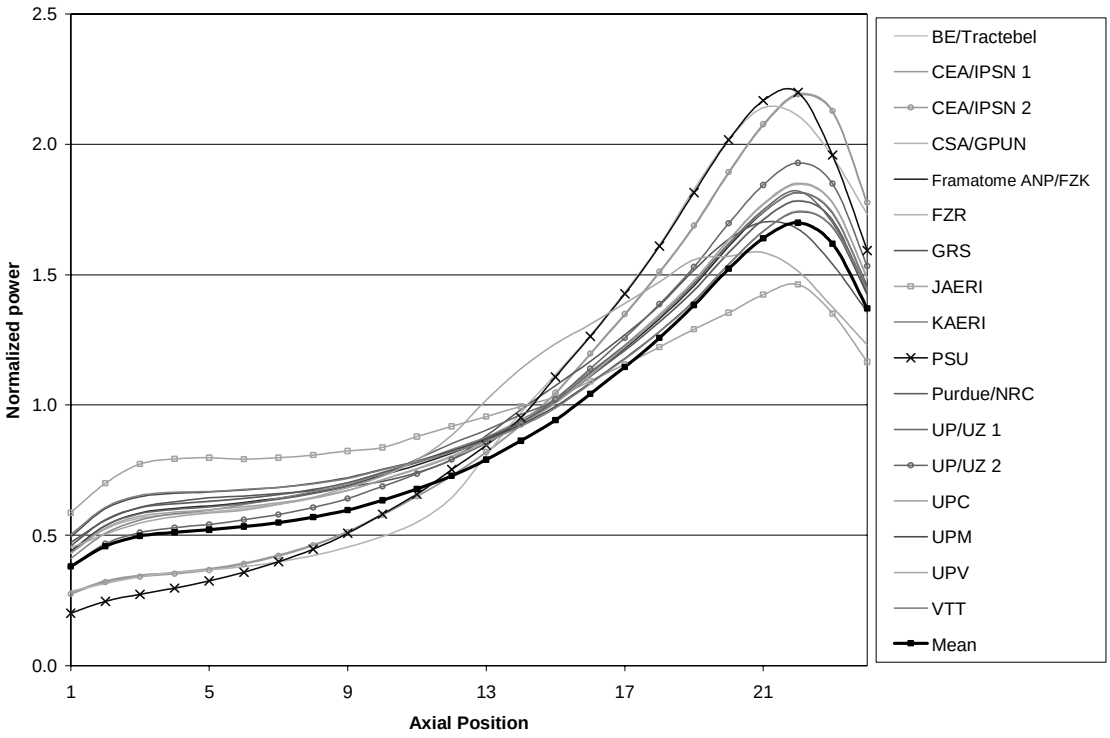

Figure 4.10. Relative axial power in stuck rod position, State 5 – 18 channels

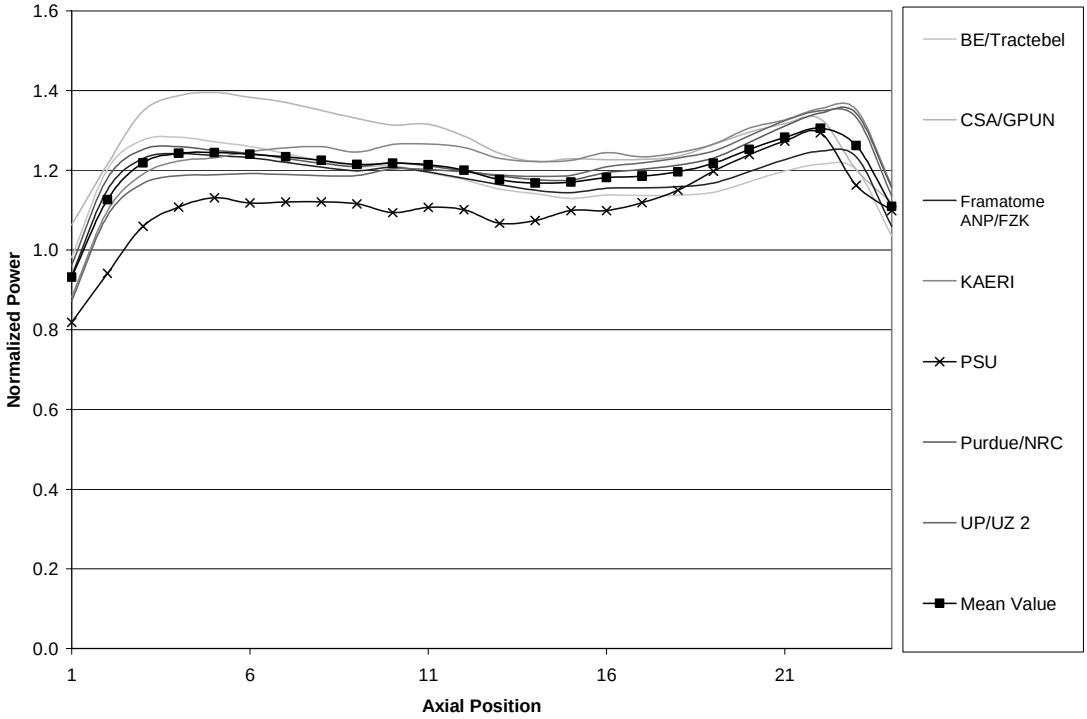

Figure 4.11. Relative axial power in stuck rod position, State 5 – 177 channels

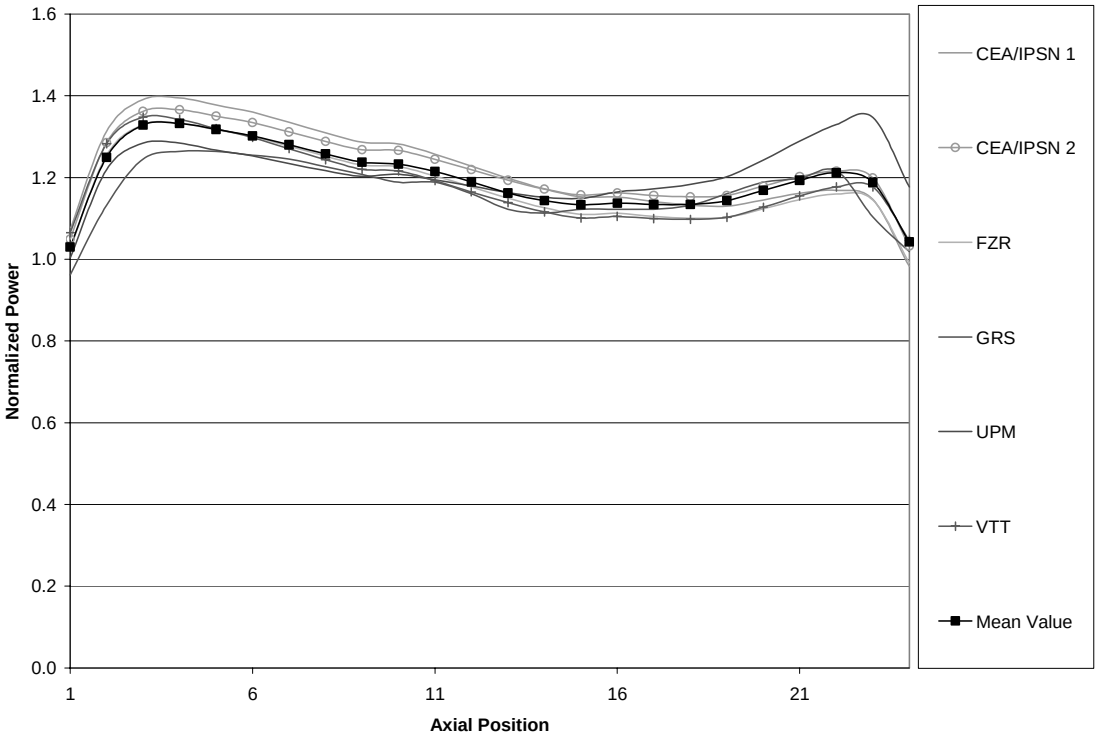

Figure 4.12. Relative axial power in stuck rod position, State 6 – 18 channels

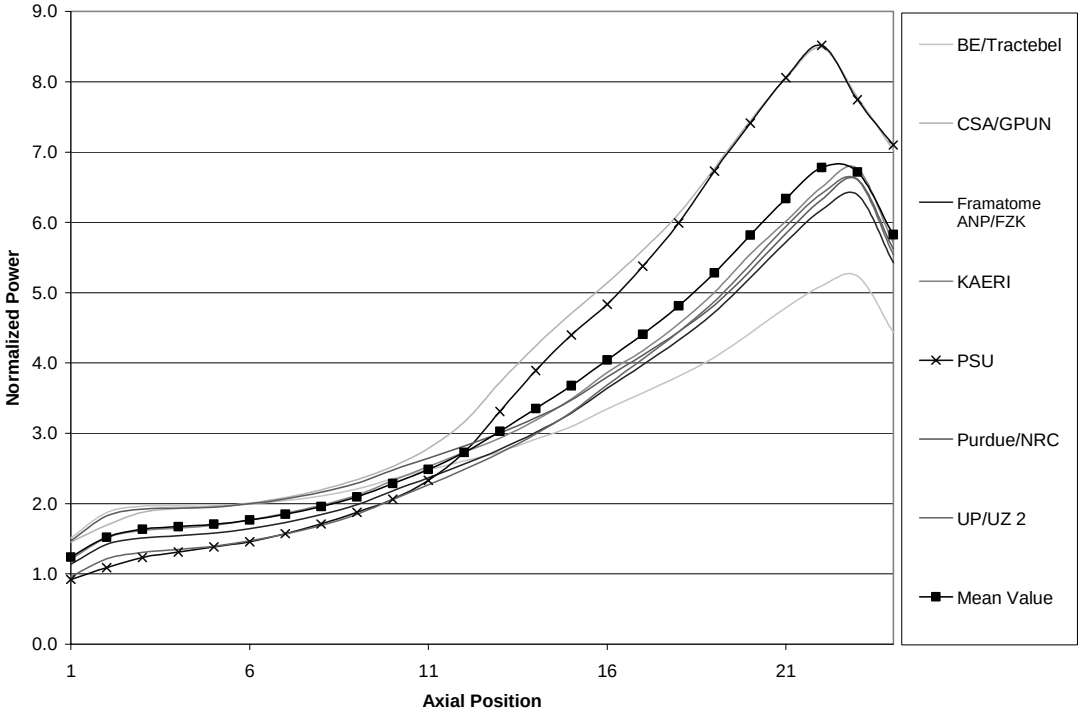

Figure 4.13. Relative axial power in stuck rod position, State 6 – 177 channels

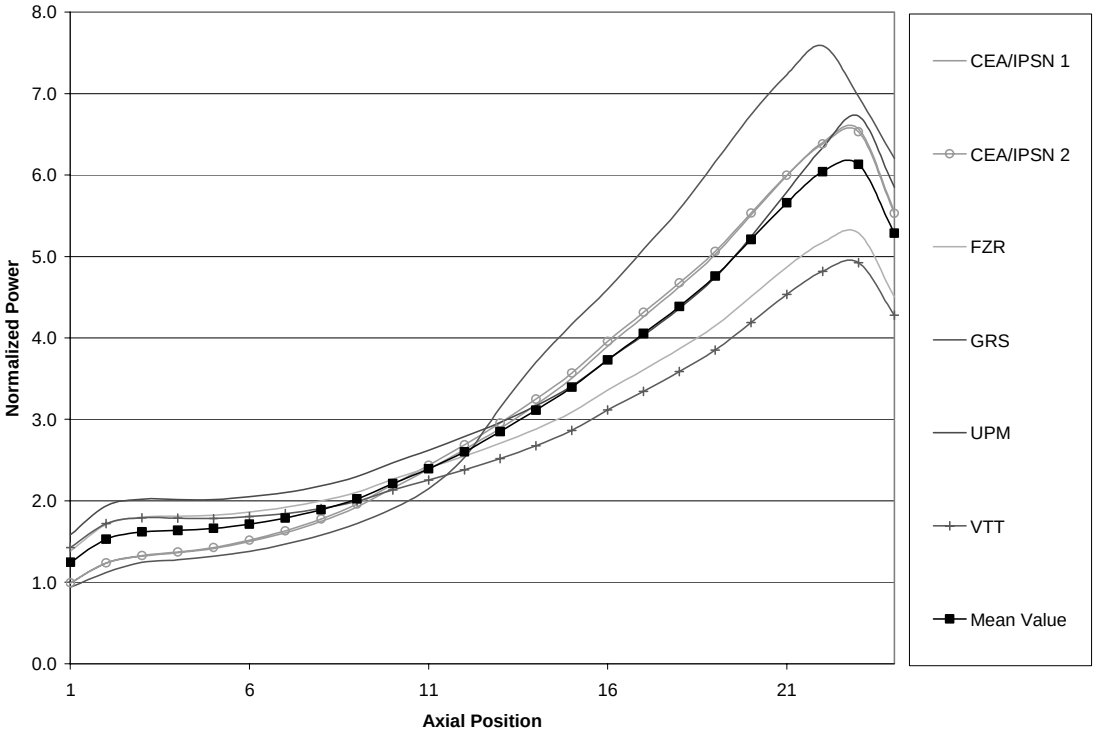

Figure 4.14. Axial Doppler temperature distribution in stuck rod position, State 6 – 18 channels

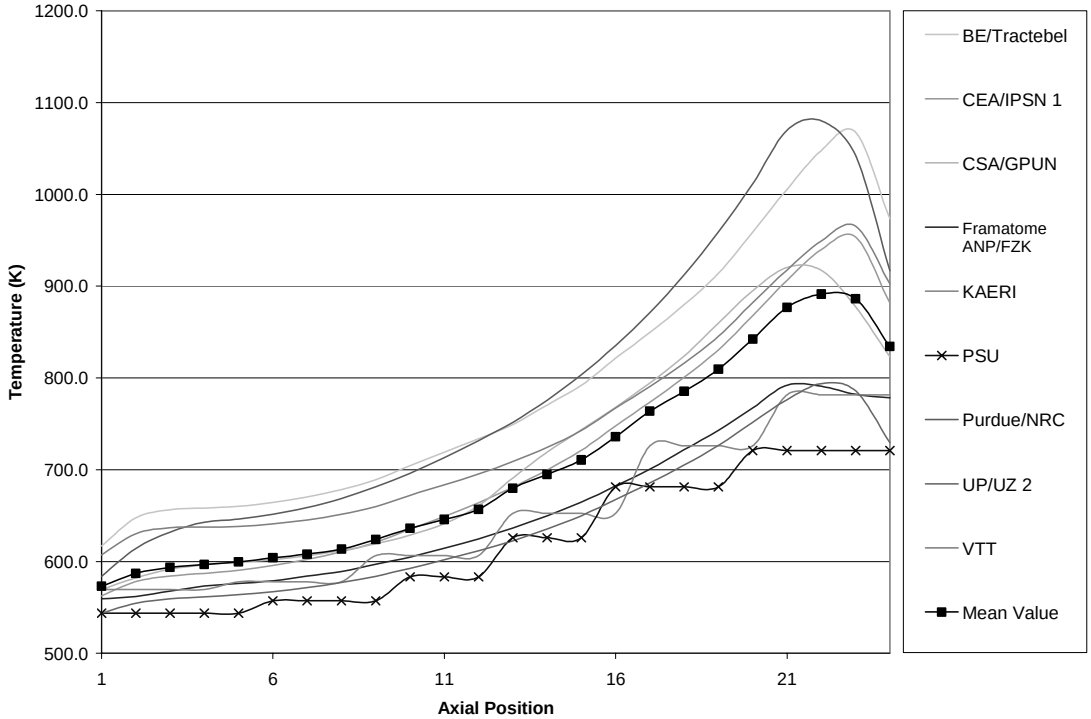

Figure 4.15. Axial Doppler temperature distribution in stuck rod position, State 6 – 177 channels

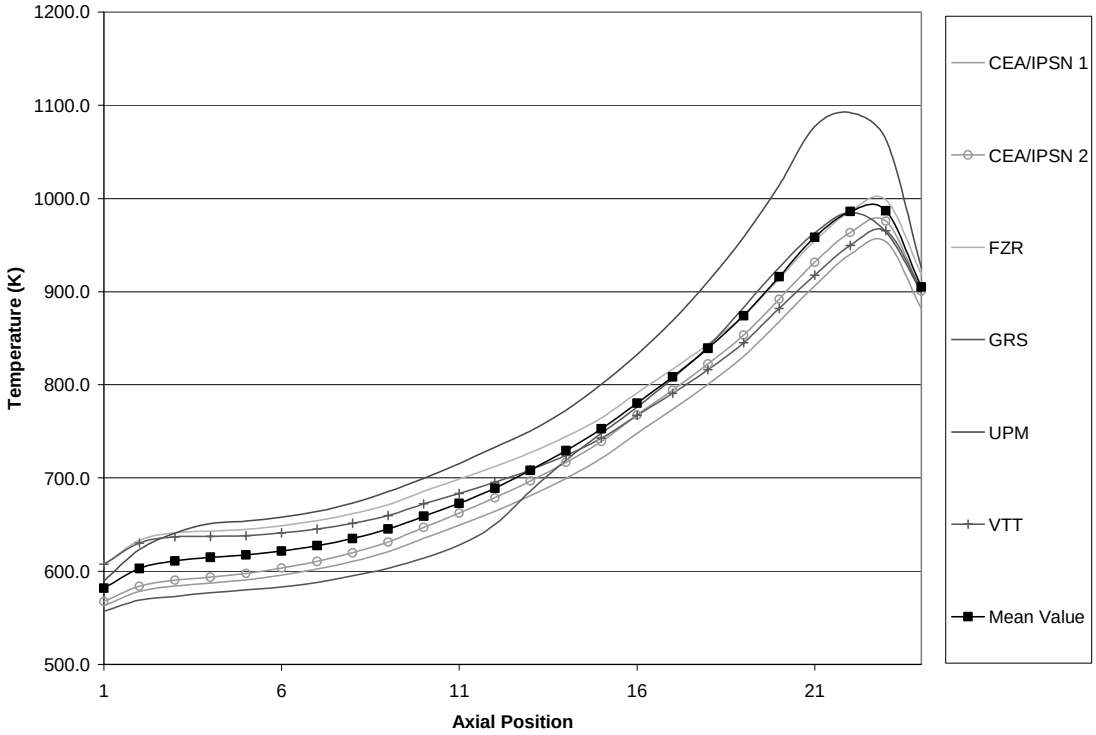

Figure 4.16. Axial coolant density distribution in stuck rod position, State 6 – 18 channels

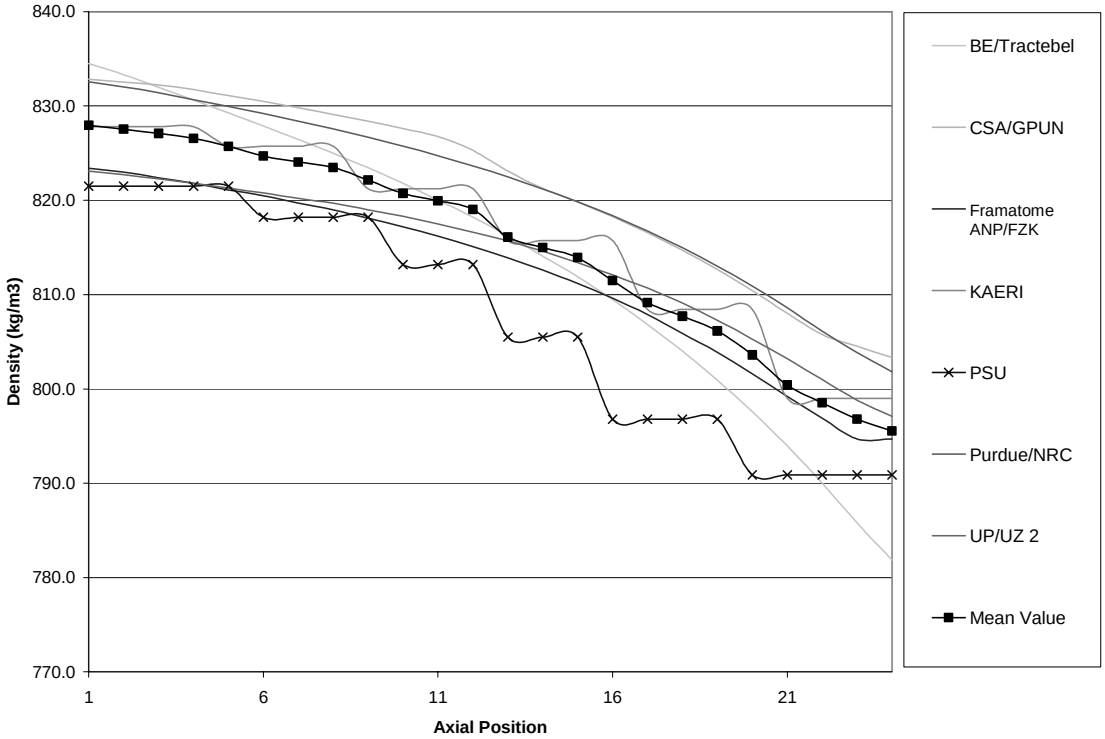

Figure 4.17. Axial coolant density distribution in stuck rod position, State 6 – 177 channels

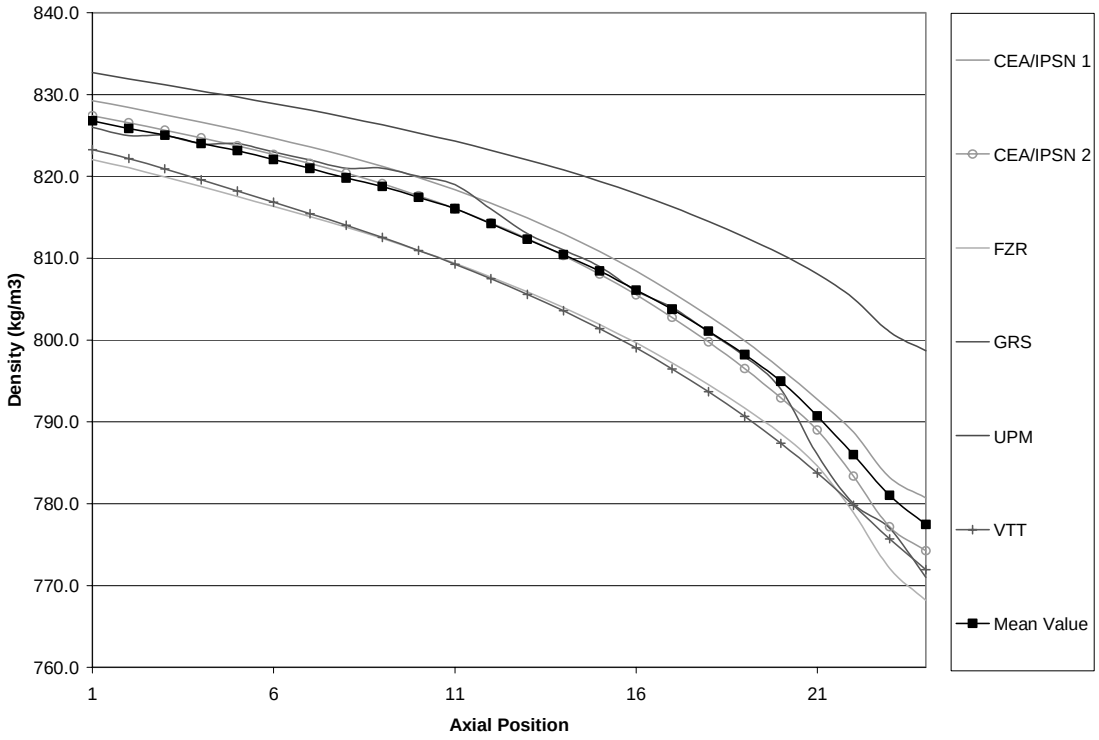

Figure 4.18. Relative axial power in stuck rod position, State 7 – 18 channels

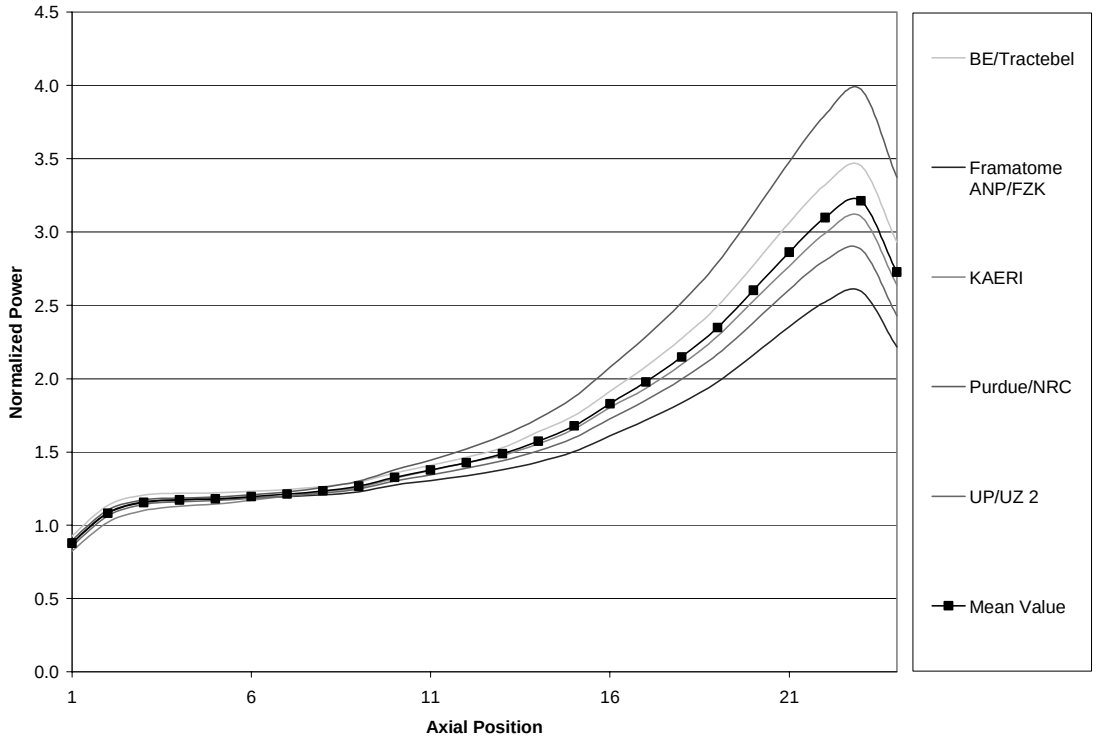

Figure 4.19. Relative axial power in stuck rod position, State 7 – 177 channels

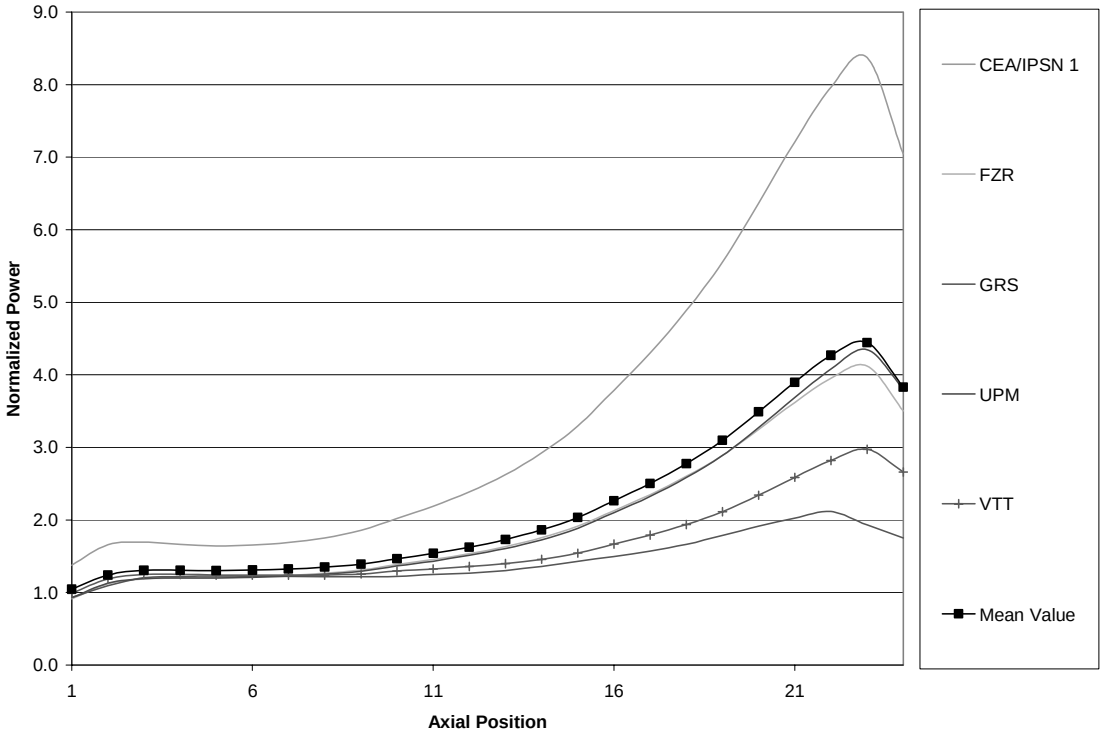

Figure 4.20. Relative axial power in stuck rod position, State 8 – 18 channels

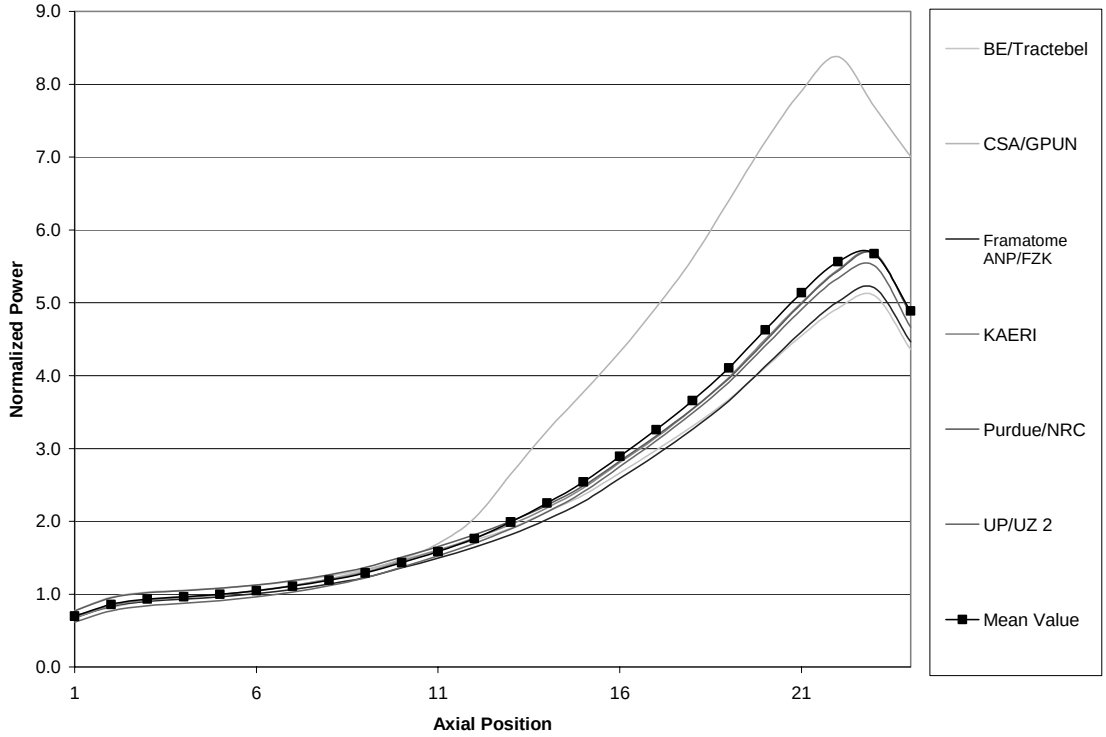

Figure 4.21. Relative axial power in stuck rod position, State 8 – 177 channels

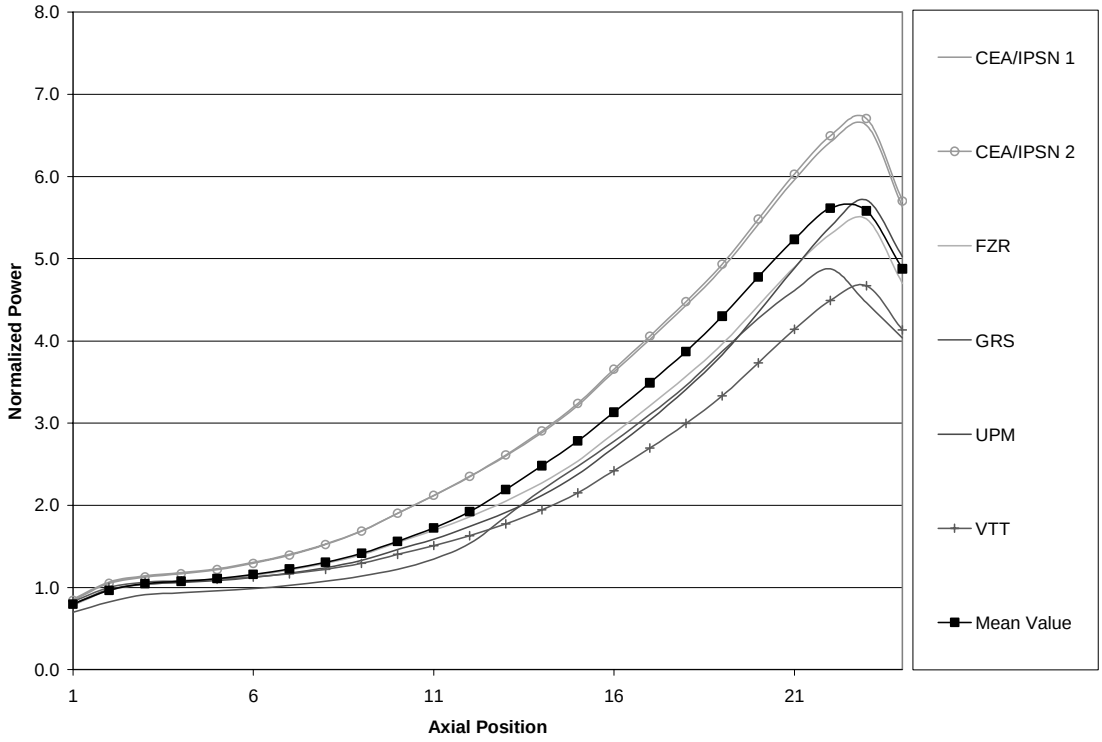

Figure 4.22. Total break flow rate for Scenario 1

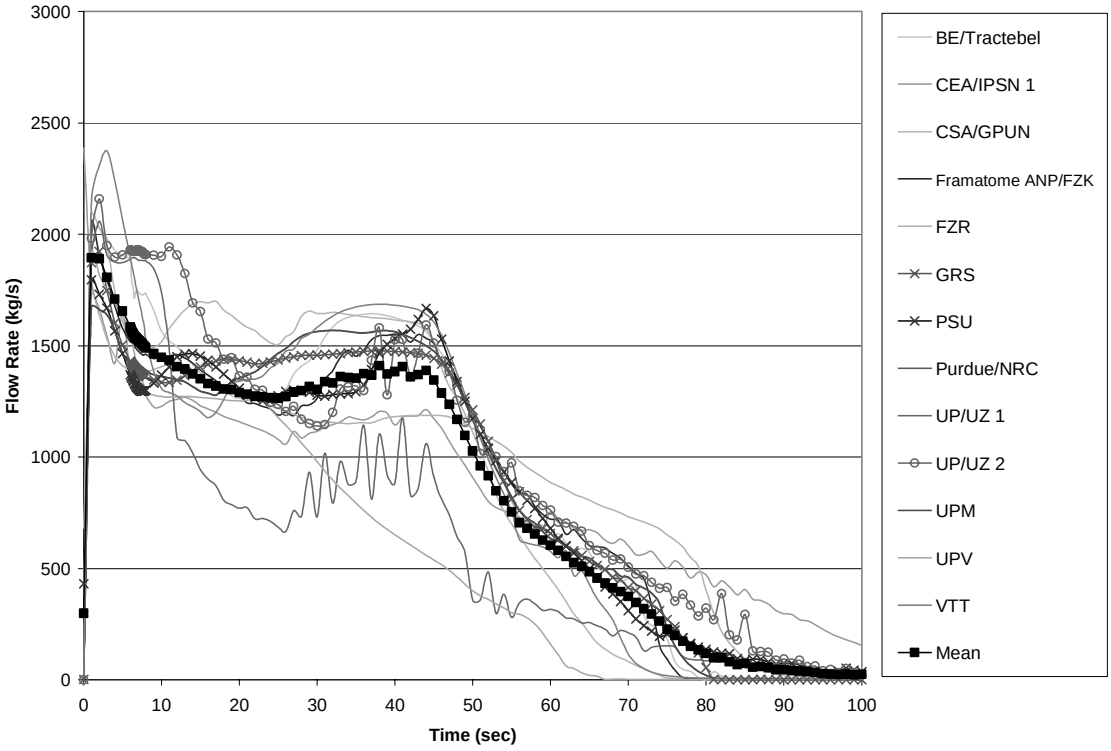

Figure 4.23. Break flow rate for Scenario 1 – 24 inch

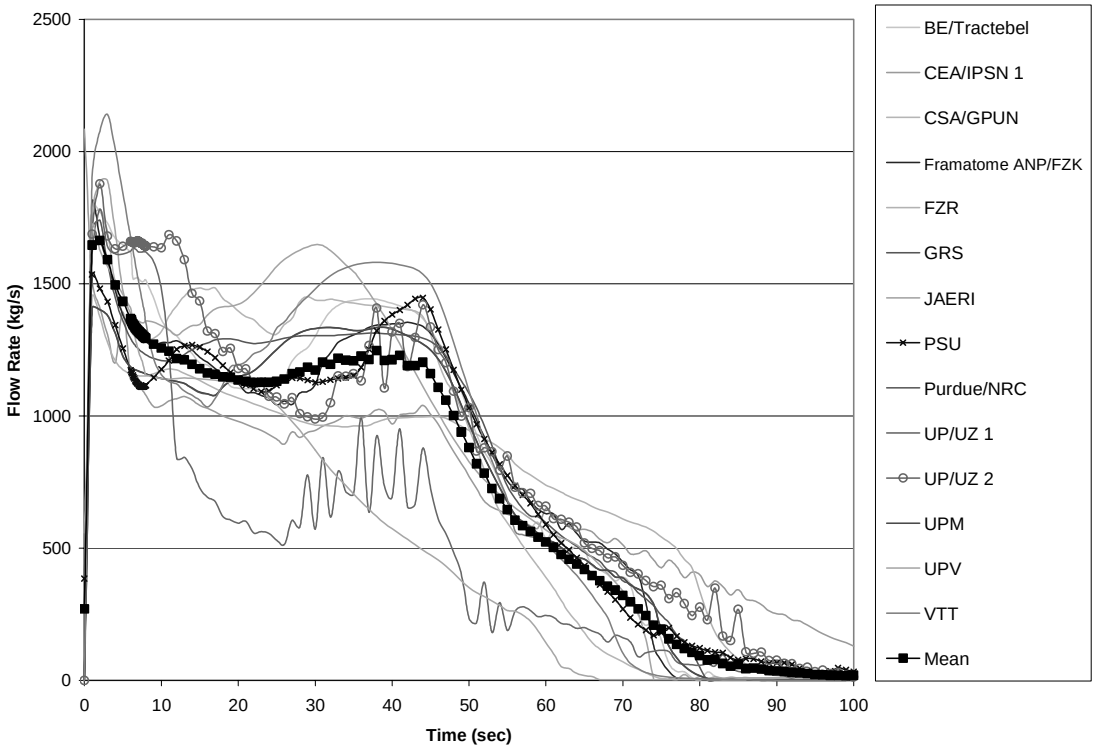

Figure 4.24. Break flow rate for Scenario 1 – 8 inch

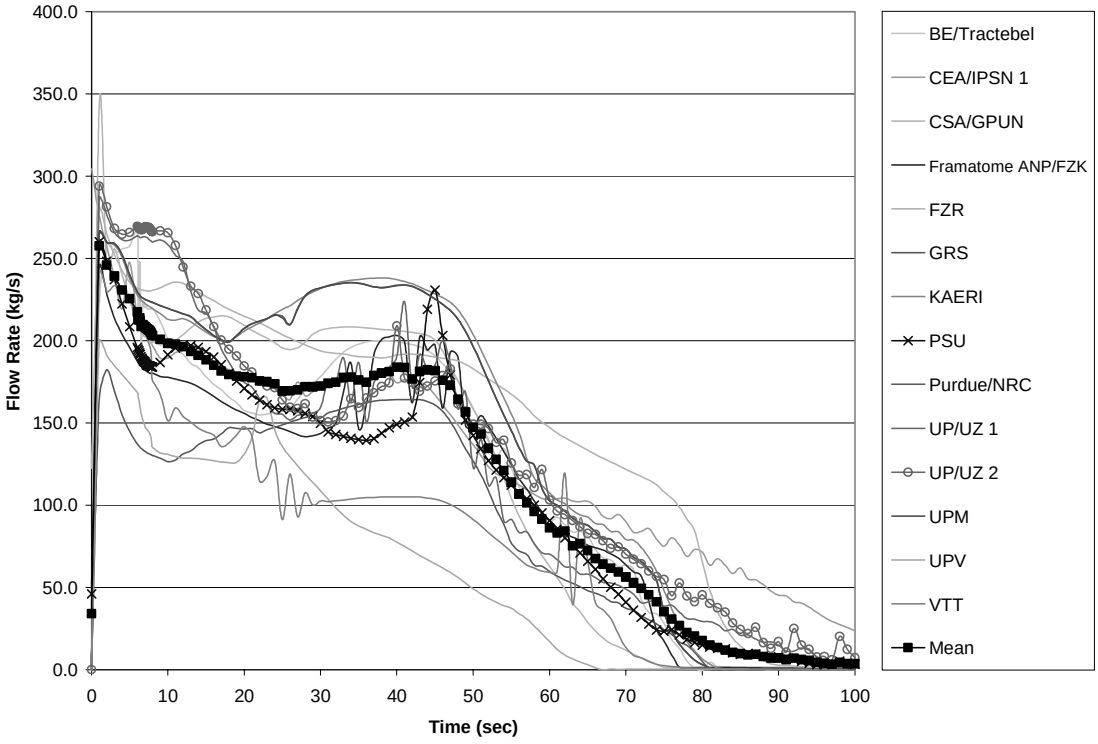

Figure 4.25. Average RCS pressure for Scenario 1

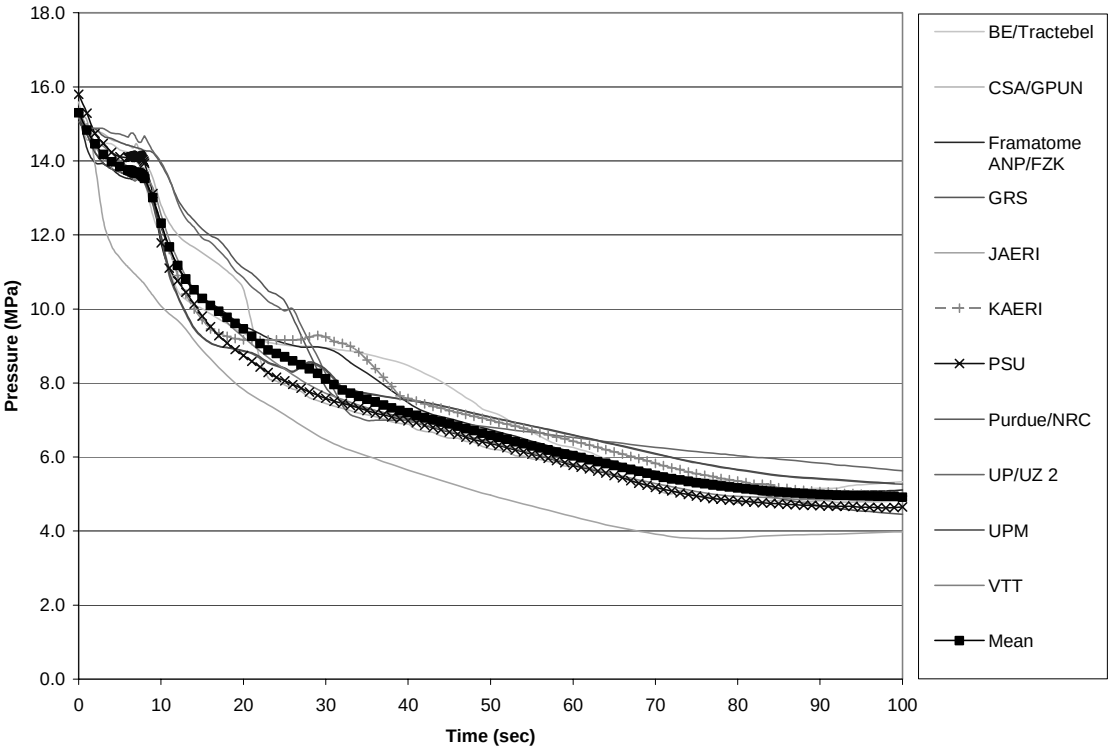

Figure 4.26. Broken loop hot leg pressure for Scenario 1

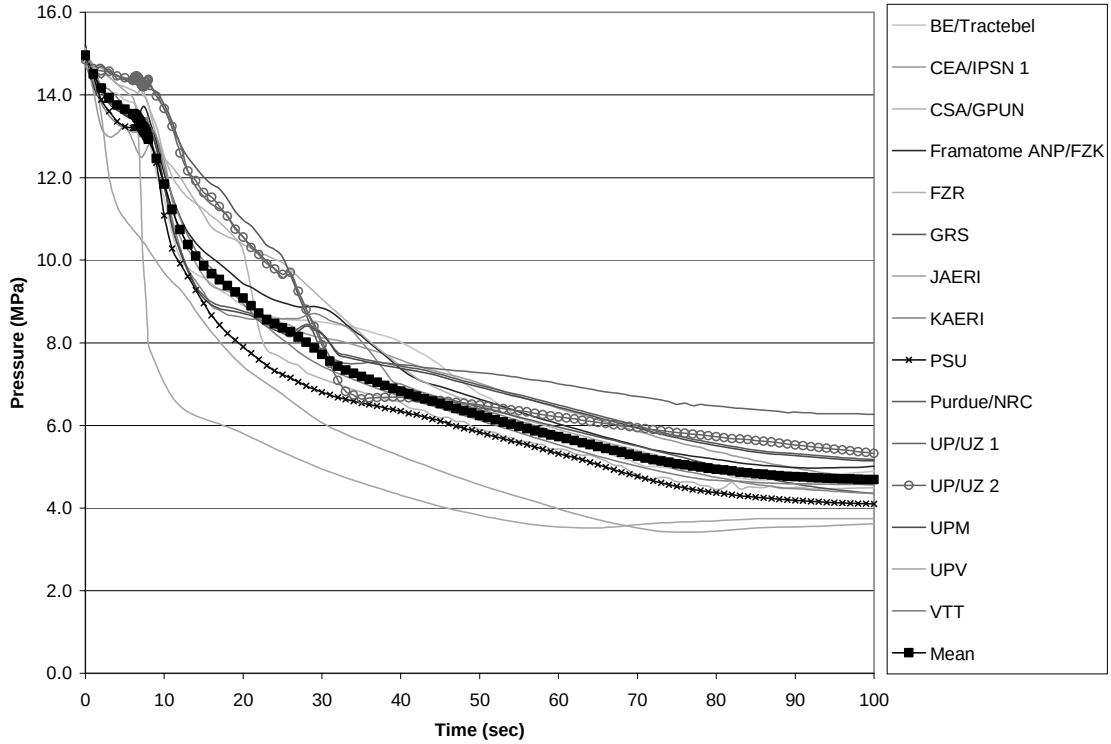

Figure 4.27. Intact loop hot leg pressure for Scenario 1

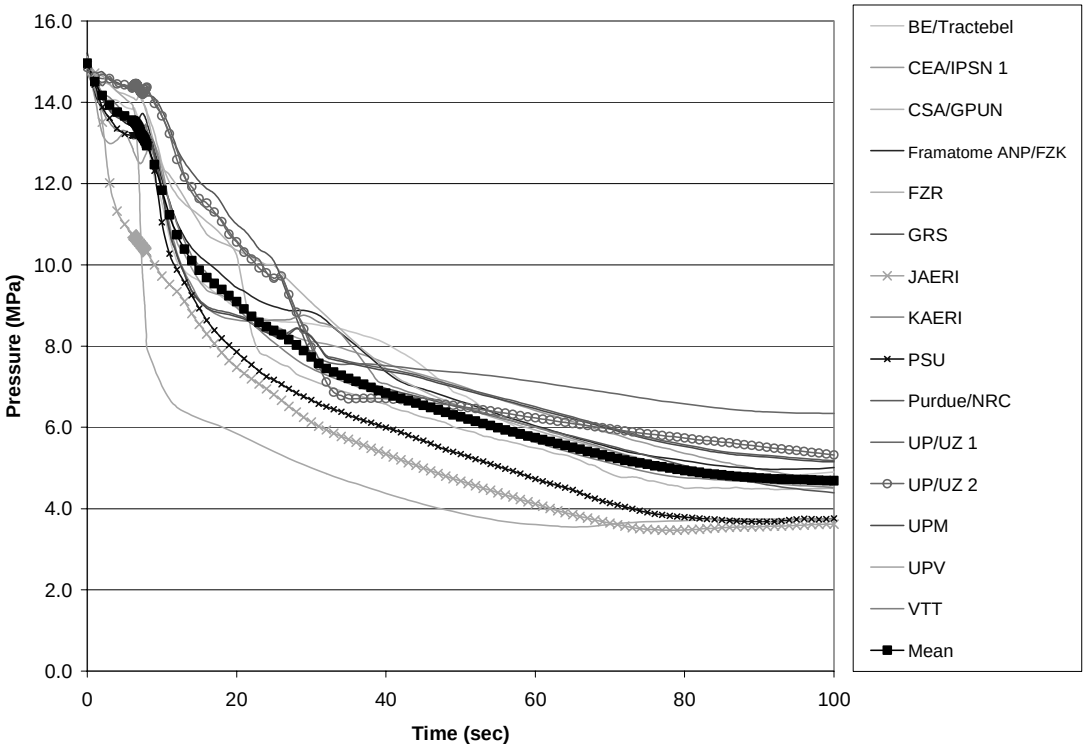

Figure 4.28. Broken loop steam line pressure for Scenario 1

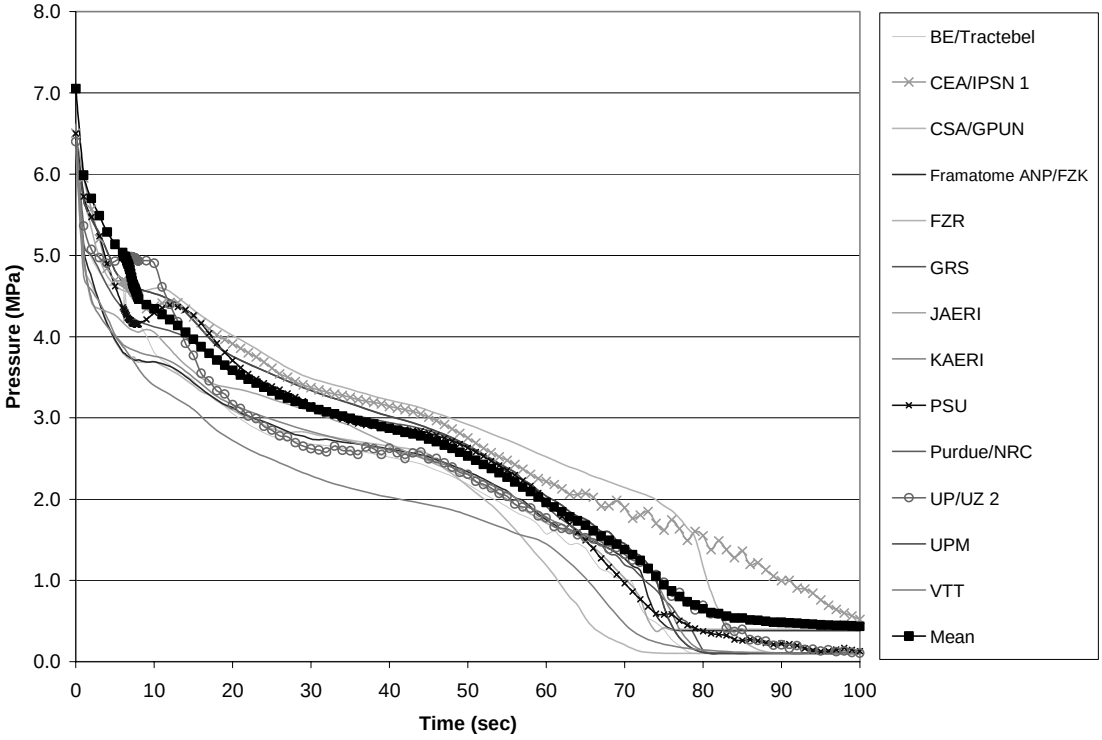

Figure 4.29. Intact loop steam line pressure for Scenario 1

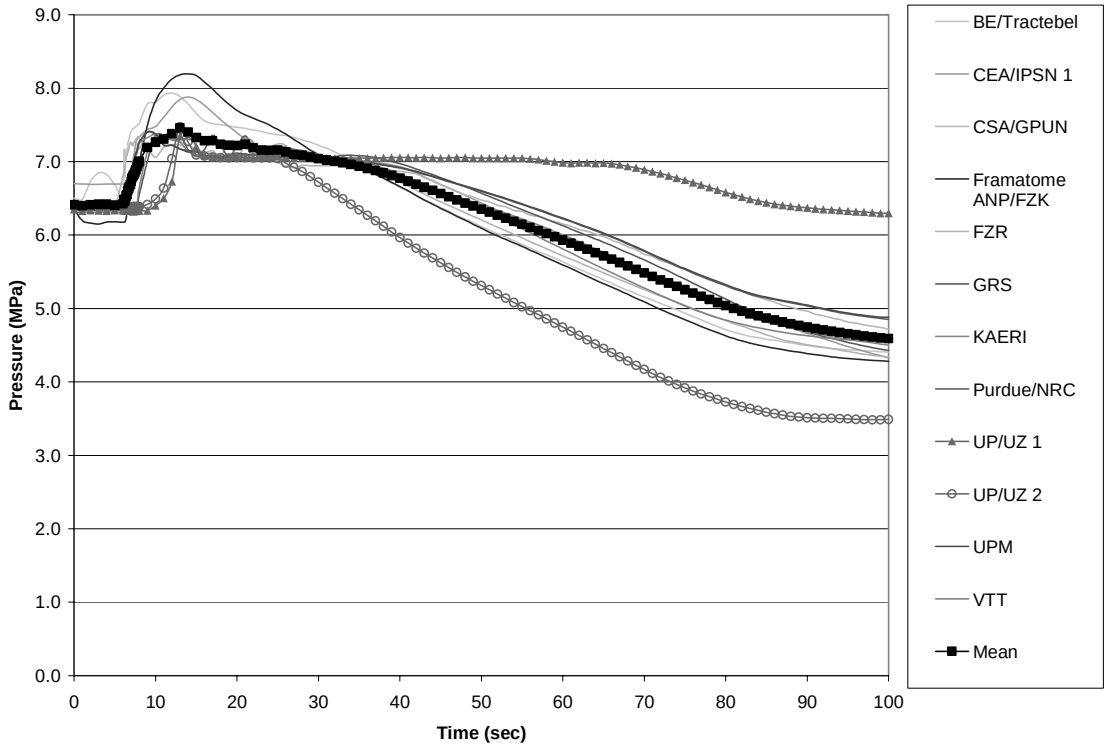

Figure 4.30. Average coolant temperature for Scenario 1

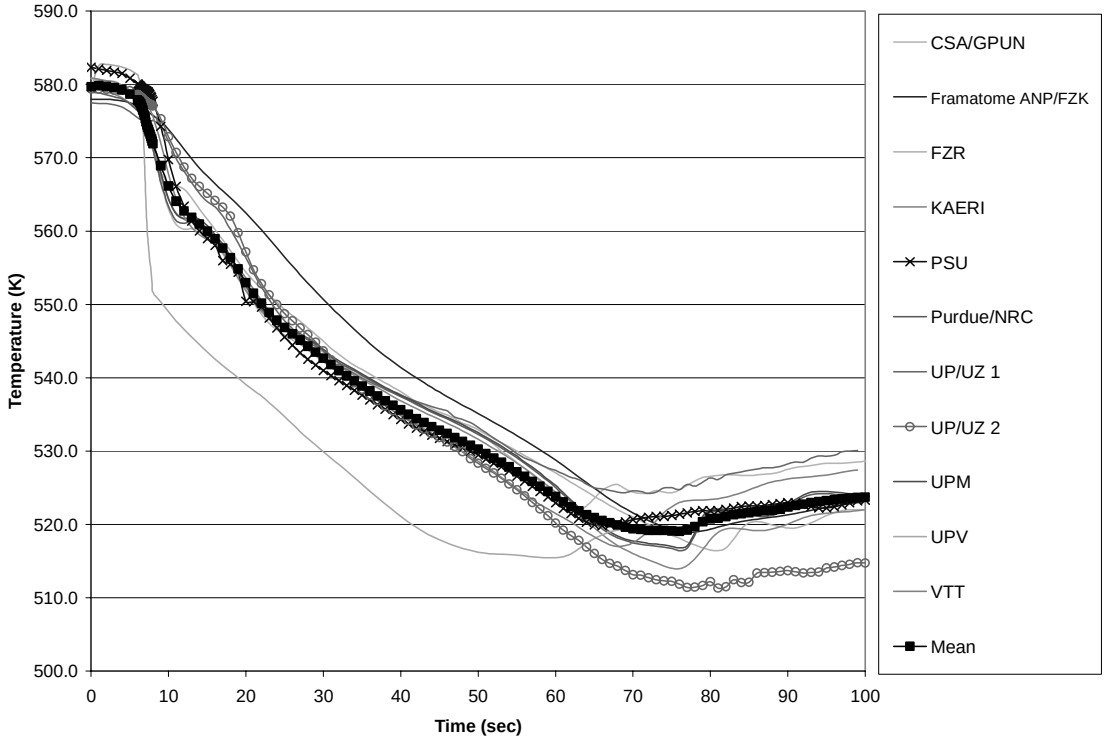

Figure 4.31. Broken loop hot leg temperature for Scenario 1

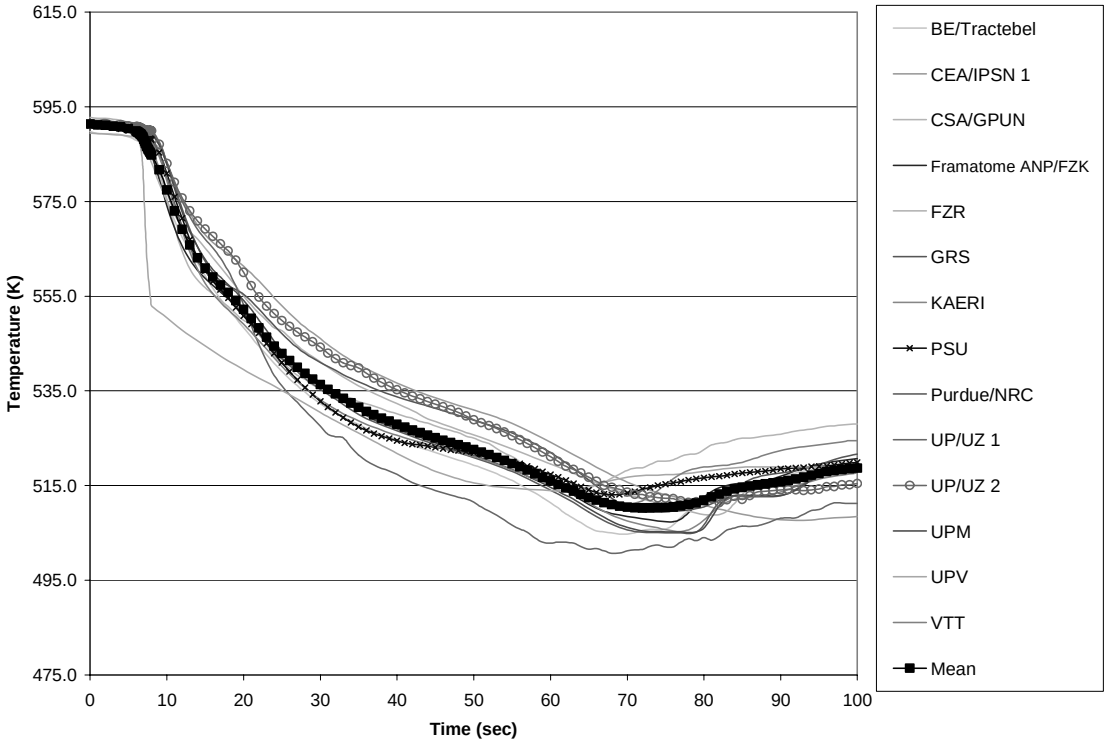

Figure 4.32. Intact loop hot leg temperature for Scenario 1

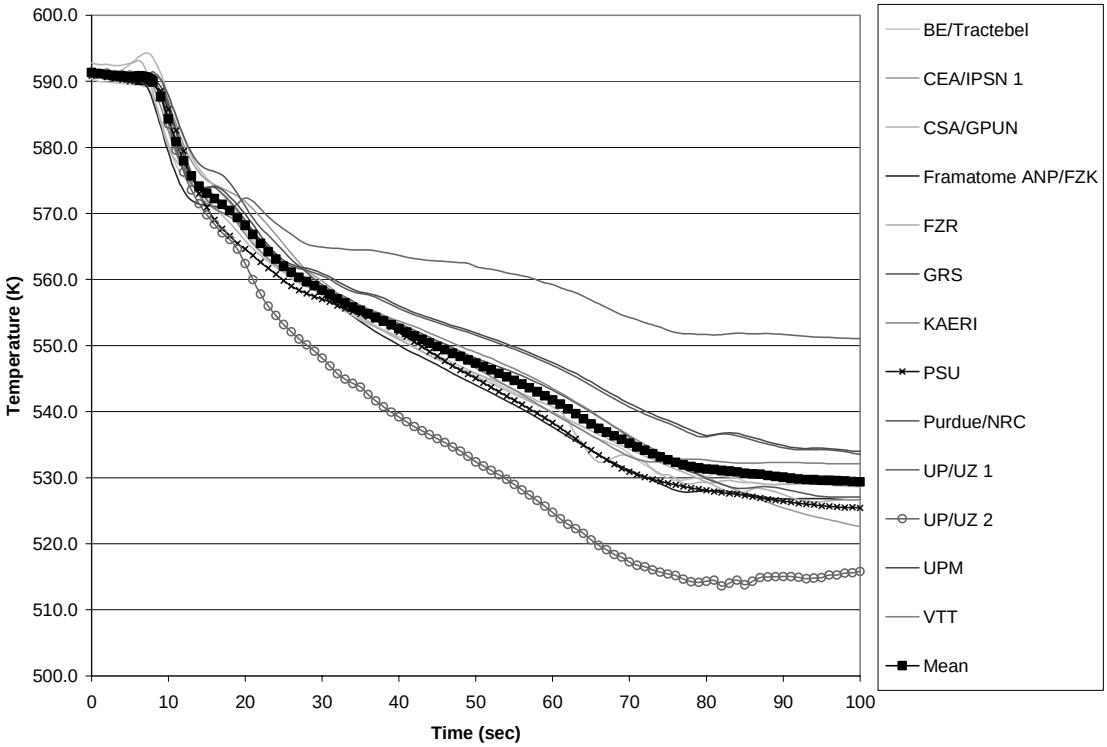

Figure 4.33. Broken loop cold leg temperature for Scenario 1

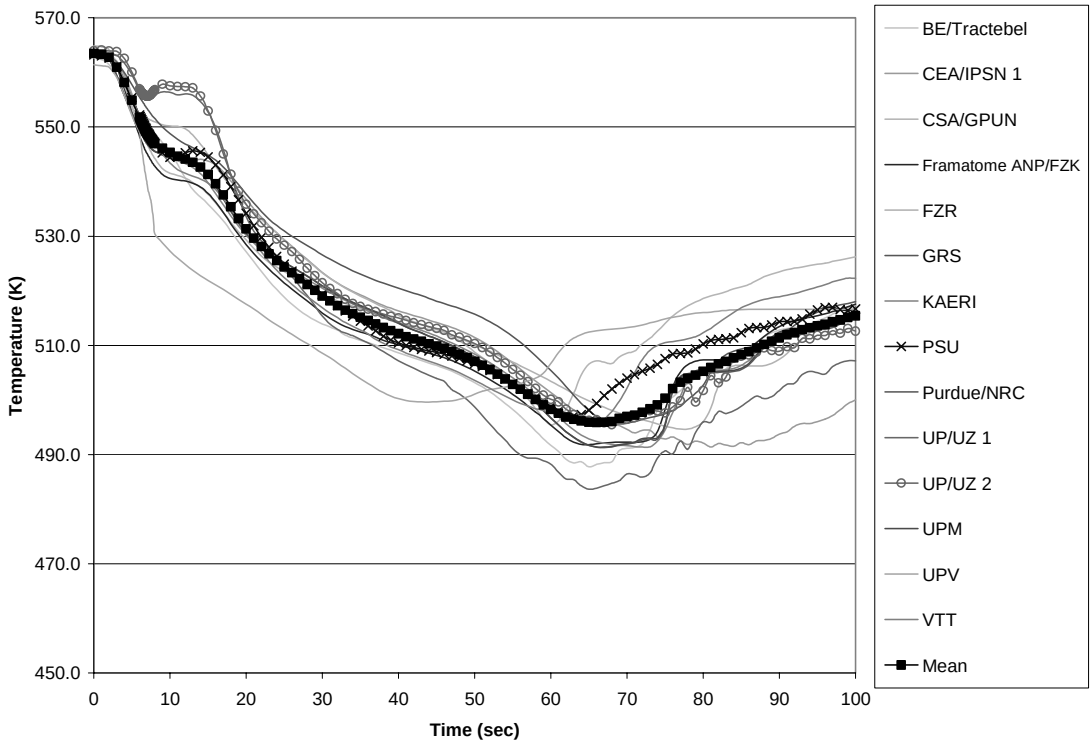

Figure 4.34. Intact loop cold leg temperature for Scenario 1

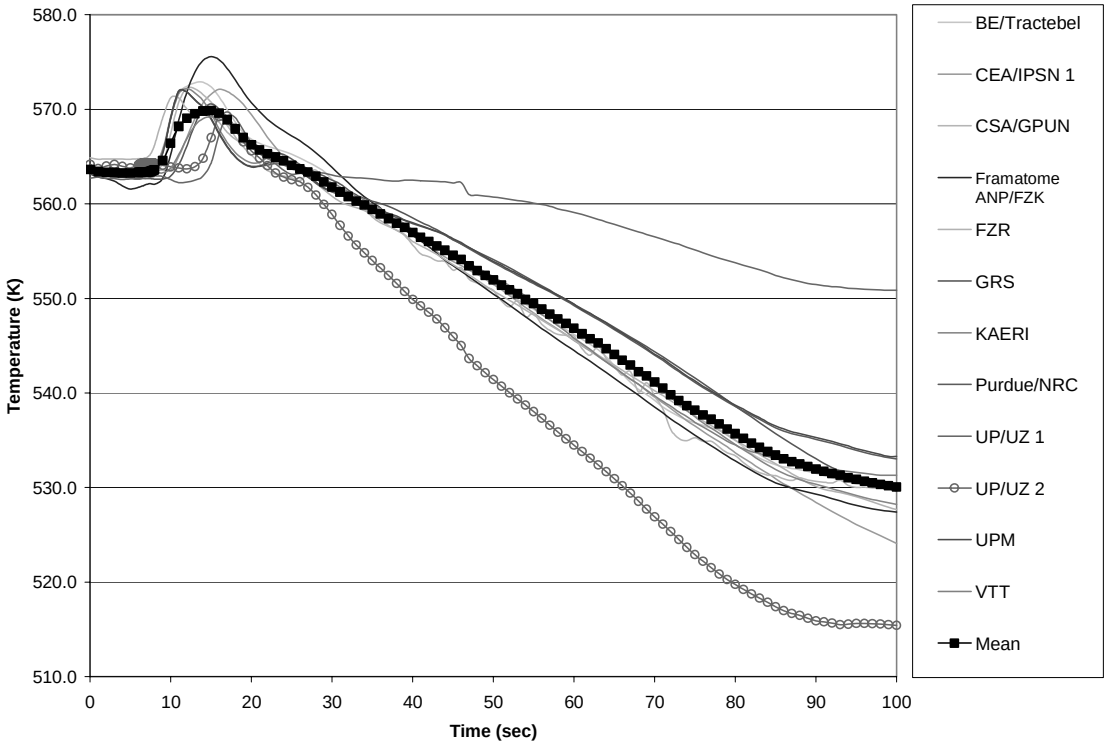

Figure 4.35. Core-averaged Doppler temperature time history for Scenario 1

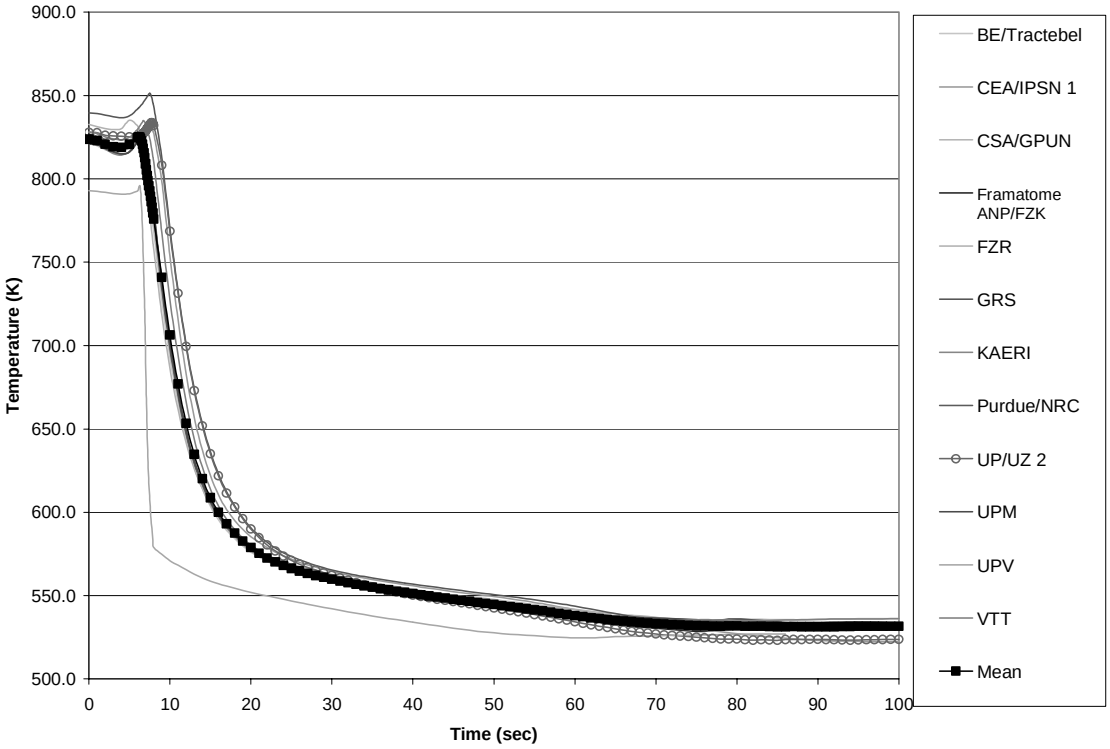

Figure 4.36. Maximum nodal Doppler temperature time history for Scenario 1

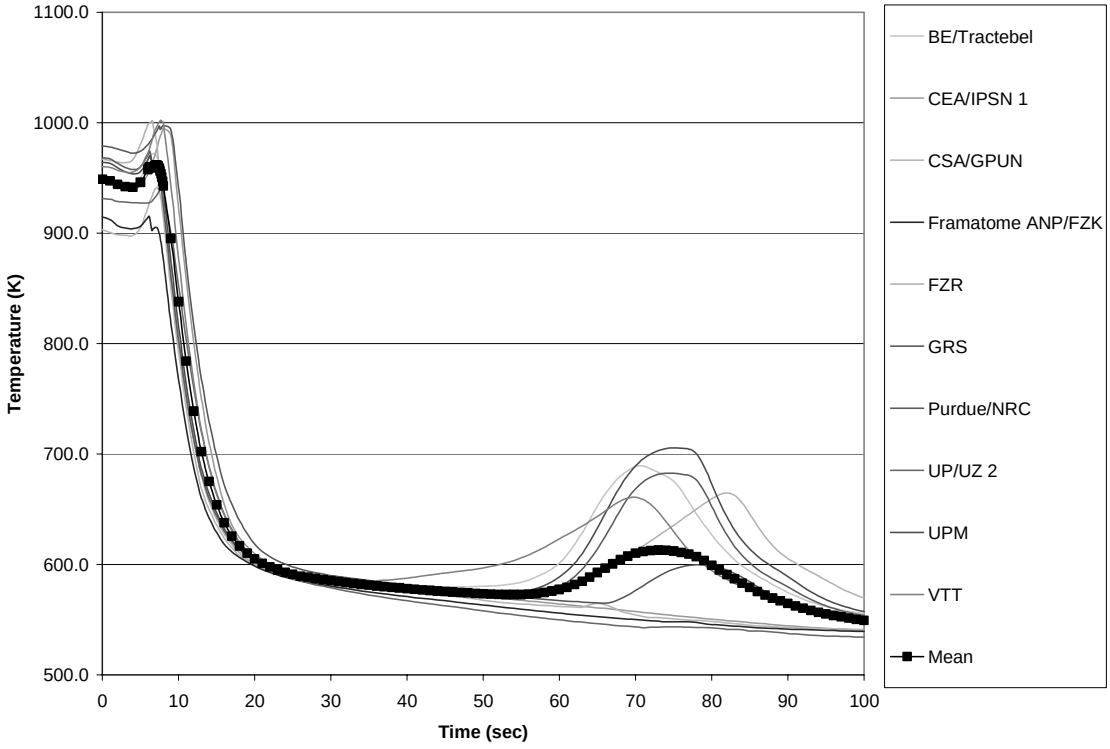

Figure 4.37. Core-averaged fission power time history for Scenario 1

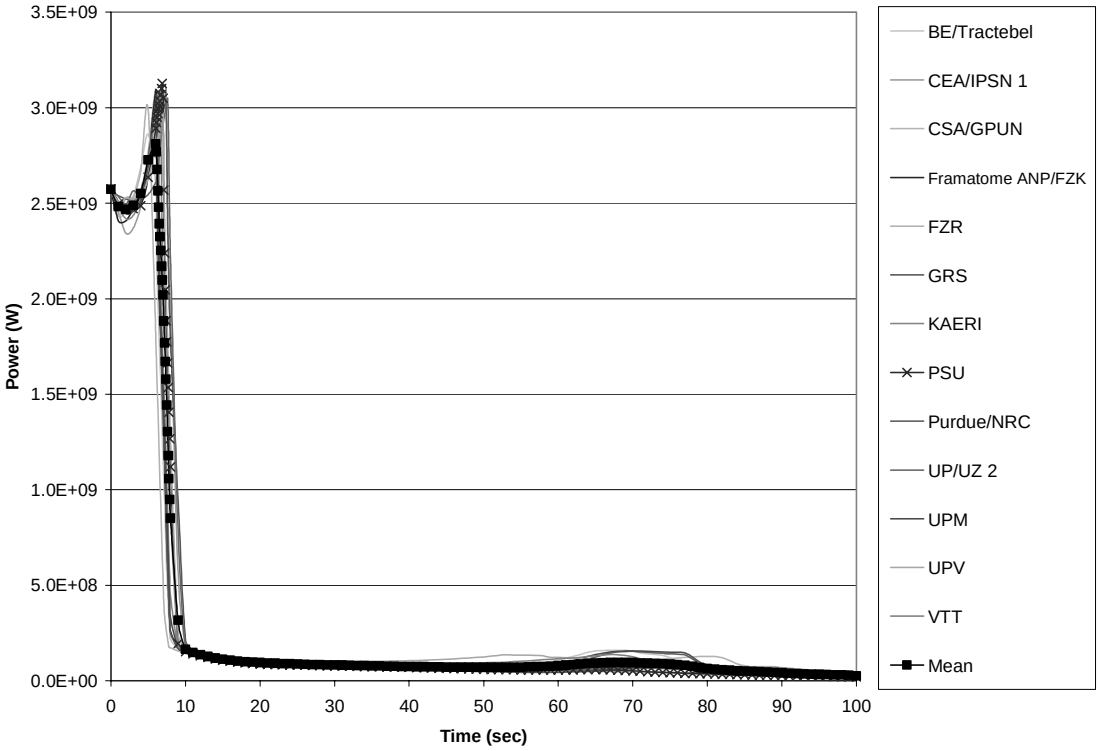

Figure 4.38. Core-averaged total power time history for Scenario 1

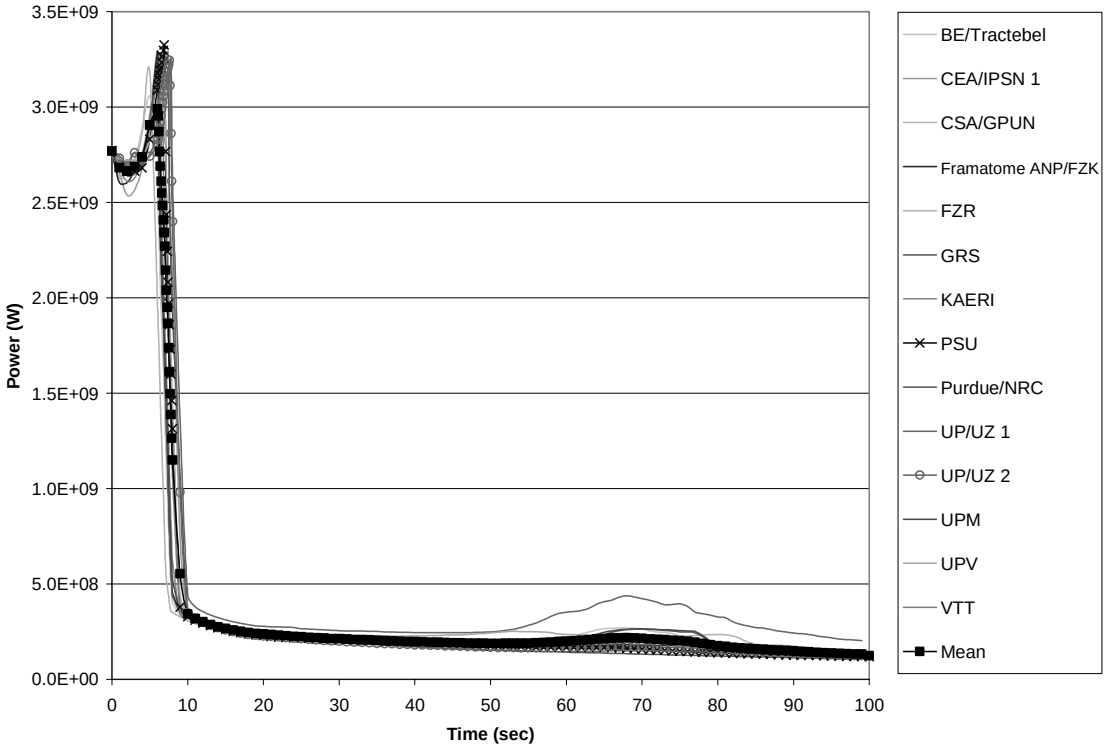

Figure 4.39. Core-averaged total reactivity time history for Scenario 1

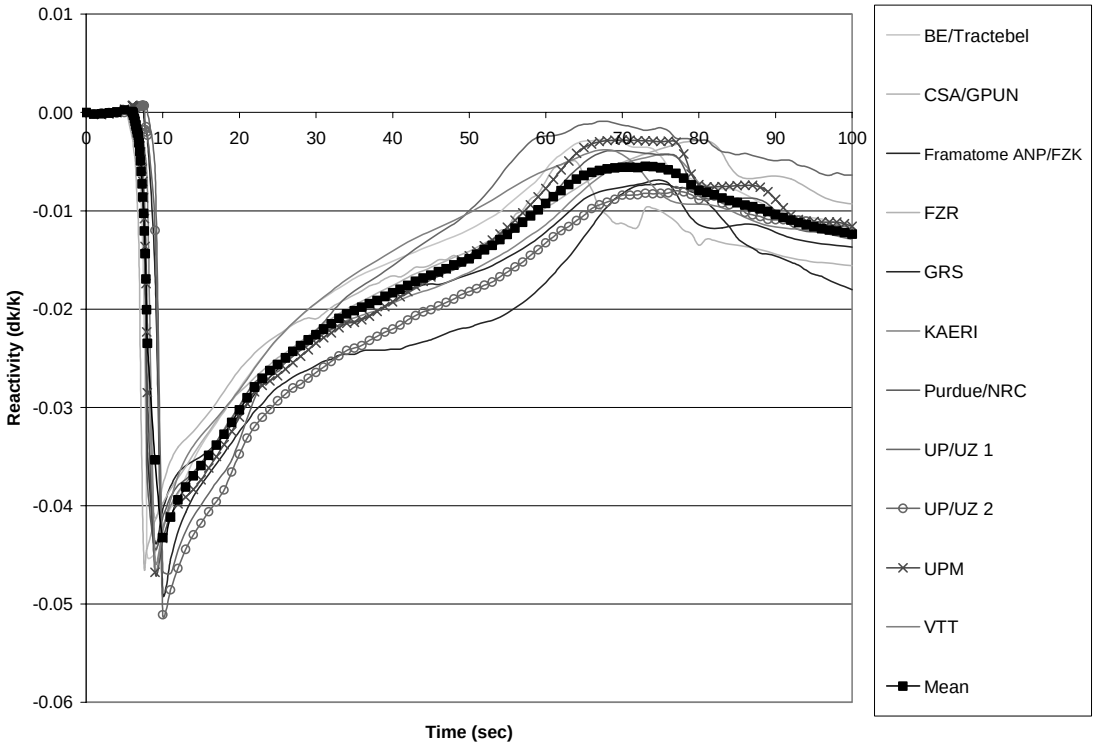

Figure 4.40. Core-averaged coolant density time history for Scenario 1

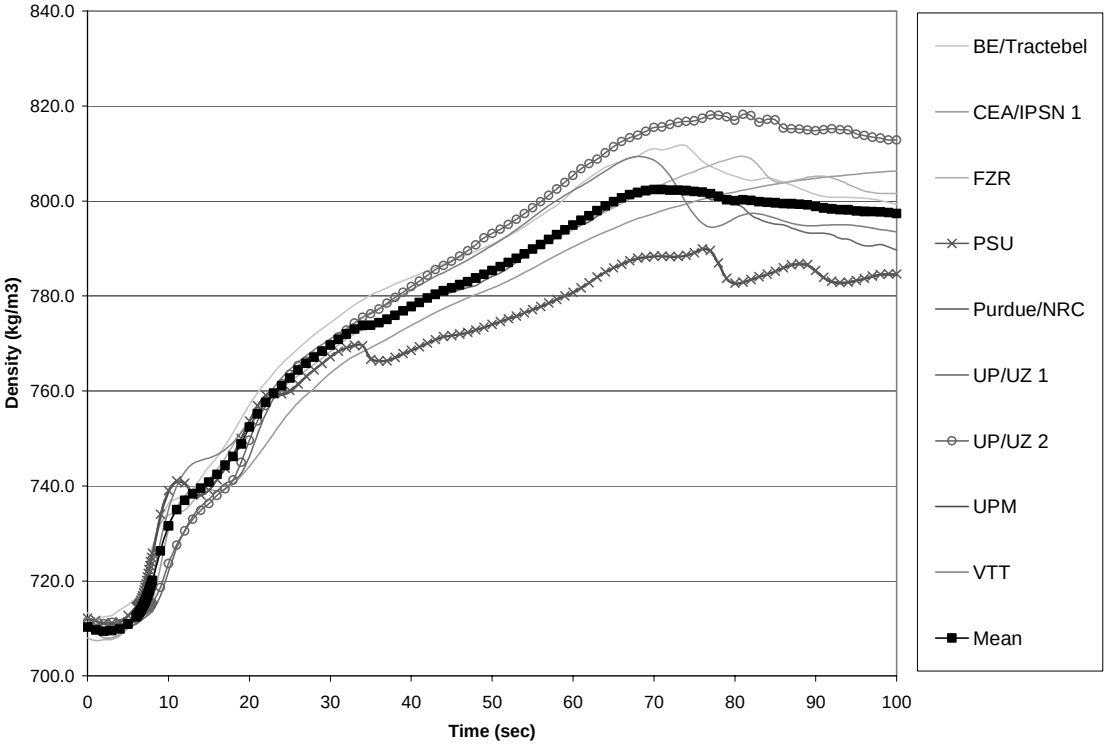

Figure 4.41. Broken SG mass for Scenario 1

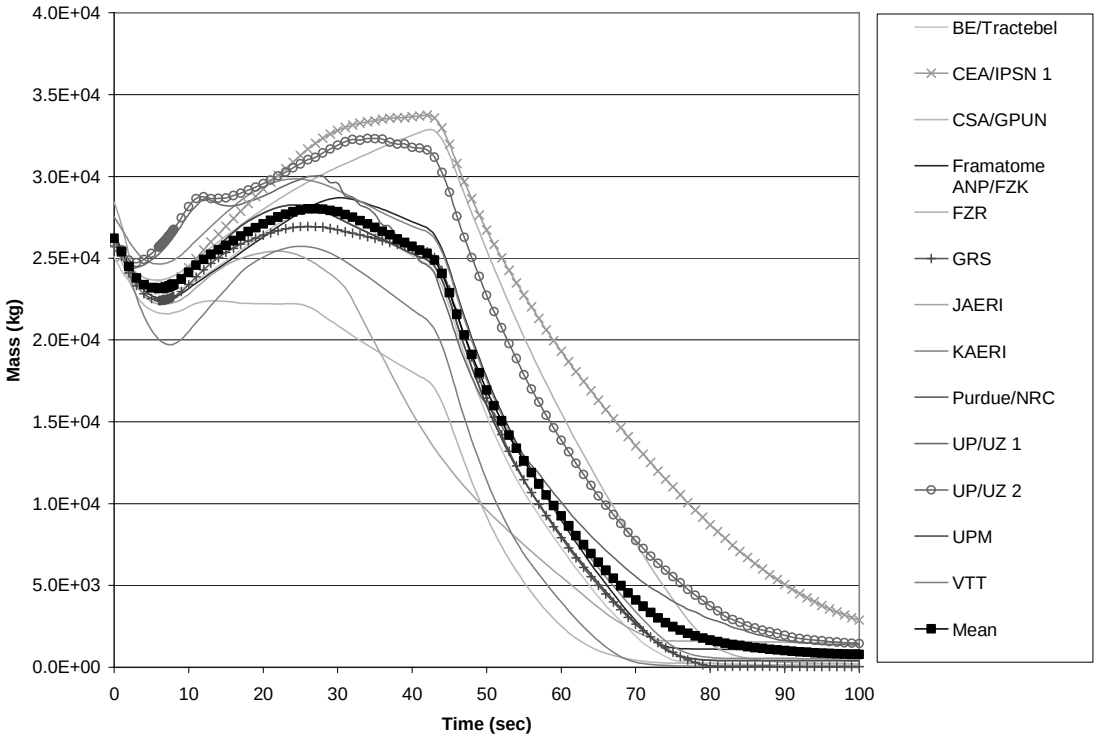

Figure 4.42. Intact SG mass for Scenario 1

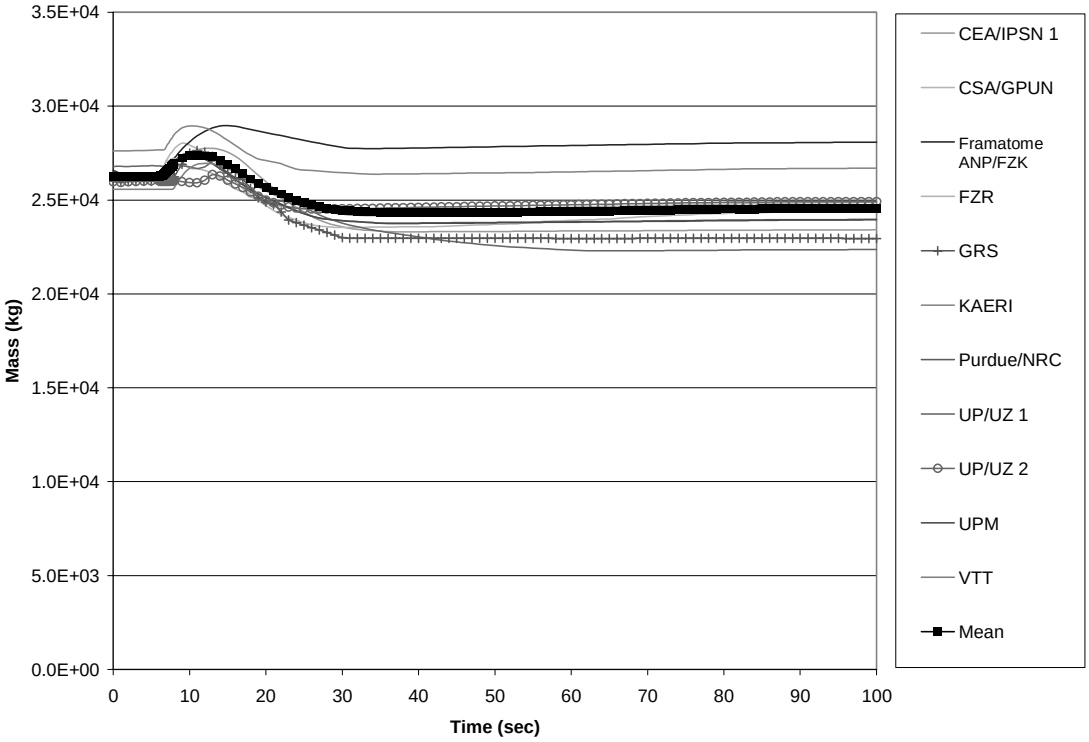

Figure 4.43. Broken SG exchanged power for Scenario 1

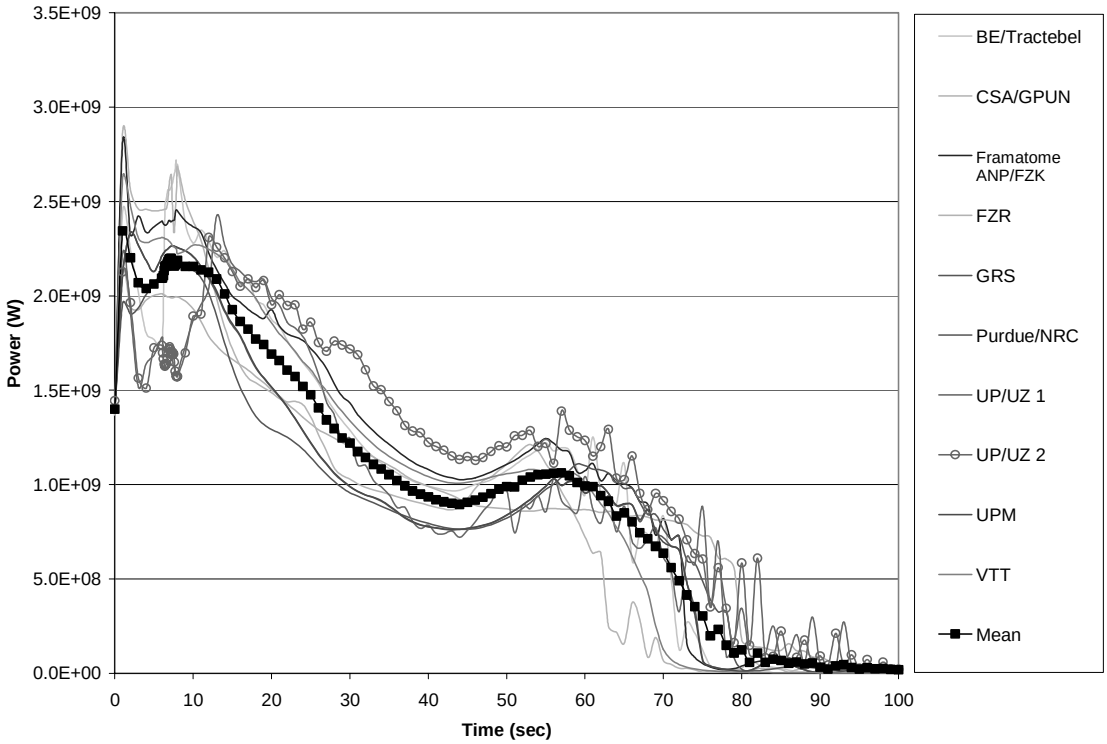

Figure 4.44. Intact SG exchanged power for Scenario 1

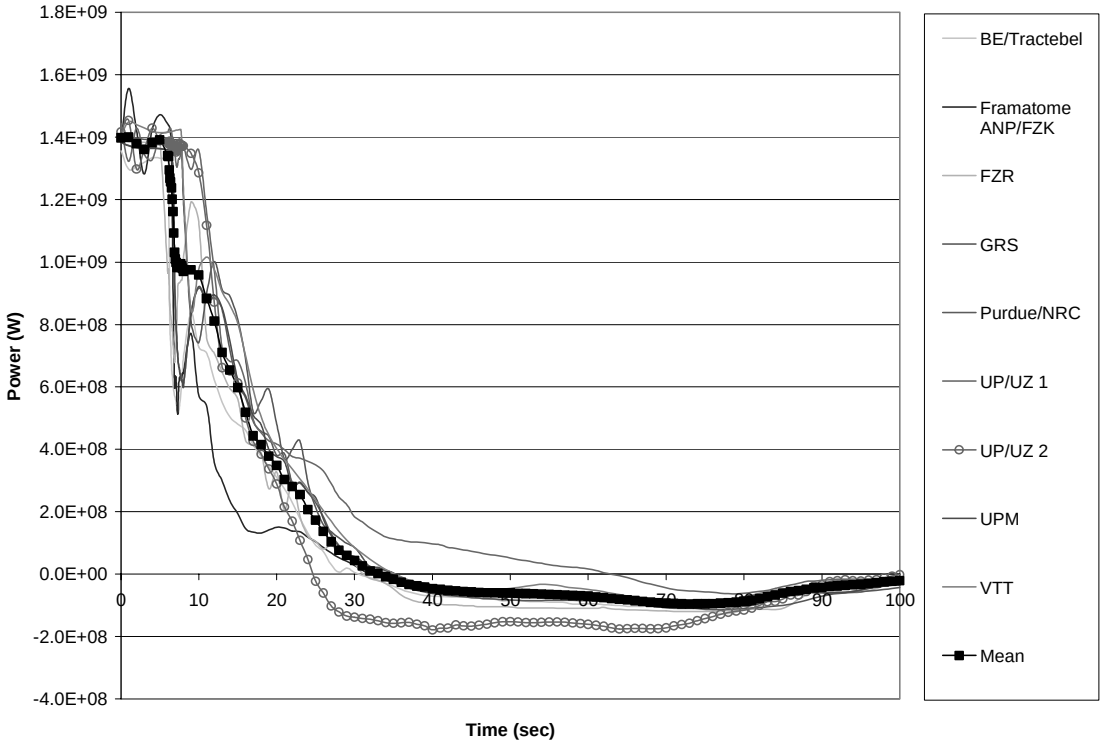

Figure 4.45. Integrated steam break flow for Scenario 1

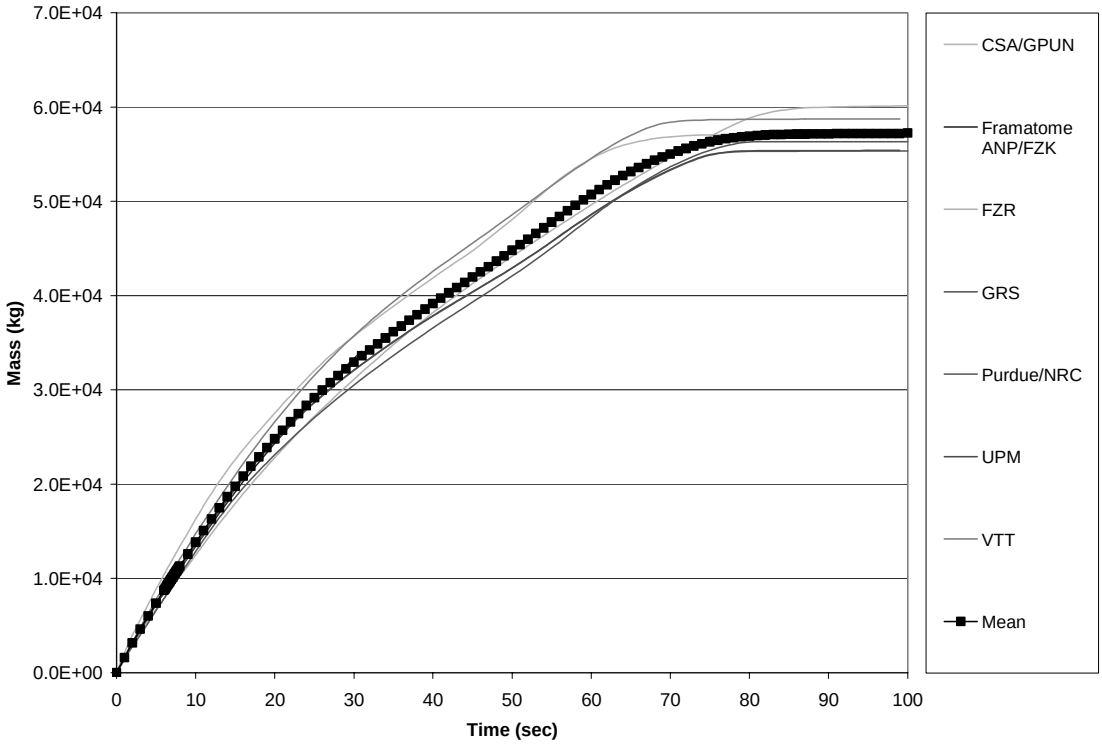

Figure 4.46. Integrated liquid break flow for Scenario 1

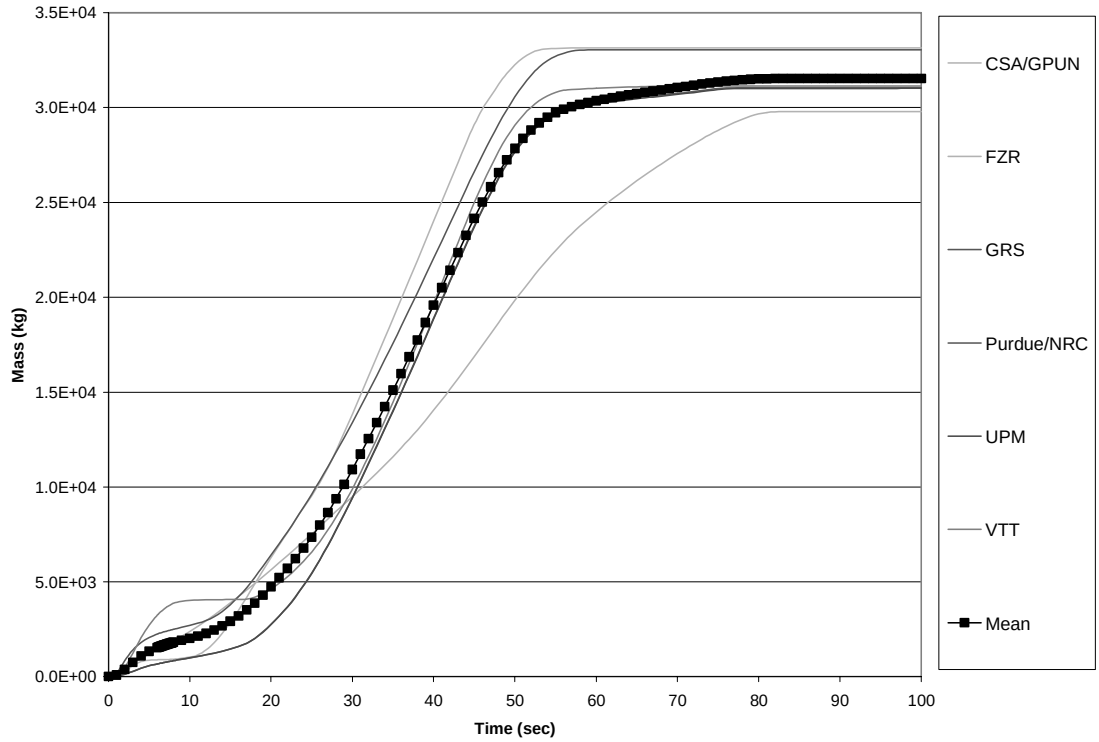

Figure 4.47. Total break flow rate for Scenario 2

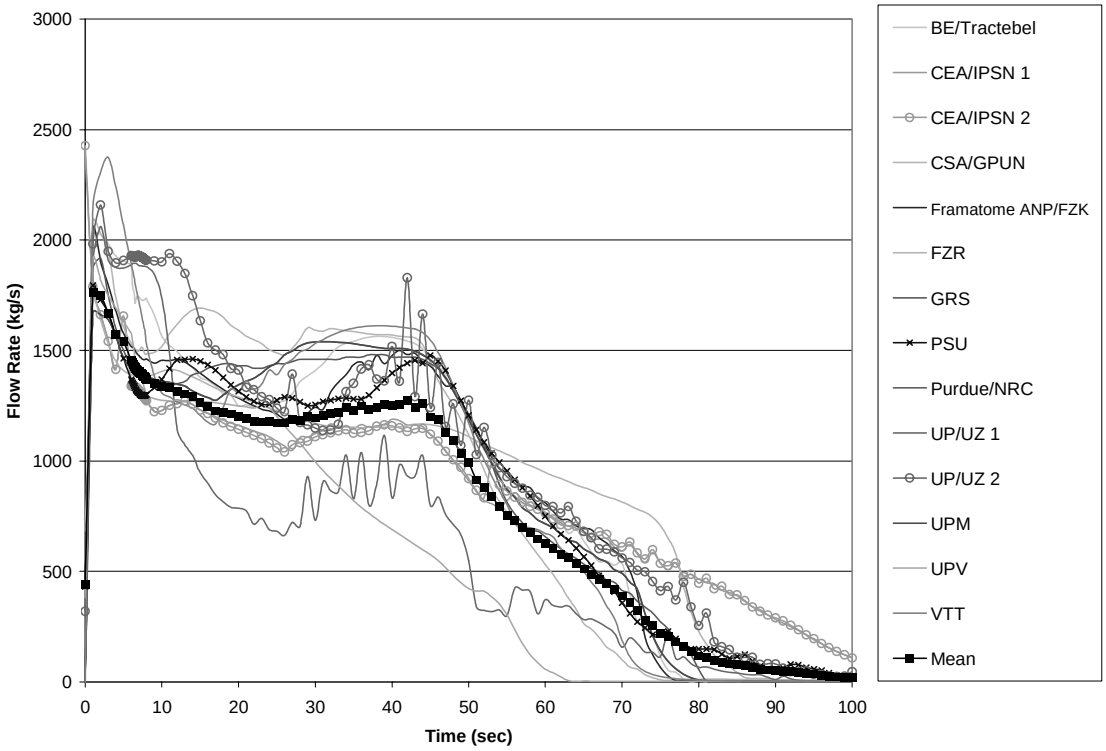

Figure 4.48. Break flow rate for Scenario 2 – 24 inch

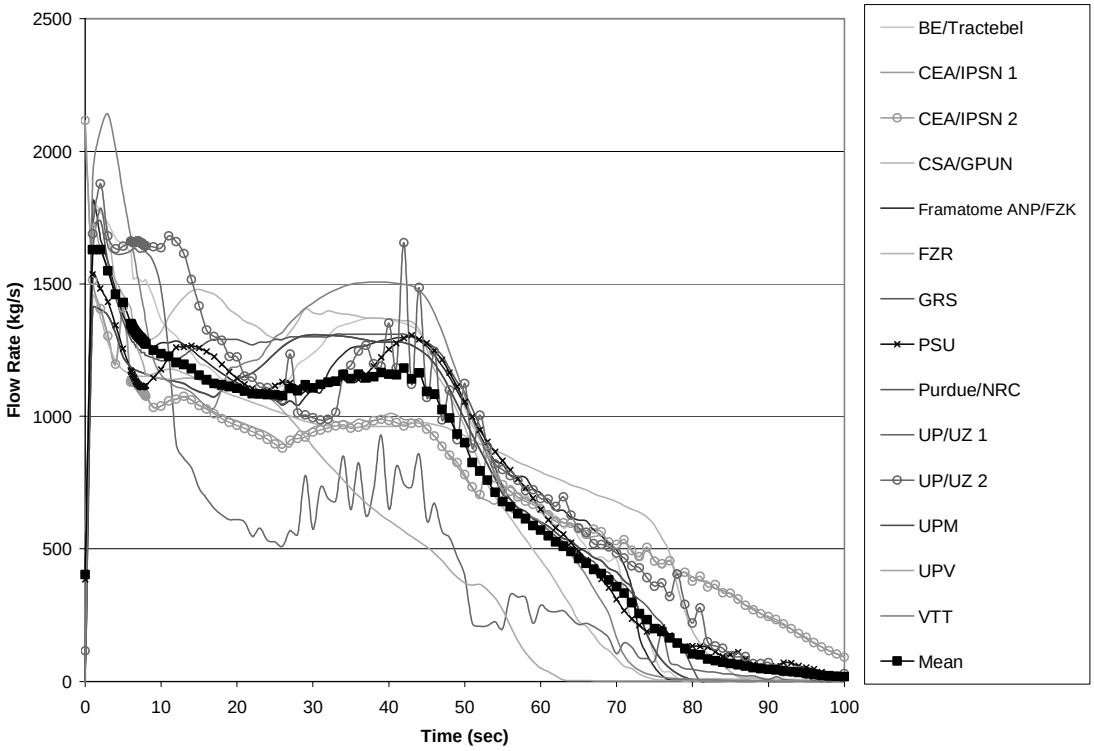

Figure 4.49. Break flow rate for Scenario 2 – 8 inch

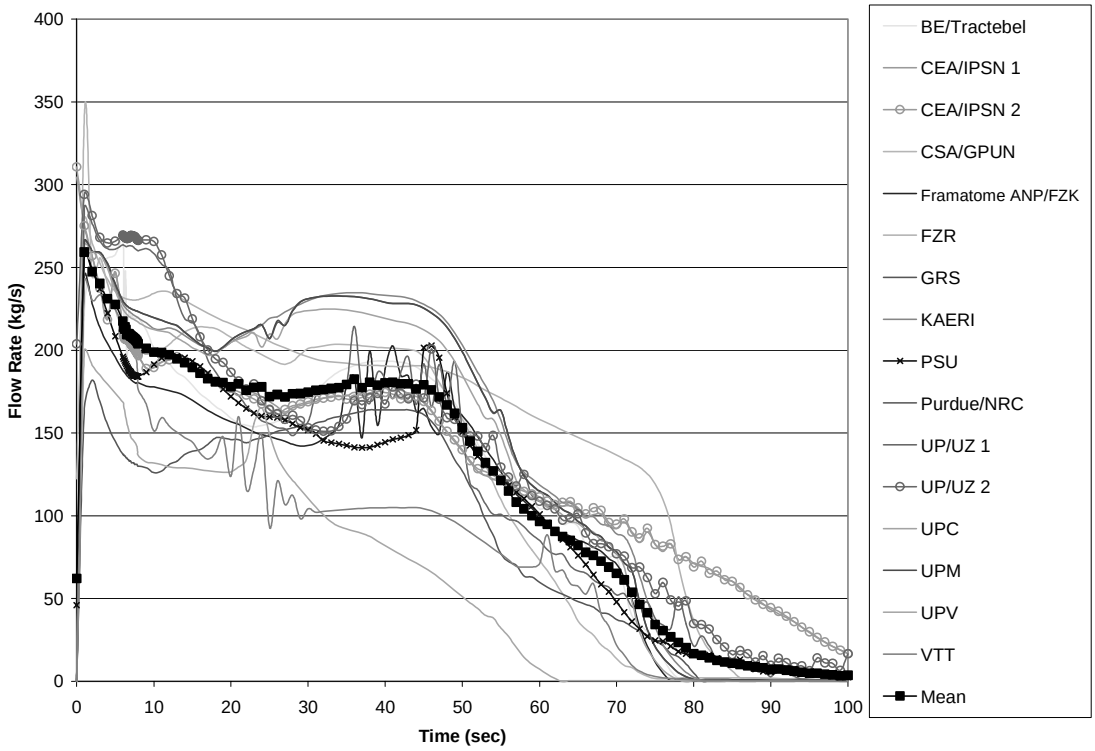

Figure 4.50. Average RCS pressure for Scenario 2

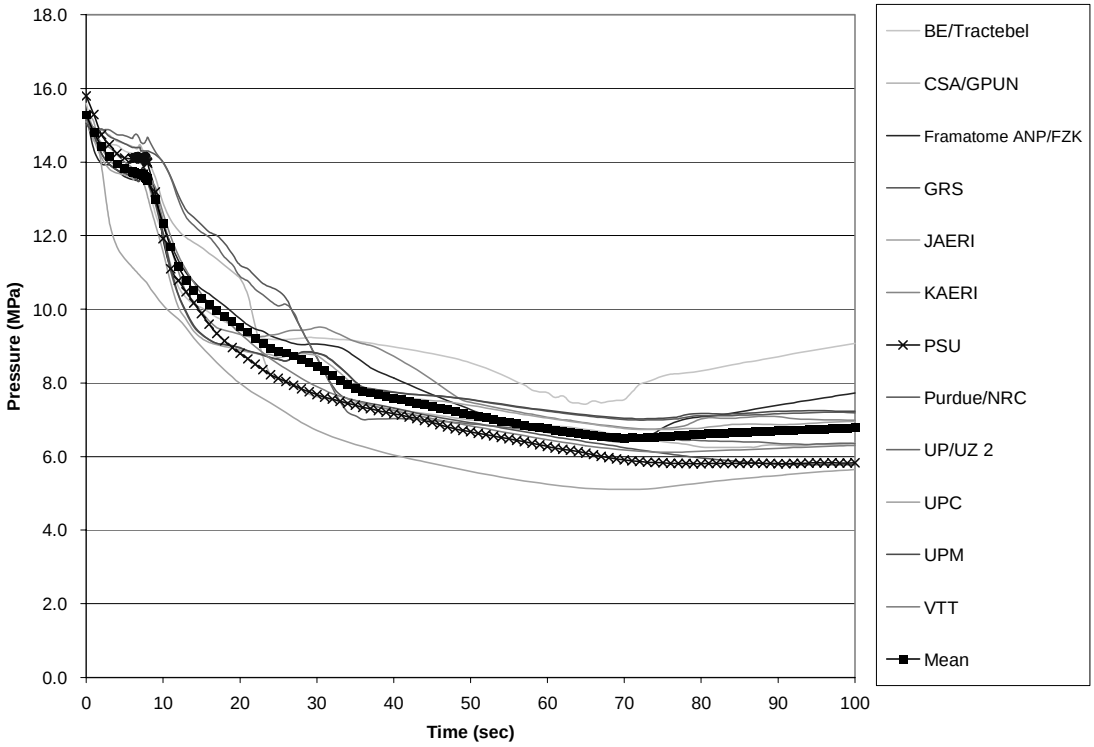

Figure 4.51. Broken loop hot leg pressure for Scenario 2

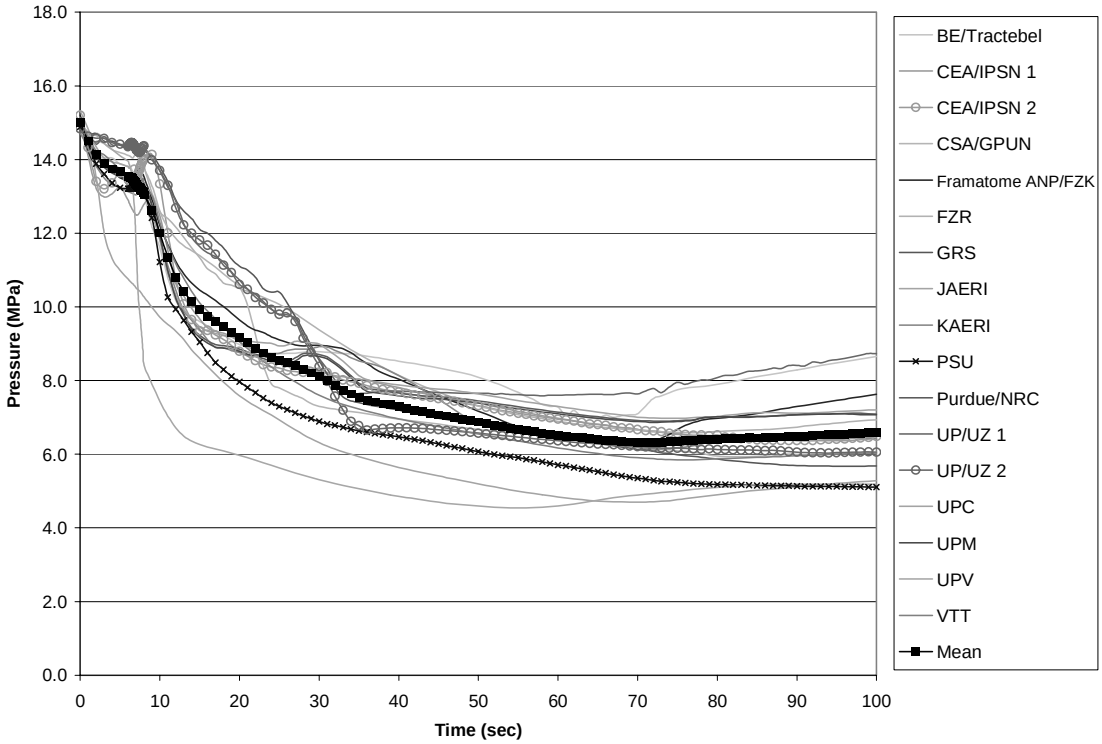

Figure 4.52. Intact loop hot leg pressure for Scenario 2

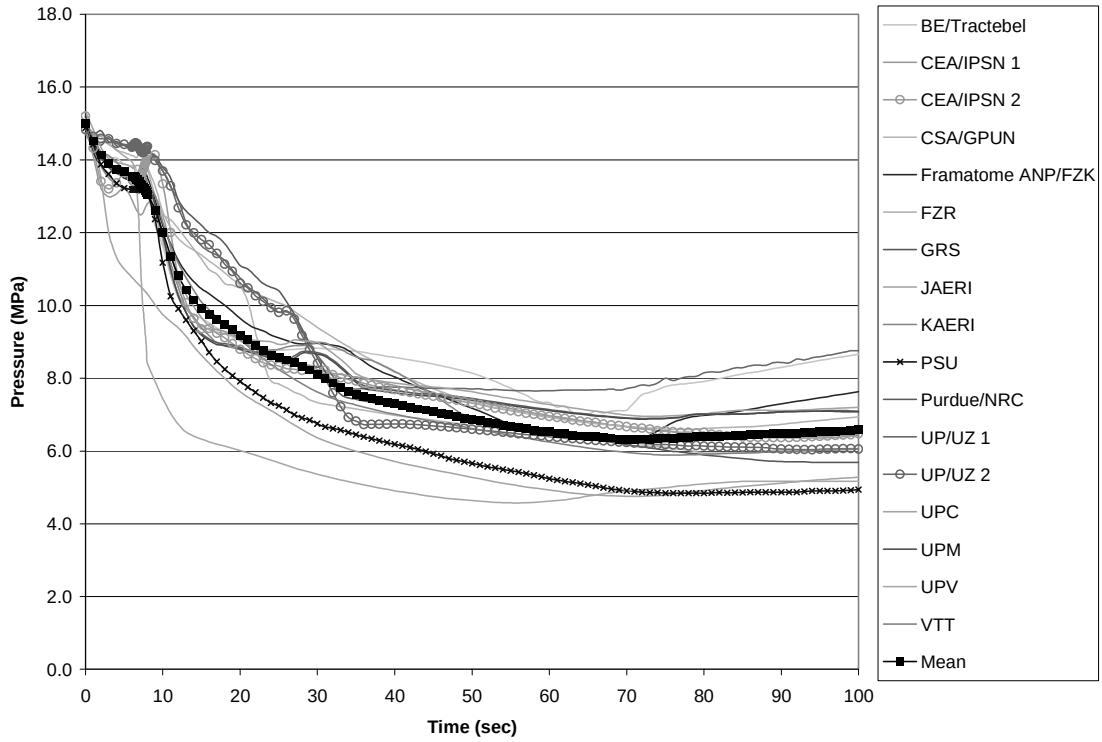

Figure 4.53. Broken loop steam line pressure for Scenario 2

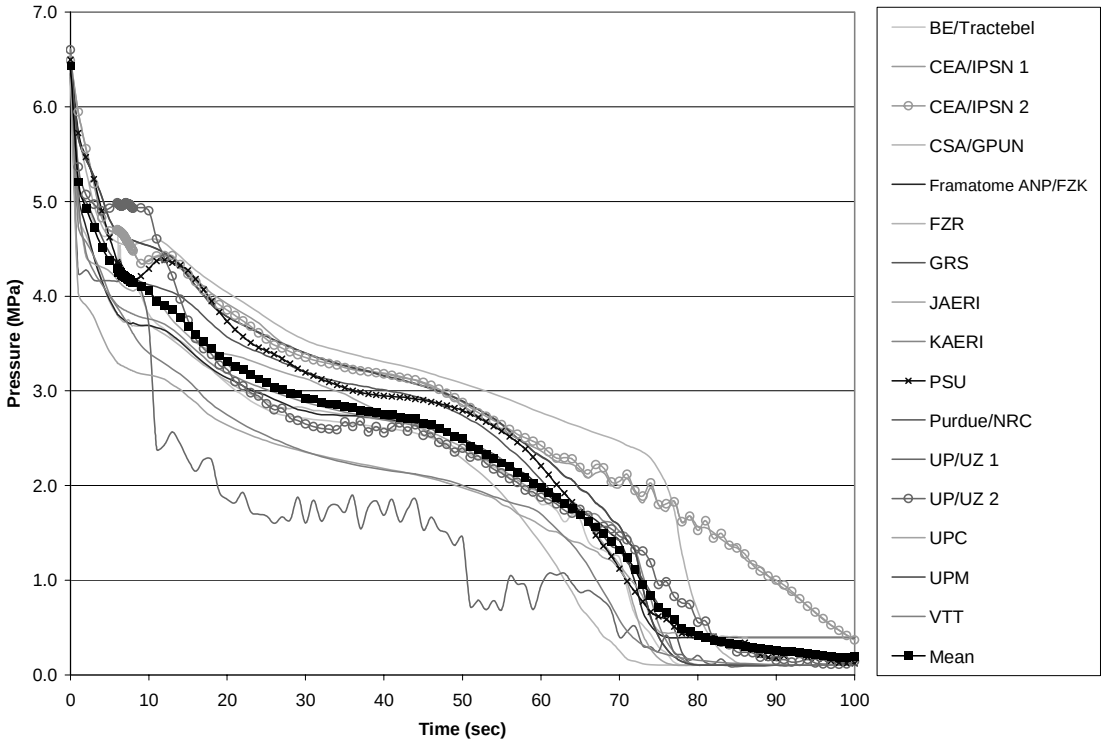

Figure 4.54. Intact loop steam line pressure for Scenario 2

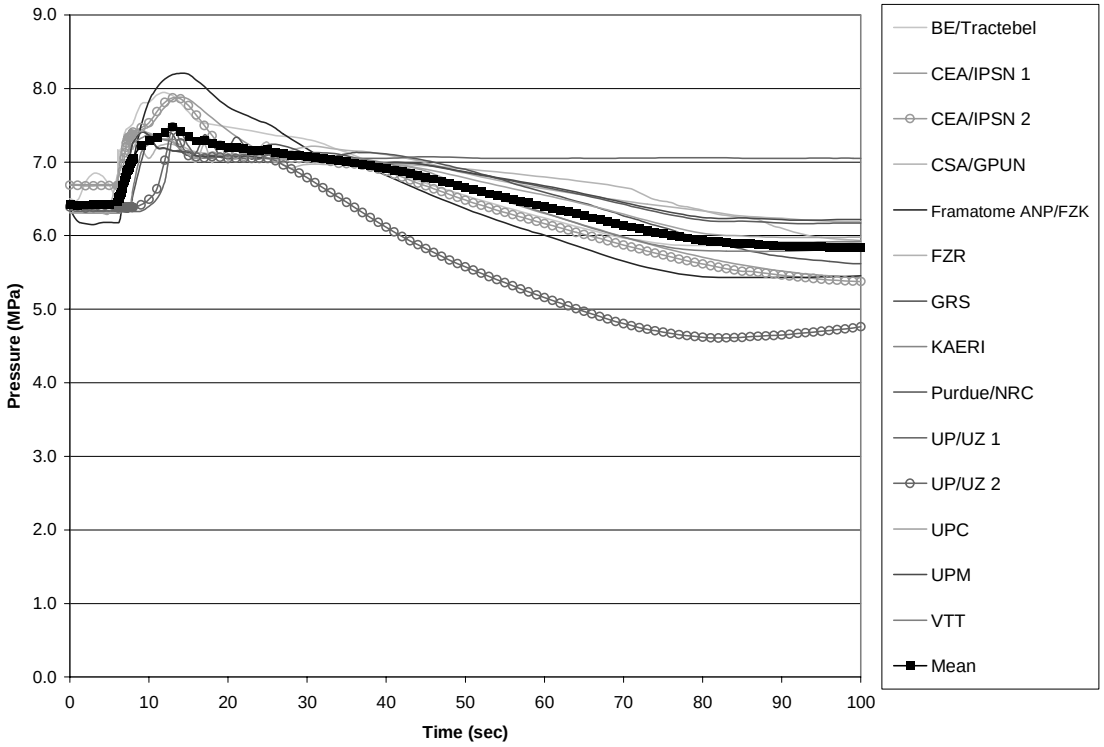

Figure 4.55. Average coolant temperature for Scenario 2

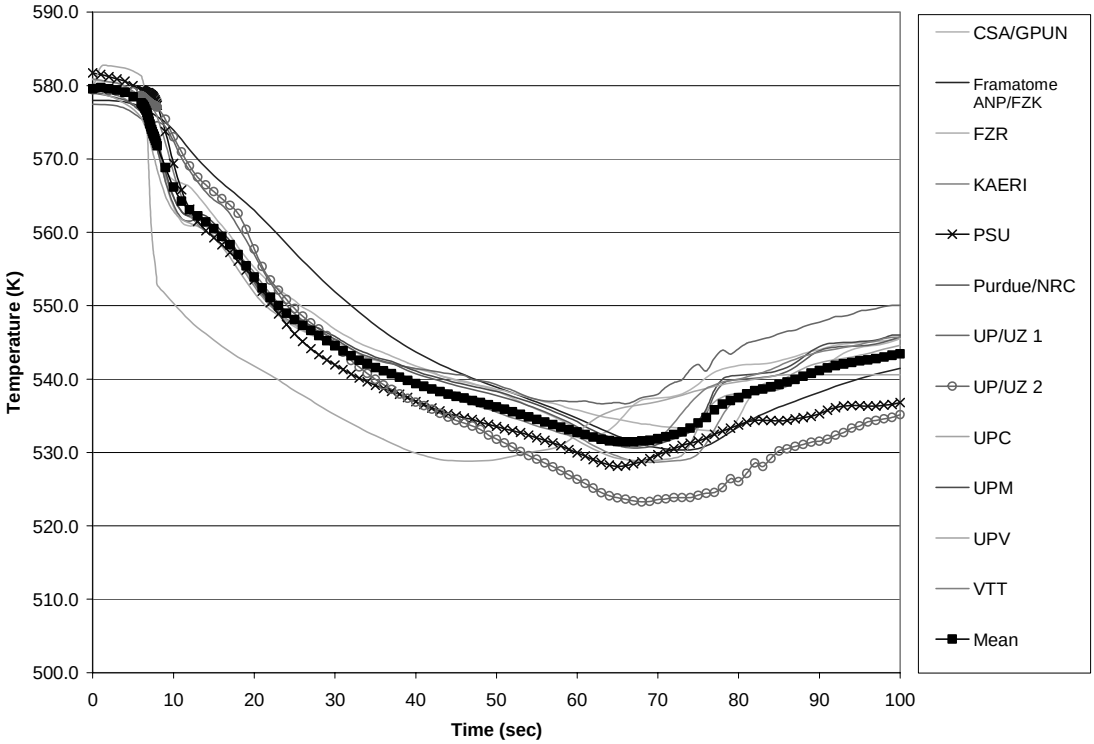

Figure 4.56. Broken loop hot leg temperature for Scenario 2

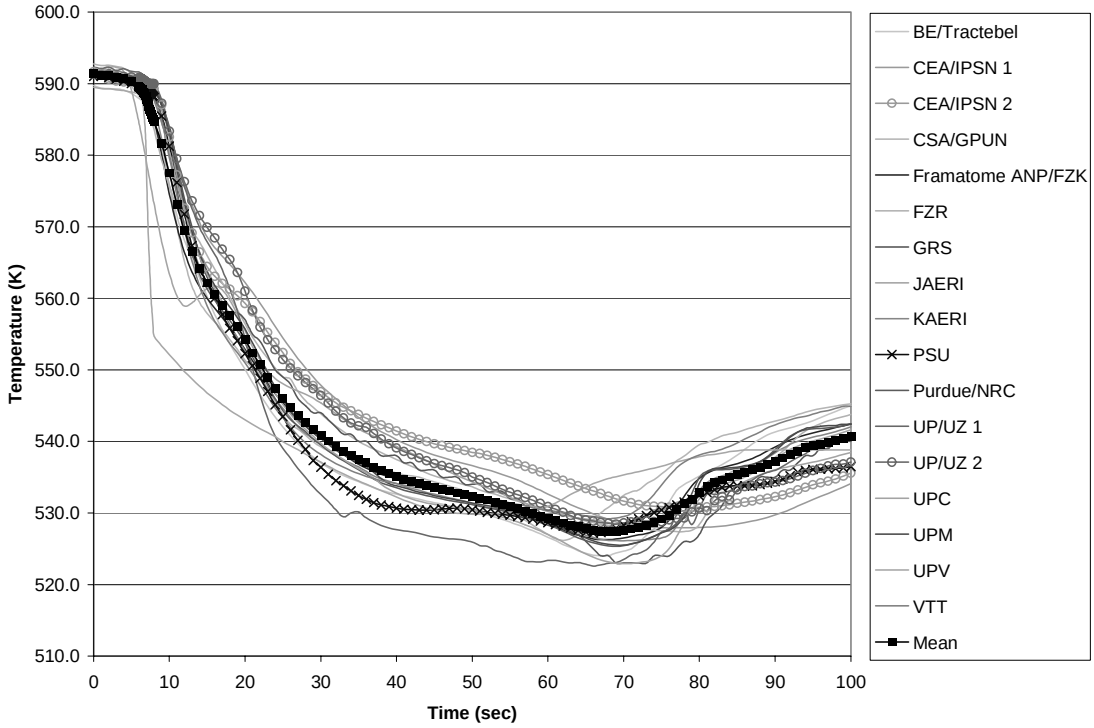

Figure 4.57. Intact loop hot leg temperature for Scenario 2

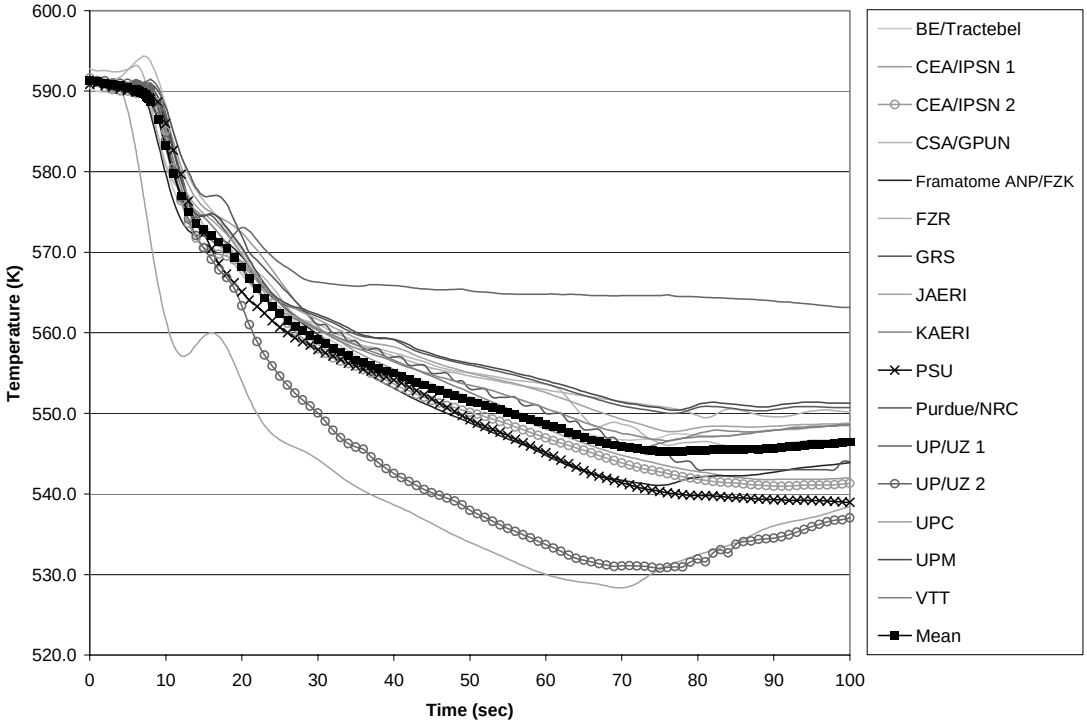

Figure 4.58. Broken loop cold leg temperature for Scenario 2

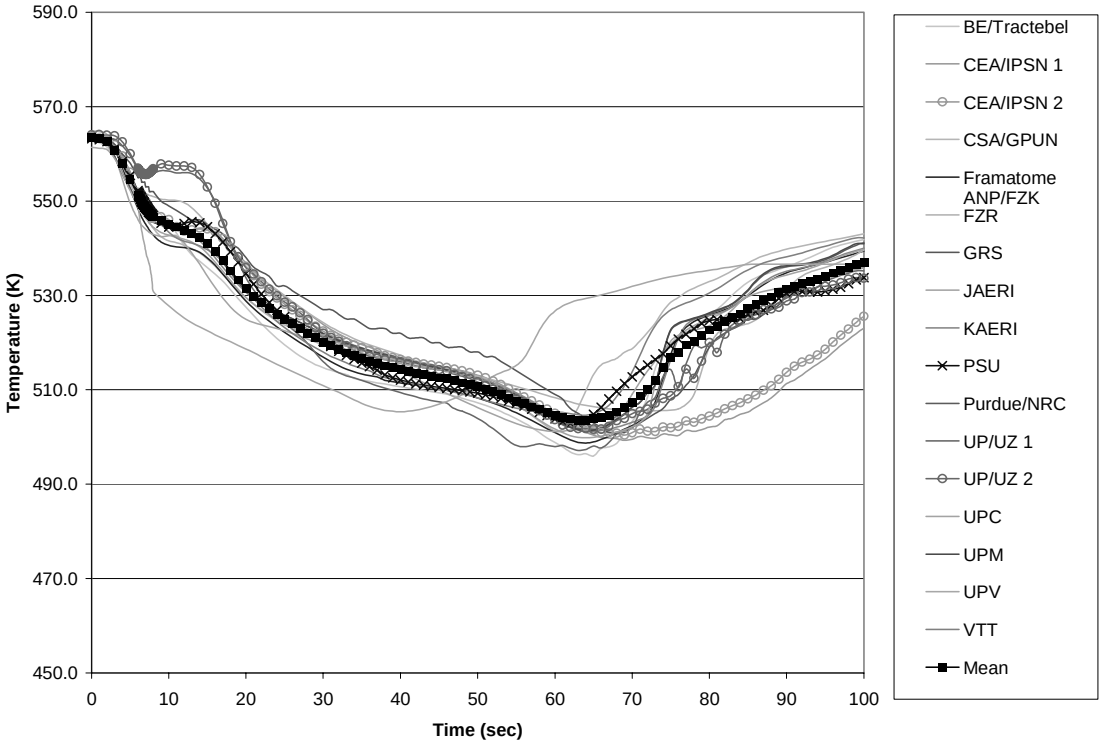

Figure 4.59. Intact loop cold leg temperature for Scenario 2

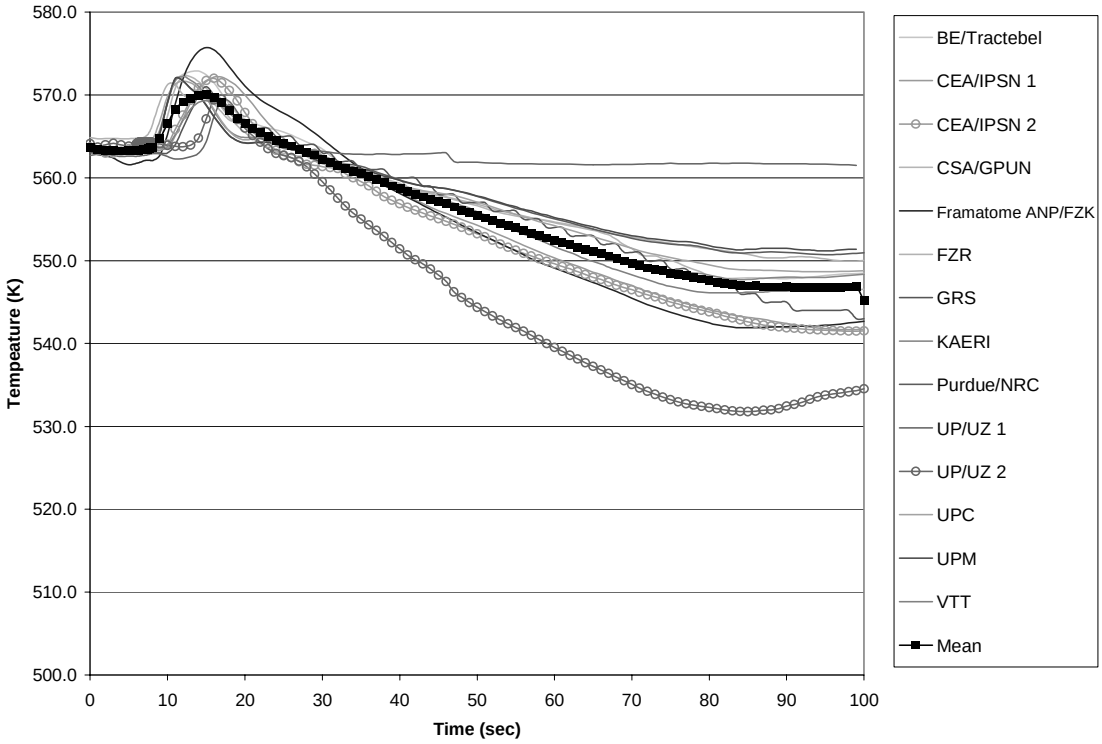

Figure 4.60. Core-averaged Doppler temperature time history for Scenario 2

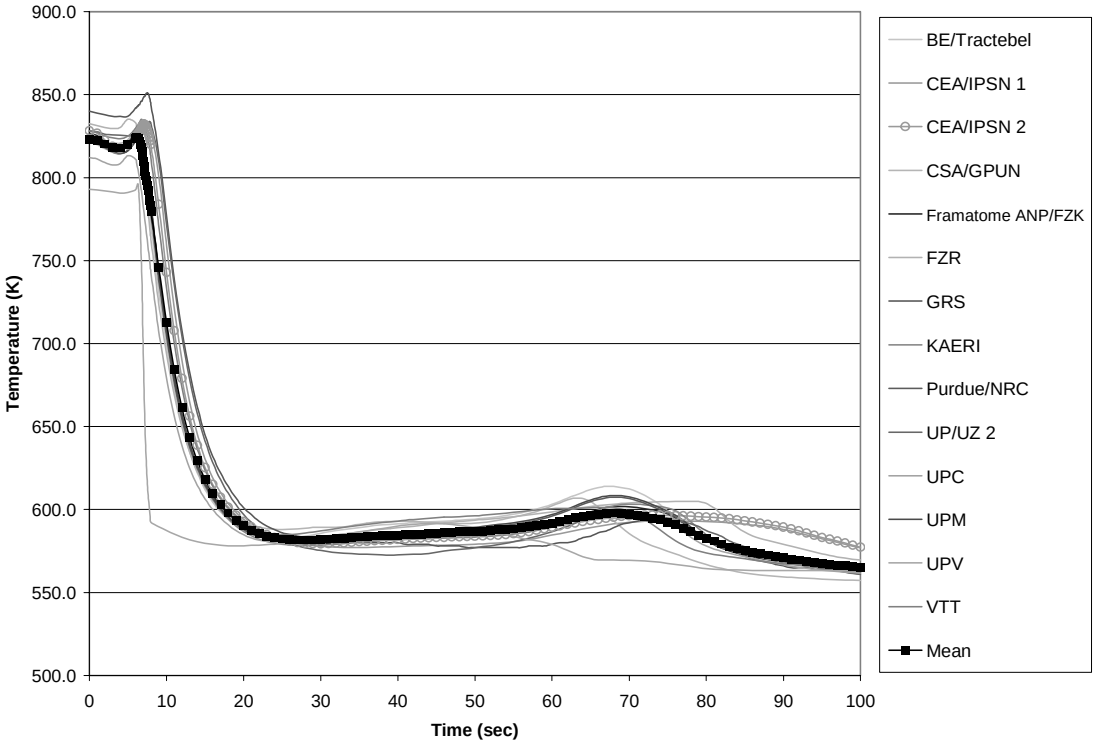

Figure 4.61. Maximum nodal Doppler temperature time history for Scenario 2

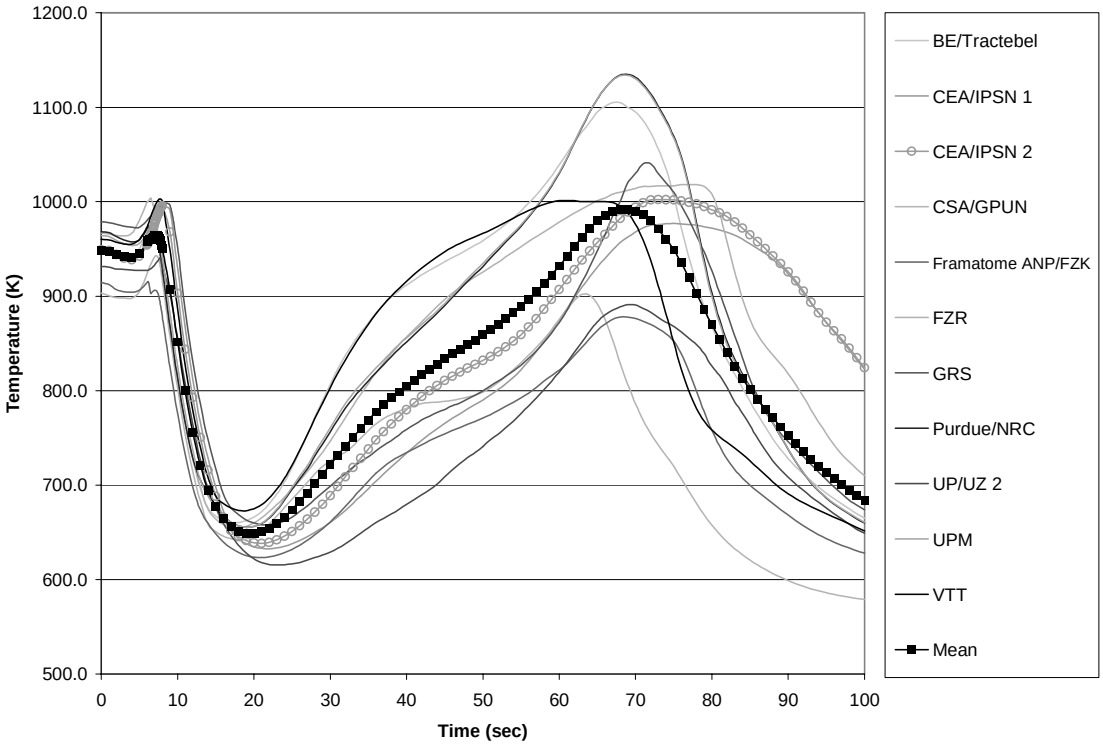

Figure 4.62. Core-averaged fission power time history for Scenario 2

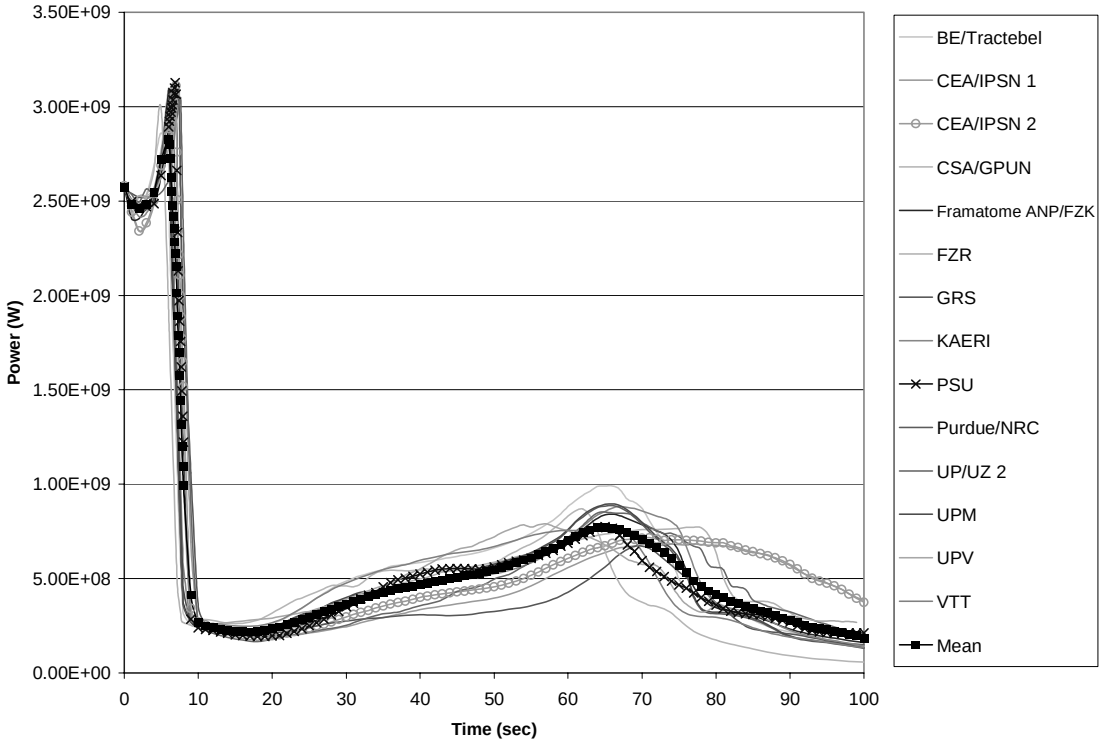

Figure 4.63. Core-averaged total power time history for Scenario 2

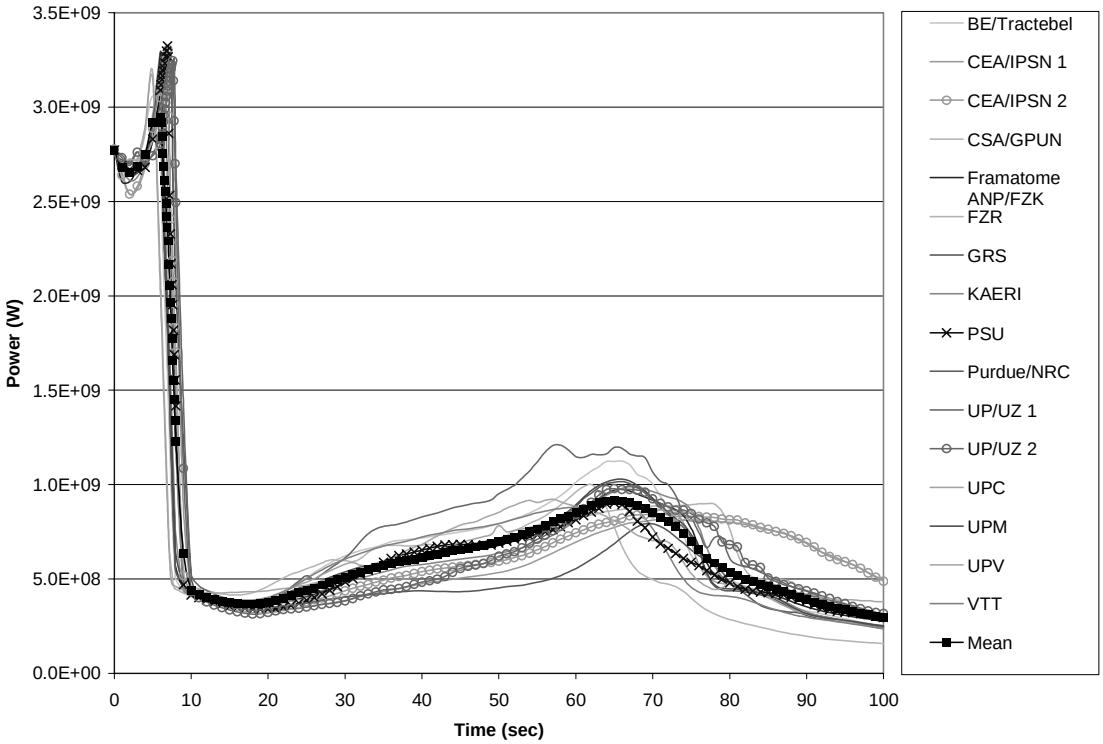

Figure 4.64. Core-averaged total reactivity time history for Scenario 2

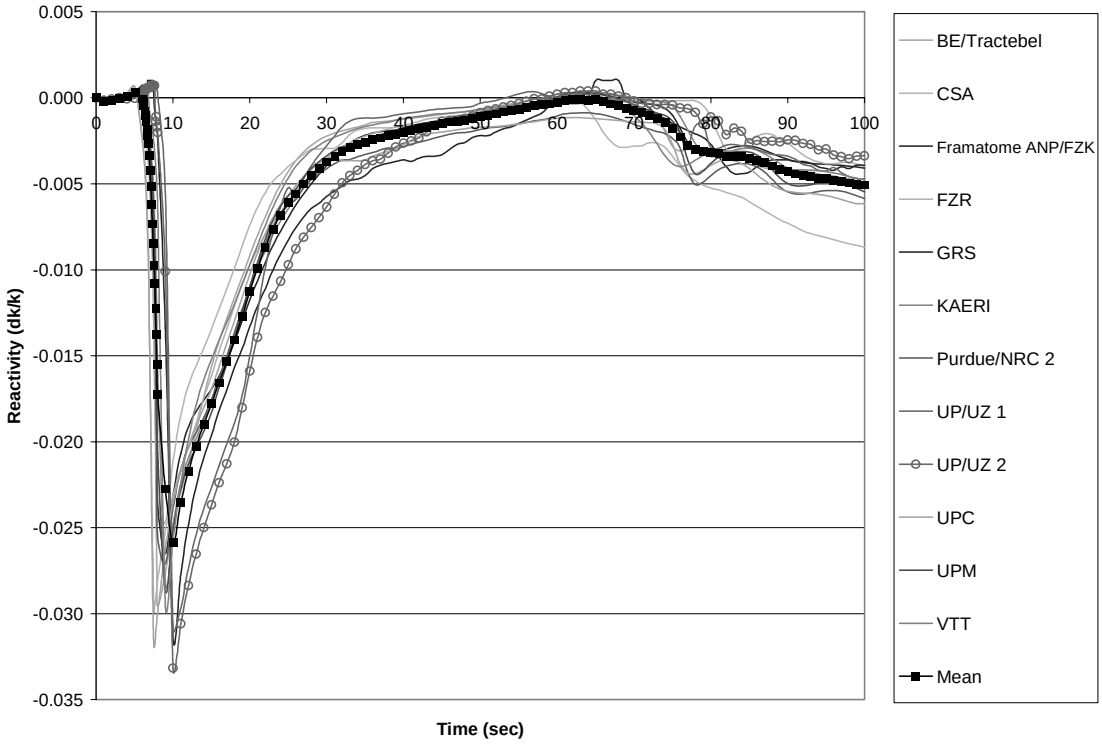

Figure 4.65. Core-averaged coolant density time history for Scenario 2

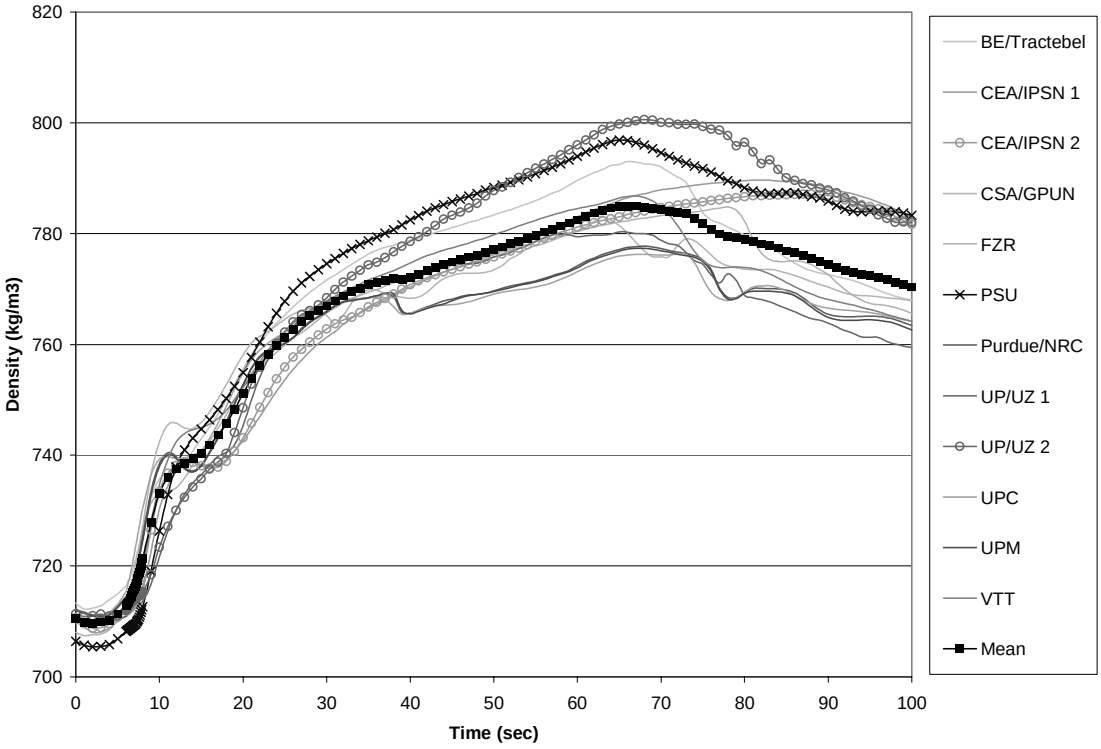

Figure 4.66. Broken SG mass for Scenario 2

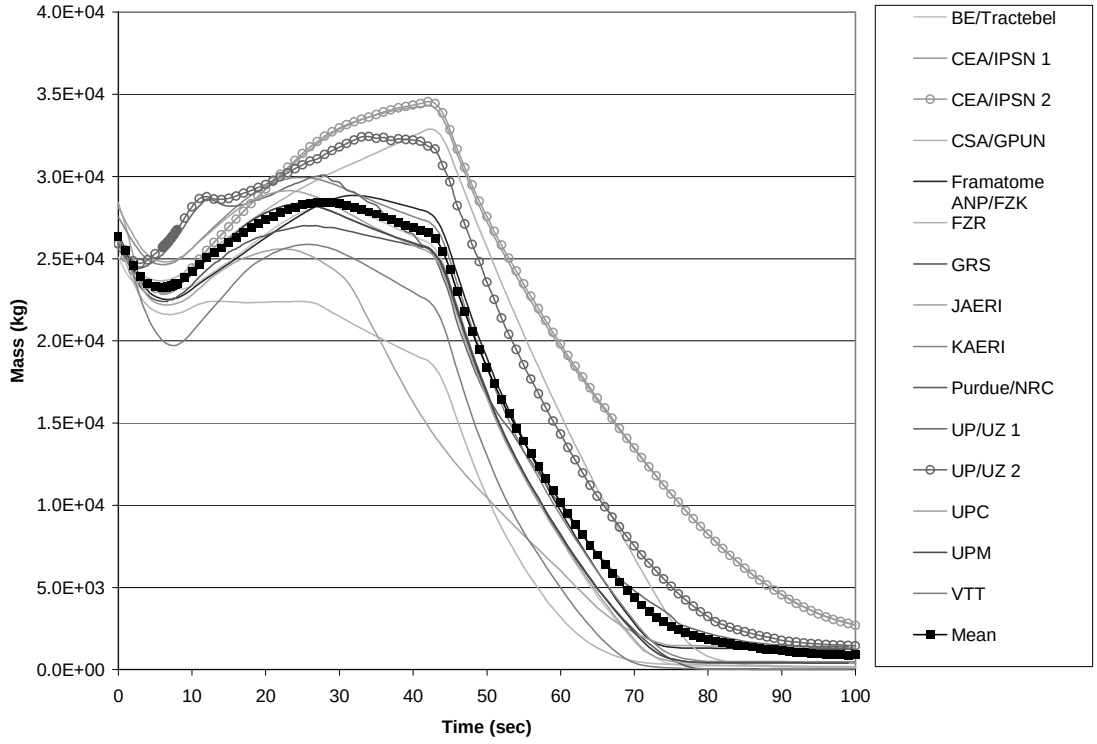

Figure 4.67. Intact SG mass for Scenario 2

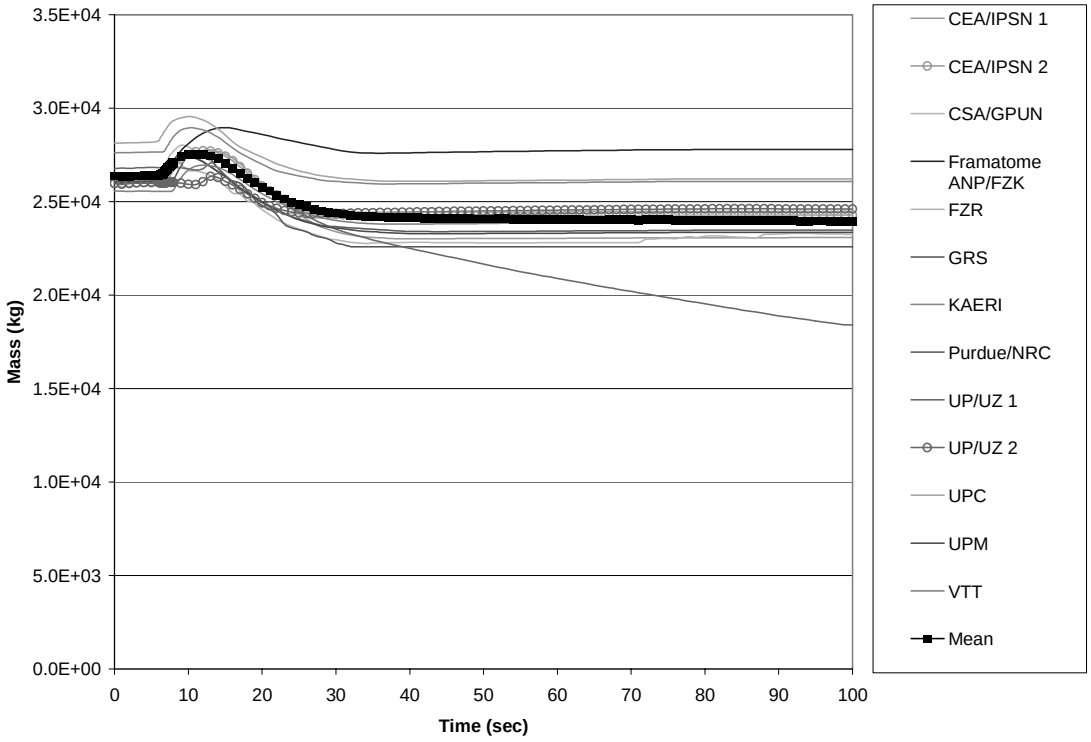

Figure 4.68. Broken SG exchanged power for Scenario 2

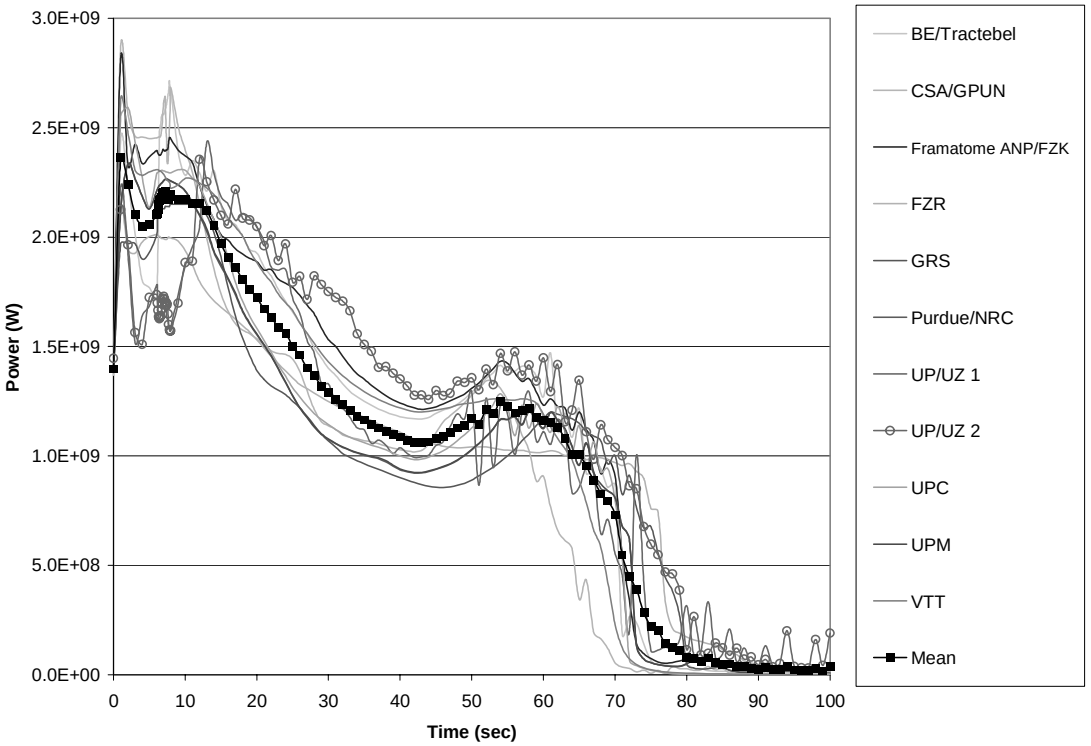

Figure 4.69. Intact SG exchanged power for Scenario 2

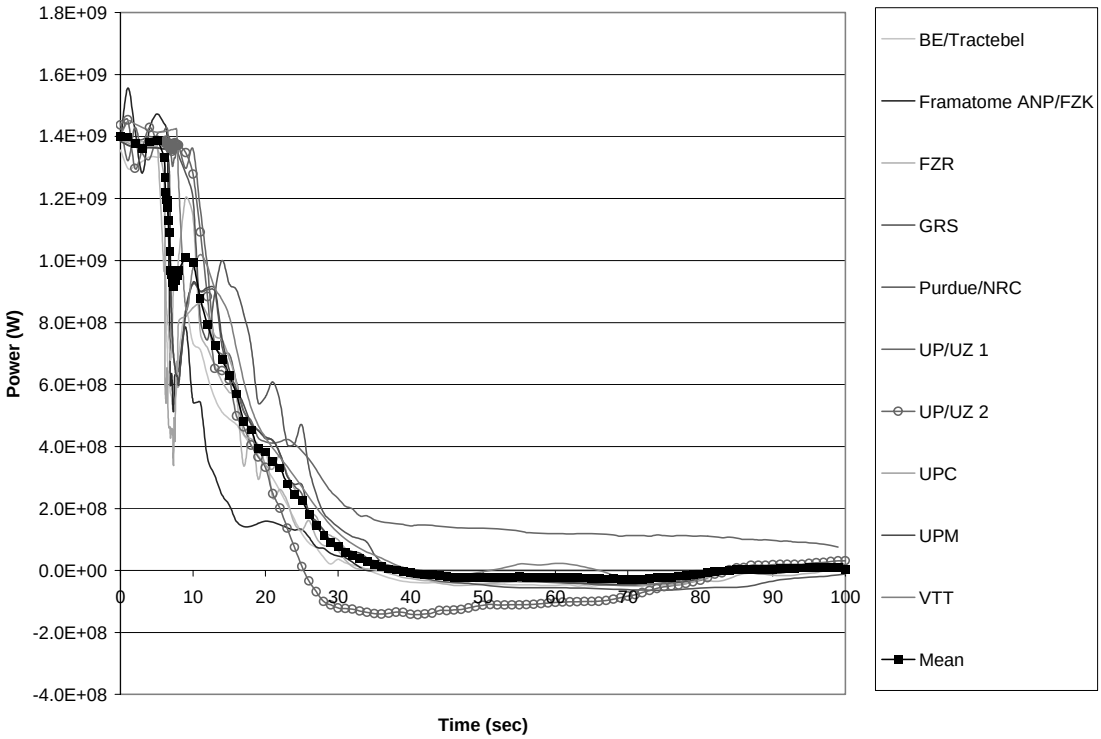

Figure 4.70. Integrated steam break flow for Scenario 2

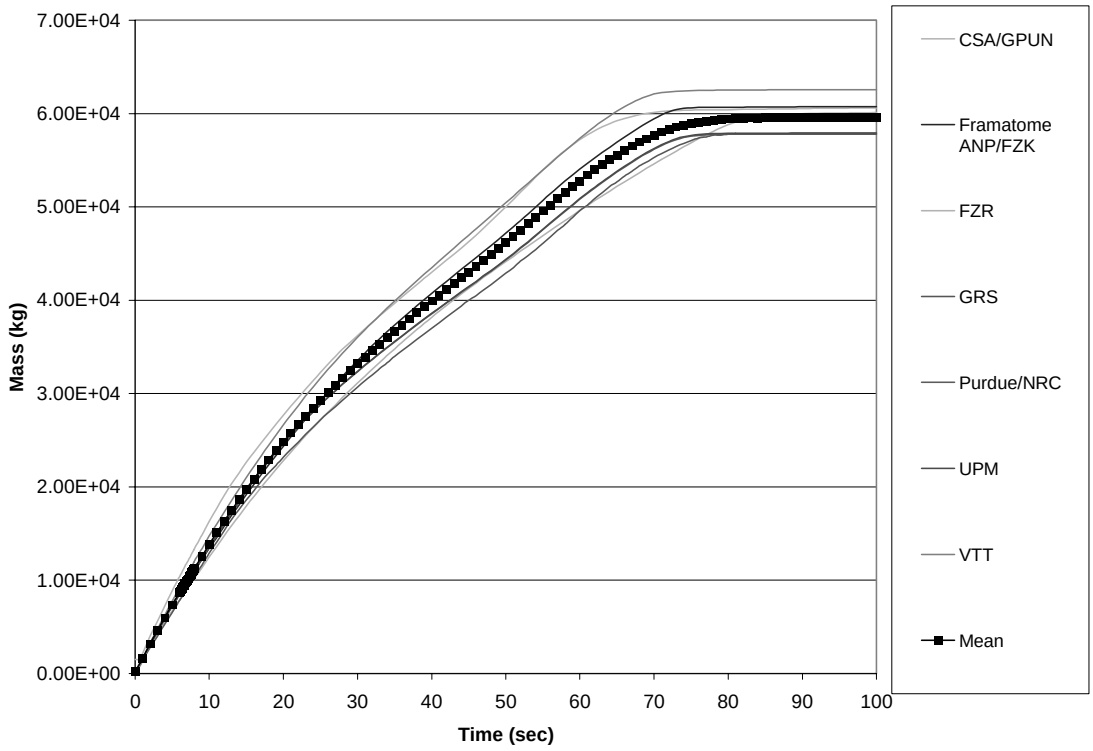

Figure 4.71. Integrated liquid break flow for Scenario 2

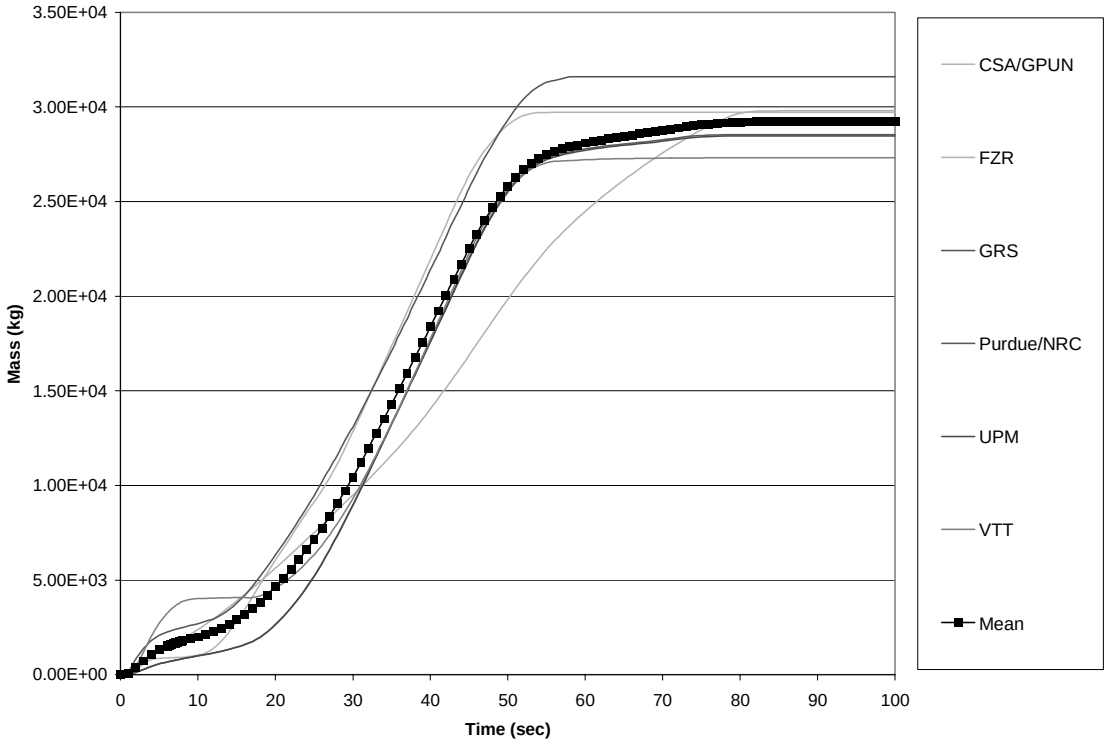

Chapter 5

CONCLUSIONS

In order to meet the objectives of the validation of best-estimate coupled codes a systematic approach has been introduced to evaluate the PWR MSLB transient. Such coupled codes use separate temporal and spatial models and numerical methods for core neutronics, core thermal-hydraulics and system thermal-hydraulics simulations. Therefore, the validation of these codes should include a testing of these models for the defined transient (in this case a MSLB) as phases (separate exercises) of the overall benchmark. The ultimate goal is to enable participants to initialise and verify these models before focusing on the major objective – testing of coupling methodologies in terms of numerics, temporal and spatial mesh overlays. This systematic approach allows one to evaluate in a more consistent manner the modelling of the combined effects (determined by neutronics/T-H as well as core/plant interactions) and removes the uncertainties introduced with the separate models. In order to perform such a comprehensive validation of coupled codes a multi-level methodology is employed. The methodology includes the application of three exercises (phases), the evaluation of several steady states and the simulation of two transient scenarios.

The analysis of the MSLB benchmark has been performed in an iterative manner. The specific list of relevant parameters for comparison in each exercise has been finally determined after preliminary calculations and comparisons were performed. The practical experience gained in this benchmark shows that only after such preliminary analysis can the peculiarities and requirements of the modelling be fixed. To this end, the international benchmark workshops and the *ad hoc* meetings (held in conjunction with international conferences) have played a very important role as forums for discussing obtained results, observed deviations, sources of modelling uncertainties and subsequent modifications to the benchmark specification [5-7]. Over the course of the benchmark activities, a professional community has been created, and its members were greatly implicated in the in-depth discussions of different aspects considered in the validation process.

In this volume, the third phase of the OECD/NRC PWR MSLB Benchmark was discussed in detail. It is anticipated that the results of this benchmark problem will assist in the understanding of the behaviour of the next generation of coupled computer codes. Overall, this benchmark has been well accepted internationally, with 15 participants representing 11 countries participating in Phase III, and a similar number participating in the first two phases. The results submitted by the participants for Phase III are used to make code-to-code comparisons and a subsequent statistical analysis. The results encompass several types of data for both thermal-hydraulic and neutronics parameters at the initial steady-state conditions and throughout the MSLB transient, including integral parameters, 1-D axial distributions, 2-D radial distributions and time histories.

Chapter 4 of this volume presented a detailed assessment of the differences among the calculated results submitted by the participants for Phase III. Overall, the participants' results for the integral parameters, the core-averaged axial distributions, and the core-averaged time histories are in good agreement; however, one exception is the core-averaged axial power distributions for the transient snapshots (especially after the scram). This parameter shows more pronounced deviations amongst participant results, both in the value and behaviour throughout the transient. Any disagreement can be

attributed to differences in the spatial decay-heat modelling as explained in Chapter 4. These differences also influence the local (in the position of the stuck rod) relative axial power distributions for the transient snapshots.

Based on the comparisons of participant's results for Phase I (defined as a point kinetics plant simulation to test the primary and secondary system model responses) it was concluded that the deviations in the predictions of system parameters time histories are due to both the modelling differences and the different theoretical models of the codes. These modelling differences were identified as follows: the conservative initial steam generator (SG) masses, the modelling of the additional feedwater to the broken SG, the steam line break flow modelling, the flow paths to the upper head of the reactor vessel and the different reactor vessel mixing models. The need to resolve these issues was addressed by carrying out parametric studies that demonstrated sensitivity of power response during the MSLB transient to key input parameters. This fact initiated an in-depth discussion concerning the main effects during a MSLB transient and their sensitivity to the modelling assumptions. As a result, a three-step procedure was applied: additional information was provided, some modelling assumptions were specified explicitly (such as the additional feedwater to the broken SG which was specified as feedwater mass flow rate vs. time) and other assumptions were made consistent (such as the SG initial mass). The lessons learned in Phase I were thus applied to Phase III.

The final results submitted by the participants for time histories for Phase III are used to make code-to-code comparisons and a subsequent statistical analysis. This information encompasses the most important thermal-hydraulic and neutronics parameters that affect the reactor behaviour during a MSLB accident, including powers, pressures, temperatures, reactivities, mass flow rates and SG masses throughout the transient. The information is presented in plots which graphically illustrate the agreement in different code predictions for each parameter. Chapter 4 of this volume presents a detailed assessment of the differences between the calculated results submitted by the participants for the time histories. The power response and the magnitude of the return to power during the transient as predicted by different codes are functions of the total reactivity time evolution. The differences arise from the different predictions of moderator feedback and Doppler feedback reactivity components, as well as the prediction of the inserted negative reactivity of the tripped rod during the dynamic scram simulation. The moderator reactivity component follows the cold leg temperature. The discrepancies in the cold leg temperature predictions are due mostly to differences in the secondary side models. It was observed that the major factors affecting the dynamics of the transient are the break flow modelling (critical flow model), the liquid entrainment, the modelling of the aspirator flow and the nodalisation of the SG downcomer. These factors affect the SG mass parameter for both the broken and the intact SGs. This parameter shows the greatest deviation amongst participant results, both in the value and behaviour of the SG masses throughout the transient. In addition, the disagreement can be attributed to differences in the heat-transfer correlations used within each code. This is especially true for the participants who use proprietary correlations that are specific to U-tube SGs in their codes; the behaviour of a OTSG is much different than a U-tube SG, and also involves superheat, something U-tube SGs do not have. The Doppler feedback reactivity predictions are sensitive to the relation used for Doppler fuel temperature as well as to the used radial and axial nodalisation of the heat structure (fuel rod).

Overall, it was determined that for the system behaviour prediction in this benchmark, the key parameters were the SG masses, the break flow rates, the coolant and fuel temperatures, and the powers. The other parameters were valuable to analyse because they helped to determine what was causing the behaviour of the key parameters. As expected, the break flow rates/modelling was very sensitive to the SG masses/modelling and vice versa. In addition, it was proven that the SG model has

a great effect on the power throughout the transient. In particular, the way the additional feedwater was introduced into the steam generator, the aspirator junction area, the downcomer nodalisation and the OTSG model in general proved to be very important.

During the second phase of this benchmark (Phase II is defined as an evaluation of the core response to imposed system T-H conditions) it was determined that the key parameters for coupled-core modelling were the thermal-hydraulic core modelling and the spatial coupling schemes with the core neutronics model, the spatial decay heat modelling, and the Doppler temperatures and density correlations used by the thermal-hydraulics codes. This conclusion was confirmed in the presented analysis of Phase III. The other parameters were useful to analyse because they helped to determine what was causing the behaviour of the key parameters. As expected, the axial distributions after the scram were very sensitive to the spatial decay heat modelling. It was also proven that the detail of the core thermal-hydraulic models has a great effect on the radial power distribution throughout the transient. In particular, the differences can be up to 15% for the snapshot at the time of highest return to power affecting local safety parameters as maximum nodal fuel temperatures. Different code formulations/correlations for Doppler temperature and moderator density affected both core averaged power and reactivity time histories and local distributions throughout the transient since these two parameters are the major feedback parameters for the cross-section modelling, impacting in this way the neutronics predictions.

The discrepancies observed in the core averaged radial distributions, local axial distributions (in the position of the stuck rod) and maximum nodal Doppler temperature time history (especially for the return to power scenario) are mostly due to the detail of spatial coupling schemes, from very detailed spatial mesh overlays (one neutronics node per thermal-hydraulic cell/channel) to coarser mesh overlays. During the course of the MSLB transient, a power spike is seen at the position of the stuck rod. However, in the 18-channel model this assembly is averaged with several of the surrounding assemblies while mapping the neutronics model to the thermal-hydraulics model. This has the significant effect of underestimating the feedback in this part of the core. On the other hand, the 177-channel model is expected to more accurately predict the feedback (as a result of a better spatial feedback resolution), and therefore the relative power shape, near the stuck rod. This can be seen very clearly from the comparisons of participants' results for the snapshot taken at time of highest return to power for the second transient scenario. The observed deviations (up to 15%) in radial power distribution are due mostly to the different thermal-hydraulic (about 5%) and heat structure (about 10%) nodalisation and mapping schemes. This result is very important since from a safety point of view, the possibility of a return to power in the later half of a MSLB transient is of great importance [6-7].

Participants' kinetics models for the benchmark utilised mostly a "one node per assembly" (npa) scheme in the radial plane [8] The benchmark team and some participants also developed a more detailed neutronic model using a 4-npa scheme in the radial plane and the subsequent mapping schemes. Comparative studies were performed for the second MSLB benchmark scenario with expected return to power. The results obtained demonstrated that the refinement of the neutronic model in the radial plane does not impact the total power transient evolution. The neutronic scheme refinement impacts local radial power distributions but not to the extent of the T-H nodalisation.

These parametric studies indicated that the MSLB calculations are mostly sensitive to the detail of the thermal-hydraulic core modelling. The MSLB simulations are less sensitive to the radial refinements of neutronic model, especially when coarser nodalisation for the thermal-hydraulic core model is used. This reflects the feedback phenomena involved in the MSLB transient since the asymmetric cooling is the driving force of the transient.

As was the case for the first two exercises, it was confirmed for the third exercise that this type of analysis requires considerably more output than was required by previous benchmarks; this is especially true of the remaining phases. In addition to requesting more output, the process of determining which parameters to request from the participants must be completed well in advance. Throughout this type of process, a great deal of consideration should be given to the level of detail required for coupled 3-D neutronic/thermal-hydraulic problems in order to evaluate the results from both a neutronic and thermal-hydraulic perspective.

It should be noted that one issue has not been incorporated into the statistical comparison techniques. In the case of time history data and 1-D axial distributions, especially axial power shapes, the overall curve shape should be compared as well. Several methods exist to complete such analysis, the most promising being the fast Fourier transform technique developed by D'Auria [9]. A number of these methods are implemented in the ACAP automatic assessment tool [10].

For the purposes of this benchmark, such a comparison was judged to be unnecessary. Curve-fit comparison would become important when the shapes differ significantly among the sets of results. However, preliminary investigations showed that the results submitted by the participants were in quite good agreement regarding the general shapes, and the only significant differences lay in the values at certain levels or points in time. For this reason, full curve analysis is not included in the comparisons for this benchmark; however, in future problems such methods should be considered.

The results of the first two exercises [2,3] were utilised to prepare the foundation of conducting the Phase III in a consistent and systematic way. Phase III is defined as a best-estimate coupled-core plant transient modelling. This exercise provides an opportunity to study the impact of different neutronics and T-H models on code predictions, as well as the coupling between them. Comparisons of the results of Phase I (performed using point-kinetics models) [2] and Phase III (performed using 3-D neutronics models) demonstrate that the 3-D analysis removes some of the conservatism inherent in point-kinetics analysis. The differences are believed to be caused by the inability of the standard point-kinetics approach to properly account for the moderator density feedback, dynamic scram simulation, local effects and flux redistribution which occur during the transient. As a result the 3-D core transient modelling provides a margin to re-criticality over the point-kinetics approach during an MSLB analysis. Such a margin is desirable due to the extended refuelling cycles and high burn-ups, which result in increasingly negative moderator temperature coefficients.

In conclusion, the application of the state-of-the-art coupled 3-D computer code systems can help to improve the performance of nuclear power plants. Developing a more in-depth knowledge of such code systems is important because 3-D kinetic/thermal-hydraulic codes will play a critical role in the future of nuclear analysis.

REFERENCES

[1] Ivanov, K., T. Beam, A. Baratta, A. Irani and N. Trikorous, *PWR MSLB Benchmark: Volume 1: Final Specifications*, NEA/NSC/DOC(99)8, April 1999.

[2] Beam, T., K. Ivanov, B. Taylor and A. Baratta, *PWR MSLB Benchmark: Volume 2: Results on Phase I on Point Kinetics*, NEA/NSC/DOC(2000)21, December 2000.

[3] Todorova, N., B. Taylor and K. Ivanov, *PWR MSLB Benchmark: Volume 3: Results of Phase II on 3-D Core Boundary Conditions Model*, NEA/NSC/DOC(2002)12, June 2002.

[4] Taylor, B. and K. Ivanov, "Statistical Methods Used for Code-to-code Comparisons in the OECD/NRC PWR MSLB Benchmark", *Annals of Nuclear Energy*, p. 27, 1589-1605 (2000).

[5] *Summary of the 2nd PWR MSLB Benchmark Workshop*, Madrid, Spain, 25-26 June 1998, NEA/NSC/DOC(98)4.

[6] *Summary of the 3rd PWR MSLB Benchmark Workshop*, Garching, Germany, 24-25 March 1999, NEA/NSC/DOC(99)6.

[7] *Summary of the 4th PWR MSLB Benchmark Workshop*, Paris, France, 24-25 January 2000, NEA/NSC/DOC(2000)2.

[8] Ivanov, K., N. Todorova, E. Sartori, "Using the OECD/NRC PWR MSLB Benchmark to Study Current Numerical and Computational Issues of Coupled Calculations", *TANSAO 84*, pp. 26-28 (2001).

[9] Ambrosini, W., R. Bovalini, F. D'Auria and F. August, "Evaluation of Accuracy of Thermal-hydraulic Code Calculations", *Energia Nucleare* (2) (1990).

[10] Kunz, R. and J. Mahaffy, "A Review of Data Analysis Techniques for Application in Automated Accuracy Assessments", *Proc. of the International Meeting BE-2000*, Washington, DC, November 2000 (Electronic Publication – CD-ROM).

APPENDIX A

Description of Computer Codes Used for Analysis in Phase III of the PWR MSLB Benchmark

CATHARE/CRONOS2/FLICA4 (CEA, France)

CATHARE is a system code with a modular structure. Zero-, one- and three-dimensional modules can be connected to model the primary and secondary circuits of any PWR. Sub-modules can be used to calculate the neutronics, the fuel thermomecanics, the pumps characteristics and other reactor components (accumulators, sources, sinks, walls, etc.)

The code has ability to model all kinds of two-phase flow patterns. Co-current and counter-current flows are modelled with prediction of counter current flow limitation. Heat transfer with wall structures and fuel are calculated taking into account all heat transfer processes (natural and forced convection with liquid or gas, sub-cooled and saturated nucleate boiling, critical heat flux, film boiling, film condensation, etc.).The interfacial heat and mass transfers describe the vaporisation caused by a superheated steam and the direct condensation cased by a sub-cooled liquid, but also the steam condensation or liquid flashing due to metastable sub-cooled steam or superheated liquid.

The latest version of CATHARE released is V1.5, which contains Revision 6. The calculations for Phase I of the MSLB Benchmark were performed with version V1.3L_1. Version V1.4U of CATHARE was used for Phase III of the benchmark. Both V1.3L_1 and V1.4U contain Revision 5.

CRONOS2 is a computer tool devoted to neutronic core computation in the SAPHYR system (SAPHYR also includes APOLLO2 for neutronic assembly calculation and FLICA4 for TH core calculation). SAPHYR codes are based on a modular structure that allows a great flexibility of use. A special user-oriented language, GIBIANE, and a shared numerical toolbox have been developed to chain the various computation modules.

CRONOS2 has been designed to provide all the computational means needed for nuclear reactor core calculations, including design, fuel management, follow-up and accidents. CRONOS2 allows steady-state, kinetic, transient, perturbation and burn-up calculations. The power calculation takes into account the thermal-hydraulic feedback effects, either by a 1-D simplified model, or by the coupling with FLICA4. All of this can be done without any limitation on any parameter (angular discretisation, energy groups, spatial meshes). As part of SAPHYR, CRONOS2 has been written with the constant goal of optimising its performance and its portability. It is based on a modular structure that allows a great flexibility of use.

The code solves either the diffusion equation or the even parity transport equation with anisotropic scattering and sources. Different geometries are available such as 1-, 2- or 3-D Cartesian, 2- or 3-D hexagonal and cylindrical geometries. Four different solvers are available: PRIAM MINOS CDIF and VNM. The PRIAM solver uses the second-order form of the transport equation and is based on S_N angular discretisation and a finite element approximation on the even flux (primal approximation); this solver is mainly devoted to accurate reference calculation for either Cartesian or hexagonal geometry. The MINOS nodal solver is based on mixed dual finite element for diffusion or simplified P_N equations; this solver performs very fast kinetic and static calculations. The CDIF solver uses finite difference approximation for the diffusion equation, and is devoted to pin-by-pin rectangular calculation. The VNM solver based on the VARIANT method will soon be connected to CRONOS2; it is based on a mixed primal method and P_N approximation and will be mainly devoted to computation of fast breeder reactors.

FLICA4 is the thermal-hydraulics code of the SAPHYR system. FLICA4 is a 3-D two-phase compressible flow code especially devoted to reactor core analysis. The fluid is modelled by a set of four equations: mass, momentum, energy conservation for the two-phase mixture and mass conservation for the vapour. The velocity disequilibria are taken into account by a drift flux

correlation. A 1-D thermal module is used to solve the conduction in solids (fuel). Thanks to the modular design of the SAPHYR codes, numerous closure laws are available for wall friction, drift flux, heat transfer and critical heat flux (CHF). A specific set has been qualified in FLICA3 for PWR applications. An extensive qualification program for FLICA4 is under way, based on recent experimental data, in order to cover a wider range of flow conditions. FLICA4 includes an object-oriented pre-processor to define the geometry and the boundary conditions. Radial unstructured meshes are available, without any limitation on the number of cells. Zooming on a specific radial zone can be performed by a second calculation using a finer mesh (for instance a sub-channel calculation on the hot assembly). The fully implicit numerical scheme is based on the finite volumes and a Roe solver. This kind of method is particularly accurate, with a low numerical diffusion.

ISAS is a general coupling tool, initially designed for the ITER project. It is based on the Parallel Virtual Machine (PVM) data exchange protocol, and provides a supervision language (GIBIANE or OCAML). Each coupled code remains independent, and is run as an individual process within a master-slave relationship. The main advantages of the coupling are fewer development needs and much reduced maintenance compared with code unification, and easy computation management (use of several machines, parallelism, etc.). As long as an ISAS interface exists in a code, this code can be coupled to any other code through ISAS without any more specific developments. This applies very conveniently to modular codes such as CATHARE2, CRONOS2 and FLICA4.

REFERENCES

Geffraye, G., B. Brun, "Validation of the CATHARE2 V1.5 Revision 6 Code for Nuclear Safety, Multiphase Flow and Heat Transfer", *Proc. of the 4th International Symposium*, Xi'an, China, 22-24 Aug. 1999.

Micaelli, J.C., F. Barre, D. Bestion, *CATHARE Code Development and Assessment Methodologies*, ANS Winter Meeting, 29 Oct.-2 Nov. 1995, San Francisco USA.

Bestion, D., "The Physical Closure Laws in the CATHARE Code", *Nuclear Engineering and Design*, 124, pp. 229-245 (1990).

Fedon-Magnaud, C., "Pin-by-pin Transport Calculation with CRONOS Reactor Code", *M&C Madrid*, 27-30 September 1999.

Lautard, J.J., D. Schneider, A.M. Baudron, "Mixed Dual Methods for Neutronic Reactor Core Calculations in the CRONOS System", *M&C Madrid*, 27-30 September 1999.

Lautard, J.J., *et al*., *CRONOS: A Modular Computational System for Neutronic Core Calculation*, IAEA meeting Cadarache, France (1990).

Toumi, I., A. Bergeron, D. Gallo, E. Royer, D. Caruge, "FLICA4: A Three-dimensional Two-phase Flow Computer Code with Advanced Numerical Methods for Nuclear Applications", *Nuclear Engineering and Design*, 200, 139-155 (2000).

Bergeron, A., D. Caruge, P. Clément, “Assessment of the 3-D Thermal-hydraulic Nuclear Computer Code FLICA4 on Rod Bundle Experiments”, *NURETH-6*, San Francisco, 3-8 October 1999.

Toumi, I., D. Caruge, “An Implicit Second Order Method for 3-D Two-phase Flow Calculations”, *Nuclear Science Engineering*, 130, 213-225 (1998).

Royer, E., I. Toumi, “CATHARE-CRONOS-FLICA Coupling with ISAS: A Powerful Tool for Nuclear Studies”, *ICONE-6 Meeting*, San Diego, USA (1998).

Toumi, I., *et al*., *Specifications of the General Software Architecture for Code Integration in ISAS*, Euratom Fusion Technology, ITER Task S81TT-01/1 (1995).

RETRAN-3D (CSA Inc., USA)

RETRAN-3D is a third-generation system transient thermal-hydraulic code. It is a realistic, best-estimate code. Its predecessor, RETRAN-02, is used extensively by the US commercial nuclear industry for modelling a wide range of safety conditions and issues. It is the basis for many utility-specific licensing and safety analyses and for various industry generic safety analysis submittals to licensing authorities. Specifically, virtually all US utilities and about 20 international organisations have used RETRAN-02 as reflected in published papers and EPRI RETRAN User group membership.

Some of the new models incorporated in RETRAN-3D include:

- Multi-dimensional neutron kinetics.
- Non-equilibrium field equations.
- Non-condensable gas flow.
- Revised numerical solution methods.

RETRAN-3D has broad capabilities to simulate plant response at all power levels and over the full spectrum of design base accidents (DBA) and some beyond-DBA events, including complex core transients. These capabilities go beyond those of the approved RETRAN-02 code and most other codes. RETRAN-3D will be used to analyse all operational transients, i.e. all FSAR Chapter 15 events except LBLOCA, such as BWR control rod drop, PWR rod ejection and PWR steam line break. It will also be used to address generic safety concerns such as boron dilution and full/partial ATWS events, and low power and shutdown cooling modes of operation in various outage configurations. RETRAN-3D contains a 3-D kinetics capability to meet the new criteria being proposed for high burn-up fuel. The 3-D kinetics option allows RETRAN-3D to properly analyse the response of mixed-oxide fuels to transients.

DYN-3D/ATHLET (FZR, Germany)

Neutron kinetic model

The 3-D neutron kinetic model is based on the solution of the three-dimensional two-group neutron diffusion equation by nodal expansion methods for the hexagonal and quadratic fuel assemblies. It is assumed that the macroscopic cross-sections are spatially constant in a node being a part of the fuel assembly. Considering hexagonal-z geometry the three-dimensional diffusion equation of each node is transformed by transverse integration in a two-dimensional equation in the hexagonal plane and a one-dimensional equation of axial direction. In the hexagonal plane the nodes can be coupled by the side averaged values or both the side averaged values and the corner point values of flux and current [1,2]. Considering the Cartesian geometry, the three-dimensional diffusion equation of each node is transformed into one-dimensional equations in each direction x,y,z by transversal integrations [3]. The equations are coupled by the transversal leakage term. The one-dimensional or two-dimensional equations are solved with the help of flux expansions in polynomials up to second order and exponential functions being the solutions of the homogeneous equation. The fission source in the fast group and the scattering source in the thermal group as well as the leakage terms are approximated by the polynomials. The outgoing partial currents are expressed by the incoming partial currents and the polynomial coefficients of the flux expansion.

Concerning the time integration over the neutronic time step an implicit difference scheme with exponential transformation is used. The exponents in each node are calculated from the previous time step or during the iteration process. In order to enable DYN3D users to independently calculate three-dimensional burn-up distributions for all possible states occurring during a reactor cycle, a burn-up version of the code has been developed.

Thermal-hydraulic model of DYN3D

The thermal-hydraulic model of the reactor core and the fuel rod model are implemented in the module FLOCAL [4], which is part of DYN3D. The reactor core is modelled by parallel cooling channels which can describe one or more fuel elements. Additionally, so-called hot channels can be considered connected to core channels with given power-peaking factors. Thermal-hydraulic boundary conditions for the core such as coolant inlet temperature, pressure, coolant mass flow rate, or pressure drop must be given as input tables for DYN3D. This option was used for the calculations during Phase II of the OECD benchmark. Applying the coupled DYN3D-ATHLET code the thermal-hydraulic boundary conditions are provided by the ATHLET code.

Mixing of coolant from different loops before entering the core can be modelled by applying mixing matrices. For VVER-440 type reactors, an analytical model for obtaining the time-dependent mixing matrices is available.

The module FLOCAL comprises:

- A one- or two-phase coolant flow model on the basis of four differential balance equations for mass, energy and momentum of the two-phase mixture and the mass balance for the vapour phase allowing the description of thermodynamic non-equilibrium between the phases.

- A heat transfer regime map from one-phase liquid up to post-critical heat transfer regimes and superheated steam.

- A fuel rod model for the calculation of fuel and cladding temperatures and the determination of some parameters for fuel rod failure estimation.

The two-phase flow model is closed by constitutive laws for heat mass and momentum transfer. Special emphasis is put on adopting the model to the conditions of RIA accidents where a combination of high heat fluxes with a high degree of coolant sub-cooling is typical and thermodynamic non-equilibrium effects are important. Different packages of water and steam thermo-physical properties presentation can be used [6].

For the estimation of fuel and cladding temperatures the heat conduction equation in one-dimensional radial geometry is solved. In the gas gap between fuel and cladding the heat transfer components due to conduction in the gas, radiation and fuel cladding contact are considered. A thermo-mechanical model of the fuel and cladding behaviour is implemented into the code. The aim of this model is the estimation of gas gap conductance behaviour for a realistic temperature calculation. Additionally, the following parameters for the diagnostic of possible fuel rod failure are provided:

- Fuel enthalpy for each axial node of the rod.

- Cladding oxide thickness.

- Signalisation of possible cladding rupture, when the cladding stress is positive (inner pressure is larger than outer pressure) and exceeds the yield point.

Coupling neutron kinetics – thermal hydraulics

For the analysis of transients that are more complex with coolant flow conditions influenced by the core behaviour, DYN3D was coupled with the ATHLET code. ATHLET was developed by the Gesellschaft für Anlagen- und Reaktorsicherheit (GRS) [5]. The code is applicable to the whole spectrum of operational and accident transients, such as small and intermediate leaks up to large breaks of coolant loops or steam lines at PWRs and BWRs. The code includes basic modules for thermal-hydraulics, heat transfer and heat conduction, neutron kinetics (point kinetics and 1-D neutron kinetics) and balance of plant simulation. Within the General Control and Simulation Module (GCSM), a general interface is available that allows coupling other independent modules to ATHLET without changes of the code architecture.

In accomplishing the coupling of ATHLET and DYN3D, two basically different methods were pursued [7]. The first one uses only the neutron kinetic part of DYN3D and integrates it into the heat transfer and heat conduction model of ATHLET. This is a very close coupling; the data have to be exchanged between all core nodes of the single models (internal coupling).

In the second coupling method, the whole core is cut out of the ATHLET plant model (external coupling). The core is completely modelled by DYN3D. The thermal-hydraulics is split into two parts: the FLOCAL model of DYN3D describes the thermal-hydraulics of the core and ATHLET models the coolant system. As a consequence of this local cut, it is easy to define the interfaces. They are located at the bottom and at the top of the core. The pressures, mass flow rates, enthalpies and concentrations of boron acid at these interfaces have to be transferred. Thus the external coupling requires only a few

parameters to be exchanged between the codes and is therefore easy to be implemented. It is effectively supported by the above-mentioned GCSM of the ATHLET code. For this reason, almost no changes of the single programs are necessary and the two codes can be developed independently. This is an important advantage of external coupling.

Different time steps are used for neutron kinetics and thermal-hydraulics. One or several time steps of neutron kinetics are performed within a thermal-hydraulic time step. The thermal-hydraulic time step is repeated to obtain convergence. The time steps are automatically controlled during the run of the code.

REFERENCES

[1] Grundmann, U., F. Hollstein, "A Two-dimensional Intranodal Flux Expansion Method for Hexagonal Geometry", *Nucl. Sci. Eng*., 133, 201-212 (1999).

[2] Grundmann, U., "HEXNEM – A Nodal Method for the Solution of the Neutron Diffusion Equation in Hexagonal Geometry", *Proceedings of the M&C'99 Conference on Mathematics and Computations in Nuclear Applications*, pp. 1086-1095, Madrid, 27-30 September 1999.

[3] Grundmann, U., *The Code DYN3DR for Steady-state and Transient Analyses of Light Water Reactor Cores with Cartesian Geometry*, Rep. FZR 114, Research Center Rossendorf (1995).

[4] Rohde, U., "Modelling of Fuel Rod Behaviour and Heat Transfer in the Code FLOCAL for Reactivity Accident Analysis of Reactor Cores", 1st Baltic Heat Transfer Conference, Göteborg (1991), published in *Transport Processes in Engineering, 2*, Elsevier Publ., Amsterdam (1992).

[5] Teschendorff, V., H. Austregesilo, G. Lerchl, "Methodology, Status and Plans for Development and Assessment of the Code ATHLET", *Proc. of the OECD/CSNI Workshop on Transient Thermal-hydraulic and Neutronic Codes Requirements*, Annapolis, USA, 5-8 Nov. 1996, p. 112, NUREG/CP-0159, NEA/CSNI/R(97)4.

[6] Rohde, U., "Modelling of Fuel Rod Behaviour and Heat Transfer in the Code FLOCAL for Reactivity Accident Analysis of Reactor Cores", 1st Baltic Heat Transfer Conference, Göteborg (1991), published in *Transport Processes in Engineering 2*, Elsevier Publ., Amsterdam (1992).

[7] Grundmann, U., D. Lucas and U. Rohde, "Coupling of the Thermohydraulic Code ATHLET with the Neutron Kinetic Core Model DYN3D", in *Proc. International Conference on Mathematics and Computations, Reactor Physics, and Environmental Analyses*, Portland, Oregon, p. 257 (1995).

MARS/MASTER (KAERI, Korea)

MARS is a multi-dimensional system thermal-hydraulic code developed for best-estimate analyses of two-phase thermal-hydraulic transients in light water reactors. The backbones of the MARS code are the RELAP5/MOD3 and COBRA-TF codes developed by the USNRC and they provide the bases for the 1-D and 3-D modules of the MARS, respectively. The 3-D module is used for a realistic representation of the thermal-hydraulic field within the reactor vessel, whereas the 1-D module is used for the rest of the system. The coupling of the 1-D and 3-D hydrodynamic models is resolved by solving an implicitly coupled system-pressure matrix equation. Since MARS retains the unique features of the two base codes, it is as versatile and robust as RELAP5 while allowing multi-dimensional nodalisation schemes as COBRA-TF. The real value of the MARS code is the enhanced solution accuracy attainable with realistic modelling. In addition, MARS has superb user-friendliness achieved by the Windows graphic feature.

MASTER is a two-group, three-dimensional neutron diffusion code capable of microscopic depletion, xenon dynamics, on-line DNB analysis and kinetics calculation in both rectangular and hexagonal geometries. The primary neutronic solver of the MASTER code is the analytic function expansion nodal (AFEN) method formulated within the framework of a coarse-mesh re-balancing technique. As optional solvers, it also has the conventional NEM as well as the non-linear ANM solvers. The transient thermal-hydraulic solution in MASTER is achieved by the COBRA III-C/P module, which employs the homogeneous equilibrium model. The mapping between the neutronic and T-H nodes is basically one-to-one. The COBRA module provides MASTER with the features of cross-flow modelling and sub-channel analysis on the fly. The types of transient calculations that can be analysed by the MASTER code include control rod perturbation (ejection, withdrawal and drop), flow perturbation (steam line break) and boron dilution events.

MARS/MASTER is a coupled 3-D kinetics/system T-H code running on a personal computer. The two codes were coupled through the dynamic link library (DLL) feature available on Windows operating systems. The use of DLL allows maintaining the integrity of each code separately and the simpler coupled-code structure. Only minor coding changes were needed for data communication and for incorporating feedback data, leaving the majority of the codes intact. In the coupled mode, the core T-H conditions are determined at each time step by MARS and they are used to update group constants in MASTER. The power distribution newly obtained by MASTER is then sent back to MARS for the next time step. The data communication is achieved by a common memory which is shared by both codes.

RELAP5/PARCS (Purdue University/NRC, USA, Universities of Piza and Zagreb, Italy and Croatia and UPC, Spain)

The RELAP5 code has been developed for best-estimate transient simulation of light water reactor coolant systems during postulated accidents. RELAP5 is a highly generic code that, in addition to calculating the behaviour of a reactor coolant system during a transient, can be used for simulation of a wide variety of hydraulic and thermal transients in both nuclear and non-nuclear systems involving mixtures of steam, water, non-condensable and solute.

The RELAP5/MOD3 code is based on a non-homogeneous and non-equilibrium model for the two-phase system that is solved by a fast, partially implicit numerical scheme to permit economical calculation of system transients. The code includes many generic component models from which general systems can be simulated. The component models include pumps, valves, pipes, heat-releasing or -absorbing structures, reactor point kinetics, electric heaters, jet pumps, turbines, separators, accumulators and control system components. In addition, special process models are included for effects such as form loss, flow at an abrupt area change, branching, choked flow, boron tracking and non-condensable gas transport.

PARCS is a modularised FORTRAN77 code which can be used to predict the transient behaviour of light water nuclear reactors resulting from external perturbations. The code solves the time-dependent two-group neutron diffusion equation in three-dimensional Cartesian geometry to obtain the transient neutron flux distribution. During the course of solution, the thermal-hydraulic feedback effects are incorporated by performing heat transfer calculations. The code is capable of performing both steady-state eigenvalue calculations for initialising the transient calculation and LWR transients such as control rod ejection/withdrawal/drop and boration/dilution events. When coupled via the NRC's general interface (GI) to the two-fluid thermal-hydraulics codes RELAP5 and TRAC-M, the PARCS code is capable of analysing boiling water reactor transients and PWR events involving a large change in coolant conditions such as steam line break accidents.

The numerical methods included in PARCS to solve the transient fixed source problem include time integration using the theta method and analytic precursor integration technique, and spatial integration using a coarse mesh finite difference solver based on a Krylov sub-space method and an analytic nodal kernel to solve the nodal coupling problems.

RELAP5/PANBOX (FRAMATOME ANP/FZK, Germany)

The coupled 3-D thermal hydraulics/neutron kinetics code RELAP5/PANBOX code was developed by FRAMATOME ANP (Germany) for the analysis of a wide range of PWR transients and accidents, where strong 3-D spatial effects and a strong coupling between core kinetics and plant thermal hydraulics are dominant.

PANBOX is a 3-D coupled neutronic/thermal-hydraulic code for steady-state and transient calculations of reactors with rectangular fuel assemblies. The basic equations of the PANBOX code are three-dimensional two-group steady-state and transient nodal diffusion equations. It uses a nodal expansion method (NEM) and/or analytical nodal integration method to solve the set of transverse-integrated one-dimensional diffusion equations for each space direction (three-dimensional discretisation of nodal neutron diffusion equations). Partial current formalism is used to couple the nodes. The code also can model the core using either one-dimensional or point kinetics equations.

Thermal-hydraulics of PANBOX is solved in the core using the COBRA 3-CP module. This code models the core as one-dimensional channels with cross flow. The balance of the system is modelled using RELAP5. Core inlet boundary conditions are passed from RELAP5 to PANBOX. This may be done on a core average or an individual channel basis depending on the transient analysed. The power distribution is then calculated in PANBOX and collapsed back for use in RELAP5. Coupling of RELAP5 and PANBOX allows both the application of the external coupling (RELAP5/PANBOX-E) and the internal coupling (RELAP5/PANBOX-I) option. In the external coupling the T-H results of COBRA 3-CP are used to update the neutronics cross-sections. In the internal coupling the RELAP5 core T-H results are directly used for the feedback to the neutronics.

The coupled code uses the EUMOD interface code to combine RELAP5 and PANBOX, enabling modelling of the entire reactor system. EUMOD consist of a set of subroutines that enable users to link external codes to RELAP5 explicitly. In this way EUMOD interface transfers data from RELAP5 to the external code, calls for execution of external code and manages the appropriate transfer of results of the external code back to RELAP5. The predicted 3-D power distribution is then collapsed onto the RELAP5 nodlaisation and passed back to RELAP5. Afterwards, a new RELAP5 time step can be performed.

A mapping procedure assures the correct interpolation and expansion of 1-D thermal-hydraulic data onto 3-D core nodalisation, so that resulting node-wise thermal-hydraulic data can be used to update nuclear data (cross-sections) for 3-D neutron kinetics calculation (PANBOX). The time integration is based on a fully implicit Euler method in combination with an exponential transformation technique to reduce truncation error. Hence, similar solution techniques can be applied for both steady-state and transient calculations.

An additional feature of RELAP5/PANBOX is a switching algorithm to select the space dimension of the neutron kinetics calculation (PK, 1-D or 3-D) automatically and selectively during the advancement of the transient calculation.

SIMTRAN/RELAP5 (University Polytechnic of Madrid, Spain)

SIMTRAN is a combination of SIMULA, a three-dimensional kinetics code, and COBRA IIIC. The COBRA code solves the thermal-hydraulic transport in the core with cross flow. External coupling to RELAP5 allows the full system to be modelled.

SIMTRAN is a 3-D PWR core dynamics code which has been being developed and validated for about 10 years. The code was developed as a single code merge, with data sharing through standard FORTRAN commons, of the 3-D neutronics nodal code SIMULA and the multi-channel thermal-hydraulics code COBRA-IIIC/MIT-2. Both codes solve the 3-D neutronic and T-H fields with maximum implicitness, using direct and iterative methods for the inversion of the linearised systems.

SIMULA is a 3-D nodal neutronics code for PWR cores. The code solves the neutron diffusion equations in one or two groups on coarse-mesh nodes (quarter of fuel assemblies). SIMULA uses a linear-discontinuous finite-difference scheme, where the interface net currents are given in terms of the actual node-average and the corrected interface-averaged fluxes, using synthetic interface flux discontinuity factors for each group and node-interface. SIMULA uses these synthetic coarse-mesh discontinuity factors in the XY directions, pre-calculated by 2-D pin-by-pin two-group diffusion calculations of whole core planes. In the axial direction the code performs embedded iterative 1-D fine-mesh two-group diffusion solutions for each node stack with the radial leakage terms interpolated from the nodal two-group solution.

COBRA-III-C/MIT-2 is a public code for thermal-hydraulics calculations, with implicit cross flows and homogeneous two-phase fluids. The code is used world-wide for DNBR analysis in PWR sub-channels, and also for 3-D whole PWR core simulation with one or more channels per fuel assembly. COBRA uses direct inversion at each plane of the axial flow equations, with cross flows updated over an outer iteration loop, for the homogenous model single-phase coolant, and finite-element direct solution of the fuel rod radial temperatures.

SIMTRAN is our coupled code for 3-D dynamic analysis of PWR cores, integrating SIMULA and COBRA as per the scheme displayed in Figure 1.

The 3-D core N-TH coupling is done internally in SIMTRAN by a semi-implicit scheme, using a staggered alternate time mesh, as shown in Figure 2.

The TH solution is advanced over one-half of the neutronic time step, thus conserving energy by taking the neutronic nodal power centred in the time step. Then, the implicitly calculated 3-D T-H variables (water density and water and fuel temperatures) are extrapolated over another half of the time step. The neutronic constants are thus nearly implicitly calculated in the next time step as a function of the extrapolated T-H variables, where the limited half-step extrapolation prevents significant oscillations, allowing for larger time steps.

REFERENCE

Aragonés, José M., Carol Ahnert, Oscar Cabellos, Nuria García-Herranz and Vanesa Aragonés Ahnert, “Methods and Results for the MSLB NEA Benchmark using SIMTRAN and RELAP-5”, to be published in OECD/NRC MSLB Benchmark Special Issue of *Nuclear Technology*.

Figure 1. Variables for the 3-D neutronics thermal-hydraulics coupling in SIMTRAN

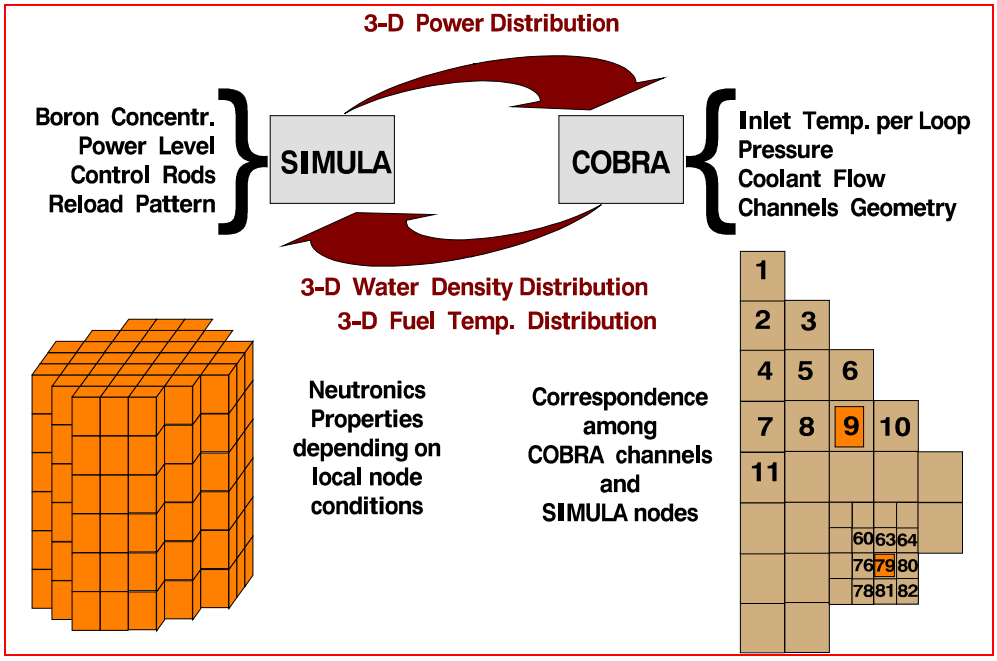

Figure 2. Temporal coupling of NK and TH for fast transients in SIMTRAN

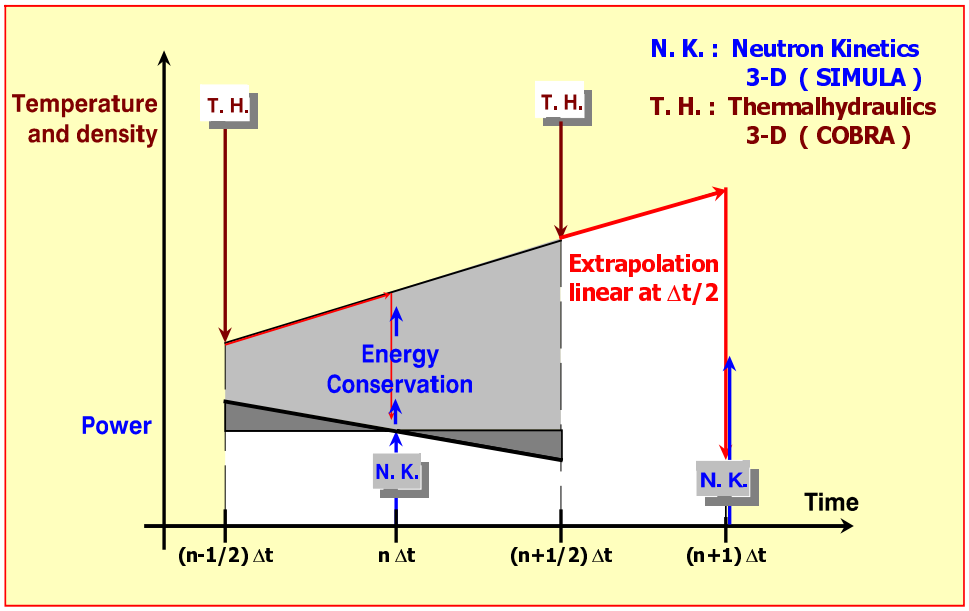

TRAB-3D/SMABRE (VTT, Finland)

TRAB-3D is the latest member of the code system developed at VTT Energy for LWR reactor dynamics calculations. The neutron kinetics model of the new code is based on the three-dimensional VVER-dynamics code HEXTRAN, but the nodal equations are solved in rectangular, instead of hexagonal, fuel assembly geometry. Special features of the solution methods are construction of the two-group nodal fluxes from two spatial modes, the asymptotic or fundamental mode and the transient mode, and approximation of the former mode by polynomials and of the latter mode by exponential functions. In addition, flux discontinuity factors can be specified on the transverse interfaces of nodes. The nodal flux model of TRAB-3D contains eight degrees of freedom per group in a transverse cross-section and they are adjusted by continuity conditions for group fluxes and currents and for their first moments at nodal interfaces.

Thermal-hydraulics models are taken from the one-dimensional dynamics code TRAB which includes descriptions of both the reactor core and the BWR-cooling circuit. Thus, the dynamic behaviour of the whole primary circuit of a reactor can be analysed with TRAB-3D. For PWR dynamics, the core model of TRAB-3D is coupled with the SMABRE PWR circuit model.

Comparisons with fine-mesh finite difference calculations have shown that TRAB-3D solves the diffusion equations for homogeneous fuel assemblies of a two-dimensional reactor core with an accuracy of better than 1% in assembly powers. The validation history of TRAB-3D, so far, includes the calculation of OECD/NEACRP 3-D light water reactor benchmark problems and verification against measurements from real BWR plant transients. Much of the validations, however, have already been done by various calculations with HEXTRAN and TRAB since the same models for neutron kinetics and thermal-hydraulics description are used in TRAB-3D.

The 1-D thermal-hydraulic model of SMABRE, developed by VTT, is able to model 3-D thermal-hydraulic effects using parallel channel nodalisation combined with the turbulent mixing model. SMABRE contains a five-equation two-phase thermal-hydraulic model, using the drift flux model. The numerical solution method used in SMABRE is a predictor-corrector type non-iterative solution. For using SMABRE without TRAB-3D, the code contains a point kinetics model. Due to the fast running capabilities of the code, it is widely used for several types of simulators in many countries.

There is a parallel coupling between the circuit model SMABRE and TRAB-3D. The coupled code TRAB-3D/SMABRE has its own main program and a few interfacing sub-programs, but in the combination TRAB-3D and SMABRE are used as if they were separate codes. Both codes use their own input, output, restart and plotting capabilities. TRAB-3D dictates the time step. SMABRE calculates the whole thermal-hydraulics of the loops and the core in a sparse geometry. Additionally, TRAB-3D performs the detailed thermal-hydraulics and fuel heat-transfer calculation in every fuel assembly of the core to get the nodal fuel and coolant conditions for the calculation of three-dimensional neutron kinetics and reactivity feedback effects.

RELAP5/QUABOX (Universities of Piza and Zagreb, Italy and Croatia)

The results are produced with RELAP5/QUABOX coupled code. RELAP5 is a NRC-sponsored code in version 3.2.2 gamma. QUABOX is a GRS QUABOX/CUBBOX-HYCA code with some modifications. Direct explicit coupling is used. RELAP5 performs all thermal-hydraulic calculations (it is responsible for control of the time step) and QUABOX solves 3-D coarse mesh neutron diffusion in two energy groups and processes interface arrays.

TRAC-PF1/NEM (The Pennsylvania State University, USA and University Polytechnic of Valencia, Spain)

The TRAC-PF1 code is a best-estimate system transient analysis code which has 3-D thermal-hydraulic analysis capability. A modified version of TRAC-PF1/MOD2 v.5.4 is currently being used at The Pennsylvania State University (PSU). Version 5.4 incorporates a 1-D decay heat model that dynamically computes the decay heat axial shape during the transient. The code solves the general transient two-phase coolant conditions in one, two, or three dimensions using a realistic six-equation two-fluid finite-difference model. This six-equation model, in conjunction with specialised empirical models for a variety of PWR primary- and secondary-loop components and control systems, allows TRAC-PF1/MOD2 v.5.4 to accurately model both mild and severe thermal-hydraulic transients.

An accurate 3-D transient neutronics model based on the nodal expansion method (NEM) was developed and integrated into TRAC-PF1 by PSU. The NEM spatial model is based on the transverse integrated procedure. Two levels of approximation are used: fourth-degree transverse-integrated flux representation and the quadratic leakage approximation. The nodal coupling relationships are expressed in a partial current formulation. The time dependence of the neutron flux is approximated by a first order, fully implicit, finite-difference scheme, whereas the time dependence of the neutron precursor distributions is modelled by a linear time-integrated approximation. The coarse-mesh rebalance and the asymptotic extrapolation methods are used to accelerate convergence of the iterative solution process. Several benchmark problems were used to assess the NEM model in both steady-state and transient conditions. Very good agreement was obtained among the reference results and those from NEM.

The coupling of the NEM neutronics to TRAC-PF1 has made use of the local thermal-hydraulic properties to simulate the core response during a transient. TRAC-PF1/NEM employs an improved semi-implicit neutronics/thermal-hydraulic coupling scheme. At the beginning of a time step, TRAC-PF1/MOD2 first performs its pre-pass stage, where fluid-state-dependent material properties and heat-transfer coefficients are calculated based on thermal-hydraulic conditions at the end of the previous time step. In the outer iteration stage, the multi-dimensional fluid-dynamic equations are solved using previous time step fuel-rod heat fluxes. Then, the 3-D transient NEM neutronics model calculates the present time step nodal power distribution using cross-section-dependent feedback parameters based on present time step fluid conditions and previous time step fuel-rod temperatures. Finally, in the post-pass stage, the new nodal power distribution is used in the numerical solution of the heat-conduction equations. To ensure symmetry between the 3-D thermal-hydraulics vessel, the heat structure, and the neutronics core model, proper radial and axial noding and mapping schemes have to be developed.

A general algorithm for detecting control-rod presence and movement was implemented in TRAC-PF1/NEM and integrated into the cross-section table's procedure. Cross-sections for nodes with control rods partially inserted are obtained by blending the rodded and un-rodded cross-sections, using a factor that is a function of the fractional amount of control-rod insertion in that cell. The control-rod algorithm is capable of modelling initial steady-state conditions with the initial positions of the control-rod groups. Movement of single rods and control-rod groups, as well as dynamic scram can also be simulated. In addition to this flexibility, there is an option in the code that allows one to perform efficient evaluations of static control-rod reactivity and shutdown margins.

APPENDIX B

Questionnaire for Phase III of the PWR MSLB Benchmark

I. Primary system

1. Vessel thermal-hydraulic (T-H) model and nodalisation (1-D, 3-D and number T-H channels or cells). How are channels/T-H cells chosen?

2. Mixing model – how is the required mixing ratio implemented?

3. Upper plenum and upper head (of reactor vessel) paths (junctions) modelling?

II. Thermal-hydraulic core model

1. Core thermal-hydraulic (T-H) model and radial and axial nodalisation (1-D, 3-D and number T-H channels or cells). How are channels/T-H cells chosen?

2. Number of heat structures (fuel rods) modelled?

3. Radial and axial heat structure (fuel rod) nodalisation?

4. Used relation for Doppler temperature?

5. Used correlations for fuel properties vs. temperature?

III. Core neutronics model

1. Number of radial neutronics nodes per assembly?

2. Axial nodalisation?

3. Radial and axial reflector modelling?

4. Spatial decay heat distribution modelling?

5. Cross-section interpolation procedure used?

6. Method used to get a critical reactor at the beginning of transient?

IV. Coupling schemes

1. Hydraulics/heat structure spatial mesh overlays (mapping schemes in radial and axial plane).

2. Hydraulics/neutronics spatial mesh overlays (mapping schemes in radial and axial plane).

3. Heat structure /neutronics spatial mesh overlays (mapping schemes in radial and axial plane).

4. Temporal coupling scheme.

5. Coupling numerics – explicit, semi-implicit or implicit?

6. Coupling way – external or internal?

7. Coupling design – serial integration or parallel processing?

V. Secondary system

1. Initial steam generator (SG) mass inventory?

2. SG downcomer nodalisation?

3. Aspirator flow modelling?

4. Steam line modelling?

5. Break flow modelling and critical flow model?

6. Are you using the updated steam safety relief valves data (see *Updated Specifications*, April 1999 – Table 5.4.2, p. 69)?

7. Are you using the updated additional feedwater mass data (between the feedwater isolation valve and the broken SG, see *Updated Specifications*, April 1999 – Table 5.4.3, p. 69)?

VI. General

1. Deviations from the updated *Final Specifications* (April 1999 – NEA/NSC/DOC(99)8)?

2. User assumptions?

3. Specific features of the used codes?

4. Number of solutions submitted per participant and how they differ?

FRAMATOME ANP/FZK, *Germany*

I. Primary system

1. Vessel thermal-hydraulic (T-H) model and nodalisation (1-D, 3-D and number T-H channels or cells). How are channels/T-H cells chosen?

   The RPV was split into two equal halves, one connected to the coolant stream of broken loop-A and the other one to coolant stream of intact loop-B. Each RPV half consists of the following 1-D fluid volumes along the main flow paths: inlet, downcomer, lower plenum, core bypass, core, core outlet, upper plenum, one annular region between baffle and core support shield and one dead-end annular region formed by core support shield and RPV-wall. Both RPV halves are connected to each other by the uppermost upper plenum volume. Hence, the RPV without the core region is represented by a total of 55 cells.

2. Mixing model – how is the required mixing ratio implemented?

   Since RPV thermal hydraulics model consists of two main flow streams (one belonging to the intact loop-B and the other one to the broken loop-A), coolant-mixing model was implemented without problems by addition of two junctions in each plenum. To get recommended mixing ratio appropriate flow areas of junctions added for mixing was necessary.

3. Upper plenum and upper head (of reactor vessel) paths (junctions) modelling?

   At the upper plenum, the main flow paths are defined by the baffle and the baffle holes as well as by the annular region between the baffle and the core support shield. Six volumes in three elevations were considered per core halves. Two additional volumes were defined (elevation 2 and 3) for mixing of both loops (A and B) occurs. The uppermost volume connects both loops. In addition, two representative guide tubes per halves were modelled that conjoin the core outlet volumes (of loop-A and loop-B) with the uppermost volume.

II. Thermal-hydraulic core model

1. Core thermal-hydraulic (T-H) model and radial and axial nodalisation (1-D, 3-D and number T-H channels or cells). How are channels/T-H cells chosen?

   <u>Thermal-hydraulic RELAP5 model (axial nodalisation)</u>: The core is represented by 19 coarse parallel thermal-hydraulic channels. No cross-flow is considered between them. Each coolant channel is represented by a pipe component with eleven equidistant axial nodes.

   <u>Thermal-hydraulic RELAP5 model (radial nodalisation):</u> Radial distribution of coarse thermal-hydraulic channels was adopted according to mapping scheme given in the Final Specifications, except for coolant channels lying on the central assembly row. They were lumped together to one additional channel.

2. Number of heat structures (fuel rods) modelled?

   <u>RELAP5 heat structure model:</u> The core is represented by 19 representative fuel rods that correspond to the 19 coarse thermal-hydraulic channels (coupled by convective boundary conditions).

<u>PANBOX heat structure model:</u> In total 241 radial nodes, 177 FA nodes and 64 reflector nodes are considered in the model.

3. Radial and axial heat structure (fuel rod) nodalisation?

   Axially each heat structure is divided in 11 equidistant nodes. In radial direction six, one and two intervals are considered inUO_2 pellet, gap and cladding, respectively. Hence, one-half of fuel pin having symmetry at the fuel centreline has 10 mesh points for temperature calculation.

4. Used relation for Doppler temperature?

   Relation given in MSLB specification.

5. Used correlations for fuel properties vs. temperature?

   Correlations given in MSLB specification.

III. Core neutronics model

1. Number of radial neutronics nodes per assembly?

   One radial node per fuel assembly.

2. Axial nodalisation?

   Twenty-eight (28) layers, 26 in core region and two for upper and lower reflector zone.

3. Radial and axial reflector modelling?

   As recommended in MSLB specifications.

4. Spatial decay heat distribution modelling?

   Three-dimensional (3-D) distribution according to the nodal fission rates. Time dependence according to specified table versus time.

5. Cross-section interpolation procedure used?

   Interpolation subroutine LINT4D. Given by PSU.

6. Method used to get a critical reactor at the beginning of transient?

   Eigenvalue calculation.

IV. Coupling schemes

1. Hydraulics/heat structure spatial mesh overlays (mapping schemes in radial and axial plane).

   RELAP5 coarse parallel channels and heat structures have the same axial nodalisation. In radial plane FAs belonging to one coarse channel were lumped together to one representative RELAP5 heat structure (according to TRAC/-PF1/NEM mapping scheme).

2. Hydraulics/neutronics spatial mesh overlays (mapping schemes in radial and axial plane).

   Thermal-hydraulic data according to RELAP5 nodalisation is passed to PANBOX via EUMOD to be mapped and interpolated onto the 3-D neutronics core nodalisation of PANBOX. Resulting node-wise thermal-hydraulic data are used to update nuclear cross-sections. Then a neutron-kinetics time step is carried out.

3. Heat structure /neutronics spatial mesh overlays (mapping schemes in radial and axial plane).

   Three-dimensional (3-D) power distribution predicted by PANBOX is collapsed to RELAP5 heat structure nodalisation and then passed back to RELAP5 for the next RELAP5 time step.

4. Temporal coupling scheme.

   Explicit coupling.

5. Coupling numerics – explicit, semi-implicit or implicit?

   Explicit coupling. Coupling process is performed when RELAP5 time step is completed.

6. Coupling way – external or internal?

   Internal coupling.

7. Coupling design – serial integration or parallel processing?

   Serial coupling.

V. Secondary system

1. Initial steam generator (SG) mass inventory?

   26 546 kg.

2. SG downcomer nodalisation?

   The steam generator downcomer is modelled by an annulus volume with four internal volumes. Feedwater is injected at the downcomer top and flows out of the downcomer to the volume representing the lower tube sheet, which is modelled as a branch. From this branch the flow is directed upwards through two volume stacks representing the boiler part of the steam generator.

3. Aspirator flow modelling?

   The aspirator is modelled by a cross-flow junction that connects the boiler (at the elevation of 9.73 m) with the downcomer top. The aspirator flow area amounts to 0.972 m² but it was reduced to 0.1858 m² to obtain an initial fluid inventory of about 26 tonnes.

4. Steam line modelling?

   The steam lines are modelled in detail considering their whole length. It was represented by a RELAP5-pipe component with eight internal volumes. In addition, a cross-connection line

was considered for intact loop-B. Four banks of main steam safety valves (MSSV) were modelled. A turbine stop valve (MSIV) per steam line, a common header and the turbine are also included in the model.

5. Break flow modelling and critical flow model?

   Break flow model uses abrupt area and homogeneous flow model for break valves. As critical flow model the RELAP5/mod3.2 default model, i.e. the Trapp & Ramson model, was used.

6. Are you using the updated steam safety relief valves data (see *Updated Specifications*, April 1999 – Table 5.4.2, p. 69)?

   Yes.

7. Are you using the updated additional feedwater mass data (between the feedwater isolation valve and the broken SG, see *Updated Specifications*, April 1999 – Table 5.4.3, p. 69)?

   Yes.

VI. General

1. Deviations from the updated *Final Specifications* (April 1999 – NEA/NSC/DOC (99) 8)?

   Use of Trapp & Ramson critical flow model instead of Moody model.

2. User assumptions?

   No.

3. Specific features of the used codes?

   Critical flow model of Trapp & Ramson as default option.

4. Number of solutions submitted per participant and how they differ?

   One.

CEA/IPSN, *France*

I. Primary system

1. Vessel thermal-hydraulic (T-H) model and nodalisation (1-D, 3-D and number T-H channels or cells). How are channels/T-H cells chosen?

   The core is separated into two 1-D channels. The lower and upper plenums are separated in three volumes for mixing requirements.

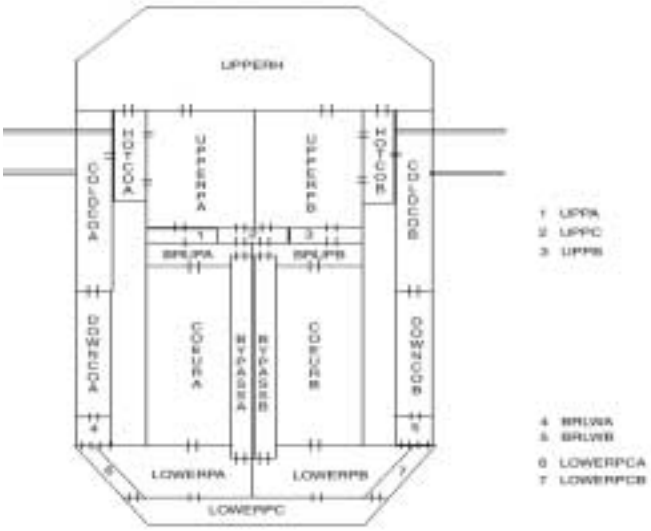

2. Mixing model – how is the required mixing ratio implemented?

   The lower plenum has been separated into three volumes:

   - *LOWERPA connected to the intact leg.*
   - *LOWERPB connected to the broken leg.*
   - *LOWERPC connected to both intact and broken legs.*

   The mixing ratio of MSLB specifications has been obtained by tuning the size of volume C for both lower (LOWERPC) and upper (UPPC) plenum.

   The upper plenum has been separated into two volumes: UPPERPA and UPPERPB.

   Three other volumes are used for the junction with core. As for lower plenum, the size of these three volumes has been calculated in order to match the mixing ratio specifications.

3. Upper plenum and upper head (of reactor vessel) paths (junctions) modelling?

   Each volume UPPERPA and UPPERPB has a junction with the upper head and two junctions with hot leg inlet.

   A 1 390 kg/s flow between upper plenum and upper head exists at initial state.

II. Thermal-hydraulic core model

1. Core thermal-hydraulic (T-H) model and radial and axial nodalisation (1-D, 3-D and number T-H channels or cells). How are channels/T-H cells chosen?

   Radial mesh: One node per assembly, i.e. 177 radial nodes.

   Axial mesh: Four nodes of 10.9 cm for the reflector, and 24 nodes of 14.88 cm for the fuel, i.e. 28 nodes.

   Global mesh: 4 956 nodes for the core (177 × 28).

   Thermal-hydraulics: fully 3-D.

2. Number of heat structures (fuel rods) modelled?

   One heat structure per assembly, i.e. 177 heat structures.

3. Radial and axial heat structure (fuel rod) nodalisation?

   Axial mesh: Four nodes of 10.9 cm for the reflector, and 24 nodes of 14.88 cm for the fuel, i.e. 28 nodes (cf. thermal-hydraulics).

   Radial mesh: 10 nodes for the pellet, and six nodes for the clad.

4. Used relation for Doppler temperature?

   Specified relation: 0.3 T_{centre} + 0.7 $T_{surface}$.

5. Used correlations for fuel properties vs. temperature?

   Specified correlations (pg. 30, Final Specifications).

III. Core neutronics model

1. Number of radial neutronics nodes per assembly?

   Radial mesh: One node per assembly, i.e. 177 radial nodes.

2. Axial nodalisation?

   Axial mesh: 53 nodes.

3. Radial and axial reflector modelling?

   Radial mesh: One node per assembly, i.e. 112 radial nodes (17 × 17 – 177).

   Axial mesh: 53 nodes (cf. fuel assemblies).

4. Spatial decay heat distribution modelling?

   Fission power distribution at steady state (time = 0 of transient), as agreed in Paris.

5. Cross-section interpolation procedure used?

   Bi-linear interpolation for fuel temperature and moderator density (regular module of CRONOS2). No extrapolation outside of the cross-section library was necessary.

6. Method used to get a critical reactor at the beginning of transient?

   Fission cross-section matrix divided by the steady-state eigenvalue (Σ_f / k_{eff}).

IV. Coupling schemes

1. Hydraulics/heat structure spatial mesh overlays (mapping schemes in radial and axial plane).

   No specific procedure as the axial mesh is the same, and there is one heat structure per radial node.

2. Hydraulics/neutronics spatial mesh overlays (mapping schemes in radial and axial plane).

   Radial mesh: Same nodalisation for neutronics and thermal-hydraulics.

   Axial mesh: Linear projection between the two nodalisations (regular procedure of FLICA4 and CRONOS2).

3. Heat structure /neutronics spatial mesh overlays (mapping schemes in radial and axial plane).

   Cf. IV.2.

4. Temporal coupling scheme.

   Same time step for thermal-hydraulic, fuel structures and neutronics.

5. Coupling numerics – explicit, semi-implicit or implicit?

   Explicit coupling between core thermal-hydraulics (FLICA4) and neutronics (CRONOS2). Semi-implicit coupling between system thermal-hydraulics (CATHARE) and core (FLICA4 and CRONOS2).

6. Coupling way – external or internal?

   External coupling through ISAS coupling software.

7. Coupling design – serial integration or parallel processing?

   Serial processing on a bi-processor computer.

V. Secondary system

1. Initial steam generator (SG) mass inventory?

   As specified, 26 000 kg.

2. SG downcomer nodalisation?

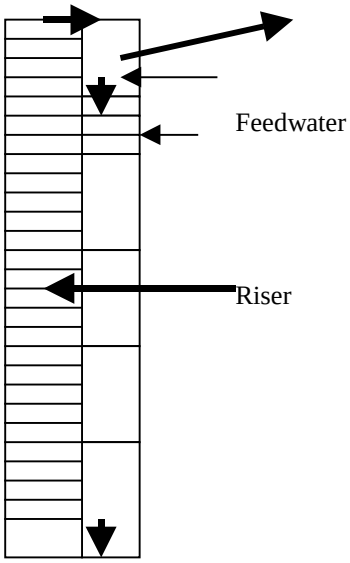

3. Aspirator flow modelling?

   A junction between the upper and lower part of downcomer.

4. Steam line modelling?

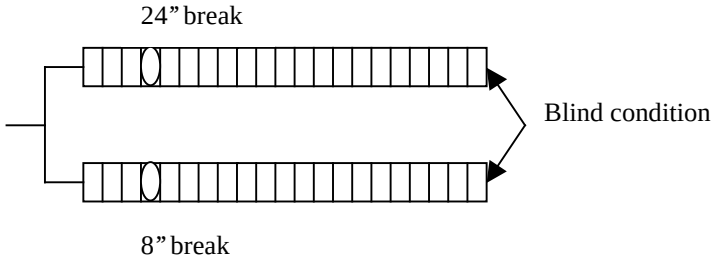

5. Break flow modelling and critical flow model?

   The 8" and 24" break flows are calculated by the Gros d'Aillon correlation.

6. Are you using the updated steam safety relief valves data (see *Updated Specifications*, April 1999 – Table 5.4.2, p. 69)?

   Yes, we used the latest specification.

7. Are you using the updated additional feedwater mass data (between the feedwater isolation valve and the broken SG, see *Updated Specifications*, April 1999 – Table 5.4.3, p. 69)?

   Yes, we used the latest specification.

VI. General

1. Deviations from the updated *Final Specifications* (April 1999 – NEA/NSC/DOC(99)8)?

   No deviation.

2. User assumptions?

   No singular pressure drop in the core (for grids), which results in tuning the friction coefficient to match the specified core pressure drop.

   Surge line singular pressure drop: Four times 12.78 (as in Phase I).

3. Specific features of the used codes?

   Use of two thermal-hydraulic codes: CATHARE (1-D) for the system and FLICA4 (3-D) for the core.

4. Number of solutions submitted per participant and how they differ?

   Two sets of solutions:

   - *Reference solution (for Scenario 2 only) based on a single core thermal-hydraulics; no core in the CATHARE circuit but only boundary conditions at core inlet and outlet. CATHARE and FLICA4 mutually exchange their core boundary conditions at each coupling step.*

   - *Simplified solution (for Scenarios 1 & 2) based on a double core thermal-hydraulics: a simplified 1-D core model in the CATHARE circuit, and a fine 3-D core model in FLICA4 (only used to provide the feedback to CRONOS2). CRONOS2 provides the core power to both FLICA4 (3-D distribution) and CATHARE (1-D distribution).*

JAERI, *Japan*

I. Primary system

1. Vessel thermal-hydraulic (T-H) model and nodalisation (1-D, 3-D and number T-H channels or cells). How are channels/T-H cells chosen?

   One-dimensional (1-D) vessel with 20 channels:

   - *Channels 1-18 – same as Figure 3.2.3 in Final Specifications (without guide tube flow).*
   - *Channel 20 – representing reflector flow.*
   - *Channel 19 – representing guide tube flow.*

2. Mixing model – how is the required mixing ratio implemented?

   In THYDE-NEU, there is no notion of "mixing ratio".

   The code is based on the "local conditions" hypothesis.

3. Upper plenum and upper head (of reactor vessel) paths (junctions) modelling?

   Upper plenum and upper head are nodalised in a usual way.

   Split downcomer noding: the downcomer and the lower plenum were radially split each into two identical nodes.

II. Thermal-hydraulic core model

1. Core thermal-hydraulic (T-H) model and radial and axial nodalisation (1-D, 3-D and number T-H channels or cells). How are channels/T-H cells chosen?

   One-dimensional (1-D):

   - *Radial nodalisation: According to Figure 3.2.3 in Final Specifications with 20 channels (refer to item II.2).*
   - *Axial nodalisation: Seven nodes per channel.*
   - *Axial node length (m):*

0.3594	*0.7440*	*0.5952*	*0.8928*	*0.5952*	*0.7440*	*0.3594*
top						*bottom*
unheated						*unheated*

2. Number of heat structures (fuel rods) modelled?

Channel	*Fuel ID*	*No. of fuel rods*
1	*1*	*1 560*
2	*2*	*1 560*
3	*3*	*1 560*
4	*4*	*1 560*
5	*5*	*1 560*
6	*6*	*1 560*
7	*7*	*2 080*
8	*8*	*2 080*
9	*9*	*2 080*
10	*10*	*2 080*
11	*11*	*2 080*
12	*12*	*2 080*
13	*13*	*2 496*
14	*14*	*2 496*
15	*15*	*2 496*
16	*16*	*2 496*
17	*17*	*2 496*
18	*18*	*2 496*
19	*(guide tube)*	*0*
20	*(reflector)*	*0*

3. Radial and axial heat structure (fuel rod) nodalisation?

   Radial nodalisation: Seven meshes for cladding and 28 meshes for fuel pellet.

   Axial nodalisation: Axial mesh lengths (m)

0.21811	*0.7440*	*0.5952*	*0.8928*	*0.5952*	*0.7440*	*0.21811*
top unheated						*bottom unheated*

4. Used relation for Doppler temperature?

   For each of 18 active channels, T_D of each fuel slab is calculated as specified by 3.3 of Final Specifications.

5. Used correlations for fuel properties vs. temperature?

   As specified by 3.3 of Final Specifications.

III. Core neutronics model

1. Number of radial neutronics nodes per assembly?

   One with the NEM.

2. Axial nodalisation?

Layer	*Axial mesh ID*	*Mesh length (cm)*	*Flow node*	*Fuel slab*
26	*28*	*10.9055*	✓	✓
26	*27*	*10.9055*		
25	*26*	*14.88*	✓	✓
24	*25*	*2.6143*	✓	✓
23	*24*	*12.266*	✓	✓
22	*23*	*14.88*	✓	✓
21	*22*	*14.88*	✓	✓
20	*21*	*14.88*		
19	*20*	*14.88*	✓	✓
18	*19*	*14.88*	✓	✓
17	*18*	*14.88*	✓	✓
16	*17*	*14.88*		
15	*16*	*14.88*	✓	✓
14	*15*	*29.76*	✓	✓
13	*14*	*29.76*	✓	✓
12	*13*	*14.88*		
11	*12*	*14.88*	✓	✓
10	*11*	*14.88*	✓	✓
9	*10*	*14.88*	✓	✓
8	*9*	*14.88*		
7	*8*	*14.88*	✓	✓
6	*7*	*14.88*	✓	✓
5	*6*	*14.88*	✓	✓
4	*5*	*10.17*	✓	✓
3	*4*	*4.71*	✓	✓
2	*3*	*14.88*		
1	*2*	*10.9055*	✓	✓
1	*1*	*10.9055*	✓	✓

3. Radial and axial reflector modelling?

   Axial noding is the same as above (item III.2).

   The reflector is radially noded as shown in Figure 3.2.3 of the Final Specifications.

4. Spatial decay heat distribution modelling?

   Decay heat at each node in the core is proportional to the transient fission power at that point.

5. Cross-section interpolation procedure used?

   It is by means of the NEA-provided routine LINT4D.

6. Method used to get a critical reactor at the beginning of transient?

   Criticality is one of many items to be simultaneously satisfied at an initial steady state. In THYDE-W, this procedure is referred to as the steady-state adjustment. For a stable system, an initial state obtained by the steady-state adjustment is expected to coincide with the null transient solution to the coupled thermal-hydraulics and neutronics problems. In the steady-state adjustment of the present problem, various parameters are varied to satisfy this requirement. Among these parameters, the most sensitive to criticality is the axial position of control rods in Bank 7 (except the one at N12).

IV. Coupling schemes

Coupling schemes for an initial steady state also are important. In THYDE-NEU, the coupling scheme for an initial steady state is complete in the sense that a steady state obtained satisfies simultaneously its thermal-hydraulics and neutronics equations without time derivatives. In other words, a steady state obtained is the solution to the null transient problem.

1. Hydraulics/heat structure spatial mesh overlays (mapping schemes in radial and axial plane).

   Thermal-hydraulically, the core is regarded as being composed of flow channels shown in Item II.2. To each active channel, a fuel rod corresponds with both having the same number of parallel units and the same axial noding (except for the unheated top and bottom).

2. Hydraulics/neutronics spatial mesh overlays (mapping schemes in radial and axial plane).

   Radial correspondence: Figure 3.2.3 in Final Specifications.

   Axial correspondence: Refer to Item III.2.

3. Heat structure /neutronics spatial mesh overlays (mapping schemes in radial and axial plane).

   Radial correspondence: Figure 3.2.3 in Final Specifications.

   Axial correspondence: Refer to Item III.2.

4. Temporal coupling scheme.

   In THYDE-NEU, three temporal integrations (thermal-hydraulics, thermal diffusion in structure and neutronics) are independent of each other at a time step, but are coupled to each other with a time step lag.

5. Coupling numerics – explicit, semi-implicit or implicit?

   Explicit.

6. Coupling way – external or internal?

   I do not understand the question.

7. Coupling design – serial integration or parallel processing?

   In THYDE-NEU, parallel processing is not implemented for three temporal integrations.

V. Secondary system

1. Initial steam generator (SG) mass inventory?

   2.84×10^4 kg (the value given by the vendor is 28 395 kg).

2. SG downcomer nodalisation?

   Mixing of the feedwater and the re-circulation flow (saturated water) is modelled.

3. Aspirator flow modelling?

   The re-circulation flow is regarded as saturated water at the initial steady state. The separation efficiency is assumed as a function of the upward mass flux of the SG secondary system.

4. Steam line modelling?

   Refer to the next question.

5. Break flow modelling and critical flow model?

   A break flow rate is bounded by critical flow rate given by Zaloudek (sub-cooled water) and Moody (saturated mixture).

   The break flow was modelled as explained in the following:

   I could explain the difference in the results between THYDE-NEU and the other codes, by using the following three figures, which show the flow modes in three phases of the transient in the right MS lines.

   Figure 1 shows the initial MS line flows of the right loop. Suppose that a break occurs at X in Figure 2. Then, the initially stagnant coolant in the cross-connect starts to flow from the intact MS line to the break (Figure 2). Simultaneously, the left break flow, which is initially positive, begin to decrease, remaining positive, but soon becoming negative. On the other hand, the right break flow always is positive.

   Since the break is double-ended (guillotine type), its size must be the same as that of the MS line, but not that of the cross-connect. The flow in the cross-connect may or may not be of critical low mode, which will be calculated by the code in accordance with the boundary condition at the break.

Figure 1. Initial MS line flows; V – valve

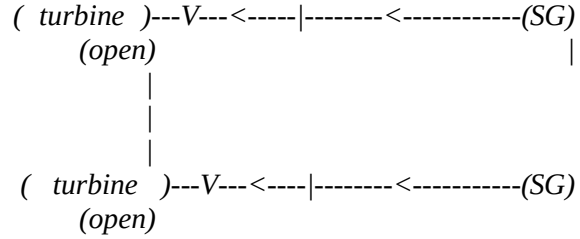

Figure 2. MS line flows just after the start of the break

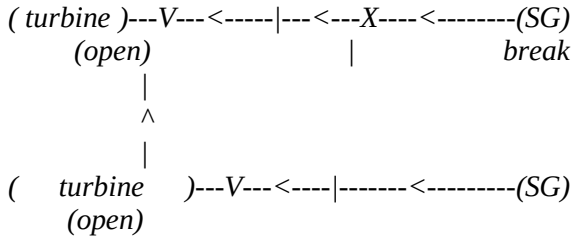

Figure 3. Persisting break flow modes

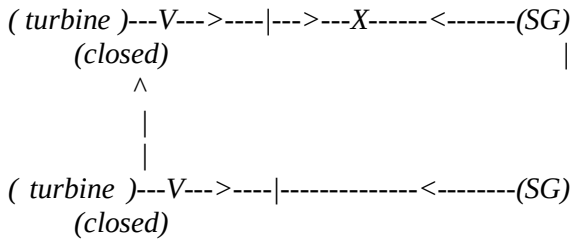

6. Are you using the updated steam safety relief valves data (see *Updated Specifications*, April 1999 – Table 5.4.2, p. 69)?

   No opening of safety/relief valves was calculated to occur since the break occurs upstream of the cross-connect (refer to above Figures). However, openings of safety/relief valves were calculated to occur when the break was assumed to take place downstream of the cross-connect.

7. Are you using the updated additional feedwater mass data (between the feedwater isolation valve and the broken SG, see *Updated Specifications*, April 1999 – Table 5.4.3, p. 69)?

   Yes.

VI. General

1. Deviations from the updated *Final Specifications* (April 1999 – NEA/NSC/DOC(99)8)?

   - *Initial SG mass inventory = 2.84 $\times 10^4$ kg. This value provided by the vendor seems to correspond to the largest capacity for the primary system cool-down.*

   - *The separation efficiency of the aspirators is assumed to decrease as the upward mass flux of the SG secondary system decreases.*

   - *Boron migration was calculated for the primary system by solving a mass equation for boron. In the benchmark, however, it does not influence the calculated results, since its concentration is low and, moreover, there is no boron injection by ECCS.*

2. User assumptions?

   The spray line of the pressuriser is connected to the cold leg. Due to a counter-current flow, a phase separation was calculated to exist in the pressuriser at the initial steady state. THYDE-NEU is capable of dealing with thermal non-equilibrium.

   The rest of the assumptions are in line with Final Specifications.

3. Specific features of the used codes?

4. Number of solutions submitted per participant and how they differ?

   One solution for Exercise 3.

KAERI, *Korea*

I. Primary system

1. Vessel thermal-hydraulic (T-H) model and nodalisation (1-D, 3-D and number T-H channels or cells). How are channels/T-H cells chosen?

   Three-dimensional (3-D) vessel T-H modelling employed.

   Reactor vessel: 59 channels, 94 gaps (a set of junctions) ⇒ 374 cells.

   Figure 1. Reactor vessel nodalisation for MARS/MASTER

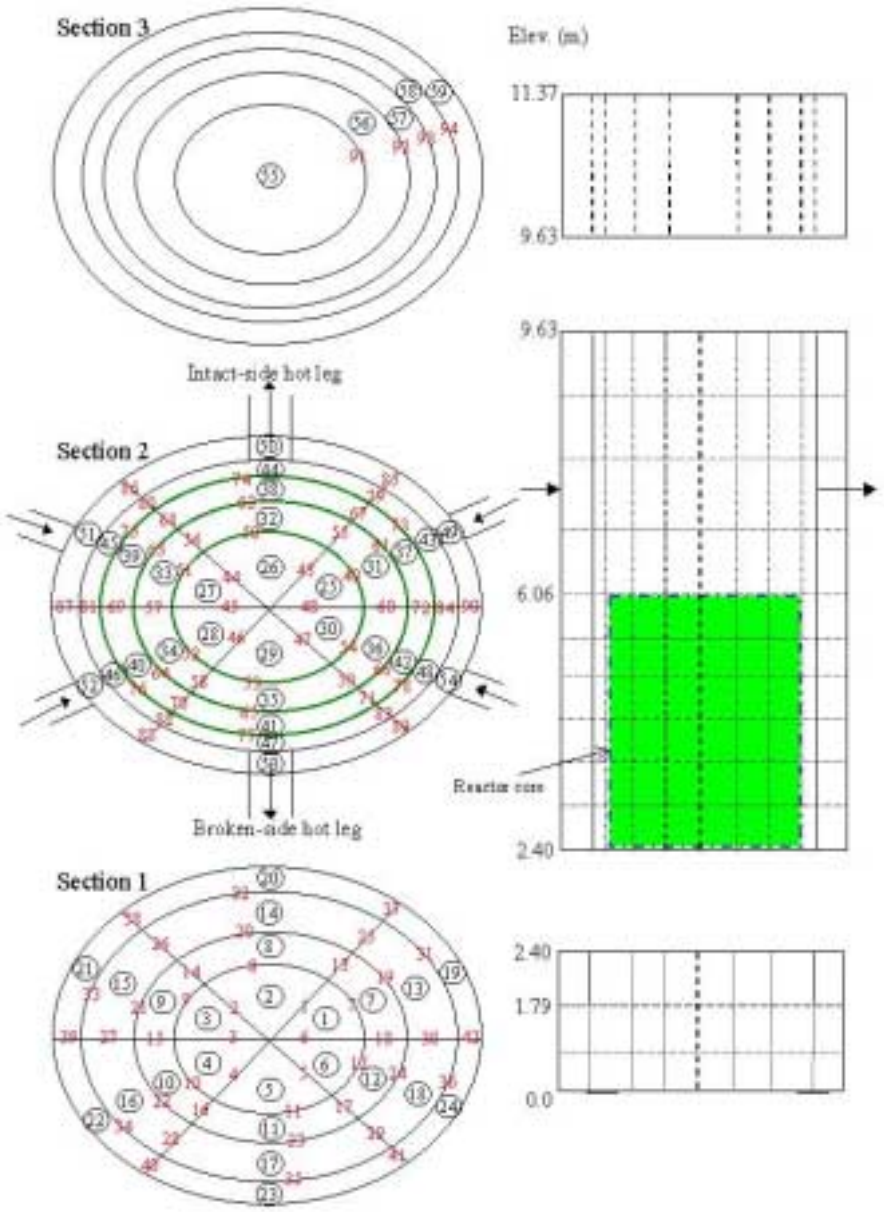

Figure 2. TMI-1 system nodalisation for MARS/MASTER

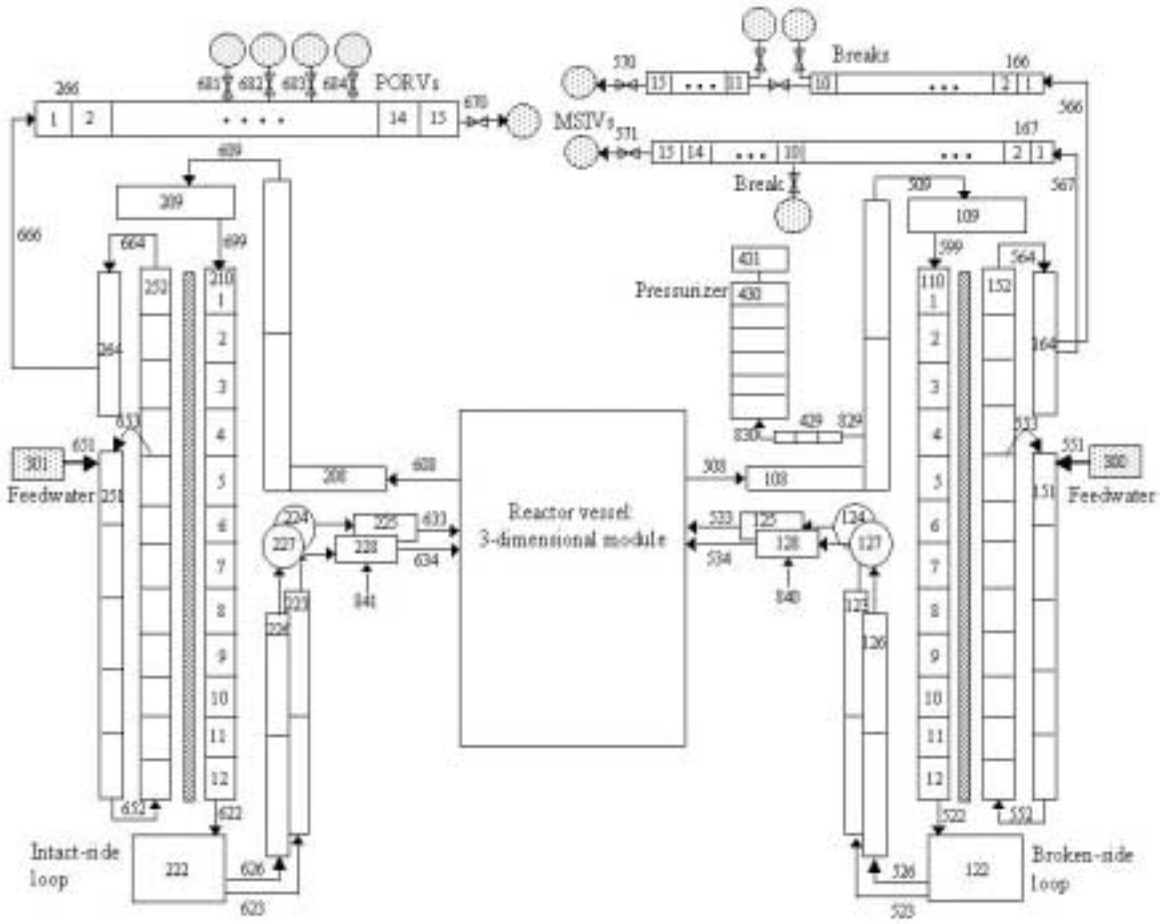

2. Mixing model – how is the required mixing ratio implemented?

   None (3-D modelling of the reactor vessel).

3. Upper plenum and upper head (of reactor vessel) paths (junctions) modelling?

   Upper plenum: 3-D modelling, 24 channels and four vertical meshes ⇒ 96 cells.

   Upper plenum: 1-D modelling, five channels and one vertical mesh ⇒ five cells.

II. Thermal-hydraulic core model

1. Core thermal-hydraulic (T-H) model and radial and axial nodalisation (1-D, 3-D and number T-H channels or cells). How are channels/T-H cells chosen?

   Eighteen (18) channels and six axial nodes (only for the active core region).

2. Number of heat structures (fuel rods) modelled?

   Eighteen (18) radial × six axial = 108 total.

3. Radial and axial heat structure (fuel rod) nodalisation?

   Six radial rings in the pellet, six uniformly spaced axial meshes.

4. Used relation for Doppler temperature?

   *0.3 * centreline temperature + 0.7 * pellet surface temperature.*

5. Used correlations for fuel properties vs. temperature?

   The NEA CRP PWR Rod Ejection Benchmark Specifications.

III. Core neutronics model

1. Number of radial neutronics nodes per assembly?

   One node/FA.

2. Axial nodalisation?

   Twenty-six (26) axial nodes.

3. Radial and axial reflector modelling?

   Modelled as is, no heat removal by reflector.

4. Spatial decay heat distribution modelling?

   Flux dependent.

5. Cross-section interpolation procedure used?

   Identical to lin4d in terms of accuracy.

6. Method used to get a critical reactor at the beginning of transient?

   Divide $\nu\Sigma_f$ by k_{eff} (1.00508).

IV. Coupling schemes

1. Hydraulics/heat structure spatial mesh overlays (mapping schemes in radial and axial plane).

   One-to-one.

2. Hydraulics/neutronics spatial mesh overlays (mapping schemes in radial and axial plane).

   One T-H nodes-to-multi neutronic nodes (about 10 neutronic nodes to one T-H node radially and four neutronic nodes per axially T-H node.

3. Heat structure /neutronics spatial mesh overlays (mapping schemes in radial and axial plane).

   Same as hydraulics.

4. Temporal coupling scheme.

   T-H leading neutronics every time step. No iteration within a time step.

5. Coupling numerics – explicit, semi-implicit or implicit?

   Explicit.

6. Coupling way – external or internal?

   Internal.

7. Coupling design – serial integration or parallel processing?

   Serial.

V. Secondary system

1. Initial steam generator (SG) mass inventory?

   Broken side one: 27 510 kg.

2. SG downcomer nodalisation?

   Five uniformly spaced vertical meshes.

3. Aspirator flow modelling?

   None.

4. Steam line modelling?

   Intact-side steam line: Lumped pipe with 15 meshes.

   Broken-side steam line: Two pipes, 15 meshes each.

5. Break flow modelling and critical flow model?

   Modified Henry-Fauske model.

6. Are you using the updated steam safety relief valves data (see *Updated Specifications*, April 1999 – Table 5.4.2, p. 69)?

   Yes.

7. Are you using the updated additional feedwater mass data (between the feedwater isolation valve and the broken SG, see *Updated Specifications*, April 1999 – Table 5.4.3, p. 69)?

   Yes.

VI. General

1. Deviations from the updated *Final Specifications* (April 1999 – NEA/NSC/DOC(99)8)?

   MASTER's internal decay heat model consistent with ISO 10645, 1992, has been used instead of the specified values.

2. User assumptions?

   None.

3. Specific features of the used codes?

   Three-dimensional (3-D) T-H modelling for the vessel.

4. Number of solutions submitted per participant and how they differ?

   One.

PSU, *USA*

I. Primary system

1. Vessel thermal-hydraulic (T-H) model and nodalisation (1-D, 3-D and number T-H channels or cells). How are channels/T-H cells chosen?

   The TRAC-PF1 VESSEL component models thermal-hydraulically the TMI-1 vessel in 3-D cylindrical geometry. The vessel model is subdivided into 14 axial layers, five radial rings, and six azimuthal sectors for a total of 420 hydrodynamic cells.

2. Mixing model – how is the required mixing ratio implemented?

   The TRAC-PF1 has a 3-D vessel fluid-dynamics capability. By explicitly modelling the radial cross-flow between the T-H cells the code accounts for thermal loop flow mixing in a best-estimate manner.

3. Upper plenum and upper head (of reactor vessel) paths (junctions) modelling?

   Three-dimensional (3-D) modelling.

II. Thermal-hydraulic core model

1. Core thermal-hydraulic (T-H) model and radial and axial nodalisation (1-D, 3-D and number T-H channels or cells). How are channels/T-H cells chosen?

   The 3-D TRAC-PF1 pressure vessel is subdivided into 14 axial layers, five radial rings and six azimuthal sectors for a total of 420 hydrodynamic cells. The core region is contained within the inner three rings and between axial layers four through nine. In the TRAC-PF1 model the four inner T-H rings have the following radiuses: R_1 = 0.945 m, R_2 = 1.3365 m, R_3 = 1.637 m and R_4 = 1.9115 m.

   The flow areas of the T-H cells in the core region are:

   - *For cell numbers 1-6 – 1.515m^2.*
   - *For cell numbers 7-12 – 1.515m^2.*
   - *For cell numbers 13-18 – 1.530m^2.*

2. Number of heat structures (fuel rods) modelled?

   Eighteen heat-structures (rods) in radial plane and six in axial plane.

3. Radial and axial heat structure (fuel rod) nodalisation?

   Eight radial and hundred axial nodes are used.

4. Used relation for Doppler temperature?

   As specified.

5. Used correlations for fuel properties vs. temperature?

   The fuel and clad properties as a function of temperature were given by the equations on pg. 30 of the Final Specifications. Furthermore, the gap conductance used in the TRAC-PF1 input was the value provided on pg. 30 of the Final Specifications.

III. Core neutronics model

1. Number of radial neutronics nodes per assembly?

   Each node in the radial plane represents one fuel assembly with the exception of the centre row of nodes, which is subdivided into two nodes. Each axial level is divided into 258 nodes, 192 fuel nodes and 66 water reflector nodes.

2. Axial nodalisation?

   Twenty-four axial nodes in the framework of the active core (as specified in Chapter 2 of the Final Specifications) plus bottom (one axial node) and top (one axial node) reflectors resulting in total of twenty-six axial neutronics nodes.

3. Radial and axial reflector modelling?

   As described in the Final Specifications.

4. Spatial decay heat distribution modelling?

   Following the fission power distribution at the initial steady state.

5. Cross-section interpolation procedure used?

   The original version without linear extrapolation.

6. Method used to get a critical reactor at the beginning of transient?

   As specified.

IV. Coupling schemes

1. Hydraulics/heat structure spatial mesh overlays (mapping schemes in radial and axial plane).

   Each heat structure is mapped to a thermal-hydraulic cell in radial and axial planes in the framework of the active core

2. Hydraulics/neutronics spatial mesh overlays (mapping schemes in radial and axial plane).

   The neutronic nodes are mapped to the T-H rings and azimuthal sectors as shown in Figures 1 and 2. Table 1 summarises the radial spatial overlays for the TRAC-PF1/NEM coupling.

Figure 1. Description of radial mapping of the T-H rings to the neutronic nodes

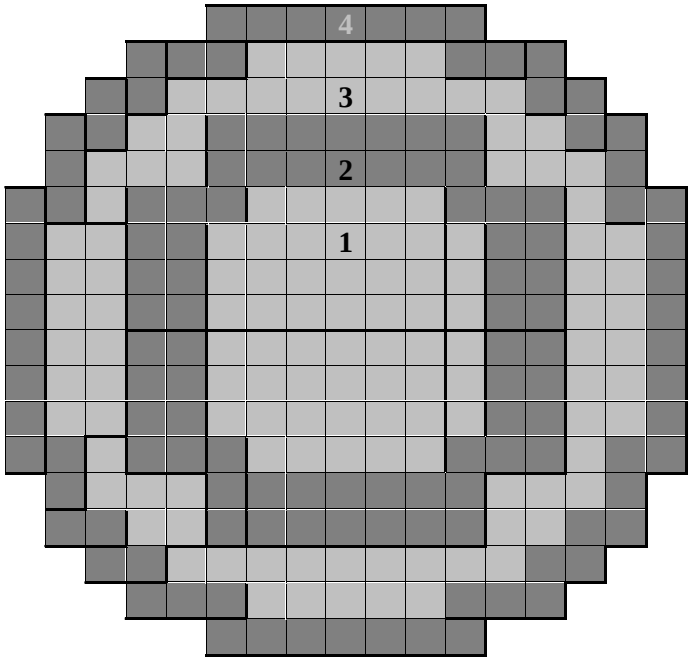

Figure 2. Description of radial mapping of the T-H sectors to the neutron nodes

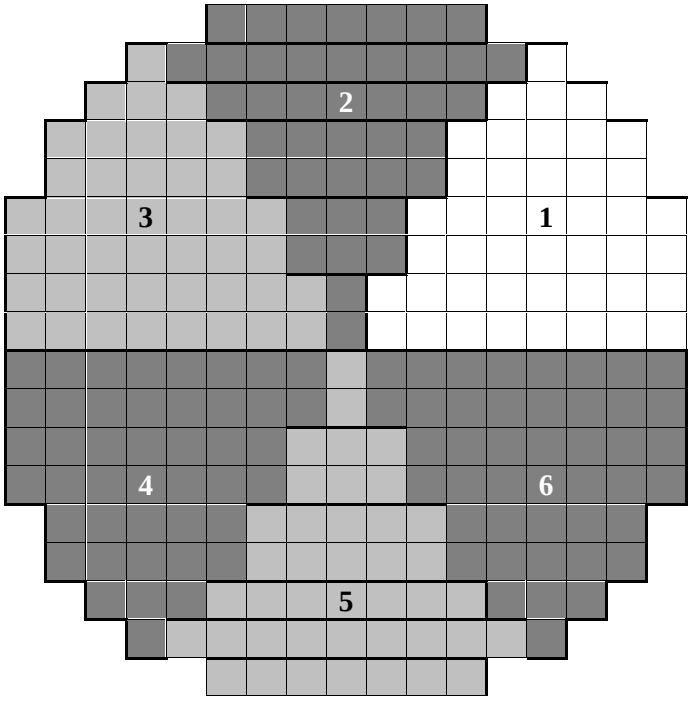

Table 1. Radial coupling summary

Thermal hydraulic (T-H) mapping	
1st (T-H) radial ring	*45 neutronic assemblies*
2nd (T-H) radial ring	*0 neutronic assemblies*
3rd (T-H) radial ring	*72 neutronic assemblies*
4th (T-H) radial ring	*64 reflector water assemblies*
Each theta zone	*29.5 neutronic assemblies*

Axially, the 24 core neutronics nodes are mapped to the six T-H nodes representing the TRAC-PF1 core. The bottom and top reflector are mapped thermal-hydraulically to VESSEL layers 3 and 10, respectively.

3. Heat structure /neutronics spatial mesh overlays (mapping schemes in radial and axial plane).

The radial spatial mesh overlays between the core neutronics model and heat structure component is shown in Figure 3, which is consistent with the original TRAC-PF1/NEM radial mapping scheme, provided in Chapter 2 of this Volume. Axial reflector regions are mapped to layers 4 and 9 for the purpose of neutronics/heat-structure coupling.

Figure 3. Description of the radial mapping of heat structures to the neutronics nodes

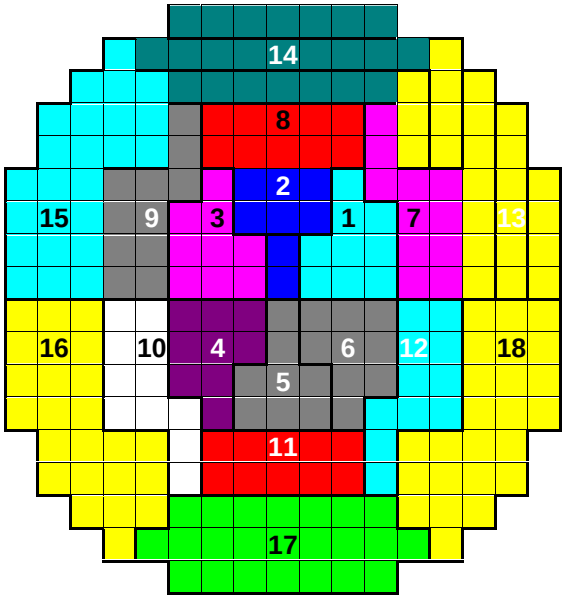

Table 2. Heat structure mapping

Inner ring heat structures	*7.5 neutronic assemblies*
Mid ring heat structures	*10 neutronic assemblies*
Outer ring heat structures	*12 neutronic assemblies*

4. Temporal coupling scheme.

One neutronics time step per one T-H step.

5. Coupling numerics – explicit, semi-implicit or implicit?

   Semi-implicit.

6. Coupling way – external or internal?

   Internal.

7. Coupling design – serial integration or parallel processing?

   Serial integration.

V. Secondary system

1. Initial steam generator (SG) mass inventory?

   26 000 kg.

2. SG downcomer nodalisation?

   Eight nodes – see figure.

3. Aspirator flow modelling?

   According to the Final Specifications.

4. Steam line modelling?

   See Figure 2.

5. Break flow modelling and critical flow model?

   The critical flow model used is a choked flow model of TRAC-PF1.

6. Are you using the updated steam safety relief valves data (see *Updated Specifications*, April 1999 – Table 5.4.2, p. 69)?

   Yes.

7. Are you using the updated additional feedwater mass data (between the feedwater isolation valve and the broken SG, see *Updated Specifications*, April 1999 – Table 5.4.3, p. 69)?

   Yes.

VI. General

1. Deviations from the updated *Final Specifications* (April 1999 – NEA/NSC/DOC(99)8)?

   None.

2. User assumptions?

   None.

3. Specific features of the used codes?

   Three-dimensional (3-D) vessel thermal-hydraulic capability.

4. Number of solutions submitted per participant and how they differ?

   One.

Purdue/NRC, *USA*

I. Primary system

1. Vessel thermal-hydraulic (T-H) model and nodalisation (1-D, 3-D and number T-H channels or cells). How are channels/T-H cells chosen?

   The following components were used:

   - *Two parallel downcomer channels, 1-D pipes.*
   - *Two parallel lower plenum channels, 1-D pipes.*
   - *Eighteen (18) parallel core channels, 1-D pipes.*
   - *One radial reflector channel, 1-D pipe.*
   - *Two parallel upper plenum channels, 1-D pipe.*
   - *Two parallel outlet plenum channels, 1-D pipe.*
   - *One upper head, 1-D pipe.*

   Eighteen (18) core channels were split in half as specified by Figure 3.2.3 and connected to the respective lower and upper plenum. The nodalisation was selected to be consistent with Figure A.2 of the Final Specifications. Cell length was adjusted to give steady-state Courant limit of about 0.1 sec.

2. Mixing model – how is the required mixing ratio implemented?

   Two parallel lower plenum channels and two parallel upper plenum channels were connected with junctions with no momentum transfer across junction (s = 3). The friction losses were adjusted to achieve the desired mixing ratio.

3. Upper plenum and upper head (of reactor vessel) paths (junctions) modelling?

   Each of the core channels was connected to one of the parallel upper plenum channels. Both upper plenums were connected to a single upper head and two parallel outlet plenums. Upper head was connected back to the outlet plenums. Outlet plenum was connected to a hot leg. The frictional losses were adjusted so that about 20% of core flow went through the upper head. This modelling was chosen to be similar to Figure A.2 of the Final Specifications.

II. Thermal-hydraulic core model

1. Core thermal-hydraulic (T-H) model and radial and axial nodalisation (1-D, 3-D and number T-H channels or cells). How are channels/T-H cells chosen?

   The flow paths through the core were represented by 19 1-D pipe components: 18 for the channels specified by Figure 3.2.3 of the Final Specifications, and an additional pipe representing flow through the radial reflector (core periphery) region. Each pipe contained 14 cells of 29.76 cm height, which includes the top and bottom (axial) reflectors. Thus, the total active core height is maintained at 357.12 cm.

2. Number of heat structures (fuel rods) modelled?

   A single heat structure component was used for each neutronic assembly in the active region of the core. This would ordinarily be 177 heat structures, except that an axis of symmetry exists in the mapping as defined by Figure 3.2.3 in the Final Specifications. Those fuel assemblies along this axis of symmetry were divided into two half-assemblies, bringing the number of heat structure components to 192. Finally, a single heat structure component was used to model the entire radial reflector region. Thus, the total number of heat structure components used in the model is 193.

3. Radial and axial heat structure (fuel rod) nodalisation?

   Throughout most of the core, each assembly is represented by an individual heat structure component. The exceptions, as mentioned above, are those fuel assemblies along the axis of symmetry and the radial reflector region. Each heat structure component contained nine radial conduction nodes, at 0.0000, 0.9391, 1.8782, 2.8173, 3.7564, 4.6955, 4.7910, 5.1275, and 5.4640 mm from the centreline of the fuel pin. The gas gap was modelled between nodes 6 and 7 (4.6955 and 4.7910 mm from the fuel centreline. Each heat structure was divided into 14 axial intervals 29.76 cm in height. The height of the heat structures corresponds to the core height of the core, including the axial reflectors.

4. Used relation for Doppler temperature?

   The common 70/30% split between fuel surface and centreline as specified on pg. 29 in the Final Specifications was used for computing Doppler temperature.

5. Used correlations for fuel properties vs. temperature?

   The fuel and clad properties as a function of temperature were given by the equations on pg. 30 of the Final Specifications. Furthermore, the gap conductance used in the RELAP input was the value provided on pg. 30 of the Final Specifications.

III. Core neutronics model

1. Number of radial neutronics nodes per assembly?

   One.

2. Axial nodalisation?

   *The core model was divided into a total of 28 axial levels. Of these, two levels are modelling the axial reflectors, while the remaining 26 levels are used to model the active core region. The nodalisation outlined in the Final Specifications was not used. Instead, the axial nodalisation was (from the bottom): 21.811, 14.88, 4.71, 10.17, 20*14.88, 12.266, 2.614, 14.88 and 21.811 cm. This does not follow the suggested nodalisation in the Final Specifications in order to match the thermal-hydraulic axial nodalisation in a more consistent manner.*

3. Radial and axial reflector modelling?

   The radial reflector was modelled in the neutronics model by a single neutronic node per reflector assembly on each axial level of the core. The axial reflector was modelled using an axial level consisting of reflector assemblies only on the top and bottom of the core.

4. Spatial decay heat distribution modelling?

   PARCS uses a six-group per neutronic node decay-heat model based on the past 3-D power history calculated by the code. The model operates under the assumption of saturation of the decay heat precursors, sometimes called "infinite operation time".

5. Cross-section interpolation procedure used?

   The method used for interpolating the cross-sections was given in the Final Specifications. This is a four-point interpolation scheme designed to interpolate the tabular format of the cross-section sets. The last results submitted also used linear extrapolation beyond the table properties range.

6. Method used to get a critical reactor at the beginning of transient?

   PARCS adjusts the fission source before beginning a transient calculation by dividing by k_{eff}.

IV. Coupling schemes

1. Hydraulics/heat structure spatial mesh overlays (mapping schemes in radial and axial plane).

   Since each assembly in the active core region is represented by a heat structure, the mapping shown in Figure 3.2.3 describes the hydraulics to heat structure mapping. Each block in this figure represents a heat structure component (with the exception of the all-black reflector, modelled by a single heat structure component), and the number in each block is the channel number coupled with that particular heat structure component. The radial reflector (channel 19) is coupled with heat structure 193. Again, there are 14 axial cells in the hydraulic components and 14 axial intervals in the heat structure components (all are of the same height).

2. Hydraulics/neutronics spatial mesh overlays (mapping schemes in radial and axial plane).

   Since each neutronic assembly in the active core is represented by a heat structure component in RELAP, the description above also demonstrates the hydraulic-to-neutronics mapping. All 64 radial reflector assemblies are mapped to channel 19 in the hydraulics model.

3. Heat structure /neutronics spatial mesh overlays (mapping schemes in radial and axial plane).

   The mapping of neutronic assemblies in the active core is one-to-one to heat structure nodalisation. All 64 radial reflector assemblies in the neutronics model are mapped to heat structure 193.

4. Temporal coupling scheme.

   Both RELAP and PARCS are locked into the same time step, and the time step size is determined by RELAP. RELAP updates its conduction solution first, followed by the hydraulics solution. These new data are passed to PARCS so the neutronics solution can be updated. The updated neutronics solution (in the form of a heat source) is passed back to RELAP and is used to update the hydraulics and conduction solution for the subsequent time step.

5. Coupling numerics – explicit, semi-implicit or implicit?

   RELAP/PARCS operates in an explicit manner.

6. Coupling way – external or internal?

   RELAP/PARCS uses an internal coupling scheme.

7. Coupling design – serial integration or parallel processing?

   Although the Parallel Virtual Machine (PVM) message passing package is used to pass the data between RELAP and PARCS, the coupled code actually operates in a serial mode, with PVM providing only an interface for passing data between the two processes.

V. Secondary system

1. Initial steam generator (SG) mass inventory?

   26 000 kg.

2. SG downcomer nodalisation?

   Five axial levels.

3. Aspirator flow modelling?

   A junction connecting SG 2/3 way up with FW inlet was used. Form losses were adjusted to achieve steady state aspirator flow equal to 10% of the steady-state outlet SG flow.

4. Steam line modelling?

   Eight axial levels, from SG outlet plenum to the MSIV. One steam line on the intact side, two steam lines on the broken side. Four relief valves connected to the four last axial levels of the intact steam line.

5. Break flow modelling and critical flow model?

   Henry-Fauske critical flow model for the break. The 24″ and 8″ breaks were connected to separate steam lines, both at 44.8 m of the steam line.

6. Are you using the updated steam safety relief valves data (see *Updated Specifications*, April 1999 – Table 5.4.2, p. 69)?

   Yes.

7. Are you using the updated additional feedwater mass data (between the feedwater isolation valve and the broken SG, see *Updated Specifications*, April 1999 – Table 5.4.3, p. 69)?

   Yes.

VI. General

1. Deviations from the updated *Final Specifications* (April 1999 – NEA/NSC/DOC(99)8)?

   Mixing ratio of 0.6 was used. The axial nodalisation of the neutronics model was finer than given in the Final Specifications. There are no axial levels in the core with a height of 29.76 cm.

2. User assumptions?

   Turbine sink pressure adjusted to achieve SL inlet pressure of 6.41 MPa. The wall roughness of the channels was 0.05% of the hydraulic diameter. This value was chosen in order to match more closely the pressure drops across the core calculated by RELAP and provided by the benchmark specifications.

3. Specific features of the used codes?

   The RELAP5 code has been developed for best-estimate transient simulation of light water reactor coolant systems during postulated accidents. RELAP5 is a highly generic code that, in addition to calculating the behaviour of a reactor coolant system during a transient, can be used for simulation of a wide variety of hydraulic and thermal transients in both nuclear and non-nuclear systems involving mixtures of steam, water, non-condensable and solute.

   The RELAP5/MOD3 code is based on a non-homogeneous and non-equilibrium model for the two-phase system that is solved by a fast, partially implicit numerical scheme to permit economical calculation of system transients. The code includes many generic component models from which general systems can be simulated. The component models include pumps, valves, pipes, heat releasing or absorbing structures, reactor point kinetics, electric heaters, jet pumps, turbines, separators, accumulators and control system components. In addition, special process models are included for effects such as form loss, flow at an abrupt area change, branching, choked flow, boron tracking and non-condensable gas transport.

   PARCS has a transient pin power capability, using form functions from the lattice physics code. The use of this feature makes best-estimate analysis and, specifically, DNB analysis easier throughout the important transient state points. ANM kernel was used for the MSLB.

4. Number of solutions submitted per participant and how they differ?

   Two solutions were submitted from RELAP/PARCS. The last one fixed valve timing, fuel conductivity correlation and minor details to match the specifications as closely as possible.

VTT, *Finland*

I. Primary system

1. Vessel thermal-hydraulic (T-H) model and nodalisation (1-D, 3-D and number T-H channels or cells). How are channels/T-H cells chosen?

   One-dimensional (1-D) nodalisation. Vessel is divided into six parallel sectors. Number of T-H cells is 128 (72 in the core and 56 in the vessel). Nodalisation is based mainly on information given for RETRAN and TRAC models.

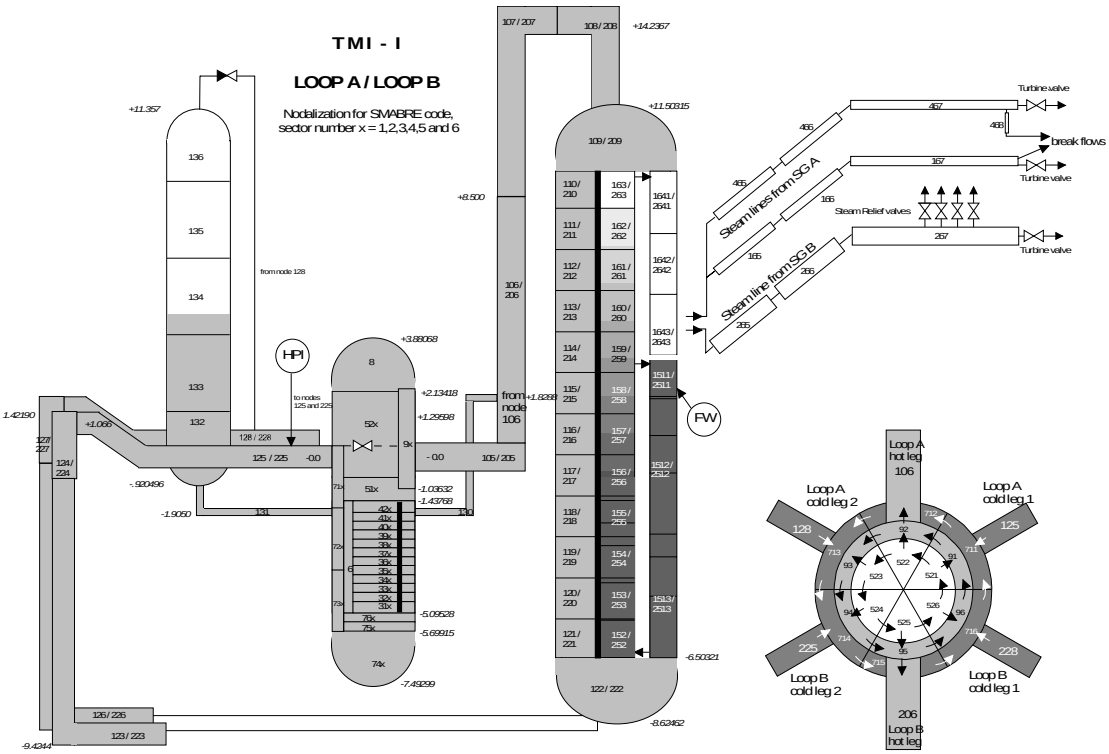

2. Mixing model – how is the required mixing ratio implemented?

   The vessel is modelled with six sectors all the way from the downcomer to outlet plenum. This creates basis to simulate mixing of cold water from the broken loop and hot water from intact loop. Mixing in the horizontal connections between the sectors is based mainly on the density difference between the nodes. Finally, the requested mixing is achieved by using the turbulent mixing model in these junctions. The turbulent mixing model consists of the mixing of the enthalpy and boron concentration between the neighbouring nodes. The amount of turbulent mixing varies according the main flow rate.

3. Upper plenum and upper head (of reactor vessel) paths (junctions) modelling?

   In the upper plenum, the mixing is mainly based on the six parallel sectors and turbulent mixing model described above. Here the uppermost node, the upper head also takes part in mixing, since part of the flow in the model goes through the single node in the upper head.

II. Thermal-hydraulic core model

1. Core thermal-hydraulic (T-H) model and radial and axial nodalisation (1-D, 3-D and number T-H channels or cells). How are channels/T-H cells chosen?

   One-dimensional (1-D), one channel/assembly, 177 channels, 24 axial nodes.

2. Number of heat structures (fuel rods) modelled?

   One hundred seventy-seven (177), one fuel rod/assembly.

3. Radial and axial heat structure (fuel rod) nodalisation?

   Twenty-four (24) axial nodes. Radially fuel rod modelled with seven points in pellet and two points in cladding.

4. Used relation for Doppler temperature?

   As specified on pg. 29 of the Final Specifications.

5. Used correlations for fuel properties vs. temperature?

   As specified on pg. 30 of the Final Specifications.

III. Core neutronics model

1. Number of radial neutronics nodes per assembly?

   One node/assembly.

2. Axial nodalisation?

   Twenty-four (24) nodes of equal height.

3. Radial and axial reflector modelling?

   Reflector nodes not modelled. Albedo boundary conditions calculated from given reflector cross-sections used.

4. Spatial decay heat distribution modelling?

   Time evolution of decay heat followed dynamically in each assembly. For axial distribution, the initial steady-state fission power distribution used through the transient.

5. Cross-section interpolation procedure used?

   Linear interpolation and extrapolation from tables.

6. Method used to get a critical reactor at the beginning of transient?

   Number of neutrons from fission divided by calculated k_{eff}.

IV. Coupling schemes

1. Hydraulics/heat structure spatial mesh overlays (mapping schemes in radial and axial plane).

   One-to-one (same nodes).

2. Hydraulics/neutronics spatial mesh overlays (mapping schemes in radial and axial plane).

   One-to-one (same nodes).

3. Heat structure /neutronics spatial mesh overlays (mapping schemes in radial and axial plane).

   One-to-one (same nodes).

4. Temporal coupling scheme.

   Core thermal hydraulics and neutronics both iterated during each time step inside the same outer iteration loop (TRAB-3D calculation). Primary loop including less detailed core T-H calculation and secondary loop calculated once in a time step (SMABRE calculation).

5. Coupling numerics – explicit, semi-implicit or implicit?

   Implicit.

6. Coupling way – external or internal?

   Parallel calculation of core T-H with both codes TRAB-3D and SMABRE.

   Coupling between codes with data exchange once in a time step (power distribution from TRAB-3D to SMABRE, core inlet and outlet T-H boundary conditions from SMABRE to TRAB-3D).

7. Coupling design – serial integration or parallel processing?

   Serial integration.

V. Secondary system

1. Initial steam generator (SG) mass inventory?

   Steam generator A: 25 977kg, steam generator B: 25 572 kg.

2. SG downcomer nodalisation?

   Three nodes (see figure in Part I).

3. Aspirator flow modelling?

   The aspirator junction, steam outtake from tube bundle to downcomer to preheat the feed water, is modelled with the given flow area, 0.96 m^2. At the steady state in SMABRE model 100 kg/s steam and also 400 kg/s of saturated water is flowing from the tube bundle to the top of downcomer. During the transient at the aspirator junction no reversal flow is allowed.

4. Steam line modelling?

   Steam line A1: three nodes until the break.

   Steam line A2: four nodes until the break.

   Steam line B: four nodes until the turbine valve.

   See picture of nodalisation in Q-I1.

5. Break flow modelling and critical flow model?

   Main steam line: Break area – 0.2462 m^2, hydraulic diameter – 0.5599 m.

   Cross-connect line: Break area – 0.0324 m^2, hydraulic diameter – 0.2031 m.

   Critical flow: The Moody model is used for critical break flow model with the contraction coefficient 1.0 for saturated flow.

6. Are you using the updated steam safety relief valves data (see *Updated Specifications*, April 1999 – Table 5.4.2, p. 69)?

   Yes.

7. Are you using the updated additional feedwater mass data (between the feedwater isolation valve and the broken SG, see *Updated Specifications*, April 1999 – Table 5.4.3, p. 69)?

   Yes.

VI. General

1. Deviations from the updated *Final Specifications* (April 1999 – NEA/NSC/DOC(99)8)?

   No reflector flux calculations (point III.3).

   Decay heat distribution (point III.4).

   Decay heat time-evolution calculated from our own fitting of ANS-79.

   The superheating of the main steam flow in SMABRE model is 26℃ instead of 19℃ given in the Final Specifications.

2. User assumptions?

3. Specific features of the used codes?

4. Number of solutions submitted per participant and how they differ?

   One solution.

FZR, *Germany*

I. Primary system

1. Vessel thermal-hydraulic (T-H) model and nodalisation (1-D, 3-D and number T-H channels or cells). How are channels/T-H cells chosen?

   One-dimensional (1-D) model, two parallel thermal-hydraulics channels from vessel inlet through downcomer and lower plenum up to the core entry, eight nodes from the vessel inlet up to the core entry, interface to the core model (DYN3D), modelling of all coolant channels, coolant is distributed according to a equal pressure drop boundary condition over the core. Each half of the assemblies is provided with the coolant temperature of the corresponding loop (after partly mixing acc. to the ratio). The row of assemblies in the middle of the core (row number 9) is provided with fully mixed coolant from the two loops.

2. Mixing model – how is the required mixing ratio implemented?

   The primary circuit is fully split into two parts; there is only one connection point for pressure balance (between the two parts of the upper head). At each time step the actual ratio is calculated, by means of a controller energy is exchanged in the lower and in the upper plenum to match the required value of 0.5.

3. Upper plenum and upper head (of reactor vessel) paths (junctions) modelling?

   Two flow paths are modelled (one for each half) from the upper plenum to the head and back to the upper plenum to ensure the cooling of the head.

II. Thermal-hydraulic core model

1. Core thermal-hydraulic (T-H) model and radial and axial nodalisation (1-D, 3-D and number T-H channels or cells). How are channels/T-H cells chosen?

   Radial T-H nodalisation: One averaged T-H channel/assembly (177 core channels and 64 reflector channels).

   Axial T-H nodalisation: 28 layers: 21.811 cm (bottom reflector), 14.88 cm, 4.7 cm, 10.17 cm, 20 × 14.88 cm, 12.266 cm, 2.614 cm, 14.88 cm, 21.811cm (top reflector).

2. Number of heat structures (fuel rods) modelled?

   One average fuel pin/T-H channel.

   Axial nodalisation: 28 layers as described in I.1.

3. Radial and axial heat structure (fuel rod) nodalisation?

   Each fuel pin in an axial layer was divided into 10 radial zones of equal area.

4. Used relation for Doppler temperature?

   Equation of pg. 29 of Updated Final Specifications (April 1999 – NEA/NSC/DOC(99)8) was used.

   The Doppler temperature of the reflectors follows the specifications on pg. 15 of Updated Final Specifications (April 1999 – NEA/NSC/DOC(99)8).

5. Used correlations for fuel properties vs. temperature?

   Correlations of pg. 30 of Updated Final Specifications (April 1999 – NEA/NSC/DOC(99)8) were used.

III. Core neutronics model

1. Number of radial neutronics nodes per assembly?

   One node per assembly.

2. Axial nodalisation?

   Twenty-eight (28) axial layers of II.1.

3. Radial and axial reflector modelling?

   One node per reflector assembly.

   Twenty-eight (28) axial layers of II.1.

4. Spatial decay heat distribution modelling?

   The decay-heat time table is calculated by using the decay heat model of DYN3D. It is based on the German standard DIN Norm 25463. The contribution of the power during the transient is taken into account. The code option that the decay heat distribution is equal to the normalised power distribution of initial state was used. The model was slightly modified to 7.1% of total power at the initial state.

5. Cross-section interpolation procedure used?

   Linear cross-section interpolation with extrapolation was used.

6. Method used to get a critical reactor at the beginning of transient?

   Node values of divided by initial k_{eff}.

IV. Coupling schemes

1. Hydraulics/heat structure spatial mesh overlays (mapping schemes in radial and axial plane).

   No overlapping, in axial direction 1:1, in radial direction 10 heat structure nodes in one hydraulics node.

2. Hydraulics/neutronics spatial mesh overlays (mapping schemes in radial and axial plane).

   No overlapping, in each direction 1:1.

3. Heat structure /neutronics spatial mesh overlays (mapping schemes in radial and axial plane).

   The same as above.

4. Temporal coupling scheme.

   DYN3D model of reactor core: Different time steps for neutronic and thermal-hydraulics with heat structure equations. Neutronics time steps smaller or equal to thermal-hydraulic time steps.

   ATHLET model of the remaining T-H system: Time step scheme of ATHLET used.

   If the time steps of ATHLET and DYN3D are different, interpolated values are transferred between the two codes.

5. Coupling numerics – explicit, semi-implicit or implicit?

   Iteration between neutronics and thermal-hydraulics (implicit scheme) in the core (DYN3D). No iteration between ATHLET and DYN3D.

6. Coupling way – external or internal?

   External coupling: Core model – DYN3D, remaining coolant system – ATHLET.

   Coupling by thermal-hydraulic core inlet and outlet conditions.

   The General Control Simulation Model (GCSM) of ATHLET was applied for this type of coupling.

7. Coupling design – serial integration or parallel processing?

   Serial integration.

V. Secondary system

1. Initial steam generator (SG) mass inventory?

   26 077 kg.

2. SG downcomer nodalisation?

   Eleven (11) nodes (one-dimensional).

3. Aspirator flow modelling?

   A junction between SG and SG downcomer is introduced; the flow is about 80 kg/s.

4. Steam line modelling?

   Broken SG: Two steam lines are modelled including the cross-connection, 10 nodes from the SG upper plenum up to the break in both lines.

   Intact SG: One two-fold steam line is modelled, same nodalisation as in broken SG.

5. Break flow modelling and critical flow model?

   Double-ended rupture within 0.1 s is modelled, after leak opening two independent leaks (8″ inch, 24″) exist. The critical 1-D flow model of ATHLET is used. This model uses a four-equation model to simulate the fluid flow in the flow path closest to the discharge plane. The field equations for this two-phase model are based on the 1-D stationary conservation laws for liquid mass, vapour mass, mixture energy and mixture momentum. Due to the separation of the mass balance, the four-equation model is capable of taking into account thermal non-equilibrium of one phase, whereas the other phase is kept at equilibrium.

6. Are you using the updated steam safety relief valves data (see *Updated Specifications*, April 1999 – Table 5.4.2, p. 69)?

   Yes.

7. Are you using the updated additional feedwater mass data (between the feedwater isolation valve and the broken SG, see *Updated Specifications*, April 1999 – Table 5.4.3, p. 69)?

   Yes.

VI. General

1. Deviations from the updated *Final Specifications* (April 1999 – NEA/NSC/DOC(99)8)?

   Not using the Moody model for critical flow.

2. User assumptions?

   No.

3. Specific features of the used codes?

4. Number of solutions submitted per participant and how they differ?

   One.

UP/UZ 1: RELAP5/PARCS, UP/UZ 2: RELAP5/QUABOX, *Italy/Croatia*

I. Primary system

1. Vessel thermal-hydraulic (T-H) model and nodalisation (1-D, 3-D and number T-H channels or cells). How are channels/T-H cells chosen?

   The vessel nodalisation is given in Figure 1 below. The vessel is subdivided into two equal parts as shown in attached Figure 2. The total number of T-H volumes in the model is 646. The single junctions were used to connect 18 core channels (R5 pipes) between volumes 115-131 and 114-130. Radial dimensions of each channel are consistent with dimensions given in Figure 3.2.3 of PWR MSLB Benchmark, Vol I: Final Specifications, April 1999.

2. Mixing model – how is the required mixing ratio implemented?

   For coupled Relap5/Parcs, four calculations are documented and have been submitted to PSU. These are identified as 9a, 9b, 10a, 10b in Table 4 of NT 398(00) of the DIMNP:

   - *Run 9a: 18 core channels, one downcomer (i.e. full mixing), Xsec without return to power.*
   - *Run 9b: 18 core channels, one downcomer (i.e. full mixing), Xsec with return to power.*
   - *Run 10a: 18 core channel, four downcomers (i.e. no mixing), Xsec without return to power.*
   - *Run 10b: 18 core channel, four downcomers (i.e. no mixing), Xsec with return to power.*

   In the case of coupled Relap5/Quabox, the mixing ratio is realised by changing flow fractions going from affected and intact loops to geometrically closer core regions during HFP steady-state runs. The mixing is realised between components 100, 111 and 100, 110 in lower plenum, and between components 131, 133 and 130, 132 in upper plenum (pressure drop characteristics of affected junctions were changed to get required flow fractions corresponding to required mixing).

3. Upper plenum and upper head (of reactor vessel) paths (junctions) modelling?

   The following bypass flow paths have been considered within the RPV:

   - *Downcomer-upper head.*
   - *Upper head- upper plenum.*
   - *Upper head-core via control rod guide tubes.*
   - *Downcomer-upper plenum.*
   - *Upper plenum-lower plenum via core.*

   In the case of coupled Relap5/Quabox, the upper plenum and upper head models are the same as in the original nodalisation except splitting of upper plenum and RCCA guide tubes in two parts and using two junctions to connect upper head to split-upper downcomer (the flow area of the communication is the same as in original model).

II. Thermal-hydraulic core model

1. Core thermal-hydraulic (T-H) model and radial and axial nodalisation (1-D, 3-D and number T-H channels or cells). How are channels/T-H cells chosen?

   Core thermal-hydraulic is a 3-D fictitious model including 18 parallel T-H channels chosen according to Figure 3.2.3 of PWR MSLB Benchmark, Volume I: Final Specification. Axial subdivisions correspond to Table 2.4.2 of the Final Specifications (24 layers). There are two parallel core bypass channels.

   In the case of coupled Relap5/Quabox, 24 equidistant layers (0.14880 m) are used for core and core bypass regions.

2. Number of heat structures (fuel rods) modelled?

   Eighteen (18) heat structures were used to model fuel rods belonging to 18 core channels (e.g. core structure attached to channel one represents 7.5 fuel elements with 1 560 fuel rods, and the one attached to channel 10 represents 10FAs with 2 080 fuel rods).

3. Radial and axial heat structure (fuel rod) nodalisation?

   The heat structure is based on real radial dimensions of fuel rod, height of axial layer and number of fuel rods belonging to the structure (e.g. for HS 01 7.5 fuel elements with 1 560 fuel rods). There are 10 radial mesh points in the structure (five mesh intervals in the fuel, two in gap and two in cladding). In the case of coupled Relap5/Quabox, 24 equidistant layers (0.14880 m) are used.

4. Used relation for Doppler temperature?

   The relation as requested in the Final Specification with weighting factor 0.7 was used.

5. Used correlations for fuel properties vs. temperature?

   Fuel and cladding properties are supplied by code users in the form of tables utilising "standard" material properties data.

III. Core neutronics model

1. Number of radial neutronics nodes per assembly?

   One node per fuel assembly was used in radial direction.

2. Axial nodalisation?

   Twenty-six (26) axial nodes were used for core region + one node for bottom and one for top reflector. The nodalisation is as requested in the Final Specification but two central regions were additionally divided in two equal parts, resulting in the following axial mesh dimensions [cm]: 14.88, 4.71, 10.17, 20 × 14.88, 12.266, 2.614 and 14.88.

3. Radial and axial reflector modelling?

   The radial and axial reflectors are explicitly modelled. The thickness of the axial reflectors is 21.881 cm. For modelling the radial reflector cells of the same size as fuel elements were used and with the same axial subdivisions. Fuel temperature used in feedback calculation for radial reflector composition is 551 K for HZP and 600 K for HFP. The moderator density as calculated in bypass channel was used for radial reflector. Fuel temperatures used for top and bottom reflector compositions are equal to corresponding fluid temperature.

4. Spatial decay heat distribution modelling?

   The decay heat is calculated internally in the code using ANS-79 decay heat model with 23 groups for ^{235}U only. Uncertainty of 2σ was used. Steady-state decay heat fraction is 0.071. In the revised calculation, the spatial distribution of decay heat is frozen at initial HFP conditions and total decay heat is calculated for each time step.

5. Cross-section interpolation procedure used?

   New version of subroutines (with extrapolation) and provided XS files were directly used in final calculation (see also the answer I.2, above).

   In the case of the coupled Relap5/Parcs, the standard procedure proposed in the Parcs Manual is adopted.

6. Method used to get a critical reactor at the beginning of transient?

IV. Coupling schemes

1. Hydraulics/heat structure spatial mesh overlays (mapping schemes in radial and axial plane).

   There are 18 core T-H channels and corresponding 18 heat structures (equivalent fuel rods). The axial subdivision of the channel and the heat structure is the same.

2. Hydraulics/neutronics spatial mesh overlays (mapping schemes in radial and axial plane).

   The fuel elements/neutronic cells are connected to core channels according to Figure 3.2.3 from the Final Specifications.

   In the case of coupled Relap5/Quabox, and related to the central row of fuel elements coolant densities used for T-H feedback calculation are based on neighbouring channel properties with weight 0.5. In axial direction, one to one mapping was used except for T-H core layers 2-3 and 24-25. In that case, two neutronic nodes correspond to one T-H node and both neutronic nodes have the same T-H conditions. The density in radial reflector is average density of two Relap5 bypass channels.

3. Heat structure /neutronics spatial mesh overlays (mapping schemes in radial and axial plane).

   Same as above.

4. Temporal coupling scheme.

   Thermal-hydraulic part of the coupled code uses semi-implicit numerics. The time step is influenced by both hydraulics and heat transfer and it is the same. Relap5 is leading part of the coupled code and either Parcs or Quabox uses the same time step. The neutronics part can influence time step size only indirectly by influence on heat transfer calculation (power of heat structure).

5. Coupling numerics – explicit, semi-implicit or implicit?

   Explicit coupling of T-H and neutronic calculation both in the cases of Parcs and Quabox.

6. Coupling way – external or internal?

   Internal coupling both in the cases of Parcs and Quabox.

7. Coupling design – serial integration or parallel processing?

   Parallel processing in the case of Relap/Parcs and serial integration in the case of Relap/Quabox.

V. Secondary system

1. Initial steam generator (SG) mass inventory?

   In the case of the coupled Relap5/Parcs, SG mass in the four runs is as described in I.2 above:

   - *Run 9a: 25 917 kg.*
   - *Run 9b: 25 917 kg.*
   - *Run 10a: 25 536 kg.*
   - *Run 10b: 25 536 kg.*

   In the case of coupled Relap5/Quabox, SG1/2 masses are 25 911 and 25 971 kg, respectively.

2. SG downcomer nodalisation?

   See Figure 1. Additional details in DIMNP NT 398(00) rev.1.

3. Aspirator flow modelling?

   All geometric and boundary/initial conditions (e.g. flow rates) available from the Final Specifications have been considered. See Figure 1. Additional details can be found in DIMNP NT 398(00) rev.1.

4. Steam line modelling?

   See Figure 1. Additional details in DIMNP NT 398(00) rev.1.

5. Break flow modelling and critical flow model?

   See Figure 3. Additional details in DIMNP NT 398(00) rev.1.

   In the case of coupled Relap5/Quabox, valve component 628 was removed and corresponding opening/closing trips adjusted (there is no influence on the results).

6. Are you using the updated steam safety relief valves data (see *Updated Specifications*, April 1999 – Table 5.4.2, p. 69)?

   Yes.

7. Are you using the updated additional feedwater mass data (between the feedwater isolation valve and the broken SG, see *Updated Specifications*, April 1999 – Table 5.4.3, p. 69)?

   Yes.

VI. General

1. Deviations from the updated *Final Specifications* (April 1999 – NEA/NSC/DOC(99)8)?

   Metal masses considered for the modelling of SGs secondary sides.

   In the case of the coupled Relap5/Parcs, the mixing has been considered as described under item I.2 above (no mixing and completed mixing cases).

2. User assumptions?

   User assumptions are unavoidable at different levels during the development of the input decks and the acceptance of steady state. It is difficult to summarise here.

3. Specific features of the used codes?

   None (in the sense that the standard code versions have not been modified).

4. Number of solutions submitted per participant and how they differ?

   UP/UZ 1 Relap5/Parcs (four solutions, see I.2 above). UP/UZ 2 Relap5/Quabox with vessel mixing.

Figure 1. Sketch of the nodalisation for the TMI-1 MSLB Benchmark

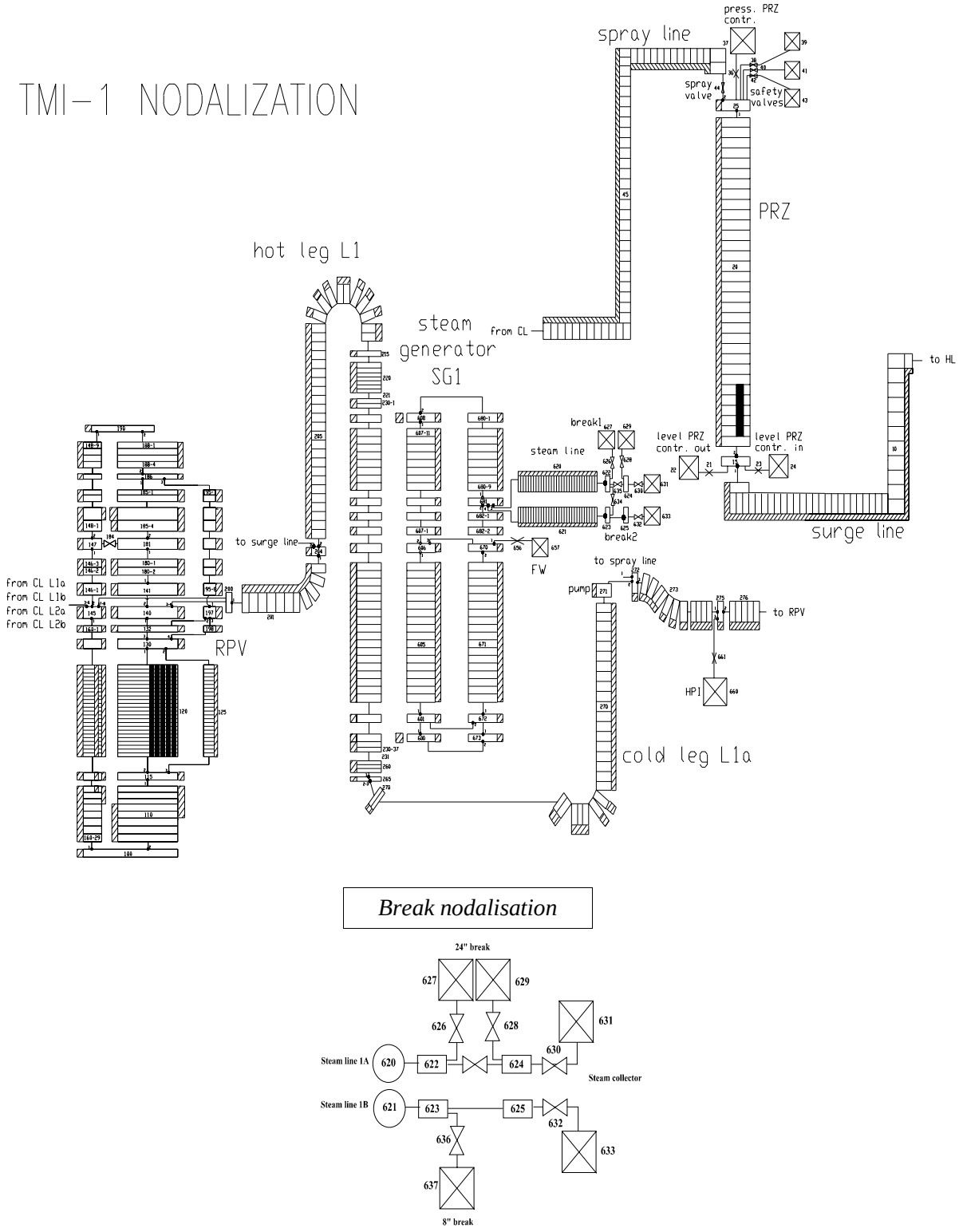

Figure 2. Nodalisation for the TMI-1 core (splitted core + mixing) with 18 channels

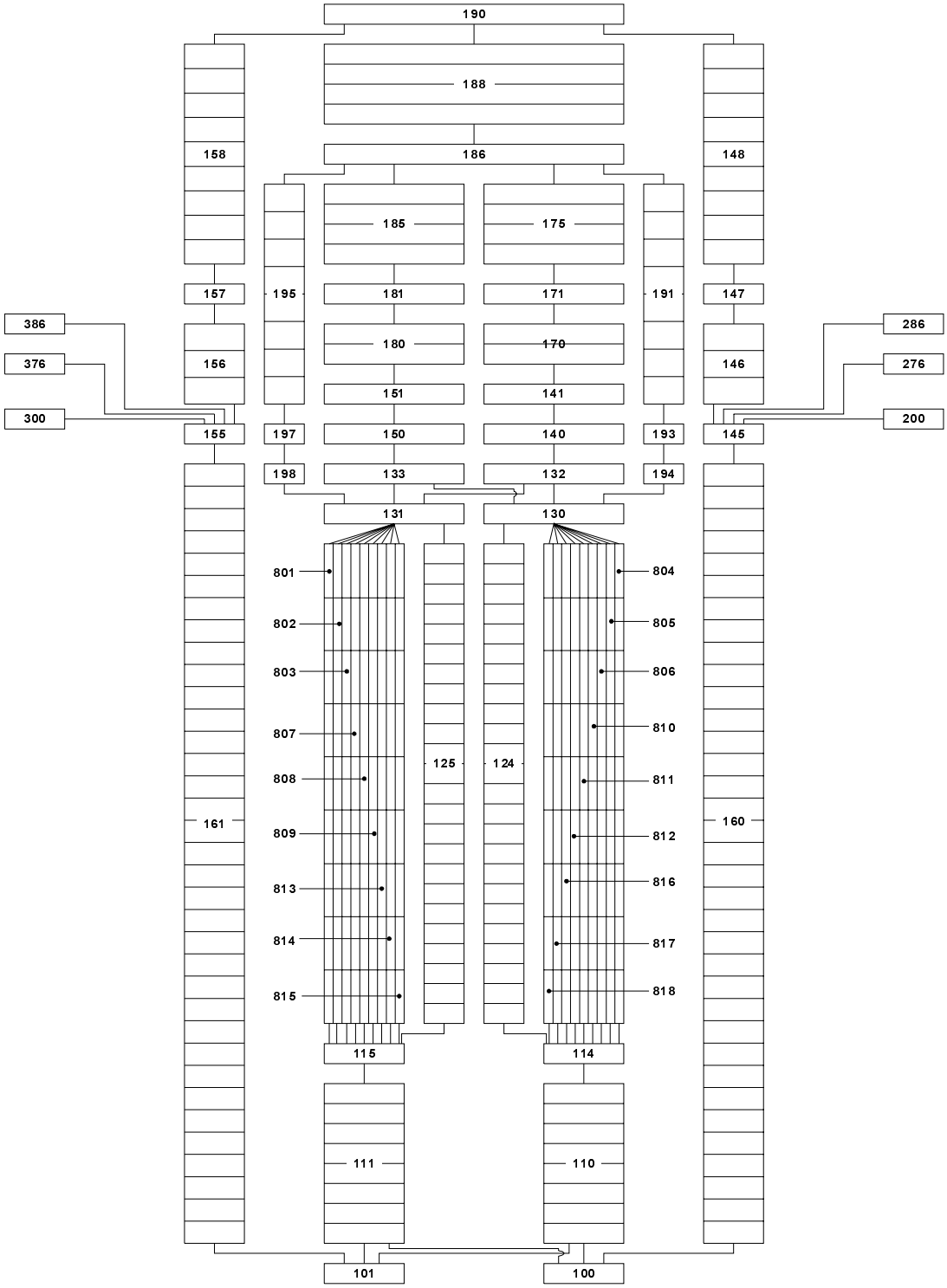

Figure 3. Break modelling

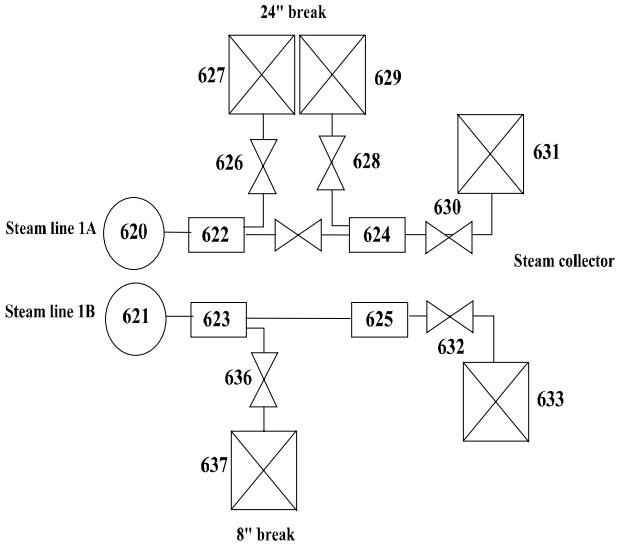

CSA/GPUN, *USA*

I. Primary system

1. Vessel thermal-hydraulic (T-H) model and nodalisation (1-D, 3-D and number T-H channels or cells). How are channels/T-H cells chosen?

   For Phase II and III, 18 parallel core channels were used (as defined in the Final Specifications). Each core channel had 24 axial T-H nodes.

   The vessel nodalisation (no core) is the same as that shown in Figure A.2 in the Final Specifications.

2. Mixing model – how is the required mixing ratio implemented?

   The mixing model was implemented by exchanging energy between the two lower plenum and two upper plenum nodes. A control system was implemented to monitor the loop temperature difference and adjust the plenum energy exchange each time step to achieve the desired loop temperature difference. The two upper and lower plenums are consistent with the vessel diagram in Figure A.2 in the Final Specifications.

3. Upper plenum and upper head (of reactor vessel) paths (junctions) modelling?

   Same as vessel diagram shown in Figure A.2 in the Final Specifications.

II. Thermal-hydraulic core model

1. Core thermal-hydraulic (T-H) model and radial and axial nodalisation (1-D, 3-D and number T-H channels or cells). How are channels/T-H cells chosen?

   For Phase II and III, 18 parallel core channels were used (as defined in the Final Specifications). Each core channel had 24 axial T-H nodes.

2. Number of heat structures (fuel rods) modelled?

   See # 3 below.

3. Radial and axial heat structure (fuel rod) nodalisation?

   Twenty-four (24) axial heat structures in each of the 18 parallel core channels.

4. Used relation for Doppler temperature?

   As defined in the Final Specifications.

5. Used correlations for fuel properties vs. temperature?

   As defined in the Final Specifications.

III. Core neutronics model

1. Number of radial neutronics nodes per assembly?

   One.

2. Axial nodalisation?

   Spacing and number as defined in the Final Specifications (24).

3. Radial and axial reflector modelling?

   As defined in the Final Specifications.

4. Spatial decay heat distribution modelling?

   As defined in the Final Specifications, proportional to initial power distribution.

5. Cross-section interpolation procedure used?

   Used FORTRAN interpolation subroutine provided by PSU.

6. Method used to get a critical reactor at the beginning of transient?

   Iterative coupling between the RETRAN-3D steady-state thermal-hydraulic module and the kinetics.

IV. Coupling schemes

1. Hydraulics/heat structure spatial mesh overlays (mapping schemes in radial and axial plane).

   One heat structure for each hydraulic node.

2. Hydraulics/neutronics spatial mesh overlays (mapping schemes in radial and axial plane).

   One hydraulic node was used for each axial neutronic spatial mesh. In the radial direction, 18 channels mapped over 177 fuel assemblies per the specification

3. Heat structure /neutronics spatial mesh overlays (mapping schemes in radial and axial plane).

   One heat structure for each neutronic spatial mesh.

4. Temporal coupling scheme.

   Three-dimensional (3-D) kinetics solution advanced with each hydraulic solution time step.

5. Coupling numerics – explicit, semi-implicit or implicit?

   Explicit.

6. Coupling way – external or internal?

   Internal.

7. Coupling design – serial integration or parallel processing?

   Serial.

V. Secondary system

1. Initial steam generator (SG) mass inventory?

   As defined in the Final Specifications.

2. SG downcomer nodalisation?

   Eight axial nodes.

3. Aspirator flow modelling?

   As defined in the Final Specifications. The aspirator flow paths (junctions 150 and 250) shown in Figure A.1 of the Final Specifications is consistent with the way it was modelled.

4. Steam line modelling?

   As defined in the Final Specifications and as shown in Figures A.3 and A.4.

5. Break flow modelling and critical flow model?

   The geometry was as defined in the Final Specifications. An isenthalpic critical flow model was used instead of the specified Moody critical flow model.

6. Are you using the updated steam safety relief valves data (see *Updated Specifications*, April 1999 – Table 5.4.2, p. 69)?

   Yes.

7. Are you using the updated additional feedwater mass data (between the feedwater isolation valve and the broken SG, see *Updated Specifications*, April 1999 – Table 5.4.3, p. 69)?

   Yes.

VI. General

1. Deviations from the updated *Final Specifications* (April 1999 – NEA/NSC/DOC(99)8)?

   There were three deviations from the Final Specifications that we are aware of in our analysis. The first is the choice of critical flow models for Phases I and III (see Q. 4 above). The second is we used the 1979 ANS decay heat model within RETRAN rather than the specified decay heat. We compare decay heat values and the differences were insignificant. The third was the core mapping for Phases II and III. RETRAN-3D requires a one to one axial correspondence between T-H, fuel and neutronic nodes. The Final Specifications had only six axial T-H/fuel nodes per channel. The Final Specifications split several assemblies between hydraulic channels. RETRAN-3D requires whole assemblies in a channel. Consequently, the Final Specifications could not be duplicated, but we approximated the specified core mapping as closely as we could.

2. User assumptions?

   None other than discussed above.

3. Specific features of the used codes?

   None.

4. Number of solutions submitted per participant and how they differ?

   Only one solution submitted.

ALSO AVAILABLE

NEA Publications of General Interest

2002 Annual Report (2003) — *Free: paper or Web.*

NEA News
ISSN 1605-9581 — Yearly subscription: € 43 US$ 48 GBP 28 ¥ 5 500

Nuclear Energy Today
ISSN 9264-10328-7 — Price : € 21 US$ 24 GBP 14 ¥ 2 700

Nuclear Science

Advanced Reactors with Innovative Fuels
Workshop Proceedings, Chester, UK, 22-24 October 2001 (2002)
ISBN 92-64-19847-4 — Price: € 130 US$ 113 GBP 79 ¥ 15 000

Physics of Plutonium Recycling
Volume VII – BWR MOX Benchmark – Specification and Results (2003)
ISBN 92-64-19905-5 — Price: € 45 US$ 45 GBP 29 ¥ 5 500
Volume VI – Multiple Pu Recycling in Advanced PWRs (2002)
ISBN 92-64-19957-8 — Price: € 45 US$ 45 GBP 28 ¥ 5 250

Basic Studies in the Field of High-temperature Engineering (2002)
Second Information Exchange Meeting, Paris, France, 10-12 October 2001
ISBN 92-64-19796-6 — Price: € 75 US$ 66 GBP 46 ¥ 8 600

Fission Gas Behaviour in Water Reactor Fuels (2002)
Workshop Proceedings, Cadarach, France, 26-29 September 2000
ISBN 92-64-19715-X — Price: € 120 US$ 107 GBP 74 ¥ 12 100

Plutonium Management in the Medium Term (2003)
ISBN 92-64-02151-5 — *Free: paper or web.*

Actinide and Fission Product Partitioning and Transmutation (2003)
Proceedings of the Seventh Information Exchange Meeting, Jeju, Republic of Korea, 14-16 October 2002
ISBN 92-64-02125-6 — *Free: paper or web.*

Burn-up Credit Criticality Benchmark (2003) — *Free: paper or web.*
Phase IV-A: Reactivity Prediction Calculations for Infinite Arrays of PWR MOX Fuel Pin Cells
ISBN 92-64-02123-X
Phase IV-B: Results and Analysis of MOX Fuel Depletion Calculations
ISBN 92-64-02124-8

CD-ROM Complete Collection of Published Reports (as of May 2003) — *Free on request.*

Accelerator-driven Systems (ADS) and Fast Reactors (FR) in Advanced Nuclear Fuel Cycles (2002)
ISBN 92-64-18482-1 — *Free: paper or web.*

Comparison Calculations for an Accelerator-driven Minor Actinide Burner (2002)
ISBN 92-64-18478-3 — *Free: paper or web.*

Speciation, Techniques and Facilities for Radioactive Materials at Synchrotron Light Sources (2002)
Workshop Proceedings, Grenoble, France, 10-12 September 2000
ISBN 92-64-18485-5 — *Free: paper or web.*

Pressurised Water Reactor Main Steam Line Break (MSLB) Benchmark
Volume III: Results of Phase II on 3-D Core Boundary Conditions Modelling (2002)
ISBN 92-64-18495-3 — *Free: paper or web.*
Volume II: Results of Phase I on Pont Kinetics (2000)
ISBN 92-64-18280-2 — *Free: paper or web.*
Volume I: Final Specifications (1999) — *Available on the web.*

A VVER-1000 LEU and MOX Assembly Computational Benchmark (2002)
Specification and Results
ISBN 92-64-18491-0 — *Free: paper or web.*

Order form on reverse side.

ORDER FORM

OECD Nuclear Energy Agency, 12 boulevard des Iles, F-92130 Issy-les-Moulineaux, France
Tel. 33 (0)1 45 24 10 15, Fax 33 (0)1 45 24 11 10, E-mail: neapub@nea.fr**, Internet: www.nea.fr**

Qty	Title	ISBN	Price	Amount
			Total*	

* Prices include postage fees.

❑ Payment enclosed (cheque payable to OECD Publications).

Charge my credit card ❑ VISA ❑ Mastercard ❑ American Express

Card No.	Expiration date	Signature
Name		
Address	Country	
Telephone	Fax	
E-mail		

OECD PUBLICATIONS, 2 rue André-Pascal, 75775 PARIS CEDEX 16
Printed in France.